The Dissertation Committee for Kwang Hoon Baek Certifies that this is the approved version of the following dissertation:

Application of Different Types of Solvents for Heavy Oil Recovery: Experimental Study on Dimethyl Ether, Organic Alkalis, and Surface Active Solvents

Committee:

Ryosuke Okuno, Supervisor

Chun Huh

David DiCarlo

Kishore K. Mohanty

Prince N. Azom

Application of Different Types of Solvents for Heavy Oil Recovery: Experimental Study on Dimethyl Ether, Organic Alkalis, and Surface Active Solvents

by

Kwang Hoon Baek

Dissertation

Presented to the Faculty of the Graduate School of

The University of Texas at Austin

in Partial Fulfillment

of the Requirements

for the Degree of

Doctor of Philosophy

The University of Texas at Austin

August 2020

To my family

Acknowledgements

I would like to express my sincere gratitude to my supervisor, Dr. Ryosuke Okuno, for his guidance on my research. I am deeply impressed by his passion, motivation, and enthusiasm for research. He shows me how to become a PhD researcher having logical thinking to come up with good research questions. I will not forget what he has taught me during my PhD program.

Besides my advisor, I am extremely grateful to my committee, Dr. Chun Huh, Dr. David DiCarlo, Dr. Kishore K. Mohanty, and Dr. Prince N. Azom for their assistance and insightful suggestions throughout my research. I would like to thank Dr. Upali P. Weerasooriya for his assistance and insight to come up with new chemicals to be studied.

My sincere thanks also go to our wonderful research staffs, Glen Baum, Gary Miscoe and Daryl Nygaard. I would not have completed my experiment without their support. I also thank my colleagues, Dr. Francisco J. Argüelles-Vivas, Dr. Gayan A. Abeykoon, Dr. Himanshu Sharma, Dr. Krishna K. Panthi, Kai Sheng, Mingyuan Wang, Young Liu, Sofiane Achour, and Haofeng Song for being not simply good colleagues, but great friends.

Last, but not the least, I would like to thank my family: my mom Taeju, my sister Jiwon, and her husband Hyungjae. My PhD study would not have been possible without their support, patience, and love. And finally, I dedicate this dissertation to my dad in heaven.

Abstract

Application of Different Types of Solvents for Heavy Oil Recovery: Experimental Study on Dimethyl Ether, Organic Alkalis, and Surface Active Solvents

Kwang Hoon Baek, Ph.D.

The University of Texas at Austin, 2020

Supervisor: Ryosuke Okuno

Various challenges in heavy oil recovery come from the low mobility of reservoir oil. For example, the heavy-oil displacement by water results in a large mobility ratio and therefore, inefficient volumetric sweep. Polymer flooding is the traditional method to improve the frontal stability of the oil displacement, but the polymer mobility is often optimized to be greater than the oil mobility because increasing the polymer viscosity adversely affects the oil production rate. The low mobility of reservoir oil also results in a large amount of steam required in steam-assisted gravity drainage (SAGD), one of the commercially successful methods of bitumen recovery. This research investigated the application of unconventional solvents for heavy oil recovery, such as dimethyl ether (DME), organic alkalis, and surface active solvents (SAS), as a potential additive to the injection fluid. These solvents are not conventionally used for enhanced oil recovery (EOR).

The first part of the dissertation presents potential methods of improving the efficiency of SAGD by using water-soluble solvents. Phase-behavior data were obtained

for mixtures of bitumen and water-soluble solvents. Experimental results indicated that use of organic alkalis at low concentrations (e.g., 0.5 wt% pyrrolidine) in low-salinity brine can yield efficient emulsification of bitumen in water. The affinity of the organic alkali for asphaltic bitumen was important for oil-in-water emulsification at a wide range of temperatures.

The second part of the dissertation presents a potential method of improving polymer flooding by SAS that reduces the interfacial tension (IFT) between the oleic and aqueous phases. Results showed that the IFT reduction by three orders of magnitude (i.e., 15.8 to 0.025 dynes/cm) gave a reduced residual oil saturation and a delayed polymer breakthrough in polymer flooding experiments with no preceding water flood. When the straight polymer flooding resulted in an oil recovery factor of 47% at 1.0 pore-volume injected (PVI), the SAS-improved polymer flooding increased it to 63% with a SAS slug of 0.1 wt% for 0.5 PVI or 0.5 wt% for 0.1 PVI.

Table of Contents

List of Tables

List of Figures

1. Introduction

1.1. Problem Description

The U.S. Geological Survey estimated that there exist more than 3,300 billion bbls of heavy oil and 5,500 billion bbls of bitumen resources in the world, and that approximately 34% of the total heavy oil and bitumen resources are distributed in North America (USGS 2007). Heavy oil recovery is often inefficient because the in-situ viscosity of heavy oil ranges from 50 to 50,000 cp (Bryan and Kantzas 2007a). Canadian extra-heavy oil or bitumen is even more viscous (Baek et al. 2019a). To decrease the mobility ratio of a displacing fluid to a displaced fluid requires either reducing the viscosity of the displaced fluid (e.g. oil) or increasing the viscosity of the displacing fluid (brine, for water flooding operation).

For conventional heavy oil (not bitumen) recovery, polymer flooding is a widely used method, in which the displacing phase with an increased viscosity improves the conformance control under reservoir heterogeneity and lowers the mobility ratio for oil displacement. In addition to polymer, alkali-surfactant-polymer (ASP) flooding has been studied as a method to improve heavy oil recovery. Heavy oils typically contain a large amount of acidic hydrocarbon components, part of which can be used as natural surfactants after the mixing and reaction with alkalis, such as sodium carbonate, sodium hydroxide, ethanolamine, and ammonium hydroxide (Baek et al. 2019b; Fu et al. 2016; Sharma et al. 2015).

ASP flooding is designed to achieve Winsor Type-III micro-emulsion phase behavior during the oil displacement (Winsor 1948), with in-situ natural surfactants, synthetic surfactants, co-solvents, and other additives (Lake et al. 2014; Sheng 2014). An optimal ASP flooding achieves a high displacement efficiency by micro-emulsion phase

behavior with ultra-low interfacial tension (IFT), and a high volumetric sweep efficiency by use of polymer.

However, ASP flooding has not been widely applied for heavy oil reservoirs. Several reports confirmed injectivity issues caused by calcite and silica scales, which were attributed partly to the injected alkalis (Delamaide 2014; Hocine et al. 2014). Apart from injectivity, ASP flooding might not be an economically feasible option depending on oil prices because of its costs for various surfactants, co-solvents, and polymers.

For an extremely viscous oil, like bitumen, the widely-used recovery method is steam injection such as cyclic steam stimulation and steam-assisted gravity drainage (SAGD). Steam injection aims to decrease the viscosity of bitumen by thermal energy. However, these methods may be inefficient and/or impractical for shallow and/or thin reservoirs that yield substantial heat losses, including many heavy oil reservoirs in Alaska and Canada (Bryan and Kantzas 2007a; Liu et al. 2006).

The main drawback of steam injection for heavy oil is the significant usage of energy and water to generate high-quality steam. To improve the efficiency of steam injection, solvent and steam co-injection methods have been studied at lab scales, and also pilot-tested (Gates 2007; Gupta et al. 2005; Gupta and Gittins 2006; Keshavarz et al. 2014 and 2015; Leaute and Carey 2002; Li et al. 2011ab; Nasr et al. 2003). The primary objective of these studies is to reduce the cumulative steam-to-oil ratio (CSOR), defined as the ratio of the cumulative volume of steam injected (cold-water equivalent) to the cumulative volume of bitumen produced.

In terms of the types of solvents, however, studies of the solvent and steam co-injection have been limited to hydrocarbon solvents. Considering that water is the dominant component in steam injection, water-soluble solvents could be potential additives to create an interaction among water, bitumen, and solvents, and as a result, give a

synergetic effect on bitumen recovery. The phase behavior of bitumen and water-soluble solvent mixtures is the key to understanding the mechanisms using water-soluble solvents for thermal recovery of bitumen.

1.2. Research Objectives

This research investigated the application of unconventional solvents for heavy oil recovery. The term "unconventional" refers to chemicals that have not been widely used for heavy oil recovery or solvent-based surfactants that are not classified in the conventional EOR surfactant category. In this research, three types of solvents, i.e. dimethyl ether (DME), organic alkalis [diethylamine (DEA), triethylenetetramine (TETA), and pyrrolidine], and surface active solvents (SAS) were studied as a potential additive in heavy oil recovery methods such as steam injection and polymer flooding. The use of these solvents for heavy oil recovery has been filed/submitted as different patents for DME (Okuno 2018) and for pyrrolidine and surface active solvents (Okuno et al. 2019; Weerasooriya et al. 2019a and 2019b).

These compounds aim to improve the recovery of highly viscous heavy oil in different ways. For steam injection, a large amount of water flowing with oil may be utilized for enhancing the efficiency of SAGD. A water-soluble solvent (e.g. DME) could reduce bitumen viscosity and reduce cumulative steam-oil ratio (CSOR). A high acidity of heavy oil opens the possibility of using an organic alkali to induce low-viscosity oil-in-water emulsions. When the induced oil-in-water emulsion contains enough bitumen, the emulsion phase could be an effective bitumen carrier during SAGD.

The fractional flow of oil in heavy oil displacement by water is small, resulting in a substantial potential for EOR. It is not a new idea to use a surfactant for polymer flooding to enhance the oil displacement efficiency by water. The new type of solvent-based

surfactant in this research could improve polymer flooding, specifically in a highly permeable reservoir of acidic heavy oil. A SAS reduces IFT by a few orders of magnitude without creating micro-emulsions of ultra-low IFT. Consequently, the expected mechanisms of the incremental oil recovery include increasing capillary number by reducing the water/oil IFT in high-permeability porous media and increasing the interfacial viscoelasticity of acidic heavy oil and water. Since a SAS is not expected to achieve an ultra-low IFT, it is unlikely to efficiently coalesce dispersed oil droplets into an oil bank in already water-flooded regions of the heavy oil reservoir. That is, the focus of the investigation is more on the secondary polymer flooding than on the tertiary.

Dimethyl ether (DME) as a water-soluble solvent in steam injection

DME is partially soluble in water and miscible with bitumen. While the vapor pressure of DME is between n-pentane (C_3) and n-butane (C_4), it could result in a different steam chamber behavior and bitumen recovery (Sheng et al. 2018). However, there is a lack of experimental data to study the detailed mechanisms of DME-steam co-injection.

The main objective is to establish the fundamental phase behavior of DME and bitumen mixtures. This research provides the comparison of DME with n-hexane in terms of the capability of viscosity reduction for Athabasca bitumen. In addition, new experimental data are presented for bubble point pressures, densities, and viscosities of Athabasca bitumen and its mixtures with DME and n-hexane.

Organic alkali for the oil-in-water emulsification of Athabasca bitumen in SAGD

The main idea of this research is to induce in-situ oil-in-water (o/w) bitumen emulsions with natural surfactants activated by an organic alkali without any additional surfactants. Because there are not many studies on the use of an organic alkali co-injected

with steam for bitumen recovery, it is crucial to conduct fundamental experimental research of emulsion phase behavior and viscosity for mixtures of Athabasca bitumen with organic alkalis.

This research aims to achieve three objectives. First, bitumen emulsification was investigated whether o/w emulsions can be formed by adding an organic alkali in the aqueous solution and mixing it with Athabasca bitumen. Second, phase behavior data was obtained for bitumen emulsification at different organic alkali concentrations, water-oil ratios (WORs), brine salinities, and temperatures. Third, bitumen contents and viscosities of o/w emulsions were measured to evaluate the effectiveness of the o/w emulsion as a bitumen carrier.

SAS for the improved polymer flooding

This topic focuses on the application of SAS as a sole chemical additive that improves the displacement efficiency of polymer flooding for heavy oil recovery. A SAS typically consists of a very short hydrophobe (e.g. carbon number lower than C_8) with a certain amount of propylene oxide (PO) units and the sufficient ethylene oxide (EO) units. The PO and EO units respectively give hydrophobicity and hydrophilicity. Surface activity depends primarily on the PO units. The aqueous stability at the desired temperature and brine composition can be adjusted by changing the EO number.

The objective of this investigation is to find conditions for the successful improved polymer flooding using SAS. It suggests a new opportunity of enhanced heavy oil recovery by adding a slug of one multi-functional solvent (i.e. SAS) to conventional polymer flooding. Experimental data are provided including emulsion phase behavior, IFT, in-situ polymer rheology, and 1-D heavy oil recovery for a glass-bead pack and a sandpack under different operating conditions.

1.3. Outline of Dissertation

Chapter 2 This chapter explains the background of this research including literature reviews.

Chapter 3 Dimethyl ether (DME) was investigated as a potential additive to steam to improve SAGD. The main objective of this research is to compare DME with n-hexane in terms of the capability of viscosity reduction for Athabasca bitumen. In addition, new experimental data are presented for bubble point pressures, densities, and viscosities of Athabasca bitumen and its mixtures with DME and n-hexane. This chapter was published in *SPE Reservoir Evaluation & Engineering*, SPE-187182-PA (Baek et al. 2019a).

Chapter 4 Organic alkalis were studied as a potential additive to steam for steam-assisted gravity drainage (SAGD). Diethylamine (DEA), Triethylenetetramine (TETA), and pyrrolidine were selected as organic alkalis in this research. This chapter provides experimental data of bitumen emulsification, viscosities of emulsions, oil contents in emulsions at different alkali concentrations, water-oil ratios (WORs), brine salinities, and temperatures. Based on comparison among results from DEA, TETA, and pyrrolidine, the effect of the chemical structure of organic alkalis on the bitumen emulsification is discussed. This chapter was published in following journals: *Journal of Petroleum Science*

and Engineering (Baek et al. 2018); *SPE Reservoir Evaluation & Engineering*, SPE-189768-PA (Baek et al. 2019b); and *Fuel* (Baek et al. 2019c).

Chapter 5 A SAS was studied for heavy oil recovery. This chapter presents the preliminary study on improved polymer flooding using a SAS with a HPAM (partially hydrolyzed polyacrylamide) polymer. Interfacial tension (IFT), phase behavior, and heavy oil recovery in a glass-bead pack were measured under simplified conditions. This chapter was published in *Energy & Fuels* (Baek et al. 2019d).

Chapter 6 Based on the previous study (Chapter 5), a comprehensive improved polymer flooding was designed for the actual heavy oil field in the North Sea. The goal of this research is to find conditions for the successful improved polymer flooding using a surface active solvent. An analogous oil, a sandpack, and a brine were matched to reservoir conditions. Interfacial tension (IFT), phase behavior, emulsion separation, in-situ polymer rheology, and heavy oil recovery in a sandpack were measured. The result suggests an opportunity of the improved polymer flooding using a SAS for high permeable heavy oil reservoirs.

Chapter 7 The conclusion of this research is described in the final chapter. Also, the future research topics are suggested.

2. Background and Literature Review

2.1. SAGD and Solvent-SAGD

SAGD has been widely used for in-situ recovery of bitumen, which is usually immobile at initial reservoir conditions. SAGD uses two horizontal wells that are approximately five meters apart vertically. The upper horizontal well is for injection of high-quality steam (e.g., 90%), and the lower well for production of heated bitumen and water. The injected steam forms a steam-saturated zone, "steam chamber". Bitumen is effectively made mobile by latent heat of the injected steam upon its condensation near the edge of a steam chamber. The main drawback of SAGD, however, is the significant usage of energy and water to generate steam.

The energy efficiency of steam injection is quantified by cumulative steam-to-oil ratio (CSOR), defined as the ratio of the cumulative volume of steam injected (cold water equivalent) to the cumulative volume of bitumen produced. In SAGD, temperatures inside the steam chamber and in its vicinity can be high (e.g., 177 - 247°C). According to Shen (2013), CSOR is generally in the range from 2 to 4 m^3/m^3 for SAGD to be economically feasible. It is desirable to lower CSOR by operating at low chamber temperatures while maintaining economically sustainable rates of oil production. SAGD is expected to be even less energy-efficient for highly heterogeneous reservoirs (Venkatramani and Okuno 2018). Therefore, there is a critical need to reduce SAGD's CSOR, which has motivated the search for alternative processes.

The co-injection of steam and solvent for SAGD (solvent-steam-assisted gravity drainage, or solvent-SAGD) has been studied and tested as a potential method to improve the drawbacks of SAGD (Gupta et al. 2005; Gupta and Gittins 2006; Leaute and Carey 2002). Solvent-SAGD processes studied in the literature, such as expanding-solvent-

SAGD (ES-SAGD) and solvent-aided-process (SAP), use a small amount of solvents (e.g., a few to 20 percent by liquid volume equivalent) (Gupta et al. 2005; Gupta and Gittins 2006; Leaute and Carey 2002). They aim to enhance the oleic-phase mobility by the dilution of oil by solvent, in addition to the thermal energy released from the injected steam. Various researchers have showed that solvent-SAGD has the potential of increasing bitumen-drainage rate and displacement efficiency, while reducing CSOR; e.g., EnCana's SAP pilot (Gates 2007; Gupta et al. 2005; Gupta and Gittins 2006; Keshavarz et al. 2014 and 2015; Leaute and Carey 2002; Li et al. 2011ab; Nasr et al. 2003).

Prior investigations into solvent-SAGD were mainly concerned with hydrocarbon solvents, such as propane (C_3), butane (C_4), and diluents, which usually consist of pentane (C_5) and heavier hydrocarbons at different concentrations (Gates 2007; Ivory et al. 2008; Keshavarz et al. 2014 and 2015; Li et al. 2011ab; Nasr et al. 2003). The suitability of hydrocarbon solvents for SAGD in terms of phase behavior has been reported to increase with increasing carbon number (or decreasing volatility), and tend to level off at a certain carbon number; e.g., approximately n-hexane (C_6) for Athabasca bitumen reservoirs (Keshavarz et al. 2015; Li et al. 2011a; Mohebati et al. 2012). However, heavy hydrocarbon solvents, as such n-hexane and diluents, are relatively expensive in general. In-situ retention of the co-injected solvent, which inevitably happens under heterogeneity, can substantially affect the project's economics. That is, the geological uncertainties associated with reservoir heterogeneity increase the uncertainty of the project's economics, if the solvent to be co-injected is expensive.

2.2. DME-SAGD

The use of DME was motivated by the question as to how we can use the water component and/or the aqueous phase to improve the efficiency of steam-based oil recovery,

such as SAGD and cyclic steam stimulation. This is because water is by far the most dominant component in steam-based oil recovery for heavy-oil and bitumen recovery (Zhu and Okuno 2016). The volume of produced water is at least a few times greater than the volume of produced oil in SAGD and cyclic steam stimulation.

Sheng et al. (2018) studied a water-soluble solvent, dimethyl ether (DME), in their phase behavior analysis and mechanistic simulations of DME-steam-assisted gravity drainage (DME-SAGD). Their results showed that DME-SAGD resulted in 35% lower SOR than SAGD while being able to maintain bitumen-production rates close to SAGD. As part of their study, they compared C_4-SAGD and DME-SAGD, because DME is between propane (C_3) and butane (C_4) in terms of vapor pressure and because C_3-SAGD did not show any improvement over SAGD in their cases due to substantially low chamber-edge temperatures. The key hypothesis that can be derived from their mechanistic simulation results is that the solvent's solubility in water makes DME-SAGD substantially different from solvent-SAGD with conventional hydrocarbon solvents through its impact on chamber-edge temperature and compositional distribution in the reservoir. Detailed investigation of how and why they are different might lead to new findings toward an efficient alternative method of bitumen recovery. Relevant results from Sheng et al. (2018) are summarized below.

Firstly, the condensation temperature for a bitumen/solvent/water mixture at a given operating pressure was shown to increase for a water-soluble solvent. It was confirmed in their thermodynamic modeling and reservoir simulations that DME-SAGD results in higher chamber-edge temperatures than C_4-SAGD, although DME is more volatile than butane (C_4). The difference in chamber-edge temperature was approximately 30°C at the operating pressure of 35 bars in their study.

Secondly, the in-situ distribution of DME in DME-SAGD was observed to be substantially different from that of butane (C_4) in C_4-SAGD. The solubility of DME in bitumen was nearly a half of that of butane (C_4) at their corresponding chamber-edge conditions at the operating pressure of 35 bars. In DME-SAGD simulations, however, approximately 50 mol% of the in-situ DME was used for dilution of bitumen, which was equivalent to the fraction of the in-situ butane (C_4) used for bitumen dilution in C_4-SAGD. This occurred likely because the partitioning of DME into bitumen and water reduced the gravity segregation of the two-liquid-phase flow along the edge of a steam chamber in DME-SAGD. The reduced gravity segregation in DME-SAGD was simulated to facilitate the mixing of condensed DME with bitumen beyond the edge of a steam chamber. This was in contrast to C_4-SAGD, in which the oleic phase diluted by a substantial amount of butane (C_4) was much less dense than the aqueous phase, impeding the contact between the butane (C_4) bank and bitumen along the edge of a steam chamber.

Thirdly, simulation results showed that the vapor fraction of the in-situ solvent was much smaller in DME-SAGD than in C_4-SAGD. Also, the injected DME was recovered not only by the oleic phase, but also by the aqueous phase in DME-SAGD because DME's solubility in the aqueous phase was properly modeled. Therefore, the recovery factor of solvent was simulated to be approximately 15% higher in DME-SAGD than in C4-SAGD.

However, the viscosity model used for the oleic phase containing DME was uncertain in the mechanistic simulation study by Sheng et al. (2018). Therefore, the main objective of this research is to quantify the dilution capability of DME in comparison with that of n-hexane (C_6) on the basis of experimental data for the same Athabasca bitumen sample. n-hexane (C_6) is used for the comparison because it has been reported to be one of the most effective solvents for solvent-SAGD for Athabasca bitumen reservoirs.

For the application of DME to heavy oil recovery, Haddadnia et al. studied vapor-liquid equilibrium data for DME/Athabasca bitumen (Haddadnia et al. 2018). They measured solubilities, densities, and viscosities of DME/bitumen mixtures and compared DME with propane (C_3) and n-butane (C_4). They found that values of solubility, density and viscosity of DME/bitumen mixtures at a given condition lie between those of propane/bitumen and n-butane/bitumen mixtures. The data presented for DME/bitumen mixtures by Haddadnia et al. (2018) are useful, but not sufficient for the purpose of DME-SAGD.

2.3. Use of Organic Alkalis in SAGD

The central hypothesis of this research is that organic alkalis can enhance in-situ bitumen transport in SAGD by inducing oil-in-water (o/w) emulsions. Organic alkalis are expected to have several mechanisms to improve the conventional SAGD when injected with steam.

First, organic alkalis create a high-pH solution (pH higher than 11) when mixed with liquid water, which is abundant near the edge of a steam chamber. Then, the aqueous phase with high pH is expected to generate natural surfactants in situ by reacting with acidic components, which are commonly present in heavy oil and bitumen.

Depending on the phase behavior, how in-situ surfactants act varies. However, steam-based recovery methods usually yield low-salinity conditions near thermal fronts, where steam condensate makes high water saturations. At low-salinity conditions (e.g., below 1,000 ppm), in-situ surfactants tend to form o/w emulsions, which transports bitumen as part of a water-continuous phase, in addition to a viscous oleic phase. In many studies, it was found that lower salinity is favorable for creating o/w emulsions than water-in-oil (w/o) emulsions with the other conditions being fixed (Al-Yaari et al. 2015;

Bahmanabadi et al. 2016; Bera et al. 2012; Cooke et al. 1974; Fortenberry et al. 2015; Healy et al. 1976; Sharma et al. 2018).

Second, once organic alkali is condensed near the edge of a steam chamber, it can also act as a diluent for the bitumen. That is, the excess amount of organic alkali residing in the oleic phase would reduce the bitumen's viscosity, in addition to the potential mechanisms associated with in-situ surfactants.

Third, organic alkalis would largely be consumed in the reactions for natural surfactants; that is, there would be little or no need to recycle the injectant, unlike the conventional solvent-SAGD using alkane-based solvents.

Many researchers have studied emulsification of heavy oil by different methods for different purposes as given below. Alkali injection for heavy oil recovery has been studied in water flooding processes, such as alkali-surfactant (AS), alkali-surfactant-polymer (ASP), and alkali-co-solvent-polymer (ACP) flooding (Bryan and Kantzas 2007ab; Bryan et al. 2008; Dong et al. 2009; Fortenberry et al. 2015; Kumar et al. 2012; Liu et al. 2006 and 2007; Pei et al. 2013; Sharma et al. 2018; Xiao et al. 2017; Zhang et al. 2016). In these prior studies, different combinations of alkalis, salts, surfactants, co-solvents and polymers were tested to achieve in-situ conditions for ultra-low interfacial tension (IFT). For pipeline transportation of heavy oil, o/w emulsion viscosity was studied with different surfactants, alkalis and solvents at different water-oil-ratio (WORs) and shear rates (Abdurahman et al. 2012; Ashrafizadeh and Kamran 2010; Ashrafizadeh et al. 2012; Hasan et al. 2010; Ghannam et al. 2012; Ghannam and Esmail 2007).

Surfactants have been also studied as steam additives for SAGD and cyclic steam stimulation (Lu et al. 2017; Srivastava and Castro 2011; Zeidani and Gupta 2013). They used commercially available hydrophilic viscosity reducers (Lu et al. 2017), hydrophilic surfactants (Zeidani and Gupta 2013), and thin film spreading agents (Srivastava and

Castro 2011) to form o/w emulsions or to demulsify w/o emulsion to enhance bitumen transport. The potential mechanisms for lowering SOR by injecting these surfactants with steam include the wettability alteration from oil-wetting to more water-wetting, and reduction of interfacial tension.

Inorganic alkali has been studied for o/w emulsification by natural surfactants (Acevedo et al. 2001; Ashrafizadeh et al. 2012). With no additional surfactants or solvents, they used sodium carbonate (Na_2CO_3) to activate natural surfactants and create o/w emulsions from Iranian heavy crude oil (Ashrafizadeh et al., 2012) and Cerro Negro bitumen (Acevedo et al., 2001). In both studies, o/w emulsions were observed at the sodium carbonate concentration range from 2,000 to 10,000 ppm.

To our knowledge, Kim et al. (2017) is the only research published on alkali-steam co-injection for SAGD. They injected steam with an alkali (not specified) into a micromodel chip, and observed significantly increased oil recovery by creating o/w emulsions. Although the size of emulsion droplets was studied, Kim et al. (2017) did not study phase behavior and rheology of emulsions created in their experiment.

Unlike other studies of heavy oil emulsification, this research is focused on bitumen-in-water emulsification by using an organic alkali without any additional surfactants or co-solvents. An organic alkali can act both as an alkali and a co-solvent, and the use of a single component with multiple functions can yield a simpler solution to enhancement of bitumen transport. To this end, it is important to find an optimal type of organic alkalis that can form o/w emulsions that are much less viscous than the original bitumen, yet has a high concentration of bitumen.

It is well known that w/o emulsions are produced with bitumen in SAGD operation (Vittoratos and Kovscek 2017). According to several simulation studies, bitumen production data in SAGD can be matched more accurately by considering w/o emulsions

(Azom and Srinivasan 2009; Ezeuko et al. 2013). Especially, w/o emulsification increases the relative permeability. As a result, in-situ emulsification enhanced the in-situ bitumen mobility and reduce CSOR (Ezeuko et al. 2013). These simulation studies indicate that o/w emulsions in SAGD could also enhance in-situ bitumen flow with the high relative permeability. The primary question, however, is whether it is possible to create o/w emulsions with organic alkalis in SAGD. In-situ properties of o/w emulsions are the next research question.

Bitumen is a complex mixture of hydrocarbons, containing asphaltenes and resins at high concentrations. These components are known to interact with water and to affect emulsion behavior (Al-Sahhaf et al. 2008; Gao et al. 2017; Jia and Okuno 2018; Kar et al. 2014; Kokal 2005; Schorling et al. 1999; Xia et al. 2004; Yan et al. 1999; Yang et al. 2007; Yarranton et al. 2000). It is crucial to conduct fundamental experimental research of emulsion phase behavior and viscosity for mixtures of Athabasca bitumen, brine, and organic alkali because such experimental research has not been presented in the literature.

2.4. Field Cases: Polymer Flooding and ASP Flooding for Heavy Oil Recovery

Field pilots of polymer flooding include East Bodo, Suffield Caen, and Seal in Canada (Liu et al. 2012; Murphy Oil Corporation 2016; Wassmuth et al. 2009). A large-scale polymer flooding was successfully conducted in Pelican Lake in Canada (Delamaide et al 2014a). In the Pelican Lake case, the incremental oil recovery after polymer flooding was 10 - 25% of the original oil in place (OOIP), in which heavy oil of 800 - 10,000 cp was displaced by polymer of 20 - 25 cp (Delamaide et al 2014b). In China, polymer flooding was performed in an offshore heavy oil field in Bohai Bay (Kang et al. 2011). After 3 years of polymer flooding, however, the incremental oil recovery was reported to

be approximately 4%. Thereafter, surfactant-polymer (SP) flooding was implemented (Lu et al. 2015).

Conventional screening criteria indicate that ASP flooding can be used effectively when the oil viscosity is below 200 cp (Chang 2013). Sheng reported 32 field projects of ASP flooding, most of which were in China (19 projects) with oil viscosities lower than 50 cp (Sheng 2014). ASP flooding, however, has been also studied for more viscous oil. Laboratory experimental results show a substantial incremental oil recovery by ASP flooding for oils with viscosities from 320 cp to 500 cp (Aitkulov et al. 2017; Kumar et al. 2010; Shamekhi et al. 2013), 2,000 cp oil (Zhang et al. 2012), and 16,000-cp oil (Shamekhi et al. 2013).

ASP floods for heavy oil in Canada include Taber South (Husky), Crowsnest (Husky), Shuffield (Cenovus), and Mooney (Black Pearl). The ASP flooding resulted in an incremental recovery of 11.1% of the OOIP for 120 cp oil in Taber South (McInnis et al. 2013), 10% for 480 cp oil in Shuffield (Cenovus Energy 2012), and 9% for 440 cp oil in Mooney (Delamaide 2017; Watson et al. 2014).

Reported issues of ASP flooding were insufficient injectivities caused by calcite and silica scales, which were attributed partly to the injected alkalis (Delamaide 2014; Hocine et al. 2014). For example, Alberta Energy Regulator reported the scale plugging and injectivity problems in the ASP flooding projects in Taber South (Husky) and Suffield (Cenovus) (Alberta Energy Regulator 2012).

To avoid the problems of alkali injection, there are a limited number of laboratory-scale experimental studies of SP flooding for heavy oil recovery (Feng et al. 2012; Hocine et al. 2014). They used self-assembled betaine surfactants, and a mixture of olefin sulfonates, alkyl aryl sulfonates, alkyl ether sulfates, and alkyl glyceryl ether sulfonates

that created ultra-low IFT micro-emulsions with their heavy oil without using alkali (Feng et al. 2012; Hocine et al. 2014).

2.5. Use of Co-Solvent for ACP Flooding

ASP flooding may involve a large number of chemicals to be injected, which tends to make the implementation of ASP flooding more complicated and costly. Alkali-cosolvent-polymer (ACP) flooding has been recently studied as a simpler alternative for heavy oils, in which only alkali and co-solvent were injected without any synthetic surfactant (Aitkulov et al. 2017; Fortenberry et al. 2015; Sharma et al. 2018). These studies used isobutanol (IBA), alkoxylated IBA (e.g. IBA-2EO, IBA-5EO, IBA-10EO, IBA-2PO), alkoxylated phenol (phenol-1PO-2EO) as co-solvents. Their results showed ultra-low IFT micro-emulsions at experimental conditions and highly efficient core floods.

Upamali et al. (2018) recently investigated the potential advantage of using short-hydrophobe co-solvents and surfactants. They used alkoxylated IBA (IBA-3EO, IBA-10EO, IBA-30EO, and IBA-1PO-2EO) and alkoxylated phenol (phenol-1PO-2EO, phenol-1PO-5EO, phenol-2EO, and phenol-4EO) as co-solvent for conventional surfactants, and achieved ultra-low IFT type III micro-emulsion phase behavior. They also used 2-ethylhexanol-xPO sulfate (2-EHS) as a surfactant along with a conventional surfactant to show ultra-low IFT type III micro-emulsion phase behavior. According to their study, the advantages of short-hydrophobe co-solvents include the short equilibrium time for micro-emulsion formation, the low micro-emulsion viscosity, and the low retention in cores.

2.6. Surface Active Solvent (SAS)

The idea is to develop a new category of surfactant with a short-hydrocarbon solvent that is applied as a co-solvent in ASP flooding (or ACP flooding). This solvent-

based surfactant is referred to as surface active solvent (SAS). A SAS was synthesized by the alkoxylation of a solvent; e.g. 2-ethylhexanol (2-EH)-xPO-yEO or phenol-xPO-yEO, where x is the number of propylene oxide (PO) and y is the number of ethylene oxide (EO).

The PO and EO groups are related to hydrophobicity and aqueous stability of a surfactant, respectively. A larger number of PO increases the affinity for oil, resulting in a higher level of hydrophobicity. Depending on brine salinity, brine hardness, and temperature, EO number can be adjusted for aqueous stability. In this research, 2-EH-xPO-yEO and phenol-xPO-yEO were tested as SAS to improve the oil recovery in polymer flooding for heavy oil. All chemicals were provided by Harcros Chemicals. The chemical structures of these SAS are illustrated in **Figure 2.1** and **Figure 2.2**.

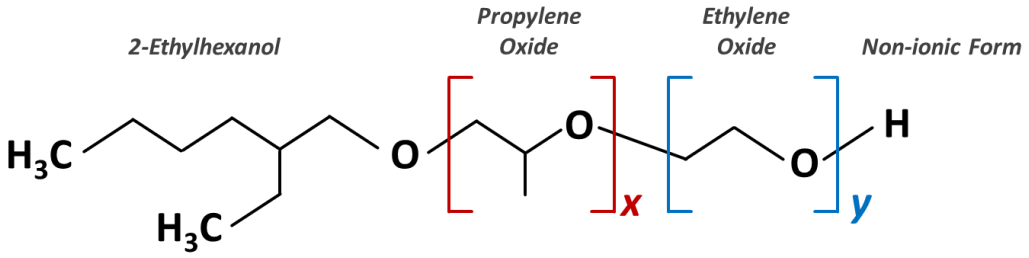

Figure 2.1 Structure of 2-ethylhexanol-xPO-yEO

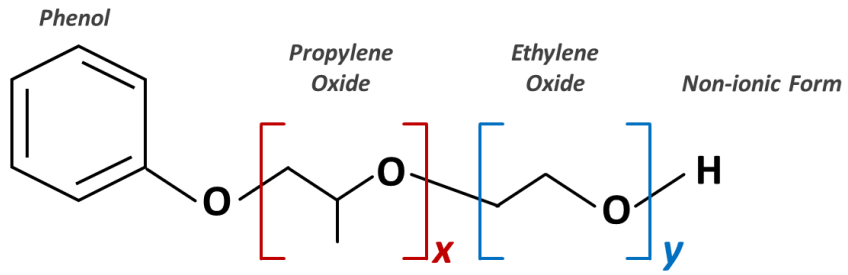

Figure 2.2 Structure of phenol-xPO-yEO

2.7. Improved Polymer Flooding for Heavy Oil Recovery

Previous studies of co-solvents and surfactants were focused on ASP or ACP floods that achieved an ultra-low IFT between the displaced and displacing phases (Aitkulov et al. 2017; Fortenberry et al. 2015; Sharma et al. 2018; Upamali et al. 2018). Their aqueous formulations consisted of an alkali, one or more surfactants, and co-solvents for ASP flooding, and an alkali with one or more co-solvents for ACP flooding.

However, this research focuses on the application of SAS as a sole chemical additive that improves the displacement efficiency of polymer flooding for heavy oil recovery. The use of SAS without any additional chemicals unlikely results in an ultra-low IFT and micro-emulsions with heavy oil. There can be the reduction of residual oil saturation by lowered IFT. The key is the incremental oil recovery by IFT reduction using SAS without creating Winsor type III micro-emulsions. Therefore, the proposed method may be more properly denoted as "improved polymer flooding" or "low-tension polymer flooding" than surfactant-polymer (SP) flooding which achieves ultra-low IFT between the displacing and displaced phases.

There are several advantages if the idea of improved polymer flooding works. First, the field application can be simpler than the conventional SP flooding. For example, there is no salinity gradient that is necessary to ASP flooding or ACP flooding. Once a suitable SAS is selected, it can be simply mixed with polymer and injected into a reservoir. Second, since only one chemical is added to polymer solution, we can reduce the operation cost compared to a multiple-chemical injection process. Third, no use of alkali can avoid the injectivity issue caused by calcite and silica scales.

The similar approach to improving polymer flooding was studied in the 1990s. Major oil companies [BP and Equinor (formerly Statoil)] studied how to improve polymer

flooding using surfactants, calling “low-tension polymer flooding” or “polymer-assisted surfactant flooding”.

BP studied the low-tension polymer flooding as a method to reduce the operation cost and improve the mobility control (Kalpakci et al. 1990). The target was a light oil recovery in a sandstone reservoir. Oil viscosity was 4 cp for a stock tank oil and 1.2 cp for a live oil. They used two different types of biopolymers (xanthan and scleroglucan) and the mixture of two surfactants synthesized by BP Research Center. A core flooding was conducted in Berea sandstone. By injecting a surfactant-polymer slug followed by polymer solution, they achieved 50 - 100 % (OOIP) oil recovery for the stock tank oil and 52 - 80 % (OOIP) oil recovery for the live oil. However, this study was similar to a conventional surfactant-polymer (SP) flooding that created Winsor type III micro-emulsion at IFT as low as 1.2×10^{-3} dynes/cm.

Equinor (formerly Statoil) studied the polymer-assisted surfactant flooding for Gullfaks Field, Norway (Maldal et al. 1998). The oil was already produced by seawater flooding, starting in 1986. They evaluated the economic feasibility of switching the injection fluid from seawater to surfactant and polymer. The reservoir conditions were favorable to the polymer flooding with a high permeable (1 - 10 Darcy) unconsolidated sand reservoir, a moderate reservoir temperature (70°C), and a low salinity formation brine (about 42,000 ppm). They tested a light oil (1.5 cp) recovery in a Bentheimer sandstone using a xanthan biopolymer and a mixture of surfactants. Injection fluids were a slug of surfactant-polymer first, then a polymer solution, and finally seawater. With the optimization of surfactant concentrations and slug sizes, oil recovery was 80 - 90 % (OOIP). Based on experimental data, they also conducted a simulation study on a two-well pilot test. They concluded that the polymer-assisted surfactant flooding was not economically feasible, mainly due to a low residual oil in the reservoir. Also, oil price and

chemical cost were not favorable. (Oil: 16 USD/bbl, Surfactant: 1.6 USD/lb, and Polymer: 3.3 USD/lb).

The improved polymer flooding using SAS in this research is different from the previous studies discussed above in that the expected application is for a highly-permeable reservoir of highly-acidic heavy oil in North Sea. This is an undeveloped heavy oil reservoir of unconsolidated sands with high porosity (30 - 35%) and high permeability (above 10 Darcy). The in-situ oil viscosity is approximately 500 cp. The salinity of the reservoir brine is about 56,000 ppm.

As a preliminary study, two scenarios are considered for oil recovery. The first one is the secondary polymer flooding (i.e. polymer injection without the water flooding stage). The second scenario is the polymer flooding after a short period of the water flooding. The polymer flooding in this North Sea reservoir can be economically more feasible than the Gullfaks Field case (Maldal et al. 1998). Since this is an undeveloped reservoir, the oil saturation prior to the project is much higher than the residual oil saturation to water flooding. Oil prices and chemical costs are highly uncertain, but they were quite unfavorable for the Gullfaks Field case. In addition, the use of a single SAS will lower the chemical cost. The price of a SAS is expected to be about 1.25 USD/lb (100% active basis) because the base solvent (e.g., 2-ehtylhexanol or phenol) is inexpensive, and also because they are non-ionic surfactants.

Recently, SAS was applied for the wettability alteration (Wang et al. 2019) and the improved polymer flooding (Panthi et al. 2019). Wang et al. (2019) tested a SAS as a wettability modifier for oil-wet limestone cores. They found that 2-etheylhexanol-4PO-15EO (or 2-EH-4PO-15EO) altered the wettability of calcite surfaces from oil-wet (contact angle = 134.1°) to water-wet (contact angle = 47.1°) after 1 day. Then, they conducted a force imbibition test for light oil recovery. Compared to water flooding, they achieved

47.3% (OOIP) incremental oil recovery with 1.6 pore volume (PV) of SAS-brine slug followed by 7.0 PV brine injection.

Panthi et al. (2019) applied a SAS for heavy oil recovery in a sandpack and sandstones. They used phenol-7PO-15EO as a single chemical additive to the polymer. Both oil and polymer viscosity were approximately 330 cp at 70°C. Before polymer flooding, water flooding was conducted until no more oil production. Then, they inject 0.4 PV of SAS-polymer slug followed by 1.5 PV polymer solution. The final oil recovery was 99.7% (OOIP) for a sandpack, 59.6% (OOIP) for a Bentheimer sandstone, and 31.5% (OOIP) for a Berea sandstone. This oil recovery result shows the clear advantage of using a SAS in a high permeability reservoir.

The experimental result by Panthi et al. (2019) looks promising, but more data are required for the application of the improved polymer flooding in an actual field. First, in this research, experimental conditions were specifically matched to the field operation plan. An analogous oil, a sandpack, and a brine were matched to reservoir conditions. Second, IFT is the key difference between the polymer flooding and the improved polymer flooding. It is important to understand the effect of SAS concentrations and brine salinity on IFT. Third, in-situ polymer rheology in a sandpack should be measured for the accurate analyze of heavy oil displacement. Last, the incremental oil recovery by the improved polymer flooding should be evaluated with the effect of the lowered IFT on the residual oil (or remaining oil) in a sandpack.

2.8. Capillary Desaturation by SAS

Incremental oil recovery by capillary desaturation is one expected mechanism of the improved polymer flooding by SAS. The residual oil saturation (or remaining oil saturation) in the reservoir decreases as capillary number (Nc) increases, which results in

enhanced oil recovery. This relationship between N_C and residual oil saturation is plotted as capillary desaturation curve (CDC). The CDCs of different reservoir types (related to pore-size distribution) are schematically shown in **Figure 2.3** (Lake et al. 2014, Chapter 3).

The critical capillary number is where the residual oil saturation starts decreasing. After the critical capillary number, a rapid decline of residual oil saturation is observed for reservoirs with more well-sorted pore-size distribution like sandstone or unconsolidated sand reservoirs. For water-wet sandstone (Berea sandstone), it was found that residual oil saturation starts reducing at the capillary number of 10^{-5} and oil recovery can be 90% (OOIP) at the capillary number of 10^{-2} (Chatzis and Morrow 1984). The key to achieving more oil recovery is to increase the capillary number above its critical capillary number. Capillary number is defined as follows (Chatzis and Morrow 1984):

$$\mathrm{Nc} = \frac{\mathrm{k}\Delta\mathrm{P}}{\sigma\mathrm{L}}$$

where k is permeability, ΔP is pressure drop, σ is interfacial tension (IFT), and L is the length of core. For a given oil displacement, permeability (k) and length (L) are fixed. Therefore, capillary number can be increased by increasing pressure drop (ΔP) or reducing IFT. However, it is unlikely that ΔP is increased in polymer flooding in comparison to water flooding in a heavy oil reservoir.

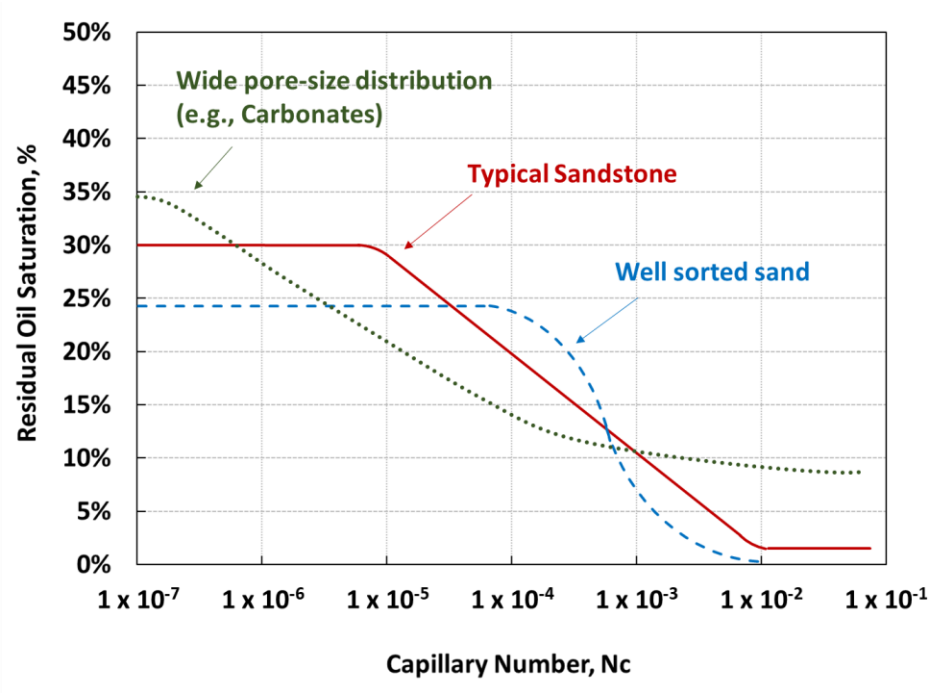

Figure 2.3 Schematic of the effect of pore-size distribution on capillary desaturation curve (CDC)

The target reservoir of the improved polymer flooding in this research is an unconsolidated sand that gives permeability higher than 10 Darcy. This can be viewed as a multiplication factor for an IFT reduction that is achieved by a simple surfactant, SAS. In addition, a rapid decline of residual oil saturation is expected with this unconsolidated high-permeability sand reservoir. If SAS could reduce IFT enough to reach a capillary number above its critical capillary number, a significant incremental oil recovery is expected.

3. Comparative Study of Bitumen Dilution Capability of Dimethyl Ether (DME) and Hexane as Steam Additives for SAGD [1]

The main drawback of SAGD is the significant usage of energy and water to generate steam. The co-injection of steam and solvent for SAGD (solvent-SAGD) has been studied and tested as a potential method to improve the drawbacks of SAGD (Gupta et al. 2005; Gupta and Gittins 2006; Leaute and Carey 2002). Prior investigations into solvent-SAGD were mainly focused on hydrocarbon solvents, such as propane (C_3), butane (C_4), and diluents, which usually consist of pentane (C_5) and heavier hydrocarbons at different concentrations (Gates 2007; Ivory et al. 2008; Keshavarz et al. 2014 and 2015; Li et al. 2011ab; Nasr et al. 2003). However, heavy hydrocarbon solvents are relatively expensive in general. The geological uncertainties associated with reservoir heterogeneity increase the uncertainty of the project's economics, if the solvent is expensive.

Water is by far the most dominant component in steam-based oil recovery for bitumen recovery (Zhu and Okuno 2016). In this research, as a potential way of utilizing water, the use of Dimethyl ether (DME) was investigated as a potential additive to steam to improve SAGD. DME is partially soluble in water and miscible with bitumen. While the vapor pressure of DME is between n-pentane (C_3) and n-butane (C_4), it could result in a different steam chamber behavior and bitumen recovery (Sheng et al. 2018). Yet, there is a lack of experimental data to study the detailed mechanisms of DME-steam co-injection.

The main objective of this research is to compare DME with n-hexane in terms of the dilution capability, i.e. viscosity reduction for Athabasca bitumen. In addition, new

[1] This chapter was published in the following paper. Baek conducted most of experiment and analyzed data as the first author of this paper.

- Baek, K., Sheng, K., Argüelles-Vivas, F.J. and Okuno, R. 2019. Comparative Study of Oil-Dilution Capability of Dimethyl Ether and Hexane as Steam Additives for Steam-Assisted Gravity Drainage. *SPE Reservoir Evaluation & Engineering* 22(03): 1030-1048. https://doi.org/10.2118/187182-PA

experimental data are presented for bubble point pressures, densities, and viscosities of Athabasca bitumen and its mixtures with DME and n-hexane.

3.1. Materials

Athabasca bitumen sample was provided by a SAGD operator. To reduce the amount of water in the bitumen sample provided, the bitumen sample was dehydrated at 120°C under atmospheric pressure. Then, basic properties of Athabasca bitumen were measured by Exova laboratory (Edmonton, Alberta, Canada).

The molecular weight (MW) of the bitumen sample was measured to be 532 g/mol by freezing point depression. Simulated distillation analysis was performed up to 720°C. The density of bitumen at 62°C and atmospheric pressure was measured to be 0.985 g/ml. SARA analysis gave the following composition: 24.5 wt% saturates, 36.6 wt% aromatics, 21.1 wt% resins and 17.8 wt% asphaltenes. The water content of the bitumen was confirmed to be less than 0.1 wt%. The properties of bitumen are summarized in **Table 3.1**, **Table 3.2**, **Table 3.3**, and **Figure 3.1**.

The purity of DME supplied by Praxair was 99.5%. n-hexane was supplied by Sigma-Aldrich at a purity higher than 99%.

Table 3.1 Dehydrated bitumen properties

Property		Value	Method
Molecular Weight		532 g/mol	Freezing Point Depression
Density		0.985 g/ml at 62°C	ASTM D 7042-12a
SARA	Saturates Aromatics Resins Asphaltenes	24.5 wt% 36.6 wt% 21.1 wt% 17.8 wt% (Pentane insoluble)	Liquid-Solid Chromatography
Water Content		less than 0.1 wt%	ASTM D 4006
Total Acid Number (TAN)		3.56 mg-KOH / g-oil	Fan and Buckley (2007)

Table 3.2 Dehydrated bitumen composition (Method: ASTM D 2887-84)

Carbon Number	Mass Fraction	Carbon Number	Mass Fraction	Carbon Number	Mass Fraction	Carbon Number	Mass Fraction
C7	0.0001	C33	0.0132	C59	0.0048	C85	0.0047
C8	0.0004	C34	0.0128	C60	0.0048	C86	0.0048
C9	0.0009	C35	0.0121	C61	0.0048	C87	0.0049
C10	0.0017	C36	0.0124	C62	0.0047	C88	0.0045
C11	0.0026	C37	0.0105	C63	0.0047	C89	0.0052
C12	0.0047	C38	0.0102	C64	0.0043	C90	0.0053
C13	0.0081	C39	0.0106	C65	0.0047	C91	0.0049
C14	0.0102	C40	0.0104	C66	0.0043	C92	0.0056
C15	0.0131	C41	0.0086	C67	0.0043	C93	0.0052
C16	0.0147	C42	0.0085	C68	0.0043	C94	0.0059
C17	0.0161	C43	0.0088	C69	0.0039	C95	0.0054
C18	0.0190	C44	0.0086	C70	0.0043	C96	0.0055
C19	0.0186	C45	0.0071	C71	0.0039	C97	0.0057
C20	0.0199	C46	0.0074	C72	0.0040	C98	0.0058
C21	0.0193	C47	0.0073	C73	0.0040	C99	0.0059
C22	0.0193	C48	0.0067	C74	0.0041	C100+	0.2555
C23	0.0190	C49	0.0066	C75	0.0041		
C24	0.0187	C50	0.0066	C76	0.0042		
C25	0.0176	C51	0.0065	C77	0.0042		
C26	0.0175	C52	0.0059	C78	0.0042		
C27	0.0163	C53	0.0059	C79	0.0038		
C28	0.0177	C54	0.0059	C80	0.0043		
C29	0.0170	C55	0.0054	C81	0.0044		
C30	0.0177	C56	0.0054	C82	0.0044		
C31	0.0143	C57	0.0053	C83	0.0041		
C32	0.0145	C58	0.0053	C84	0.0046		

Table 3.3 Dehydrated bitumen simulated distillation (Method: ASTM D 7169-05 Modified)

Mass Recovered [%]	Temperature [°C]	Mass Recovered [%]	Temperature [°C]	Mass Recovered [%]	Temperature [°C]
0.5	192.1	26	423.2	52	584.2
1	215.1	27	428.4	53	591.1
2	238.7	28	433.5	54	598.4
3	256.3	29	438.7	55	605.9
4	269.3	30	443.7	56	613.4
5	280.4	31	449.0	57	620.7
6	290.7	32	455.1	58	628.0
7	299.9	33	461.0	59	635.1
8	307.9	34	466.9	60	642.1
9	315.1	35	472.9	61	649.4
10	322.7	36	478.5	62	655.7
11	330.0	37	484.5	63	663.1
12	337.2	38	490.6	64	670.4
13	344.0	39	496.4	65	676.5
14	350.5	40	503.1	66	682.6
15	356.7	41	509.0	67	688.0
16	363.4	42	515.7	68	693.2
17	370.0	43	521.6	69	697.3
18	375.7	44	528.4	70	702.1
19	381.5	45	535.4	71	705.8
20	387.3	46	541.9	72	709.4
21	393.1	47	548.1	73	712.9
22	399.0	48	556.0	74	716.4
23	405.2	49	563.1	75	720.0
24	411.3	50	569.5		
25	417.5	51	576.7		

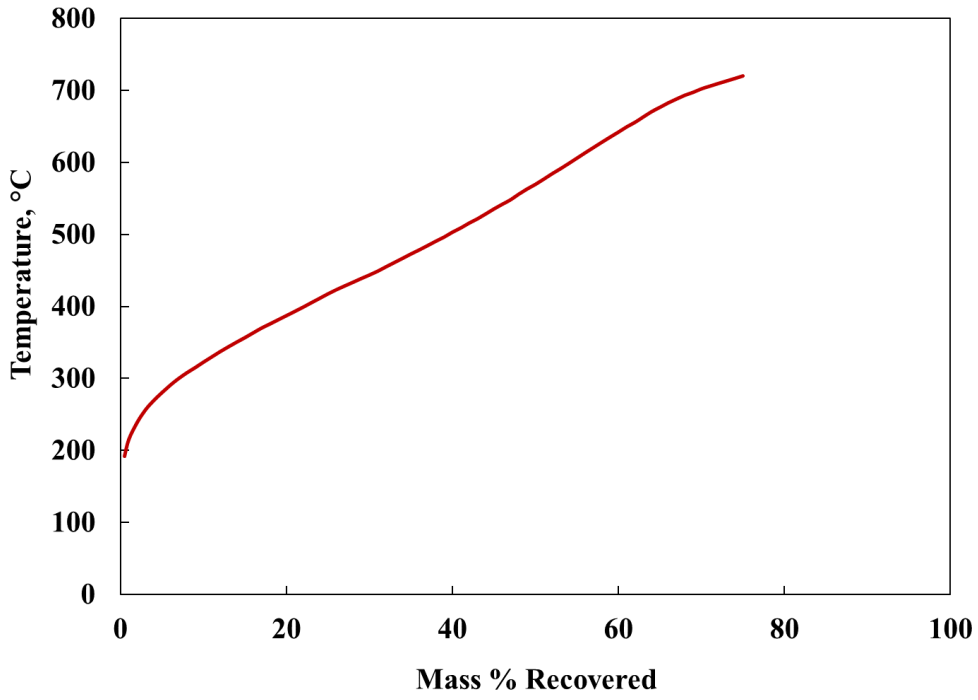

Figure 3.1 Dehydrated bitumen simulated distillation

3.2. Experimental Procedure

3.2.1. Bubble Point Measurements

A PVT apparatus was set up to measure bubble points of solvent/bitumen mixtures at temperatures between 81 and 121°C. **Figure 3.2** presents a schematic diagram for the PVT apparatus. A DBR PVT cell (model: DBR-0150-100-200-200-286-155) was installed in an oven (Blue M, model: DC-1406F). The confining pressure for the PVT cell was controlled by Teledyne ISCO pump (model: 100DX). The PVT cell temperature was measured in °C by a calibrated T-type thermocouple. The accuracy of this thermocouple

is ± 1°C. The confining pressure was measured in psi by an Ashcroft digital pressure gauge. The accuracy of this pressure gauge is ± 0.17 bar.

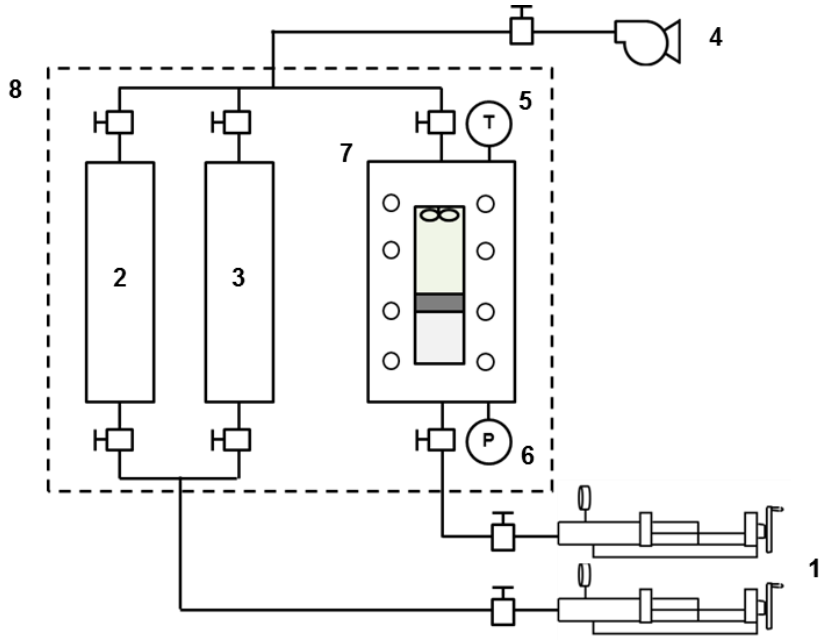

1. Pressurization pump 2. Bitumen accumulator 3. Solvent accumulator
4. Vacuum pump 5. Temperature gauge 6. Pressure gauge
7. PVTcell 8. Oven

Figure 3.2 Experimental set up for bubble point measurement

Before each measurement, the system was cleaned with hexane and toluene. After cleaning, all lines, valves, and feed accumulators were flushed with dry air. The PVT cell was then evacuated for six hours at 80°C. Feed accumulators were prepared to store the solvent and bitumen to be injected into the PVT cell. The amount of feed injection was controlled by the ISCO pump. The injection flow rate was set below 8 ml/hr to measure an accurate injection volume. The mass and mole fractions of components were calculated by use of MW and density data from National Institute of Standards and Technology

(NIST) for n-hexane, and the literature for DME (Wu et al. 2003 and 2004; Ihmels and Lemmon 2007; Wu and Yin 2008).

For each mixture, the solvent was injected first into the PVT cell. To measure a precise volume, solvent was injected in the liquid-phase state at room temperature. Because of its high viscosity, bitumen was heated for one day and injected into the PVT cell at 60°C. After the injection of solvent and bitumen, the oven was set to a target temperature (81 - 121°C), and the magnetic mixer equipped inside the PVT cell was operated to enhance the mixing of components. The PVT-cell pressure was set sufficiently higher than the vapor pressure of the solvent at the temperature, in order to have the mixture as a single liquid phase. The system was left for at least one day while using the magnetic mixer. An equilibrium state of the mixture was confirmed by constant temperature and pressure in the PVT cell and also constant volume in the pump.

Bubble points were measured by the constant mass expansion method, in which the total fluid volumes were recorded at different pressures. The pressure of the mixture was initialized at a high pressure so that it was a single-phase liquid, and then it was decreased by 1.4 bars per hour. While decreasing the pressure, the mixture was stirred by the magnetic mixer to accelerate the equilibration process at a new pressure. After the PVT-cell pressure reached the next target pressure, the magnetic mixer was turned off. The mixture was then kept in static for at least two hours. This period of time was sufficient for a mixture to reach a single-phase equilibrium state. While the system reached an equilibrium state, the pressure was kept constant. Equilibrium was confirmed when the PVT-cell pressure was stable with no volume change. When a mixture formed two equilibrium phases, it took a longer period of time for equilibration. After a vapor phase appeared, pressure was decreased by 0.34 - 0.69 bars for every 5 hours while the magnetic mixer was on. After the PVT-cell pressure reached a target pressure, the magnetic mixer

was turned off, and the mixture was kept in static for at least 10 hours. Equilibrium was confirmed by a stable pressure in the PVT cell and a constant fluid volume.

After one constant mass expansion was completed at a given temperature, the PVT cell was pressurized above the vapor pressure of the solvent. Then, a new temperature was set and left for at least one day to reach a new equilibrium state. The magnetic mixer was kept on during this time. After reaching a new equilibrium state, the same procedure of constant mass expansion was repeated to measure a new bubble point.

The volume changes and the pressure of the PVT cell were recorded at each expansion step. The volume change was also detected through the visual window with the cathetometer. Three bubble point measurements for DME/bitumen mixtures and two bubble point measurements for n-hexane/bitumen mixtures were carried out in this research.

3.2.2. Density and Viscosity Measurements

A schematic of the system for density and viscosity measurements is shown in **Figure 3.3**. It consists of automated pumps, a mixing accumulator, an in-line density meter, an in-line viscometer, an oven, a back pressure regulator (BPR), and an accumulator for the effluent. The pump (Teledyne ISCO 100DX) pressurizes and maintains the pressure of the system automatically by de-ionized water. A mixing accumulator was used as an equilibrium cell, where the fluid sample is prepared homogeneously. The capacity of the mixing accumulator is 1,290 ml.

In the density measuring cell (Anton Paar), the density of fluid is measured in a U-shaped tube, in the range from 0 to 3 g/ml. The accuracy of the density meter is ±0.001 g/ml. The pressure and temperature ranges of the density meter are 0 to 1,400 bars and -7 to 200°C, respectively. For this research, it was calibrated with water and nitrogen for

temperatures in the range from 20 to 200°C and pressures from 1.01 to 100 bars. Density values for calibration were taken from NIST. The in-line viscometer (Hydramotion's XL7 series) measures the viscosity of fluid in the range from 0.1 to 10,000 cp. The pressure limit is 700 bars and the temperature limit is 450°C. This is a resonant (or vibrational) viscometer that creates waves within the liquid being measured. The viscosity accuracy is ±1% of the reading, and the repeatability is ±0.3% of the reading.

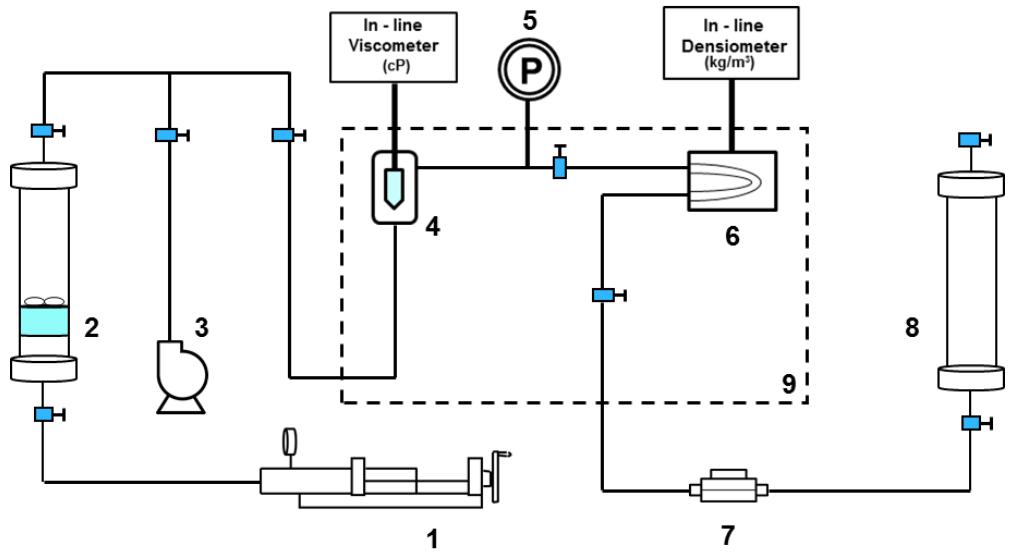

1. Pressurization pump
2. Mixing accumulator
3. Vacuum pump
4. In-line viscometer
5. Pressure gauge
6. In-line density meter
7. Back pressure regulator
8. Effluent collector
9. Oven

Figure 3.3 Experimental set up for density and viscosity measurement

Both the viscometer and the density meter were installed inside a Despatch oven (LAC2-18-8). LED screens that display measured data from density meter and viscometer were connected outside the oven. The absolute pressure of the system was measured in bar

with a pressure gauge (Omega, PX459-2.5KGI-EH) located between the density meter and viscometer. The pressure of the system was maintained with the BPR installed outside of the oven. The temperature for the density meter was measured in °C with an accuracy ±0.1°C.

Before each measurement, the system was cleaned thoroughly with toluene, and dried with air. Cleaning was complete when the density meter and viscometer read the NIST density and viscosity values for toluene at the specific temperature and pressure conditions. Then, the system was evacuated for at least six hours, and then it was filled with helium at 68.6 bars. The pressure was monitored for one day to ensure that no leakages occurred for the setup. The total fluid volume of the system is 30 ml.

At 23°C and 20.7 bars, mixtures containing bitumen and solvent were prepared at two mixing ratios (in volume): 11.6 vol% of solvent and 88.4 vol% of bitumen, and 19.8 vol% of solvent and 80.2 vol% of bitumen. Mixtures were completely stirred for at least one day. To start an experiment, the mixture was first injected from the mixing accumulator at 5 ml/hr and 68.6 bars to remove the helium of the system. Helium was used to prevent the flash vaporization of the mixture inside the system. Once 30 ml of the sample was injected, the flow rate was change to 50 ml/hr for a total volume of 60 ml. This injection procedure is to remove trapped helium inside the system. Density and viscosity of 100% bitumen, DME /bitumen mixtures, and n-hexane/bitumen mixtures were measured from 50 to 170°C and 15 to 70 bars. Measurements were performed at a fixed temperature by increasing pressure within the closed system inside the oven.

3.3. Experiment Results and Correlations

Bubble points, densities, and viscosities were measured for the bitumen and its mixtures with solvents at a wide range of temperatures and pressures. As summarized in

Table 3.4, nine mixtures were studied for the experiments: five DME/bitumen mixtures (DB-1, -2, -3, -4, and -5) and four n-hexane/bitumen mixtures (HB-1, -2, -3, and -4). Bubble points were measured for DB-1, DB-2, DB-3, HB-1, and HB-2. Densities and viscosities were measured for DB-4, DB-5, HB-3, and HB-4.

Table 3.4 Compositions of the DME/bitumen and n-hexane/bitumen mixtures studied in this research

Mixture	DME [mol%]	Bitumen [mol%]	Mixture	n-hexane [mol%]	Bitumen [mol%]
DB-1	80.0	20.0	HB-1	80.0	20.0
DB-2	47.0	53.0	HB-2	92.0	8.0
DB-3	20.0	80.0	HB-3	50.0	50.0
DB-4	65.4	34.6	HB-4	34.6	65.4
DB-5	50.0	50.0			

3.3.1. Bubble Point Data

Table 3.5 presents the bubble points measured for the three DB mixtures and the two HB mixtures. One of the observation points was whether liquid-liquid separation occurs for these mixtures, especially for HB-2 because of the high solvent concentration.

In Gao et al. (2017), a mixture of 97.24 mol% n-butane (C_4) and 2.76 mol% Athabasca-bitumen exhibited liquid-liquid separation of hydrocarbons for a wide range of temperatures from 50 to 170°C at pressures relevant to solvent-SAGD for Athabasca bitumen reservoirs. Since such liquid-liquid separation is expected to affect bitumen transport beyond the edge of a steam chamber, Gao et al. (2018) later conducted a phase behavior study for n-hexane/Athabasca-bitumen and n-octane (C_8)/Athabasca-bitumen mixtures. They did not observe liquid-liquid separation for these mixtures even at high solvent concentrations, such as 97.53 mol% n-hexane and 93.71 mol% n-octane in their mixtures with Athabasca bitumen.

Table 3.5 Experimental results for bubble point pressures

Mixture	Temperature [°C]	Bubble Point Pressure [bar]	Mixture	Temperature [°C]	Bubble Point Pressure [bar]
DB-1	81	19.6	HB-1	111	3.5
	93	27.2		121	3.8
	121	42.0			
DB-2	81	11.0	HB-2	106	3.6
	92	13.8		121	4.1
	121	19.2			
DB-3	81	5.0			
	93	6.6			
	121	8.5			

Zou et al. (2007) detected liquid-liquid separation by using x-ray transmission tomography and in-line density measurement. Gao et al. (2017, 2018) applied back-light to observe color differences among different phases for bitumen/solvent mixtures and bitumen/solvent/water mixtures. This was effective for detecting the separation of solvent-rich liquid and bitumen-rich liquid in Gao et al. (2017). Gao et al. (2017, 2018) also used pressure-volume plots to detect phase changes.

Liquid-liquid separation was not observed in the current research. First, no color difference was observed in the liquid phase. Second, pressure-volume plots in this research indicated only the transition from single liquid (L) to two phases (V-L). Note that the bitumen sample in the current research is different from the one used in Gao et al. (2017, 2018). For example, the MW of the Athabasca-bitumen sample in Gao et al. (2017, 2018), 635 g/mol, is approximately 19% higher than the Athabasca-bitumen sample used in this research.

3.3.2. Density and Viscosity Data

Densities of the Athabasca bitumen were measured at temperatures from 43 to 178°C and pressures from 1.6 to 100 bars (**Table 3.6** and **Figure 3.4**). Figure 3.4 shows that bitumen density decreases with increasing temperature and with decreasing pressure. For example, the density of bitumen at 28 bars was approximately 0.997 g/ml at 43°C, but decreased to approximately 0.913 g/ml at 178°C.

Viscosities of the same bitumen were measured at temperatures from 55 to 170°C and pressures from 1.7 to 100 bars (**Table 3.7** and **Figure 3.5**). As expected, the bitumen viscosity is sensitive to temperature. The bitumen viscosity at 28 bars was measured to decrease from approximately 2,479 cp at 55°C to 3.5 cp at 170°C.

For bitumen mixtures with DME and n-hexane, density and viscosity measurements were conducted for DB-4, DB-5, HB-3, and HB-4. The solvent/bitumen mixing ratio was set to be 14 wt% solvent and 86 wt% bitumen for DB-4 and HB-3, and 8 wt% solvent and 92 wt% bitumen for DB-5 and HB-4. With these four mixtures, comparison of measured viscosities for DME and n-hexane can be made at the same mixing ratios in mole and weight; i.e., DB-5 and HB-3 at 50 mol% dilution, DB-4 and HB-3 at 14 wt% dilution, and DB-5 and HB-4 at 8 wt% dilution. The measured densities and viscosities are tabulated as follows: **Table 3.8** for DB-4, **Table 3.9** for DB-5, **Table 3.10** for HB-3, and **Table 3.11** for HB-4.

At the equimolar condition (50 mol% solvent and 50 mol% bitumen), the viscosity of n-hexane/bitumen was lower than that of DME/bitumen at the same pressure and temperature. However, the viscosity of the two mixtures became closer at higher temperatures. For example, comparison of DB-5 and HB-3 at 60 bar indicates that the viscosity of DME/bitumen was 30 cp higher at 55°C, but only 1.2 cp higher at 109°C (**Figure 3.6**).

Table 3.6 Experimental results for the bitumen density

Temperature: 43°C		Temperature: 56°C		Temperature: 80°C	
Pressure [bar]	Density [g/ml]	Pressure [bar]	Density [g/ml]	Pressure [bar]	Density [g/ml]
1.6	0.995	1.9	0.987	1.8	0.972
3.5	0.996	2.0	0.987	13.8	0.972
6.9	0.996	3.6	0.987	27.7	0.973
10.3	0.996	6.9	0.988	41.3	0.974
13.8	0.996	10.3	0.988	55.2	0.975
17.3	0.996	13.7	0.988	69.0	0.976
20.7	0.996	17.2	0.988	82.9	0.977
24.1	0.997	20.7	0.988	100.1	0.978
27.6	0.997	24.2	0.988		
27.6	0.997	27.6	0.989		
31.0	0.997	31.1	0.989		
34.4	0.997	34.5	0.989		
38.0	0.997	41.3	0.989		
41.3	0.998	48.3	0.990		
44.9	0.998	55.3	0.990		
48.3	0.998	62.2	0.991		
51.7	0.998	69.0	0.991		
55.1	0.998	75.9	0.991		
58.6	0.998	82.8	0.992		
62.1	0.999	89.7	0.992		
65.5	0.999	96.6	0.992		
69.0	0.999	100.0	0.992		
72.4	0.999				
75.9	0.999				
79.3	0.999				
82.7	1.000				
86.2	1.000				
89.6	1.000				
93.1	1.000				
96.6	1.000				
100.0	1.000				

Table Continued

Table Continued

Temperature: 111°C		Temperature: 146°C		Temperature: 178°C	
Pressure [bar]	Density [g/ml]	Pressure [bar]	Density [g/ml]	Pressure [bar]	Density [g/ml]
1.7	0.953	1.7	0.931	1.7	0.910
13.8	0.954	13.8	0.932	13.8	0.912
27.7	0.955	27.7	0.933	27.6	0.913
41.4	0.956	41.4	0.934	41.4	0.914
55.2	0.957	55.3	0.935	55.2	0.916
69.0	0.958	69.1	0.936	69.0	0.917
82.8	0.959	83.1	0.937	82.8	0.918
100.1	0.960	100.0	0.938	100.1	0.919

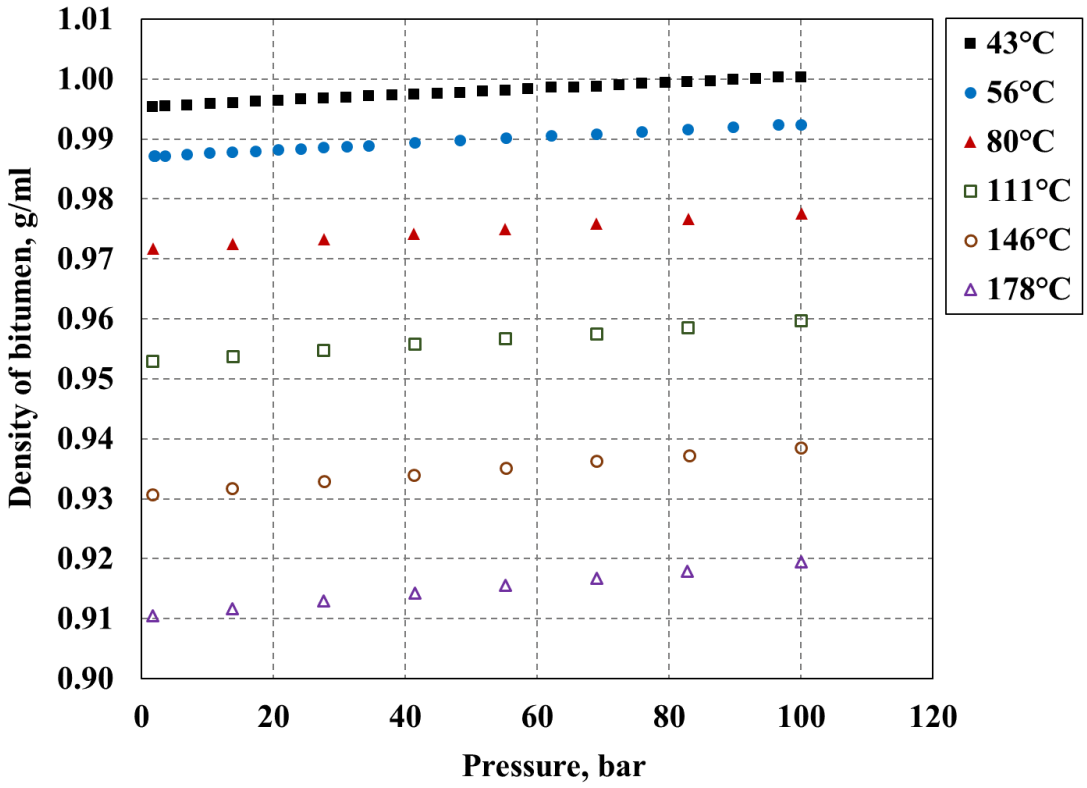

Figure 3.4 Experimental results for the bitumen density

Table 3.7 Experimental results for the bitumen viscosity

Temperature: 55°C	
Pressure [bar]	Viscosity [cp]
1.7	2290
13.8	2380
27.7	2470
41.4	2580
55.2	2690
70.0	2810
82.9	2940
100.0	3110

Temperature: 79°C	
Pressure [bar]	Viscosity [cp]
1.8	271
13.8	286
27.7	293
41.3	305
55.2	317
69.0	330
82.9	344
100.1	362

Temperature: 107°C	
Pressure [bar]	Viscosity [cp]
1.7	44.4
13.9	45.9
27.7	47.6
41.4	49.5
55.9	51.3
69.0	53.2
82.8	55.2
100.1	57.7

Temperature: 140°C	
Pressure [bar]	Viscosity [cp]
1.7	9.3
13.8	9.6
27.7	9.9
41.4	10.2
55.3	10.6
69.1	11.0
82.9	11.3
100.0	11.8

Temperature: 170°C	
Pressure [bar]	Viscosity [cp]
1.7	3.3
13.8	3.4
27.6	3.5
41.4	3.5
55.2	3.7
69.0	3.8
82.8	3.9
100.1	4.0

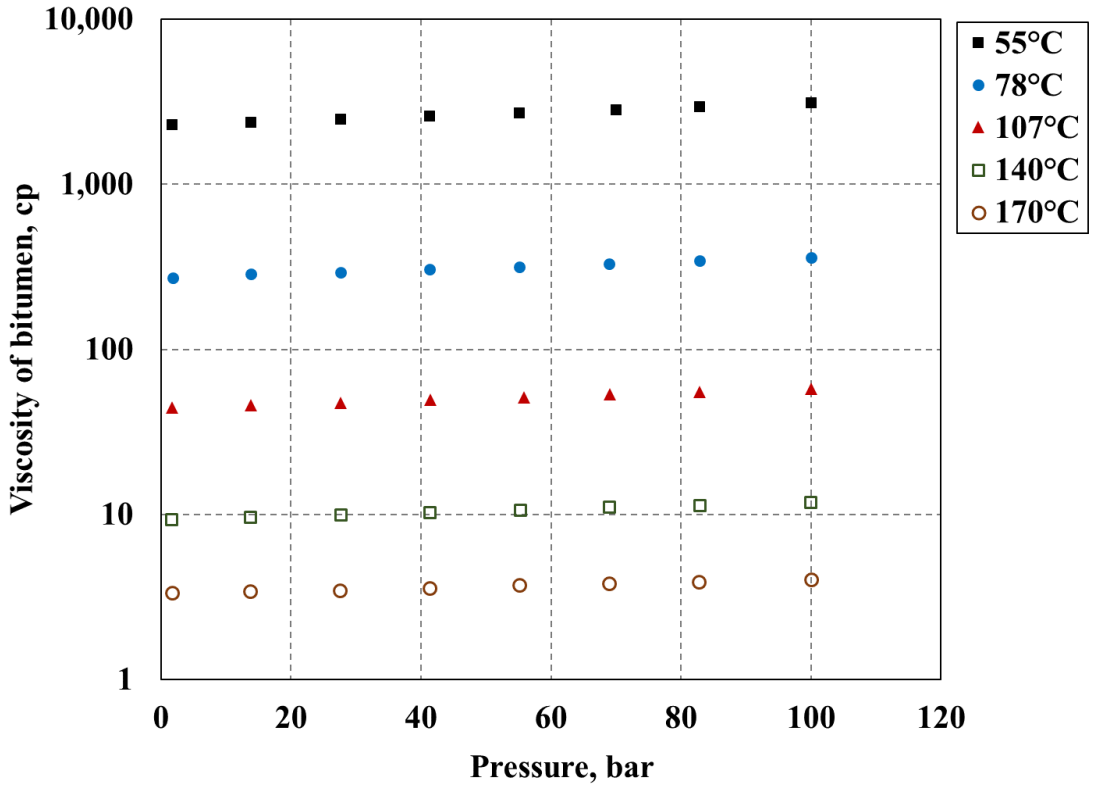

Figure 3.5 Experimental results for the bitumen viscosity

Table 3.8 Experimental results for the density and viscosity of DB-4

Density			Viscosity		
Temperature [°C]	Pressure [bar]	Density [g/ml]	Temperature [°C]	Pressure [bar]	Viscosity [cp]
55	30.0	0.927	54	30.0	17.2
	35.0	0.927		35.0	19.7
	40.0	0.928		40.0	21.1
	50.0	0.928		50.0	22.4
	60.0	0.929		60.0	23.6
	70.0	0.930		70.0	24.6
82	30.0	0.906	81	30.0	4.7
	35.0	0.907		35.0	5.3
	40.0	0.907		40.0	5.8
	50.0	0.908		50.0	6.3
	60.1	0.909		60.1	6.7
	70.0	0.910		70.0	7.0
111	35.0	0.884	109	35.0	1.9
	40.0	0.885		40.0	2.1
	50.0	0.886		50.0	2.3
	60.0	0.887		60.0	2.5
	70.0	0.888		70.0	2.6
145	50.0	0.860	141	50.0	1.0
	60.0	0.861		60.0	1.1
	70.0	0.862		70.0	1.2

Table 3.9 Experimental results for the density and viscosity of DB-5

Density			Viscosity		
Temperature [°C]	Pressure [bar]	Density [g/ml]	Temperature [°C]	Pressure [bar]	Viscosity [cp]
55	20.1	0.948	55	20.1	38.2
	25.0	0.948		25.0	36.7
	35.1	0.949		35.1	36.7
	40.0	0.949		40.0	48.1
	50.0	0.950		60.0	79.0
	60.0	0.950		70.1	87.5
	70.1	0.951			
82	30.0	0.930	82	30.0	10.9
	35.0	0.930		35.0	10.4
	40.0	0.931		40.0	11.2
	50.0	0.931		50.0	14.2
	60.0	0.932		60.0	17.8
	70.1	0.933		70.1	21.2
111	30.1	0.909	109	30.1	3.8
	35.0	0.909		35.0	3.7
	40.0	0.910		40.0	3.5
	50.0	0.911		50.0	5.5
	60.0	0.911		60.0	4.7
	70.0	0.912		70.1	5.6
144	40.0	0.886	141	40.0	1.9
	50.0	0.887		50.0	1.9
	60.1	0.888		60.1	1.6
	70.0	0.889		70.0	1.9
173	50.1	0.865	170	50.0	1.6
	60.0	0.867		70.0	0.9
	70.0	0.868			

Table 3.10 Experimental results for the density and viscosity of HB-3

Density			Viscosity		
Temperature [°C]	Pressure [bar]	Density [g/ml]	Temperature [°C]	Pressure [bar]	Viscosity [cp]
55	15.0	0.919	54	15.0	22.4
	35.0	0.921		35.0	30.6
	60.0	0.922		60.0	49.0
81	15.0	0.902	80	15.0	6.0
	35.0	0.903		35.0	7.4
	60.0	0.905		60.0	11.8
110	15.0	0.882	108	15.0	2.4
	35.0	0.883		35.0	2.5
	60.0	0.885		60.0	3.5
144	15.0	0.858	141	15.0	1.2
	35.0	0.860		35.0	1.2
	60.0	0.863		60.0	1.3
173	15.1	0.838	170	15.0	1.0
	35.0	0.840		35.0	1.0
	60.0	0.843		60.0	0.7

Table 3.11 Experimental results for the density and viscosity of HB-4

Density			Viscosity		
Temperature [°C]	Pressure [bar]	Density [g/ml]	Temperature [°C]	Pressure [bar]	Viscosity [cp]
55	14.7	0.948	54	15.0	80.5
	35.0	0.949		35.0	223
	60.0	0.951		60.0	246
82	15.0	0.930	81	15.0	14.0
	35.0	0.931		35.0	31.1
	60.1	0.933		60.0	45.2
111	15.0	0.911	109	15.0	4.0
	35.0	0.913		35.0	7.0
	60.1	0.914		60.0	11.1
145	15.0	0.888	141	15.0	1.6
	35.0	0.890		35.0	1.9
	60.0	0.893		60.0	3.2
174	15.0	0.868	170	15.0	1.1
	35.0	0.871		60.2	1.4
	60.2	0.873			

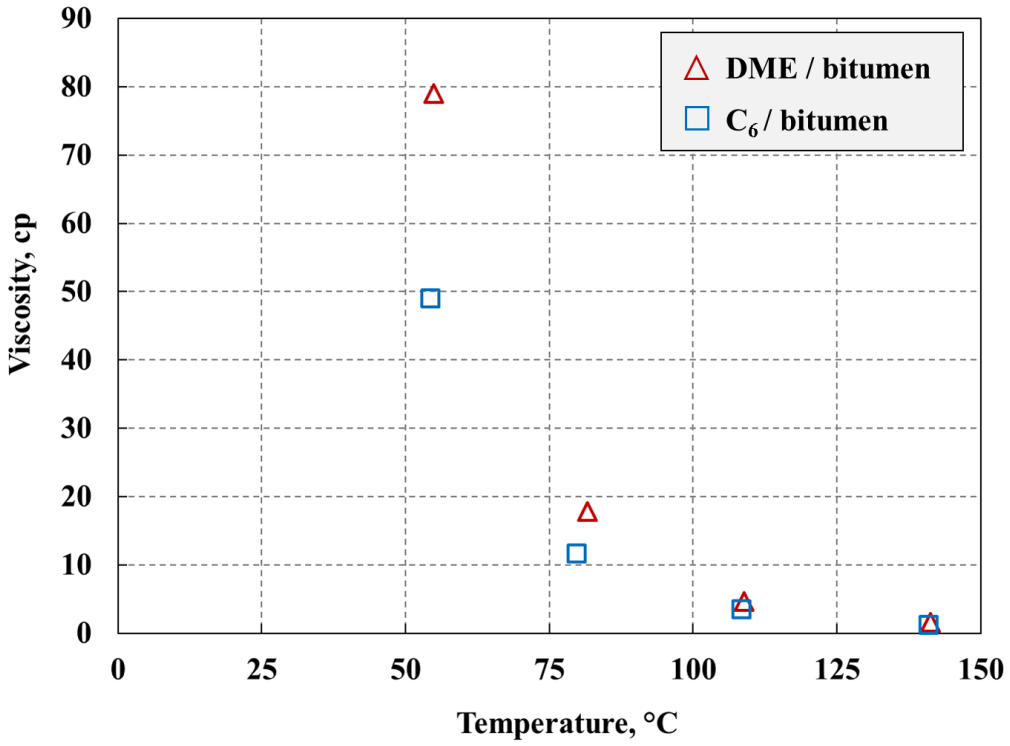

Figure 3.6 Experimental results for the equimolar mixture of solvent and bitumen, DB-5 and HB-3, at 60 bars

3.3.3. Correlations for Density and Viscosity of Solvent/Bitumen Mixtures

The density data measured for the bitumen in this research have been correlated with the equation used by Nourozieh et al. (2015a):

$$\rho_{bit} = \rho_0 \exp(\alpha P) \quad (1)$$

$$\rho_0 = a_1 + a_2 T + a_3 T^2 \quad (2)$$

$$\alpha = a_4 \exp(a_5 T) \quad (3)$$

where ρ_{bit} is bitumen density in kg/m^3 and P is pressure in MPa, and T is temperature in °C. Five parameters a_1 to a_5 are adjusted to match the experimental data in this research. The resulting AAD and AARD are 0.75 kg/m^3 and 0.08%, respectively, with a_1 = 1022.11, a_2 = -0.61, a_3 = 0, $a_4 = 3.53 \times 10^{-4}$ and $a_5 = 3.30 \times 10^{-4}$.

The viscosity data measured for the bitumen in this research are correlated by use of the correlation of Mehrotra and Svrcek (1986):

$$\ln(\mu_{bit}) = \exp(b_1 + b_2 \ln(T + 273.15)) + b_3 P_g \quad (4)$$

where T is temperature in °C and P_g is gauge pressure in MPa. The resulting AAD and AARD are 32.7 cp and 18.3%, respectively, with b_1= 33.33463, b_2 = -5.40032 and b_3 = 0.023782.

Wu et al. (2003) presented the following correlation for saturated-liquid DME:

$$\log_{10} \mu_{DME} = -5.7282 + \frac{631.031}{T} + 0.01453T - 1.8225 \times 10^{-5} T^2 \quad (5)$$

where μ is DME's viscosity in cp, and T is temperature in K. This correlation gave 0.5% AARD from experimental data measured from -46 to 70°C (227 to 343 K). Viscosities of n-hexane are taken from NIST, in which n-hexane's viscosities are calculated by use of the correlation presented in Michailidou et al. (2013). In terms of solvent viscosity, DME is less viscous than n-hexane. For example, the viscosity of DME and n-hexane at 35 bar is compared in **Figure 3.7**.

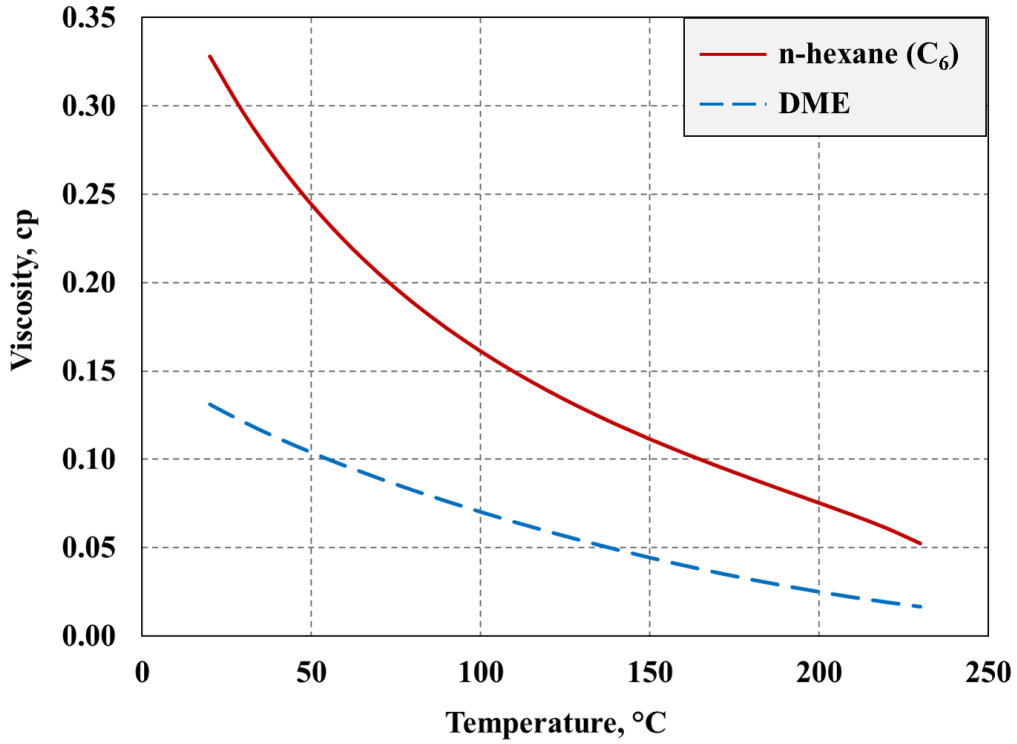

Figure 3.7 Viscosity of DME and n-hexane (C_6) at 35 bar

The viscosity data for the two mixtures, DME/bitumen and n-hexane/bitumen, are correlated with the following three models: a modified Arrhenius model, the power law model, and Walther's model. The modified Arrhenius equation is used because it is implemented in a commercial reservoir simulator, CMG STARS (Computer Modelling

Group 2014). Therefore, the calibrated model can be directly used to perform numerical simulation of steam-DME co-injection.

The original Arrhenius equation (Arrhenius, 1887) based on kinetic theory is

$$\ln \mu_{mix} = \sum_{i=1}^{Nc} x_i \ln \mu_i \tag{6}$$

where μ_{mix} is the viscosity of a mixture, μ_i is the viscosity of component i, and x_i is the mole fraction of component i. The modified Arrhenius model used in this research is

$$\ln \mu_L = \sum_{i=1}^{Nc} q_i x_{iL} \ln \mu_{iL} \tag{7}$$

subject to

$$\sum_{i=1}^{Nc} q_i x_{iL} = 1.0 \tag{8}$$

where μ_{iL} and x_{iL} are the viscosity and mole fraction of component i in the oleic phase, respectively. qi is weighting factor for component i. Weighting factors for components except for bitumen are set to be equal, subject to equation 8.

For mixtures of bitumen/solvent/water, Venkatramani and Okuno (2017) used the following equation for the weighting factor q_{CD} for the dead bitumen component (C_D):

$$q_{CD} = 1 + \alpha \left\{ \frac{(1-x_{CDL})[1-(1-x_{CDL})^8]}{x_{CDL}} \right\} \tag{9}$$

where α is a constant specific to the solvent in the mixture of interest. They used this equation to account for the difference between the two binaries, bitumen/water and bitumen/solvent, in terms of the viscosity mixing rules as presented in Glandt and Chapman

(1995). In this research, the α parameters for DME and n-hexane have been determined by matching the viscosity data as follows: 0.291 for DME and 0.0381 for n-hexane.

The α parameter tends to increase from zero as the solvent mixed with bitumen becomes lighter according to the optimized α values by Venkatramani and Okuno (2017) on the basis of published data for bitumen/solvent mixtures. The modified Arrhenius equation (equation 7) reduces to the original Arrhenius (equation 6), which is the log-linear mixing rule, when α is set to zero ($q_i = 1.0$ for all i).

Figure 3.8 compares the viscosities calculated for DB-5 and HB-3 at 60 bars by use of the two equations with the corresponding experimental data. The original Arrhenius equation reasonably correlates the data for HB-3 (Figure 3.8a). With the small value of α, 0.0381, optimized for n-hexane/bitumen mixtures, the modified Arrhenius equation is only slightly more accurate. However, Figure 3.8b clearly shows that accurate representation of the DB-5 data requires the modified Arrhenius equation.

In addition to the modified Arrhenius model, the power law model and Walther's model (Walther 1931) are applied to correlate the viscosity data obtained. The power model is

$$\mu_{mix} = [x_s \mu_s^n + (1 - x_s)\mu_{bit}^n]^{1/n} \tag{10}$$

where μ_s and μ_{bit} are the viscosities of solvent and bitumen, respectively. x_s is the solvent mole fraction in the mixture. The n parameter was determined to be 0.1416 for bitumen/DME mixtures and 0.0175 for bitumen/n-hexane mixtures.

Walther's model (Walther 1931) is

$$\ln(\ln(\mu_{mix}) + C) = v_s \ln(\ln(\mu_s + C)) + (1 - v_s)\ln(\ln(\mu_{bit} + C)) \tag{11}$$

where v_s is the solvent volume fraction in the mixture. The *C* parameter was determined to be 0.9641 for bitumen/DME mixtures and 0.9128 for bitumen/n-hexane mixtures.

Figure 3.9 compares the three viscosity models with the experimental data for DB-5 and HB-3 at 60 bars. It is observed that Walther's model gives higher values than the other two models, and therefore, it gives more accurate correlation at high-viscosity regions. For the n-hexane/bitumen mixtures, all correlations are in reasonable agreement with the experimental data. The modified Arrhenius model and power law model are similar in correlative accuracy for the n-hexane/bitumen mixtures. For the DME/bitumen mixtures, Walther's model is more accurate at high-viscosity values, but the modified Arrhenius model is more accurate at low-viscosity values.

For all viscosity data measured for HB-3 and HB-4, the modified Arrhenius equation gives an AAD of 11.9 cp and an AARD of 25.4%. The power law model gives an AAD of 11.2 cp and an AARD of 26.6%. Walther's model gives an AAD of 10.6 cp and an AARD of 42.7%.

For the DB-4 and DB-5 data, the modified Arrhenius equation gives an AAD of 4.2 cp and an AARD of 22.5%. The power law model gives an AAD of 6.1 cp and an AARD of 39.6%. Walther's model gives an AAD of 6.2 cp and an AARD of 40.2%.

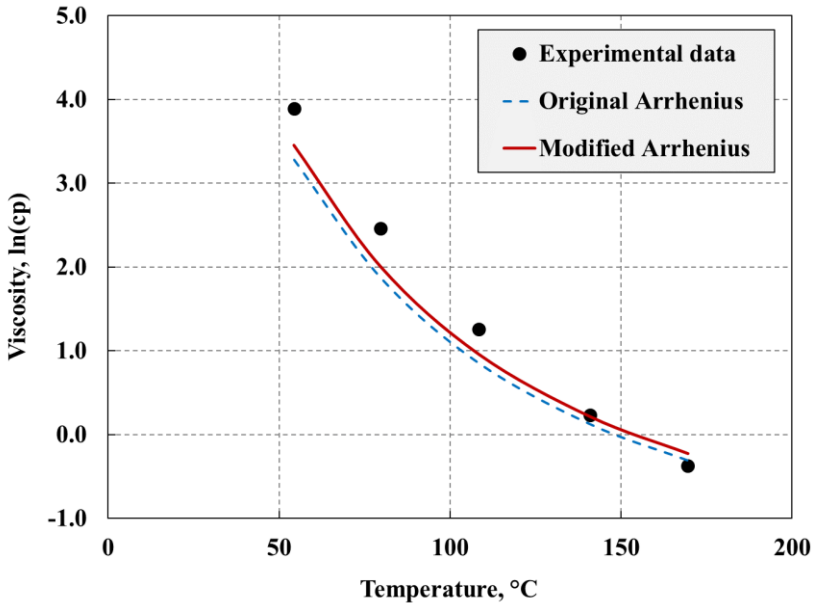

(a) n-hexane (C_6) 50 mol% / bitumen 50 mol% (HB-3) at 60 bars

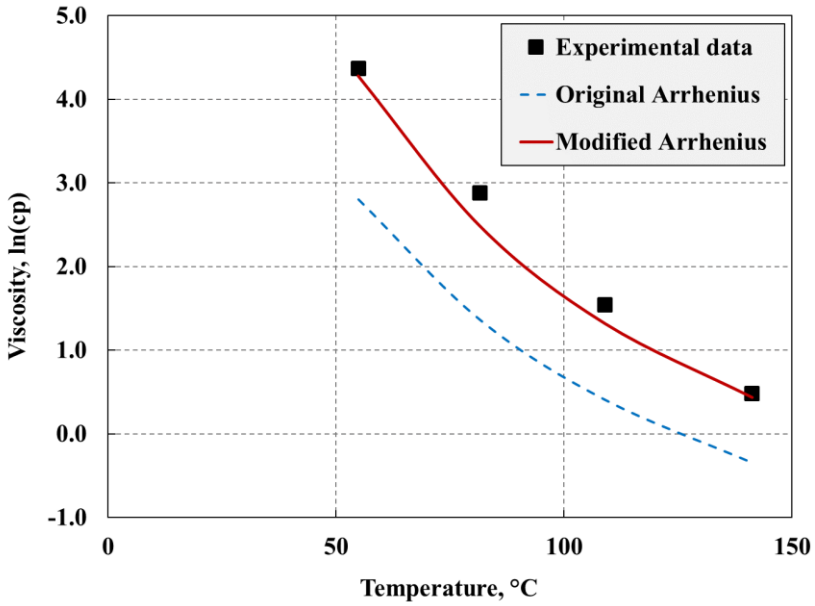

(b) DME 50 mol% / bitumen 50 mol% (DB-5) at 60 bars

Figure 3.8 Correlations by use of the original and modified Arrhenius equations are compared with the experimental data (50 mol% solvent / 50 mol% bitumen) at 60 bars

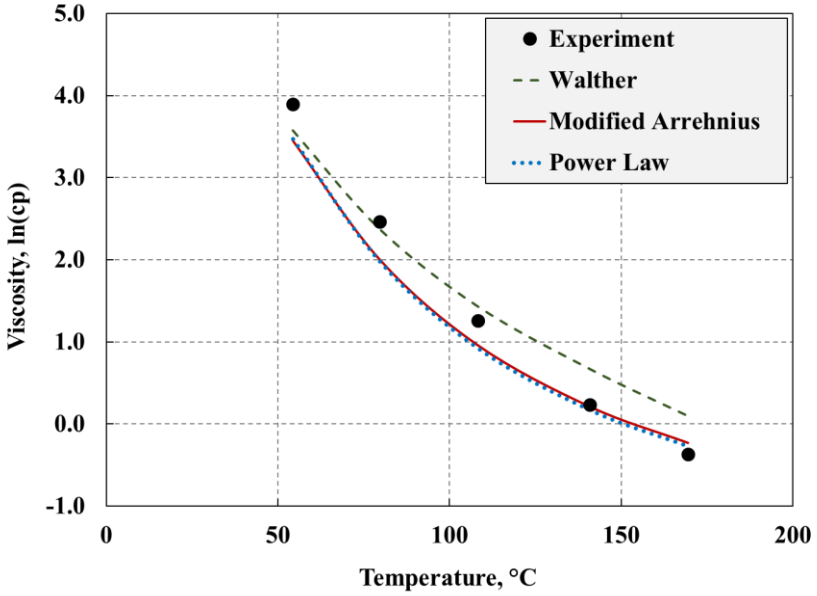

(a) n-hexane (C_6) 50 mol% / bitumen 50 mol% (HB-3) at 60 bars

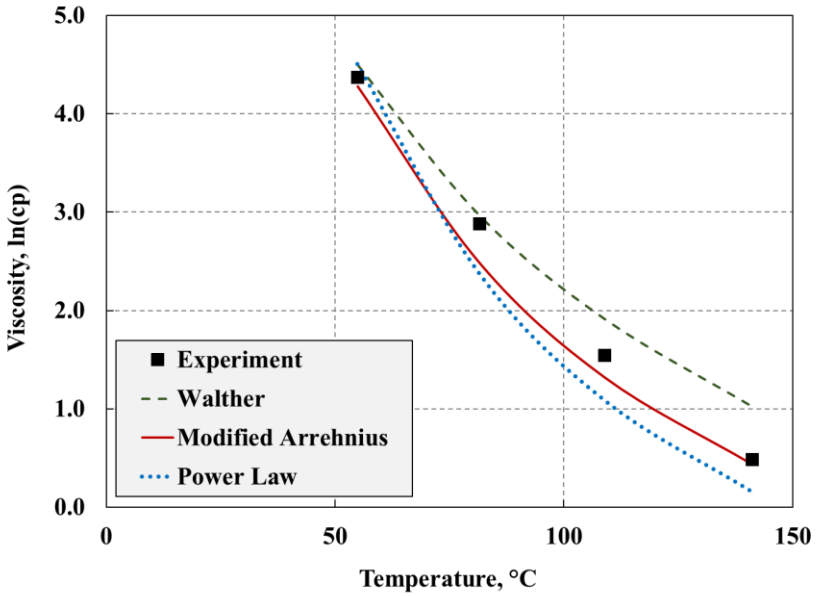

(b) DME 50 mol% / bitumen 50 mol% (DB-5) at 60 bars

Figure 3.9 Correlations by use of the modified Arrhenius equation, the power law equation, and Walther's equation are compared with the experimental data (50 mol% solvent / 50 mol% bitumen) at 60 bars

3.4. Dilution Capability of DME and n-alkanes with Bitumen

This section consists of two subsections. In the first subsection, the viscosity data measured for the bitumen and HB-3 and HB-4 are analyzed and compared with the data reported by Nourozieh et al. (2015b) for another Athabasca bitumen sample and its mixtures with n-hexane. In the second subsection, n-hexane and DME are compared in terms of viscosity reduction of the oleic phase by dilution, for which the modified Arrhenius equation calibrated with the new data is used.

3.4.1. Bitumen and n-hexane/Bitumen Viscosity Data

Nourozieh et al. (2015b) measured viscosities of n-hexane/Athabasca-bitumen mixtures. The Athabasca bitumen sample used by them (Nourozieh et al. 2015abc) was provided by ConocoPhillips. The molecular weight (MW) was reported to be 539.2 g/mol, which is close to the MW, 532 g/mol, measured for the Athabasca bitumen sample used in this research (both results were obtained by using benzene as the solvent). However, the SARA composition of their bitumen sample is markedly different from that of the bitumen used in this research as shown in **Table 3.12**. The Athabasca bitumen sample in this research is richer in saturates than that used in Nourozieh (2015abc). Table 3.12 also shows the coefficients for equation 4 for the two Athabasca bitumen samples.

Figure 3.10 clearly shows that the bitumen studied in this research is less viscous at all temperatures than the bitumen studied by Nourozieh et al. (2015abc). This viscosity difference can be explained by the difference in the SARA composition (Table 3.12). Malkin et al. (2016) analyzed the effect of saturates, aromatics, resins, and asphaltenes on the viscosity of nearly 200 crude oil samples. They observed that saturates tend to decrease the oil viscosity, but asphaltenes, resins, and aromatics tend to increase it. The concentration of saturates is twice higher in the bitumen in this research than in the bitumen

used in Nourozieh et al. (2015abc) (24.5 wt% in comparison with 12.26 wt%). This clear difference in SARA is likely the main reason for the observed difference in Figure 3.10. Note that different solvents were used to measure the asphaltene content for the bitumen in this research and the bitumen studied by Nourozieh et al. (2015abc). The asphaltene was pentane-insoluble in this research, but heptane-insoluble in Nourozieh et al. (2015abc).

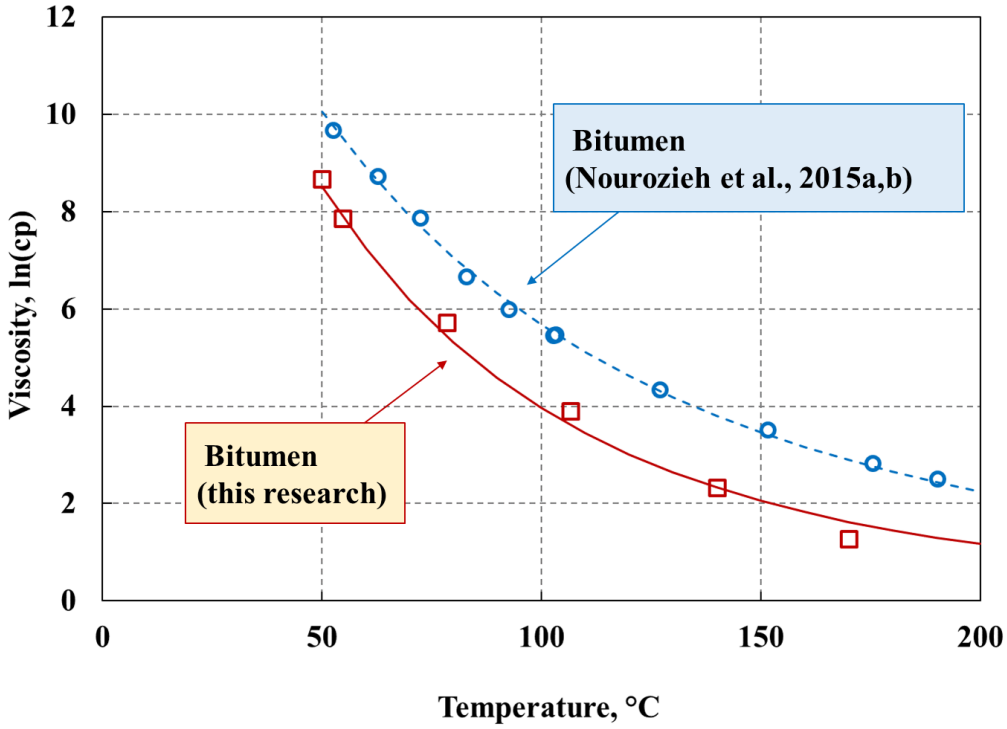

Figure 3.10 Viscosity for bitumen in this research and bitumen from Nourozieh et al. (2015ab).

o: Experimental data for the bitumen viscosity taken from Nourozieh et al. (2015ab) at 40 bars;
□: Experimental data for the bitumen viscosity at 40 bars in this research;
- -: Mehrotra and Svrcek (1986) correlation (equation 4) for the bitumen of Nourozieh et al. (2015ab);
—: Mehrotra and Svrcek (1986) correlation (equation 4) for the bitumen studied in this research. Parameters of Mehrotra and Svrcek (1986) correlation for two bitumens are tabulated in Table 3.12.

Table 3.12 Properties of bitumen in this research and bitumen used in Nourozieh et al. (2015abc).

The two bitumen samples are similar in terms of molecular weight, but markedly different in terms of the saturate concentration. The viscosity model developed by Mehrotra and Svrcek (1986) shows good agreement with both bitumens with different values for parameters, b_1, b_2 and b_3. Note that the asphaltene was pentane-insoluble in this research, but heptane-insoluble in Nourozieh et al. (2015abc).

		Bitumen (this research)	Bitumen (Nourozieh et al., 2015abc)
MW [g/mol]		532	539.2
SARA [wt%]	Saturates	24.5	12.26
	Aromatics	36.6	40.08
	Resins	21.1	36.53
	Asphaltenes	17.8 (pentane insoluble)	11.13 (heptane-insoluble)
Bitumen viscosity model (Mehrotra and Svrcek, 1986)	b_1	33.33463	26.65193
	b_2	-5.40032	-4.04208
	b_3	0.023782	0.031101

To validate the experimental viscosity data for the HB-3 and HB-4 mixtures, the power-law model (equation 10) with *n* parameter from Nourozieh et al. (2015b) is applied. The *n* parameter was determined to be 0.0186 for the mixtures of n-hexane with Athabasca-bitumen in Nourozieh et al. (2015b). **Figure 3.11a** shows that the viscosities for HB-3 are correlated with the power-law correlation given in Nourozieh et al. (2015b), although the bitumens studied by them and in this research are different from each other (Table 3.12).

In addition, the modified Arrhenius model with $\alpha = 0.0381$ is applied to the experimental data of Nourozieh et al. (2015b). **Figure 3.11b** shows that the modified Arrhenius model (equation 7) correlates well the viscosity values for the mixtures of n-hexane/Athabasca-bitumen measured by Nourozieh et al. (2015b). This indicates that the mixing behavior of the current bitumen sample with n-hexane is similar to that of Nourozieh et al.'s (2015b) bitumen sample with n-hexane.

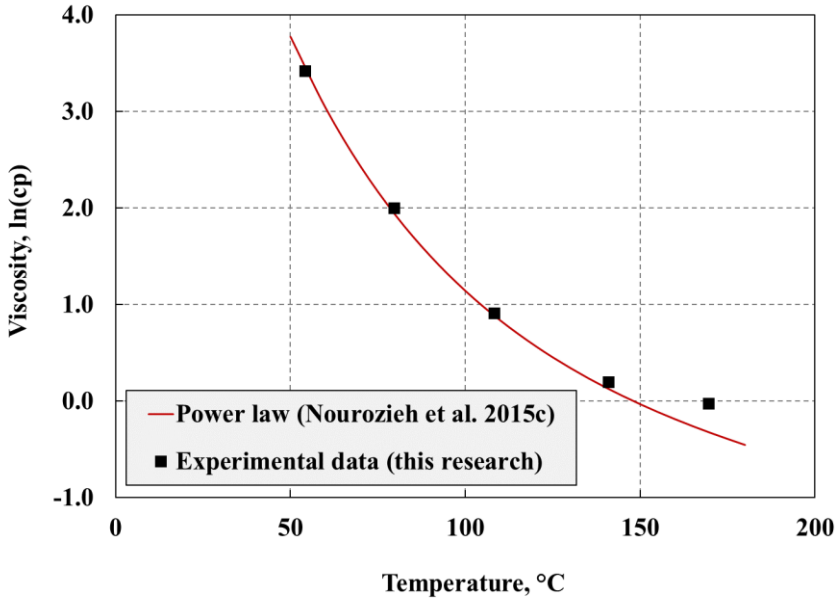

(a) Bitumen (in this research): 50 mol% n-hexane (C_6) / 50 mol% bitumen (HB-3) at 35 bars

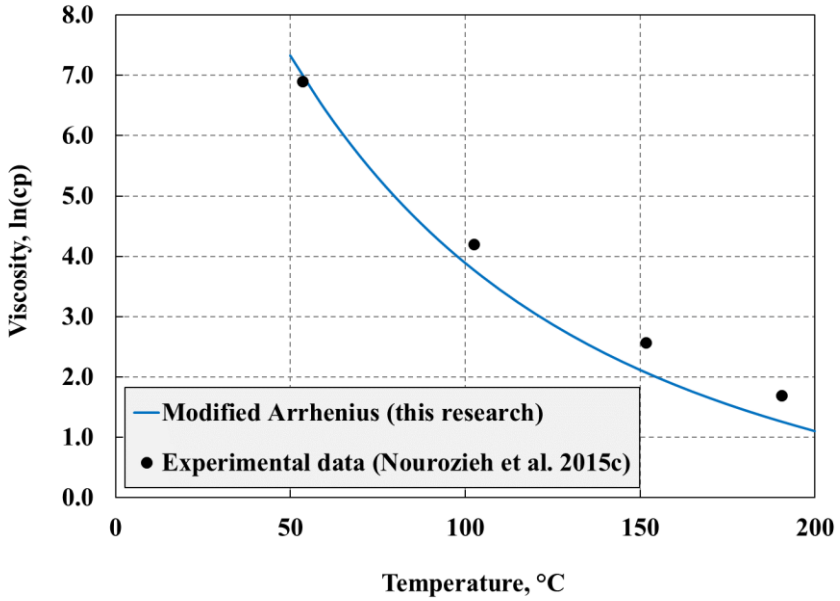

(b) Bitumen (Nourozieh et al. 2015c): 24.8 mol% n-hexane (C_6) / 75.2 mol% bitumen at 41 bars

Figure 3.11 Cross-check of power law model and modified Arrhenius model to correlate experimental data

3.4.2. Dilution Capability of DME and n-hexane

The dilution capabilities of DME and n-hexane are compared in terms of oleic-phase viscosity, by use of the modified Arrhenius equation calibrated with the new data. The comparison is made for the temperature range from 50 to 200°C, which are deemed relevant to in-situ conditions for the L-phase flow in SAGD and solvent-SAGD.

Figure 3.12 shows the L-phase viscosities calculated for the bitumen, and the equimolar mixtures of n-hexane/bitumen and DME/bitumen at 35 bars. Overall, DME/bitumen and n-hexane/bitumen exhibit similar viscosities. The viscosity of the DME/bitumen mixture is approximately 66 cp higher than that of the n-hexane/bitumen mixture at 50°C. However, the difference is calculated to be less than 1 cp at temperatures above 110°C. This trend is calculated also at different pressures.

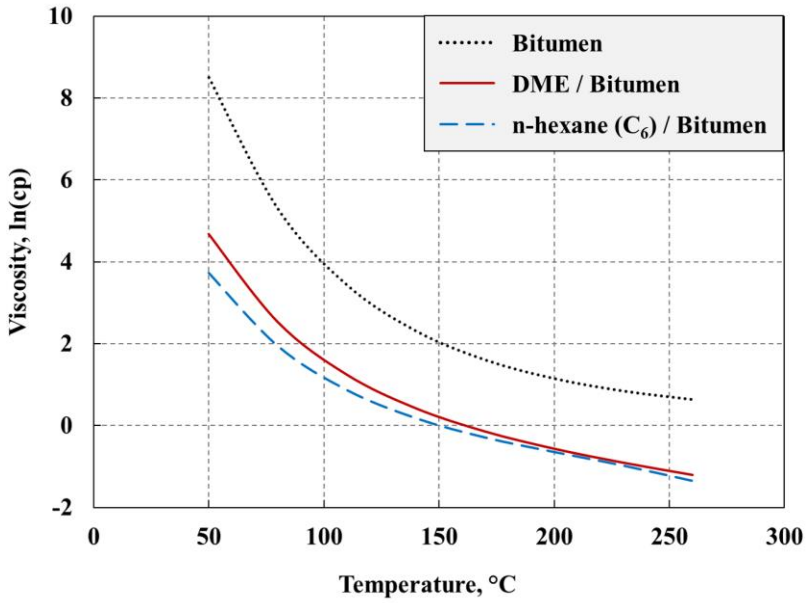

Figure 3.12 The viscosity comparison for bitumen, the equimolar mixtures of bitumen with DME and bitumen with n-hexane (C_6) at 35 bars

Figure 3.13 shows the L-phase viscosities calculated at 35 bars for 100% bitumen, and n-hexane/bitumen and DME/bitumen mixtures with two different solvent concentrations, 30 mol% and 70 mol%. Again, the overall effect of DME on bitumen dilution is close to that of n-hexane.

The experimental results and viscosity correlations indicate that n-hexane/bitumen mixtures give lower L-phase viscosities than DME/bitumen mixtures and that they become similar with increasing temperature. This indicates that the viscosity of a less viscous solvent with bitumen does not necessarily result in lower viscosity than that of bitumen mixtures with a more viscous solvent at the same concentration. This trend can be also found in the experimental data by Nourozieh et al. (2013), Kariznovi et al. (2013), and Ramos-Pallares et al. (2015).

Ramos-Pallares et al. (2015) measured the viscosity of a bitumen sample from Western Canada mixed with a series of n-alkanes: ethane, propane, butane, pentane, and heptane. Because their experimental data were given by use of mass fractions, the concentrations of solvent were converted into the mole fractions with the assumed MW of 500 g/mol for their bitumen sample. It was found that, under the same mole fraction of solvent, the heptane/bitumen mixture was less viscous than the mixtures of the bitumen with ethane and propane, as presented in **Figure 3.14a**. Furthermore, a similar observation can be made by use of the power-law models made by Nourozieh et al. (2013) and Kariznovi et al. (2013) for n-decane and n-tetradecane, respectively. That is, the viscosity of n-tetradecane/bitumen is calculated to be slightly lower than that of n-decane/bitumen, as presented in **Figure 3.14b**.

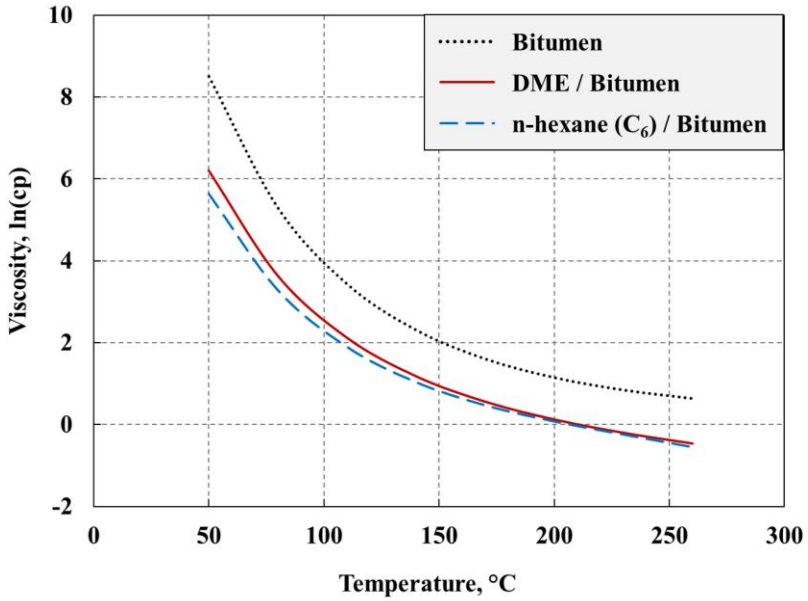

(a) 30 mol% Solvent / 70 mol% Bitumen at 35 bars

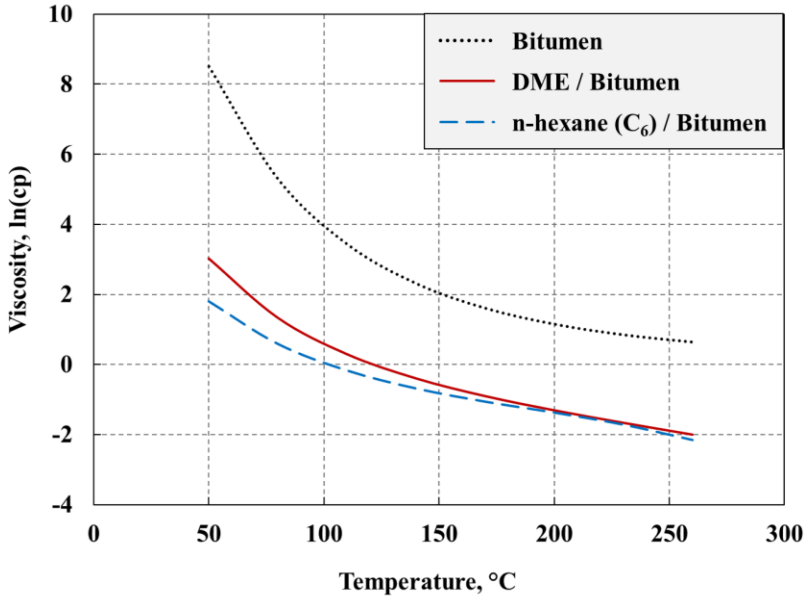

(b) 70 mol% Solvent / 30 mol% Bitumen at 35 bars

Figure 3.13 The viscosity comparison for DME/bitumen, n-hexane (C_6)/bitumen and bitumen at 35 bars with different concentrations of solvent: 30 mol% and 70 mol%

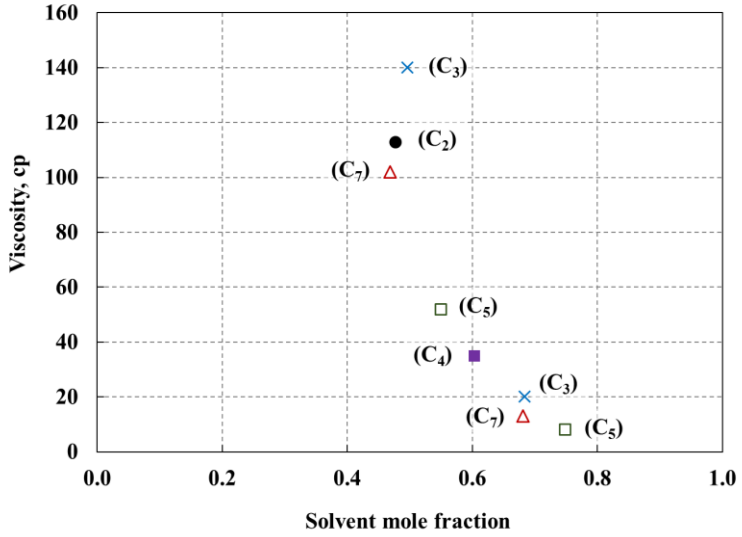

(a) Experimental data for the viscosity of bitumen with different solvents at 100°C (Ramos-Pallares et al., 2015). At the same molar concentration of solvent, n-heptane(C_7) gives lower viscosity than ethane(C_2) or propane(C_3) when it is mixed with the same bitumen (Western Canada).

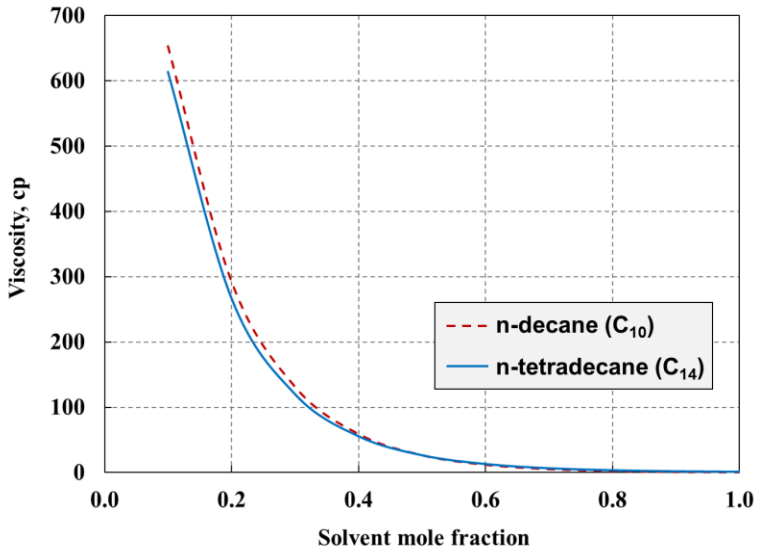

(b) The viscosities calculated for n-decane (C_{10}) and n-tetradecane(C_{14}) with Athabasca bitumen at 70°C and 40 bars by the power law model of Nourozieh et al. (2013) and Kariznovi et al. (2013). n-tetradecane (C_{14}) gives lower viscosity than n-decane(C_{10}) when mixed with Athabasca bitumen.

Figure 3.14 Experimental data and viscosity correlations show that bitumen mixed with heavier solvent results in lower viscosity than that with lighter solvent

To further investigate the dilution capability of DME in comparison with n-alkane solvents, the modified Arrhenius equation has been calibrated with the viscosity data measured by Nourozieh et al. (2015d and 2017) for mixtures of Athabasca bitumen with propane (C_3) and n-butane (C_4). The bitumen sample used for these papers is the same as that in Nourozieh et al. (2015b) for n-hexane. Liquid viscosities of propane and butane were estimated from saturated liquid viscosity reported in NIST. For supercritical temperatures, Reynolds' model for a single component was used in the following form to perform the extrapolation:

$$\mu_{\text{solvent}} = \text{A} \exp(-\text{BT}) \tag{12}$$

where A and B are two fitting parameters obtained from regression on NIST saturated-liquid viscosities. Viscosity and temperature are in cp and °C. A and B for C_3 are 0.1317 and 0.0124, and those for C_4 are 0.2147 and 0.011. **Figure 3.15** presents the result of regression to NIST's data for liquid C_3 and C_4. Then, the α value for the modified Arrhenius equation is 0.36 for C_3 and 0.376 for C_4. The resulting modified Arrhenius correlation gives AARD of 54.4% and 17.4% for C_3/bitumen (Nourozieh et al., 2015d) and C_4/bitumen (Nourozieh et al., 2017), respectively.

Now, the viscosities of mixtures of the bitumen studied in this research with C_3, C_4, C_6 and DME are calculated by use of equation 7 along with the obtained α values. **Figure 3.16** presents the viscosity trends calculated at the solvent concentration of 50 mol% at 35 bars. The results show that the dilution of the bitumen is most significant with C_6. The other solvents are similar in terms of the capability of viscosity reduction at the 50 mol% dilution level.

As described above, a less-viscous solvent does not necessarily yield a lower viscosity when it is mixed with bitumen at a given molar concentration. Another point of discussion regarding DME is that the hydrogen bonding that can occur between DME and various components in the bitumen sample may cause the viscosity of the DME/bitumen mixture to increase.

Hansen (1967) considered that the total energy holding liquid mixture together consists of the energy associated with dispersion, polarity, and hydrogen bonding,

$$\delta^2 = \delta_d^2 + \delta_p^2 + \delta_h^2 \tag{13}$$

where δ is the energy density with a unit of 1/MPa. Subscripts d, p and h represent the contributions of dispersion, polarity and hydrogen bonding, respectively. Hansen's theory has been used to show the tendency of solvent interaction with polymers. Argillier et al. (2005) conducted a study of how intermolecular forces affect solvent's capability of diluting heavy oil based on Hansen's dimensional solubility parameters (1967). They concluded that a good solvent should have a high polarity parameter and a low hydrogen-bonding parameter. δ_p and δ_h values for commonly seen solvents were presented in Barton (1991). Alkanes has δ_p and δ_h of zero. Ether generally has a δ_p value from 3 to 5, and δ_h from 7 to 8. Methanol, which was reported by Argillier et al. (2005) to increase the viscosity of bitumen, has $\delta_p = 12$ and $\delta_h = 22$. In comparison, water has a $\delta_p = 16$ and $\delta_h = 42$.

Results in this research showed that the DME/bitumen mixture is slightly more viscous than the n-hexane/bitumen mixture at the same concentration and temperatures below 107°C. This may be attributed to stronger intermolecular forces between DME and polar components in bitumen than those between n-hexane and bitumen. Complex

compounds typically contained in bitumen include asphaltenes, which may form hydrogen bonds with DME molecules. At higher temperatures, the effect of hydrogen bonding on viscosity can be reduced, which might improve the capability of DME for viscosity reduction. This is in line with the observation that DME gives a similar level of viscosity reduction to n-hexane at higher temperatures (above 107°C). In contrast, no hydrogen bonding occurs between bitumen components and alkane solvents. Therefore, alkanes may perform well even at low temperatures based on the theory of Hansen (1967).

A good example for the effect of hydrogen bonding was reported by Dehaghani and Badizad (2016) for mixtures of methanol and a heavy oil, as shown in **Figure 3.17**. In their study, viscosities of methanol/heavy-oil mixtures were measured to be clearly higher than the viscosity of 100% heavy oil. The authors attributed this viscosity increase to methanol's self-association and the cross-association between methanol and asphaltene molecules. The viscosities for their n-heptane- and methanol-heavy oil mixtures were calculated from their reported kinematic viscosities and densities for this figure.

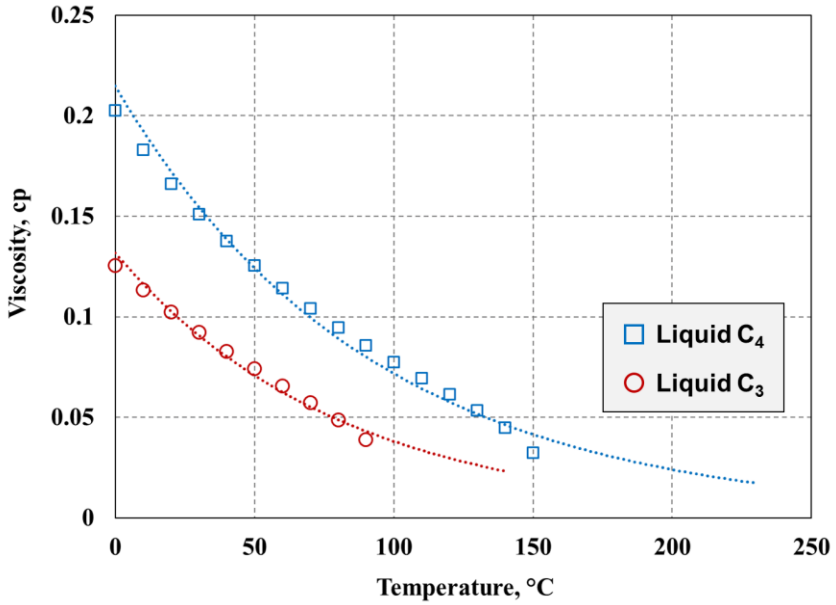

Figure 3.15 Regression result with viscosities of liquid propane (C_3) and n-butane (C_4) given by NIST

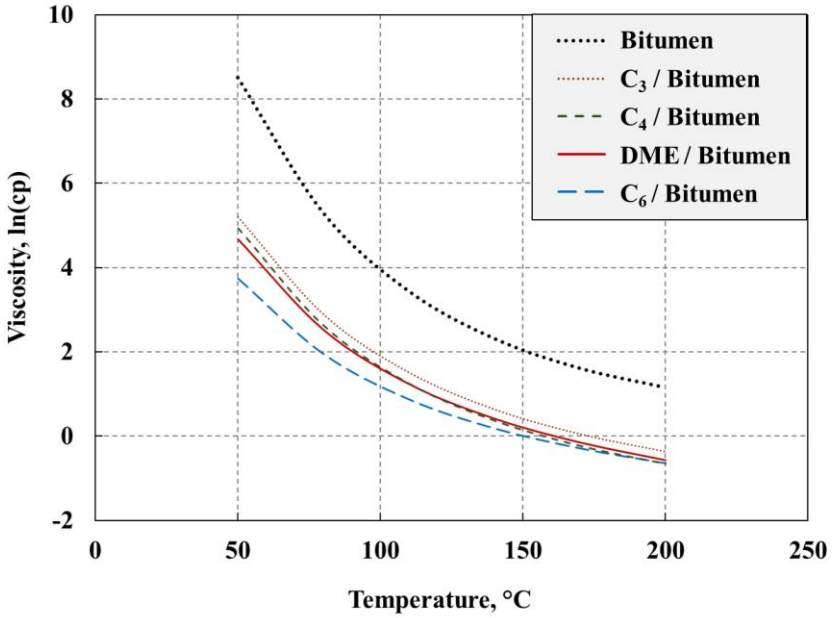

Figure 3.16 Comparison between n-alkanes and DME in terms of bitumen dilution at 50 mol% solvent concentration at 35 bars

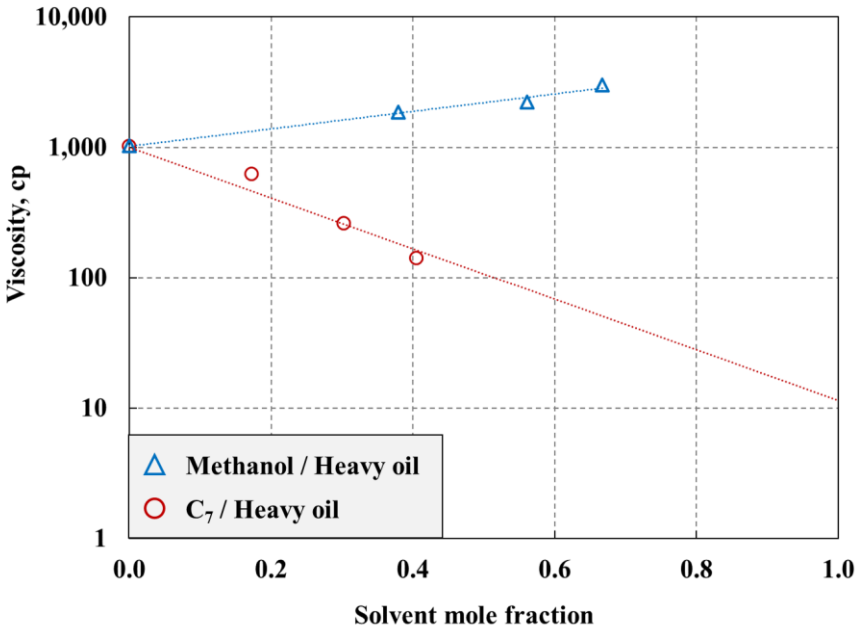

Figure 3.17 Comparison of viscosities measured for n-heptane (C_7)/heavy oil and methanol/heavy oil mixtures at 20°C and atmospheric condition

The heavy oil has an API gravity of 20°. The viscosity is calculated from their reported kinematic viscosity assuming the heavy oil's molecular weight is 500 g/mol. (Dehaghani and Badizad, 2016)

3.5. Conclusions

The capability of DME as diluent for Athabasca bitumen was compared with that of n-hexane by use of measured viscosities and correlations. New experimental data were presented for phase behavior of Athabasca bitumen, five mixtures of Athabasca bitumen with DME, and four mixtures of Athabasca bitumen with n-hexane. Conclusions are as follows:

- Liquid-liquid separation of solvent/bitumen mixtures, which occurred for n-butane/Athabasca-bitumen in Gao et al. (2017), was not observed for any of the DME/bitumen and n-hexane/bitumen mixtures in this research. The highest solvent concentration in this study was 80 mol% DME (DB-1) for the DME/bitumen system and 92 mol% n-hexane (HB-2) for the n-hexane/bitumen system.
- The Athabasca bitumen studied in this research was measured to be less viscous than the Athabasca bitumen studied by Nourozieh et al. (2015abcd and 2017). Although the two bitumens are similar in terms of molecular weight, the concentration of saturates in the bitumen studied in this research is twice higher than that of the other bitumen. This likely explains the lower viscosity of the bitumen studied in this research.
- Three viscosity models were used to correlate the experimental data: a modified Arrhenius model, the power law model, and Walther's model. In terms of AARD, the modified Arrhenius equation resulted in the best correlative accuracy among the three models. Although Walther's correlation gave a low AAD, it showed the largest AARD because of relatively large deviation for low-viscosity conditions. The power law model was similar to the modified Arrhenius model for correlation of the n-hexane/bitumen mixtures, but it did not give an accurate correlation for the DME/bitumen mixtures.

- The modified Arrhenius equation with a weighting factor, q_i, as a function of α was able to capture the deviation of solvent/bitumen from the original Arrhenius (log-linear mixing) rule. It correlated well the viscosity data for the Athabasca bitumen diluted by n-hexane and DME. The relatively large α value, 0.291, for DME/bitumen mixtures in comparison with α of 0.0381 for n-hexane/bitumen mixtures indicates that the viscosity of DME/bitumen mixtures deviates more from the log-linear mixing rule.
- The new experimental results showed that the equimolar mixture of DME with Athabasca bitumen was 79 cp, and that of n-hexane with the same bitumen was 49 cp at 55°C and 60 bars. However, the two solvents were equivalent as diluent at temperatures above 107°C for the bitumen studied. For example, the difference was approximately 1 cp at 109°C and 35 bars between the equimolar mixture of Athabasca bitumen with DME and that with n-hexane. The new experimental data and viscosity correlations indicate that the dilution capability of DME becomes similar to n-hexane at higher temperature and higher solvent concentration conditions.

4. Oil-in-Water Emulsification of Athabasca Bitumen with Organic Alkalis [2]

Organic alkalis were studied as a potential additive to steam for steam-assisted gravity drainage (SAGD). Diethylamine (DEA), Triethylenetetramine (TETA), and pyrrolidine were selected as organic alkalis in this research. The main idea is to induce in-situ oil-in-water (o/w) bitumen emulsions with natural surfactants activated by an organic alkali without any additional surfactants. An organic alkali can act both as an alkali and a co-solvent, and the use of a single component with multiple functions can yield a simpler solution to enhancement of bitumen transport. To this end, it is important to find an optimal type of organic alkalis that can form o/w emulsions that are much less viscous than the original bitumen, yet has a high concentration of bitumen.

Bitumen is a complex mixture of hydrocarbons, containing asphaltenes and resins at high concentrations. These components are known to interact with water and to affect emulsion behavior (Al-Sahhaf et al. 2008; Gao et al. 2017; Jia and Okuno 2018; Kar et al. 2014; Kokal 2005; Schorling et al. 1999; Xia et al. 2004; Yan et al. 1999; Yang et al. 2007; Yarranton et al. 2000). It is crucial to conduct fundamental experimental research of emulsion phase behavior and viscosity for mixtures of Athabasca bitumen, brine, and organic alkali because such experimental research has not been presented in the literature.

[2] This chapter was published in following three papers. Baek conducted all experiment and analyzed most of data as the first author of these papers.

1) Baek, K., Argüelles-Vivas, F.J., Okuno, R., Sheng, K., Sharma, H. and Weerasooriya, U.P. 2018. Emulsification of Athabasca Bitumen by Organic Alkali: Emulsion Phase Behavior and Viscosity for Bitumen/Brine/Triethylenetetramine. *Journal of Petroleum Science and Engineering* 168: 359-369. https://doi.org/10.1016/j.petrol.2018.04.063
2) Baek, K., Argüelles-Vivas, F.J., Okuno, R., Sheng, K., Sharma, H. and Weerasooriya, U.P. 2019. An Experimental Study of Emulsion Phase Behavior and Viscosity for Athabasca Bitumen/Diethylamine/Brine Mixtures. *SPE Reservoir Evaluation & Engineering* 22(2): 628-641. https://doi.org/10.2118/189768-PA
3) Baek, K., Okuno, R., Sharma, H. and Weerasooriya, U.P. 2019. Oil-in-Water Emulsification of Athabasca Bitumen with Pyrrolidine Solution, *Fuel* 246: 425-442. https://doi.org/10.1016/j.fuel.2019.02.123

This research provides experimental data on bitumen emulsification, viscosities of emulsions, oil contents in emulsions at different alkali concentrations, water-oil ratios (WORs), brine salinities, and temperatures. Based on comparison of DEA, TETA, and pyrrolidine, the effect of the chemical structure of organic alkalis on the bitumen emulsification is discussed.

4.1. Materials

Oil

The same dehydrated Athabasca bitumen (in the previous chapter) was used for experiments in this research. The total acid number was measured to be 3.56 mg-KOH/g-oil by using the method of Fan and Buckley (2007) (Table 3.1). Cooke et al. (1974) studied that the required acid number for an alkali-based oil recovery method was 1.5 mg-KOH/g-oil. Ge et al. (2012) showed in their sandpack flooding experiment that a higher acid number resulted in a higher oil recovery among four oil samples with acid numbers between 1.85 and 4.66 mg-KOH/g-oil. Therefore, the acid number of the bitumen sample in this research, 3.56 mg-KOH/g-oil, indicates that the bitumen contained the sufficient amount of acidic components to create natural surfactants by reacting with an organic alkali.

Organic Alkalis

Diethylamine (DEA), triethylenetetramine (TETA), and pyrrolidine were selected as organic alkalis, considering the different chemical structures. DEA is a short carbon-chain amine. The chemical formula is $(CH_3CH_2)_2NH$ and the molecular weight (MW) is 73 g/mol. The DEA was supplied by Sigma-Aldrich. The purity of DEA was higher than

99.5%. DEA is one of the suitable organic alkalis that meet the main requirements for organic alkali-steam co-injection. That is, DEA is between pentane (n-C_5) and hexane (n-C_6) in terms of volatility. Therefore, it is expected to effectively propagate in the reservoir as part of the vapor phase and to condense at thermal fronts.

Compared to DEA, TETA is a long carbon-chain amine. TETA has a chemical formula, $C_6H_{18}N_4$, and the molecular weight (MW) of 146 g/mol. The boiling temperature is 267°C due to its chemical structure. TETA was provided by Harcros Chemicals.

Unlike DEA and TETA, pyrrolidine contains a cyclic structure. The molecular weight (MW) and the boiling temperature are 71 g/mol and 87°C, respectively. Pyrrolidine is also suitable for organic alkali-steam co-injection. The pyrrolidine was provided by Sigma-Aldrich, and the purity was higher than 99.5%.

As shown in **Table 4.1**, it was confirmed that these organic alkalis can create high pH aqueous phases when it dissolves into the aqueous phase. Sheng (2015) studied that high pH condition in aqueous solutions is favorable for creating natural surfactants by reactions of alkali with acidic components in bitumen.

Brine

For aqueous solutions, different concentrations of brine were prepared with deionized water and NaCl. NaCl was chosen as the only salt in brine because, in general, brine in the steam injection operation is very fresh (low salinity) and NaCl is the main component in brine as shown in other literature (Petersen and Grade 2011; Razi et al. 2016).

Table 4.1 pH of alkali solutions at the room temperature

Alkali Concentration [wt%]	pH		
	DEA	TETA	Pyrrolidine
0.5	10.5	10.2	10.6
1	11.2	10.5	11.4
2	11.3	10.7	11.4
5	11.2	10.9	11.5
10	11.5	11.0	11.6
20	11.5	11.4	11.6
30	11.5	11.2	11.7
50	11.5	11.4	11.6
70	11.2	11.3	11.5
90	10.4	10.9	10.7

4.2. Experimental Procedure

4.2.1. Emulsion Phase Behavior

Samples were prepared at 10 different alkali concentrations (0.5, 1, 2, 5, 10, 20, 30, 50, 70, and 90 wt% in aqueous phase) with 4 different salinities (0, 1,000, 30,000, and 100,000 ppm) for 3 different water-oil-ratios (WORs) (5:5, 7:3, and 9:1). Due to the aqueous phase stability, the maximum alkali concentration was limited to 70 wt% for 30,000 ppm brine, and 50 wt% for 100,000 ppm brine.

For each sample, 4-ml volume of sample was prepared in a 10-ml Pyrex pipette. The preparation procedure is as follows: First, the tip of a pipette was sealed by flame. Then, a specified volume of the brine, the alkali, and the bitumen was injected into the pipette. The bitumen was heated up to 80°C before injection to make it more mobile. After injecting all components, an argon gas was injected into the pipette as a blanket gas.

Finally, the neck of the pipette was sealed by flame. The samples were aged in an oven at 100°C for 3 weeks. During the aging period, samples were mixed 4 times a day. Then, samples were rested for 2 days before reporting emulsion phase behavior at 100°C.

The pH values after mixing indicated that all acidic components in bitumen had reacted with an alkali (**Table 4.2**). The minimum pH values (0.5 wt% alkali at WOR 5:5) were 9.9 for DEA, 9.7 for TETA, and 9.8 for pyrrolidine.

Table 4.2 pH of aqueous phase after mixing bitumen with 0.5 wt% alkali

0.5 wt% Alkali	pH	
	WOR 7:3	WOR 5:5
DEA	10.3	9.9
TETA	9.8	9.7
Pyrrolidine	10.2	9.8

Emulsion types (water-external and oil-external) were identified by several different methods: a visual observation, an emulsion volume, emulsion fluidity in the pipette, and the method used in Kumar et al. (2012). Kumar et al. (2012) determined emulsion types by putting emulsion droplets into deionized water and toluene each. They observed that oil-in-water (o/w) emulsion droplets spread in deionized water, but not in toluene. The opposite behavior was observed for water-in-oil (w/o) emulsions.

4.2.2. Viscosity and Bitumen Content in Emulsion

After the emulsion phase behavior scan, the viscosity and bitumen content in emulsions were measured for selected samples: 5 alkali concentrations (0.5, 2, 5, 50, and 90 wt% in aqueous phase) at 1,000 ppm and WOR 7:3. The salinity and WOR were

selected by considering typical operating conditions in the oil field from which the bitumen sample was taken for this research.

For this detailed analysis of specific emulsion samples, 8-ml of the sample was prepared in a 10-ml Pyrex pipette using the same preparation procedure of emulsion phase behavior. The phase behavior of these samples was observed at 3 different temperatures (25°C, 50°C, and 80°C) for DEA samples, and 4 different temperatures (25°C, 50°C, 80°C, and 100°C) for TETA and pyrrolidine samples.

The viscosity of an emulsion phase was measured by a rheometer (Model: ARES LS-1 from TA Instruments) with 50-mm diameter parallel bottom and upper plates at 3 different temperatures (25°C, 50°C, and 80°C). Viscosity measurement temperature was limited by the boiling temperature of each organic alkali.

For each viscosity measurement, an emulsion sample taken from a pipette was transferred on the bottom parallel plate of the rheometer. Different gap sizes were applied for different viscosity ranges by considering the maximum torque of this rheometer. The gap size was set to 0.4 mm for o/w emulsions, and 0.8 mm for w/o emulsions. The range of shear rates was from 0.1 to 100 sec^{-1}. The lower limit of torque during viscosity measurement was set to 0.74 μNm because measurements at lower torques might be unreliable. For each emulsion sample, an average viscosity was reported based on 2 - 4 times of repeated measurements.

The special care was taken as described in Tagavifar et al. (2018) to avoid any possible errors in the viscosity measurement using this particular rheometer. For each measurement, a new sample was used to prevent any alteration of emulsion rheology through experiencing high shear rates. Although it is ideal to measure viscosity right after the loading of a sample, samples were placed on the rheometer for several minutes during viscosity measurements at 50°C and 80°C to reach the target temperature.

To measure the amount of bitumen in o/w emulsions, hydrochloric acid (HCl) was added in the emulsion phase to separate bitumen. For 1 ml of the o/w emulsion, 2 ml of 3.5 molarity HCl solution was added. Then, the sample was stirred until transparent water was separated from bitumen along with the protonated alkali. Then, the volume of bitumen was obtained by measuring the volume of separated water. The material balance for the entire sample (2.4 ml of bitumen in the total sample of 8 ml) was confirmed for the determination of the bitumen amount in o/w emulsions. For w/o emulsions, the bitumen content in emulsion was not measured since bitumen was existing only in the emulsion phase.

4.3. Experiment Results

4.3.1. Emulsion Phase Behavior

Results of the emulsion phase behavior at 100°C are summarized in following figures: **Figure 4.2**, **Figure 4.3**, **Figure 4.4**, **Figure 4.5**, and **Figure 4.6** for DEA, **Figure 4.7**, **Figure 4.8**, **Figure 4.9**, **Figure 4.10**, and **Figure 4.11** for TETA, and **Figure 4.12**, **Figure 4.13**, **Figure 4.14**, **Figure 4.15**, and **Figure 4.16** for pyrrolidine. For samples with DEA, the phase behavior can be categorized into 7 types: 3 types for a single phase and 4 types for two phases. The single-phase types are “o/w emulsion”, “w/o emulsion”, and “diluted bitumen”. The two-phase types are “o/w emulsion with an excess oil phase”, “two o/w emulsions (bitumen-rich and water-rich)”, “w/o emulsion with an excess-water phase”, and “w/o emulsion with o/w emulsion”.

Emulsions with DEA were kinetically stable for at least 6 months, but not thermodynamically; hence, two co-existing o/w emulsions were formed through separation

of the bitumen-rich and water-rich o/w emulsions, resulting from flocculation of droplets in the water-continuous phase (Ballard et al. 2015; Bibette et al. 1992; Robins and Hibberd 1998). The droplet size of o/w emulsions created by DEA was measured with high resolution camera **(Figure 4.1).** It shows that most of the droplets were of a few microns. A similar emulsion droplet size distribution can be found at Kim et al. (2017), in which 90% of o/w emulsion droplets were smaller than 15 microns.

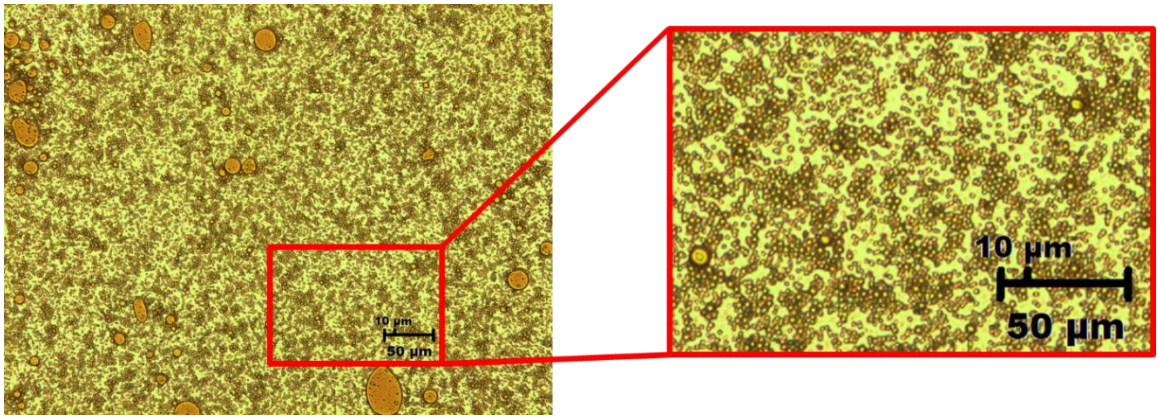

Figure 4.1 Emulsion droplet size (o/w emulsion created by DEA)

For samples with TETA, three types of phase behavior were observed: (1) a single-phase emulsion, (2) two emulsion phases, and (3) diluted bitumen with TETA. The first type, a single-phase emulsion, was "o/w emulsion". The two emulsion phases consisted of the "water-external and oil-external emulsions". However, different levels of solubilization in emulsion (oil in water and water in oil) made it possible to observe three sub-types: (2a) "o/w emulsion with an excess oil phase", (2b) "bitumen-rich w/o emulsion with water-rich o/w emulsion", and (2c) "w/o emulsion with an excess-water phase". The

third type of phase behavior was observed only for 90 wt% TETA samples, which was "diluted bitumen".

For samples with pyrrolidine, the phase behavior can be categorized into 5 types: 2 types for a single-phase and 3 types for two phases. The single-phase types are "o/w emulsion" and "diluted bitumen". The two-phase types are "o/w emulsion with an excess-oil phase", "w/o emulsion with an excess-water phase", and "bitumen-rich w/o emulsion with water-rich o/w emulsion".

Observations on emulsion phase behavior are as follows: First, o/w emulsion was dominant at low salinity (0 and 1,000 ppm) and w/o emulsion was dominant at high salinity (30,000 and 100,000 ppm). The inversion of emulsion types with increasing salinity was also observed in many literature (Al-Yaari et al. 2015; Bahmanabadi et al. 2016; Bera et al. 2012; Cooke et al. 1974; Fortenberry et al. 2015; Healy et al. 1976; Sharma et al. 2018). With increasing salinity, the interaction between water molecules and salt ions increases compared to that between water molecules and surfactants. As a result, the interfacial tension (IFT) between the emulsion and the oil decreases whereas the IFT between the emulsion and the water increases with increasing salinity, as experimentally shown by Bera et al. (2012) and Healy et al. (1976). Acevedo et al. (2001) observed in their experiment that the IFT between the oil and the aqueous solution increased with increasing NaCl concentrations, resulting in the disappearance of the ultra-low IFT region that existed at lower NaCl concentrations.

Second, o/w emulsions were dominant at low alkali concentrations, and w/o emulsion appeared with increasing alkali concentrations. At the alkali concentration of 90 wt%, single-phase bitumen was highly mobile, indicating a solvent-diluted bitumen phase. Winsor (1948) presented that the addition of water-soluble organic liquid can invert o/w emulsions to w/o emulsions. This kind of inversion was also found by Salager et al. (1982),

in which o/w emulsions were inverted into w/o emulsions with increasing pentanol concentration at a fixed salinity and WOR. Indeed, in this research, the inversion from the o/w emulsion to the w/o emulsion was observed with increasing the organic alkali concentration. This indicates that the excess amount of the organic alkali worked as a co-solvent in the system, and changed the emulsion type. Also, the optimal concentration of an organic alkali to induce o/w emulsification of bitumen could be low, e.g. as low as 0.5 wt%.

Third, with increasing WOR, o/w emulsions became lean in bitumen owing to a smaller amount of natural surfactants. The inversion from o/w emulsions to w/o emulsions with increasing WOR was studied in other studies (Bahmanabadi et al. 2016; Fortenberry et al. 2015; Sharma et al. 2018). The effect of WOR on the emulsion phase behavior depends on properties of the oil and therefore, the type of natural surfactants activated by alkalis. For example, Fortenberry et al. (2015) studied the effect of WOR on emulsion phase behavior with different co-solvents, where o/w emulsions became more dominant with increasing WOR.

In general, it was observed that the higher temperature was more favorable for creating the single-phase o/w emulsion. The effect of temperature on the emulsion phase behavior could be explained by the temperature effect on the IFT between the oil and the aqueous solution. However, the uncertainty in natural surfactant properties makes it difficult to give a systematic explanation of the temperature effect.

At a given surfactant concentration, IFT can either decrease or increase with increasing temperature depending on the salinity (Isaacs and Smolek 1983; Saki et al. 2017). At a given salinity, it was observed that IFT decreased up to a certain temperature and increased at higher temperatures (Ye et al. 2008). The IFT reduction between the bitumen and the surfactant solution with increasing temperature was measured by Isaacs and Smolek

(1983). In their experiment, the IFT between the bitumen and the surfactant solution was decreased from 50 to 100°C at the NaCl salinity range between 0 and 2,500 ppm. Natural surfactants in this research may have given a similar trend, in which the natural surfactants at 1,000 ppm NaCl brine decreased the IFT between bitumen and aqueous phase as the temperature increased from 25 to 100°C.

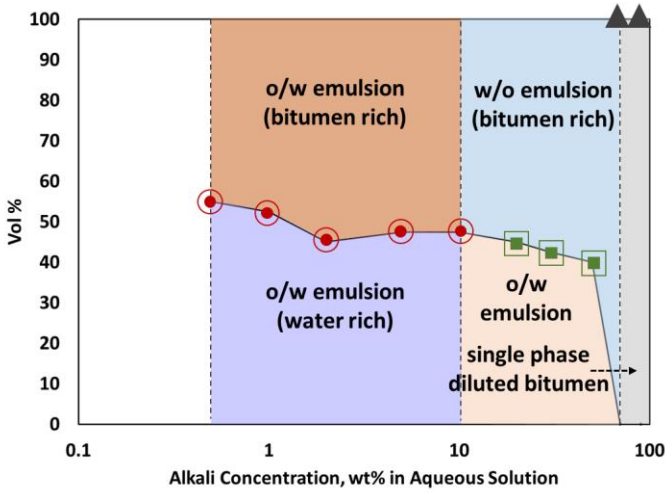

(a) Alkali: DEA, WOR 5:5, Salinity: 0 ppm

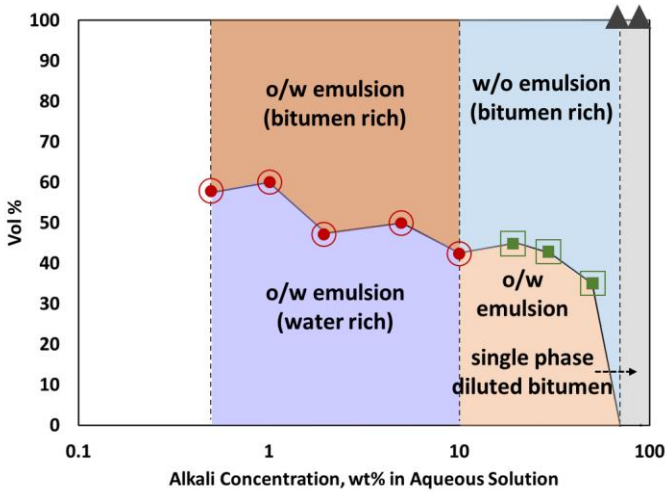

(b) Alkali: DEA, WOR 5:5, Salinity: 1,000 ppm

Figure 4.2 Emulsion phase behavior of DEA samples at WOR 5:5 and 100°C

At 0 ppm and 1,000 ppm, two o/w emulsions (bitumen-rich and water-rich) were observed up to 10 wt%. Two-phase w/o and o/w emulsions were observed from 20 wt%.

▲ : a single phase diluted bitumen
⦿ : oil-in-water emulsions (bitumen rich) with oil-in-water emulsions (water rich)
▣ : water-in-oil emulsions (bitumen rich) with oil-in-water emulsions (water rich)

Figure continued

Figure continued

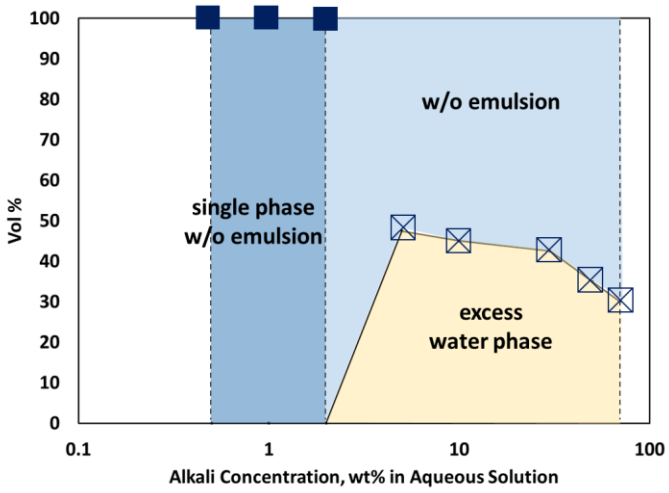

(c) Alkali: DEA, WOR 5:5, Salinity: 30,000 ppm

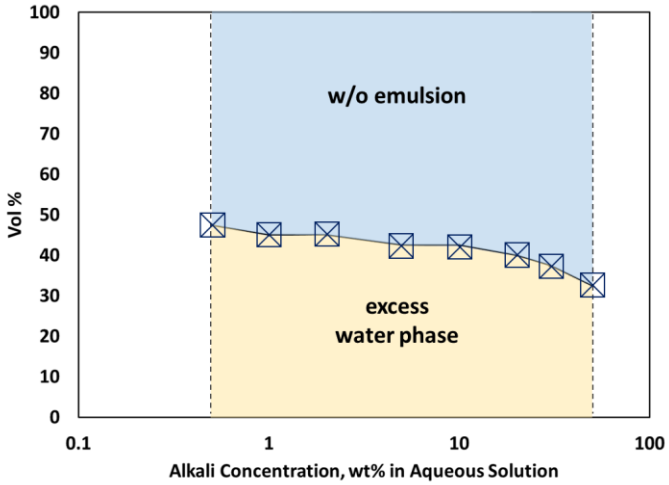

(d) Alkali: DEA, WOR 5:5, Salinity: 100,000 ppm

Figure 4.2 Emulsion phase behavior of DEA samples at WOR 5:5 and 100°C

For 30,000 ppm samples, a single phase w/o emulsion was observed at low DEA concentration up to 2 wt%. Otherwise, w/o emulsions with an excess water-rich phase were observed. For 100,000 ppm samples, w/o emulsions with an excess water-rich phase were observed.

■ : a single phase water-in-oil emulsion

⊠ : water-in-oil emulsions with excess water phase

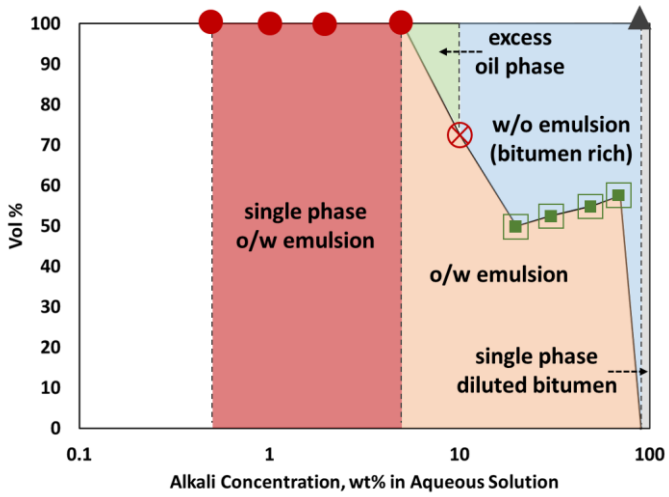

(a) Alkali: DEA, WOR 7:3, Salinity: 0 ppm

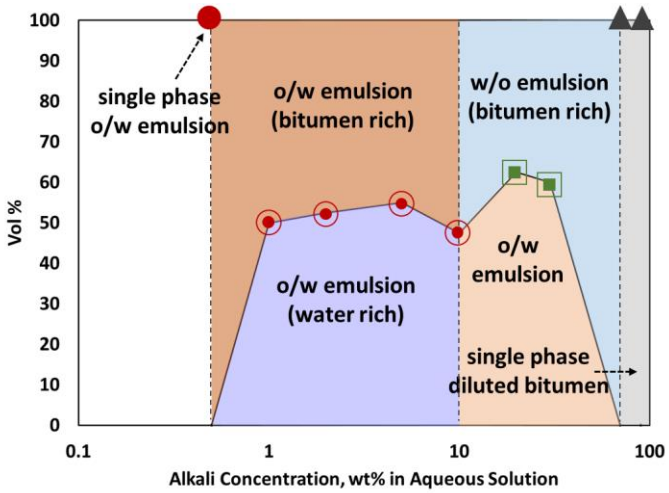

(b) Alkali: DEA, WOR 7:3, Salinity: 1,000 ppm

Figure 4.3 Emulsion phase behavior of DEA samples at WOR 7:3 and 100°C

Single-phase o/w emulsions were observed at low DEA concentrations. At 0 ppm, o/w emulsion with an excess oil phase was observed at 10 wt%. At 1,000 ppm, two o/w emulsions were observed up to 10 wt%.

- ● : a single phase oil-in-water emulsion
- ▲ : a single phase diluted bitumen
- ⊗ : oil-in-water emulsions with excess oil phase
- ⊙ : oil-in-water emulsions (bitumen-rich) with oil-in-water emulsions (water-rich)
- ▣ : water-in-oil emulsions (bitumen-rich) with oil-in-water emulsions (water-rich)

Figure continued

Figure continued

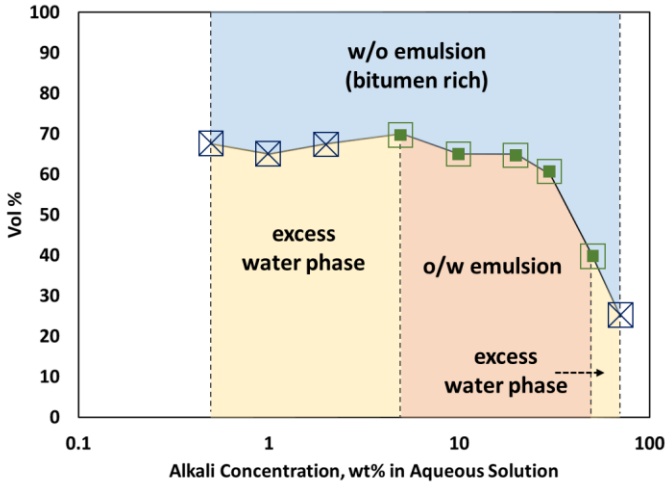

(c) Alkali: DEA, WOR 7:3, Salinity: 30,000 ppm

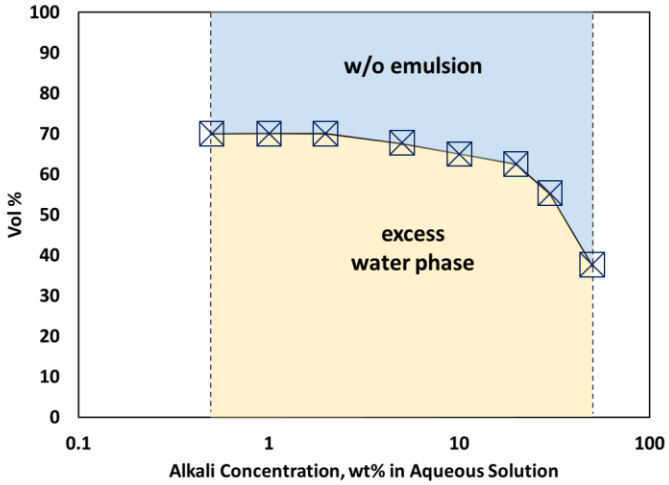

(d) Alkali: DEA, WOR 7:3, Salinity: 100,000 ppm

Figure 4.3 Emulsion phase behavior of DEA samples at WOR 7:3 and 100°C

For 30,000 ppm samples, w/o emulsion with o/w emulsion or excess water-rich phase were observed. For 100,000 ppm samples, w/o emulsions with excess water-rich phase were observed.

▣ : water-in-oil emulsions (bitumen-rich) with oil-in-water emulsions (water-rich)

⊠ : water-in-oil emulsions with excess water phase

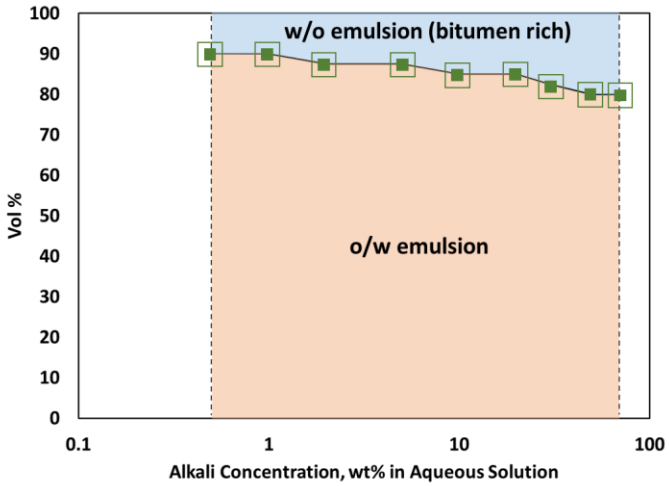

(a) Alkali: DEA, WOR 9:1, Salinity: 0 ppm

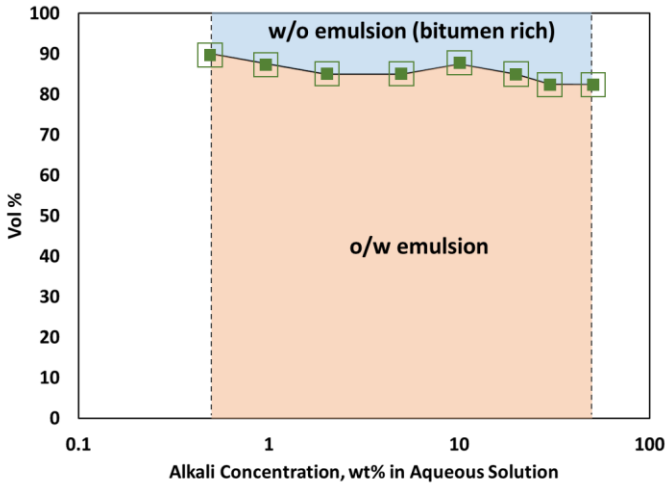

(b) Alkali: DEA, WOR 9:1, Salinity: 1,000 ppm

Figure 4.4 Emulsion phase behavior of DEA samples at WOR 9:1 and 100°C

Two phase w/o – o/w emulsions were observed for 0 ppm and 1,000 ppm samples.
▣ : water-in-oil emulsions (bitumen rich) with oil-in-water emulsions (water rich)

Figure continued

Figure continued

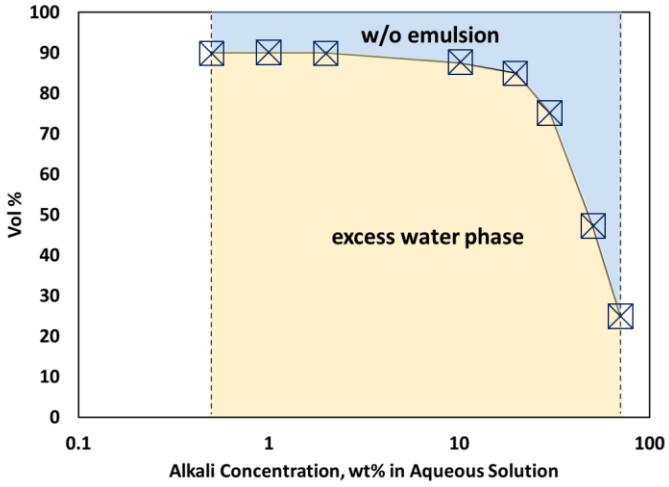

(c) Alkali: DEA, WOR 9:1, Salinity: 30,000 ppm

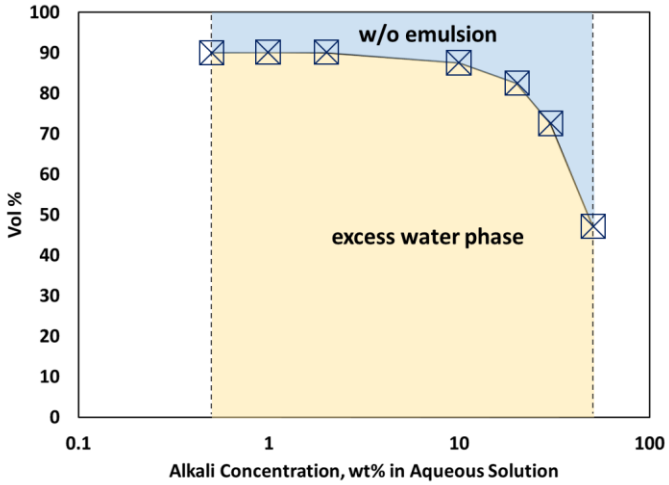

(d) Alkali: DEA, WOR 9:1, Salinity: 100,000 ppm

Figure 4.4 Emulsion phase behavior of DEA samples at WOR 9:1 and 100°C

For 30,000 ppm and 100,000 ppm samples, w/o emulsions with excess water-rich phase were observed.

⊠ : water-in-oil emulsions with excess water phase

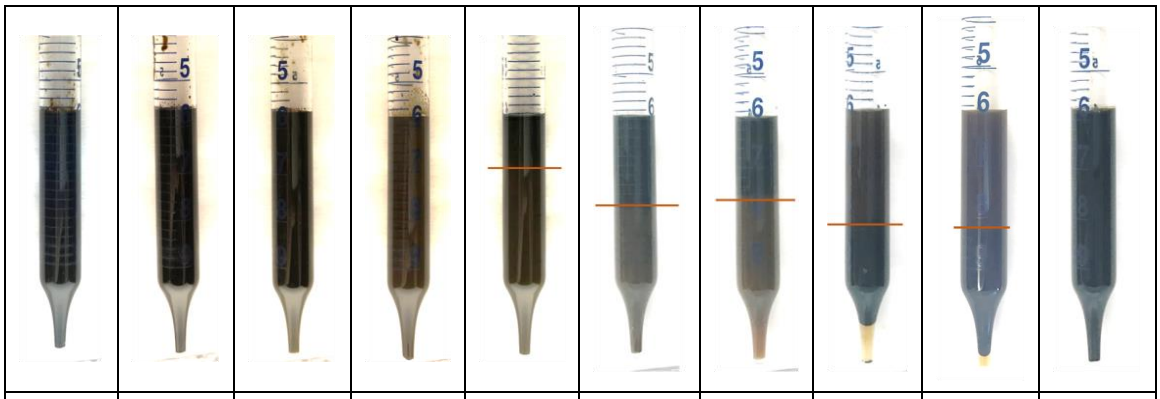

0.5 wt%	1 wt%	2 wt%	5 wt%	10 wt%	20 wt%	30 wt%	50 wt%	70 wt%	90 wt%

Figure 4.5 Emulsion phase behavior at different DEA concentrations: 0 ppm salinity, WOR 7:3, 100°C

From 0.5 wt% to 5 wt%, the single-phase o/w emulsion was created. The o/w emulsion with the excess oil phase were observed at 10 wt%. From 20 wt% to 70 wt%, the w/o emulsion (bitumen-rich) with the o/w emulsion (water-rich) were observed.

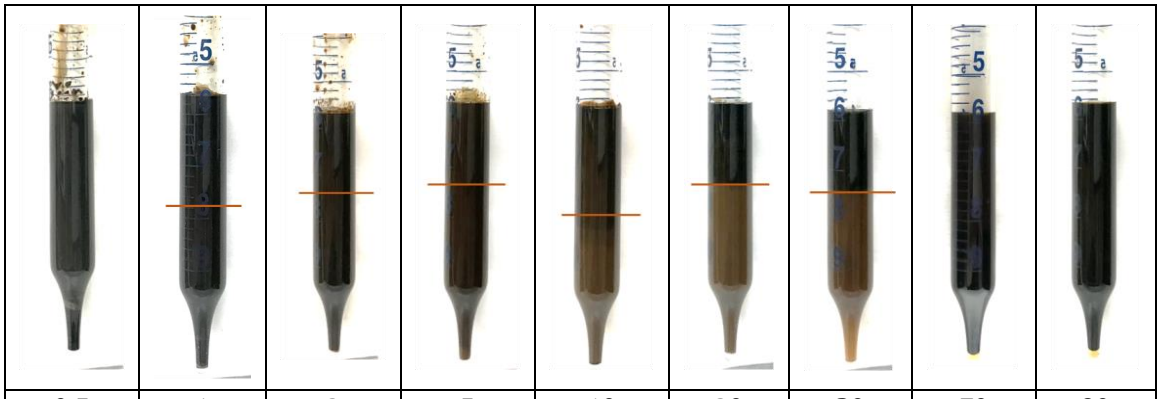

0.5 wt%	1 wt%	2 wt%	5 wt%	10 wt%	20 wt%	30 wt%	70 wt%	90 wt%

Figure 4.6 Emulsion phase behavior at different DEA concentrations: 1,000 ppm salinity, WOR 7:3, 100°C

For 0.5 wt%, the single-phase o/w emulsion was created. Two o/w emulsions (bitumen-rich and water-rich) were observed up to 10 wt%. From 20 wt% to 30 wt%, w/o emulsions (bitumen-rich) with o/w emulsion (water-rich) were observed.

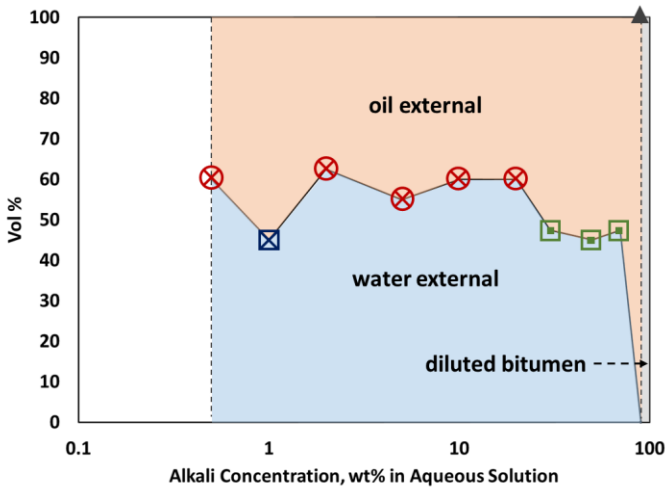

(a) Alkali: TETA, WOR 5:5, Salinity: 0 ppm

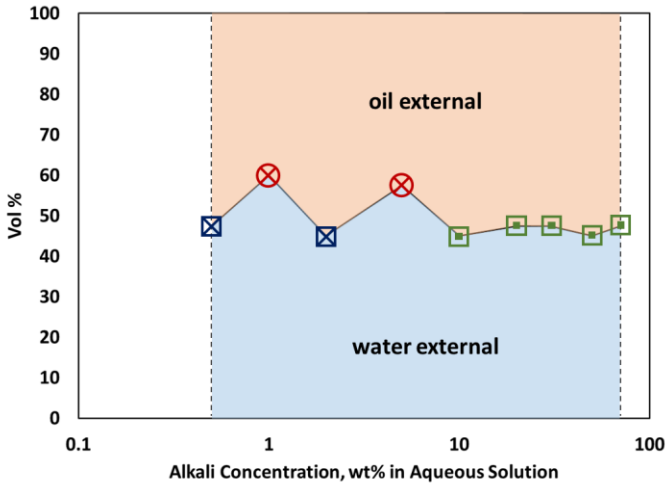

(b) Alkali: TETA, WOR 5:5, Salinity: 1,000 ppm

Figure 4.7 Emulsion phase behavior of TETA samples at WOR 5:5 and 100°C

At 0 ppm, o/w emulsions were observed up to 20 wt% except the w/o emulsion at 1 wt%. At 1,000 ppm, o/w emulsions were observed at 1 wt% and 5 wt%, and w/o emulsions were observed at 0.5 wt% and 2 wt%. Other than those points, w/o emulsion (bitumen rich) with o/w emulsions (water-rich) were observed.

⊗ : oil-in-water emulsions with excess oil phase
⊠ : water-in-oil emulsions with excess water phase
▣ : water-in-oil emulsions (bitumen rich) with oil-in-water emulsions (water rich)
▲ : diluted bitumen

Figure continued

Figure continued

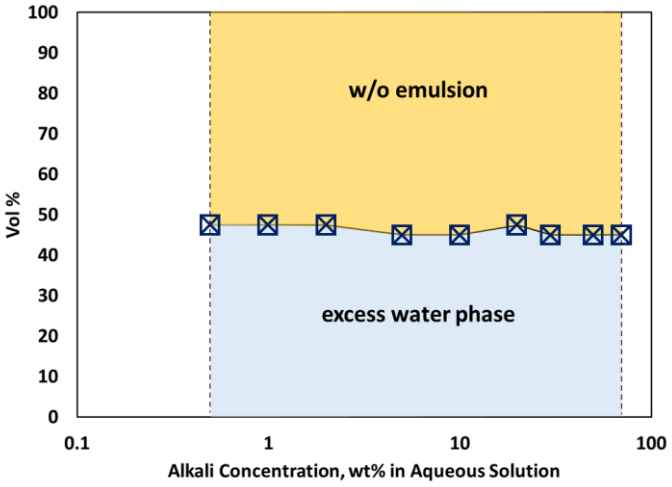

(c) Alkali: TETA, WOR 5:5, Salinity: 30,000 ppm

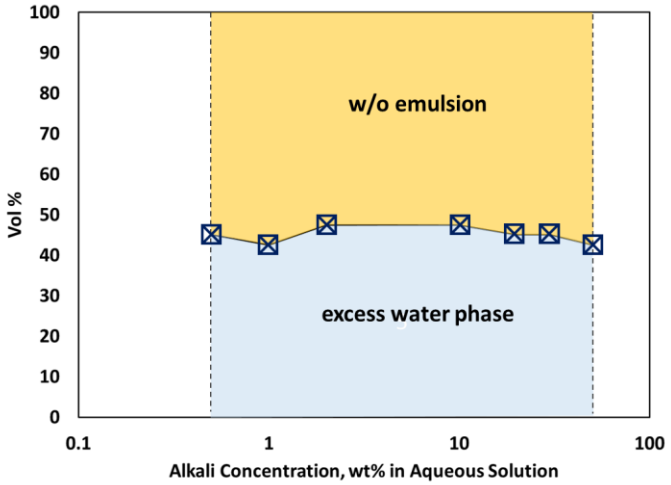

(d) Alkali: TETA, WOR 5:5, Salinity: 100,000 ppm

Figure 4.7 Emulsion phase behavior of TETA samples at WOR 5:5 and 100°C

For 30,000 ppm and 100,000 ppm, all samples showed w/o emulsions with excess water phase.

☒ : water-in-oil emulsions with excess water phase

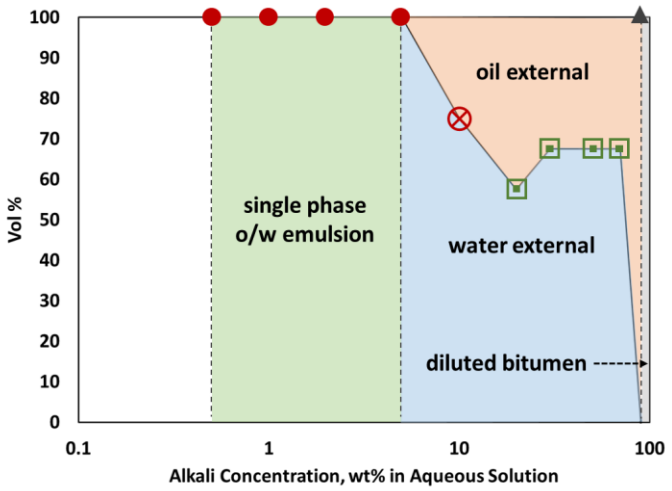

(a) Alkali: TETA, WOR 7:3, Salinity: 0 ppm

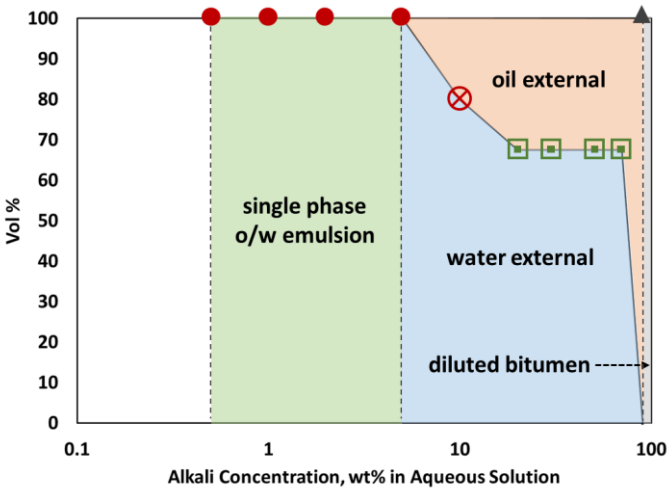

(b) Alkali: TETA, WOR 7:3, Salinity: 1,000 ppm

Figure 4.8 Emulsion phase behavior of TETA samples at WOR 7:3 and 100°C

Single-phase o/w emulsions were observed up to 5 wt% at 0 ppm and 1,000 ppm. At 10 wt%, o/w emulsions with excess oil phase were observed. From 20 wt%, w/o emulsion (bitumen rich) with o/w emulsions (water-rich) were observed.

- ● : a single phase oil-in-water emulsion
- ⊗ : oil-in-water emulsions with excess oil phase
- ▣ : water-in-oil emulsions (bitumen-rich) with oil-in-water emulsions (water-rich)
- ▲ : diluted bitumen

Figure continued

Figure continued

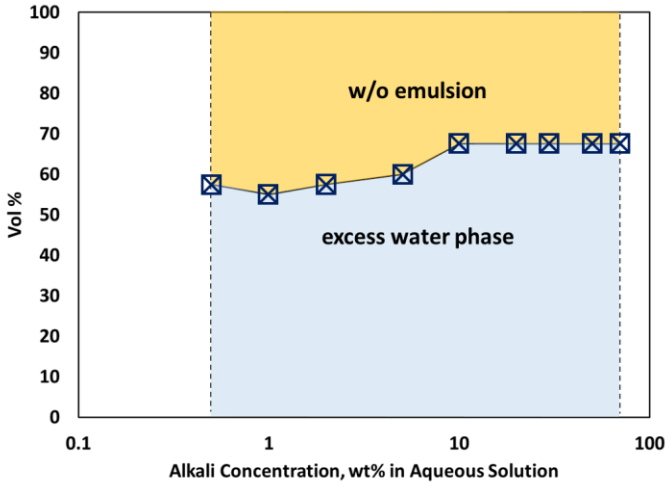

(c) Alkali: TETA, WOR 7:3, Salinity: 30,000 ppm

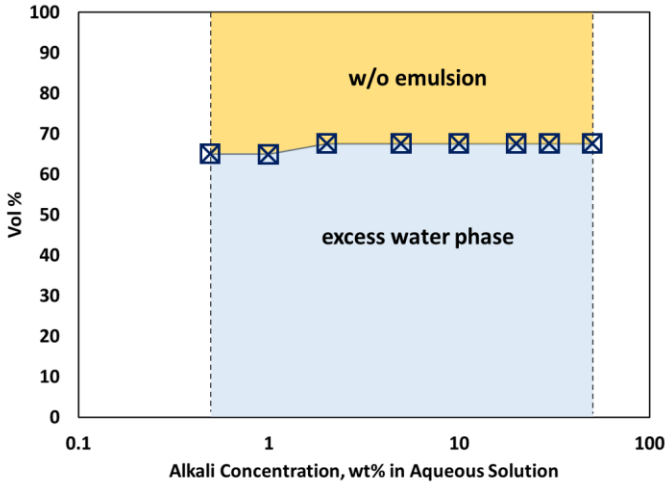

(d) Alkali: TETA, WOR 7:3, Salinity: 100,000 ppm

Figure 4.8 Emulsion phase behavior of TETA samples at WOR 7:3 and 100°C

For 30,000 ppm and 100,000 ppm, all samples showed w/o emulsions with excess water phase.

☒ : water-in-oil emulsions with excess water phase

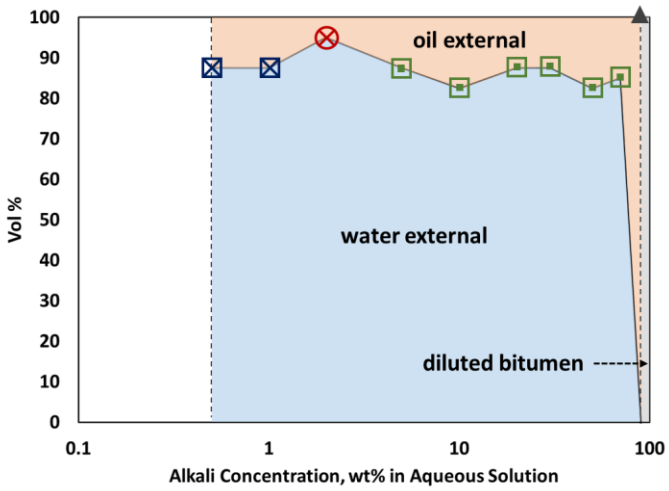

(a) Alkali: TETA, WOR 9:1, Salinity: 0 ppm

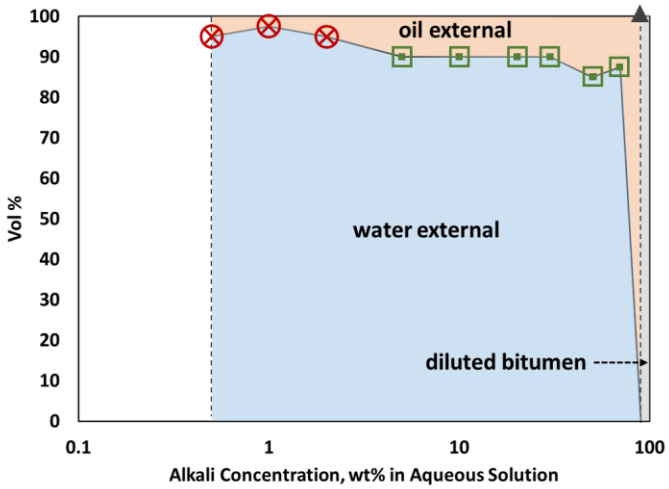

(b) Alkali: TETA, WOR 9:1, Salinity: 1,000 ppm

Figure 4.9 Emulsion phase behavior of TETA samples at WOR 9:1 and 100°C

At 0 ppm, w/o emulsions with excess water phase were observed at 0.5 wt% and 1 wt%. At 2 wt%, o/w emulsions with excess oil phase were observed. From 5 wt%, w/o emulsion (bitumen rich) with o/w emulsions (water-rich) were observed. At 1,000 ppm, o/w emulsions with excess oil phase were observed up to 2 wt%. From 5 wt%, w/o emulsion (bitumen rich) with o/w emulsions (water-rich) were observed.

⊗ : oil-in-water emulsions with excess oil phase
▣ : water-in-oil emulsions (bitumen-rich) with oil-in-water emulsions (water-rich)
⊠ : water-in-oil emulsions with excess water phase
▲ : diluted bitumen

Figure continued

Figure continued

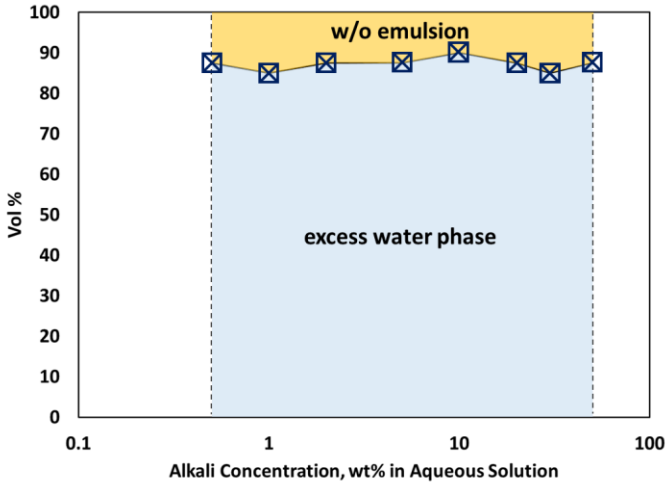

(c) Alkali: TETA, WOR 9:1, Salinity: 30,000 ppm

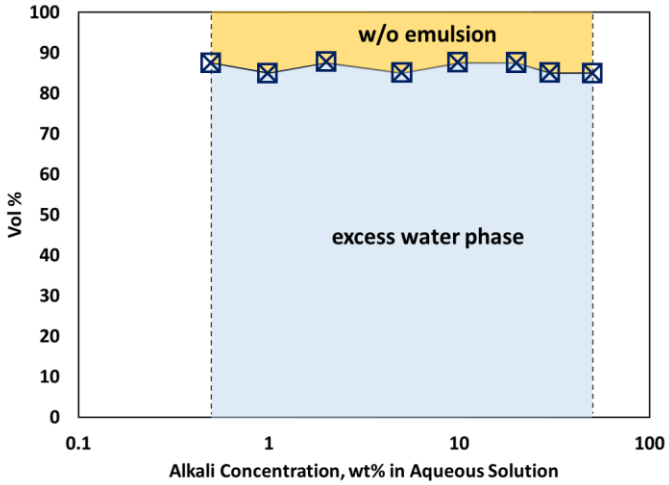

(d) Alkali: TETA, WOR 9:1, Salinity: 100,000 ppm

Figure 4.9 Emulsion phase behavior of TETA samples at WOR 9:1 and 100°C

For 30,000 ppm and 100,000 ppm, all samples showed w/o emulsions with excess water phase.

☒ : water-in-oil emulsions with excess water phase

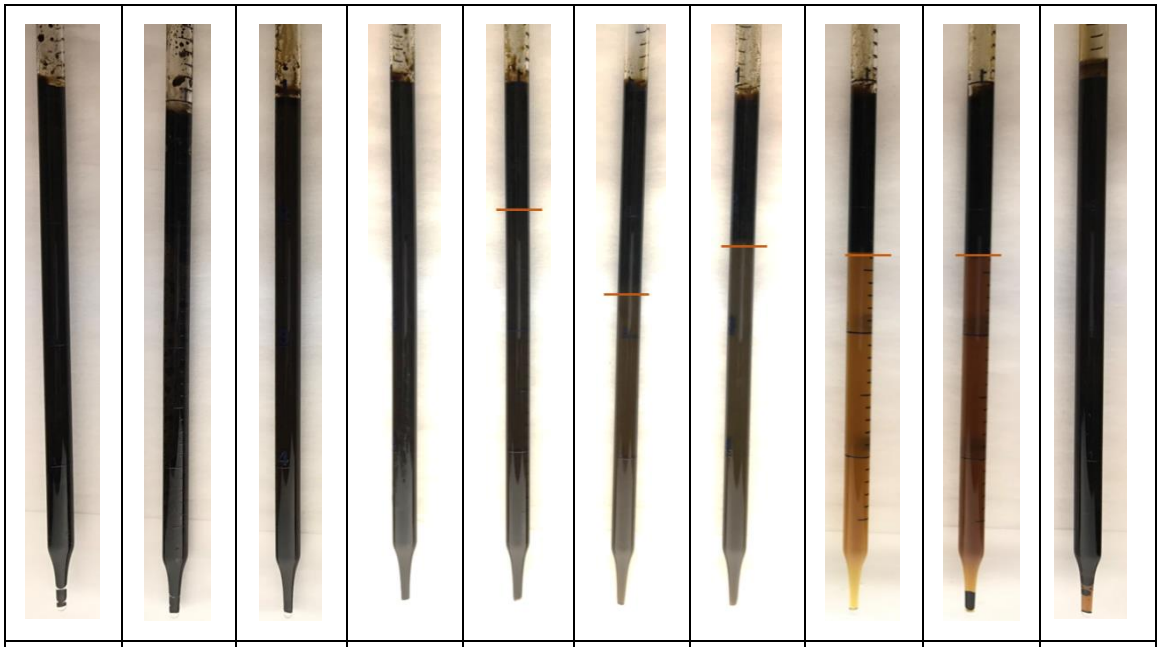

0.5 wt%	1 wt%	2 wt%	5 wt%	10 wt%	20 wt%	30 wt%	50 wt%	70 wt%	90 wt%

Figure 4.10 Emulsion phase behavior at different TETA concentrations: 0 ppm salinity, WOR 7:3, 100°C

From 0.5 wt% to 5 wt%, a single-phase o/w emulsion was created. The o/w emulsion with the excess oil phase was observed at 10 wt%. From 20 wt% to 70 wt%, w/o emulsions (bitumen-rich) with o/w emulsion (water-rich) were observed.

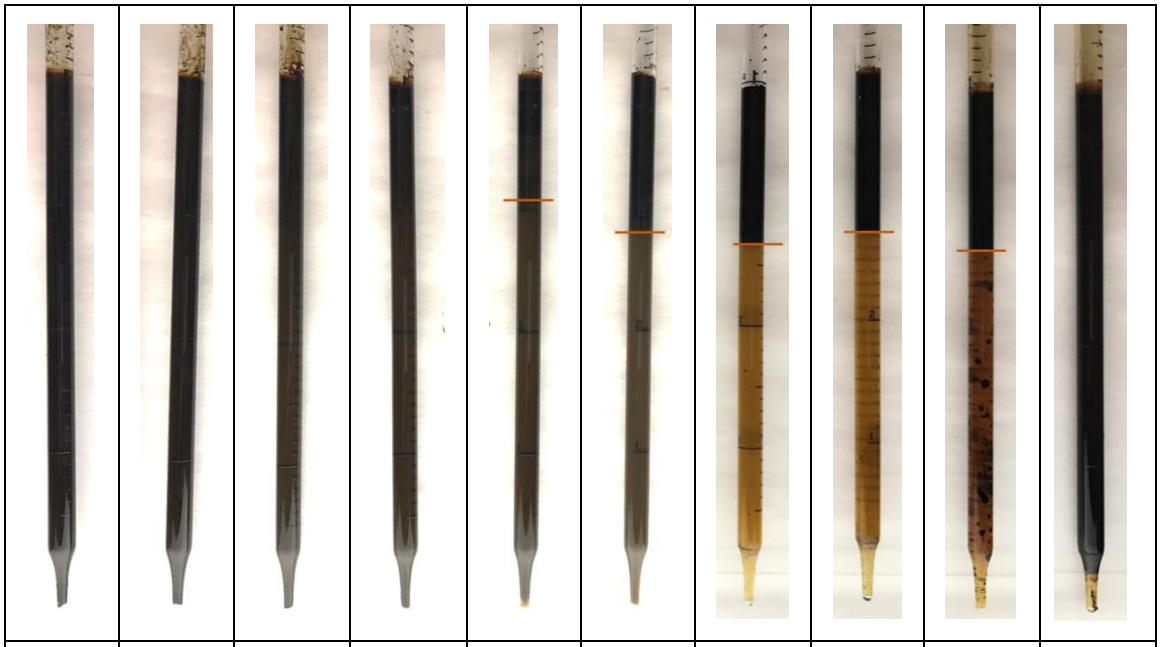

0.5 wt%	1 wt%	2 wt%	5 wt%	10 wt%	20 wt%	30 wt%	50 wt%	70 wt%	90 wt%

Figure 4.11 Emulsion phase behavior at different TETA concentrations: 1,000 ppm salinity, WOR 7:3, 100°C

From 0.5 wt% to 5 wt%, a single-phase o/w emulsion was created. The o/w emulsion with the excess oil phase was observed at 10 wt%. From 20 wt% to 70 wt%, w/o emulsions (bitumen-rich) with o/w emulsion (water-rich) were observed.

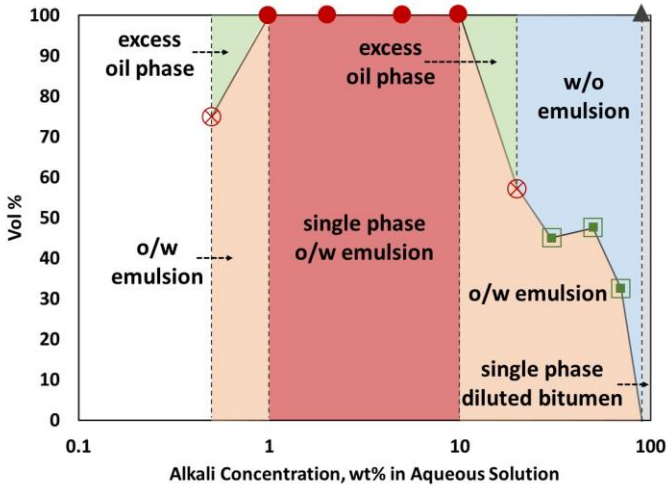

(a) Alkali: Pyrrolidine, WOR 5:5, Salinity: 0 ppm

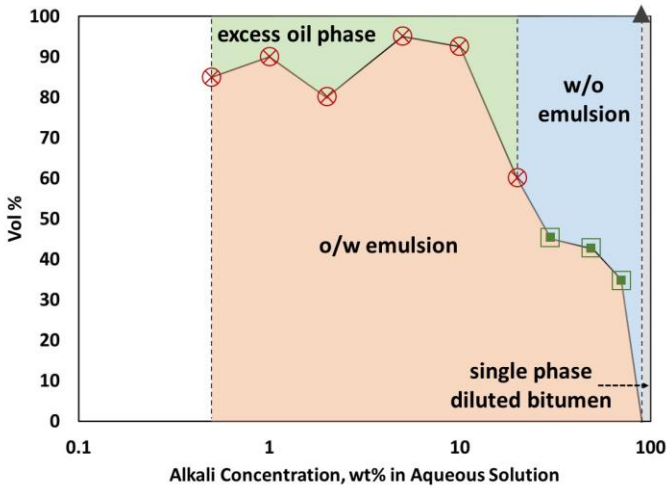

(b) Alkali: Pyrrolidine, WOR 5:5, Salinity: 1,000 ppm

Figure 4.12 Emulsion phase behavior of pyrrolidine samples at WOR 5:5 and 100°C

Single-phase o/w emulsions were observed at 0 ppm. At low salinities (0 and 1,000 ppm), o/w emulsions with excess oil phase were dominant below 20 wt% pyrrolidine concentration.

- ● : single-phase oil-in-water emulsion
- ⊗ : oil-in-water emulsions with excess oil phase
- ▣ : water-in-oil emulsions (bitumen-rich) with oil-in-water emulsions (water-rich)
- ▲ : diluted bitumen

Figure continued

Figure continued

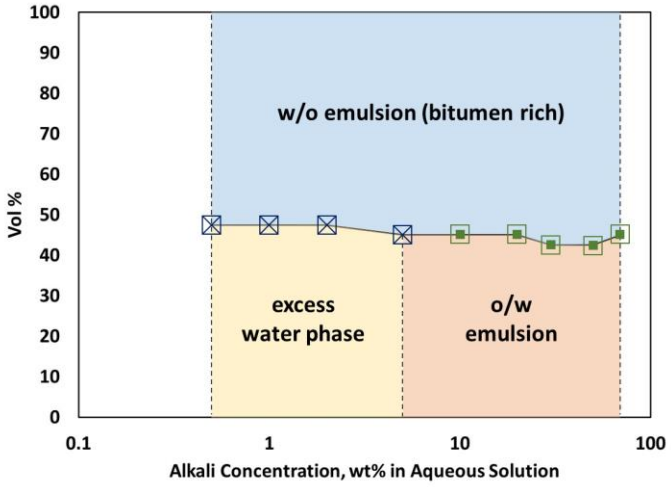

(c) Alkali: Pyrrolidine, WOR 5:5, Salinity: 30,000 ppm

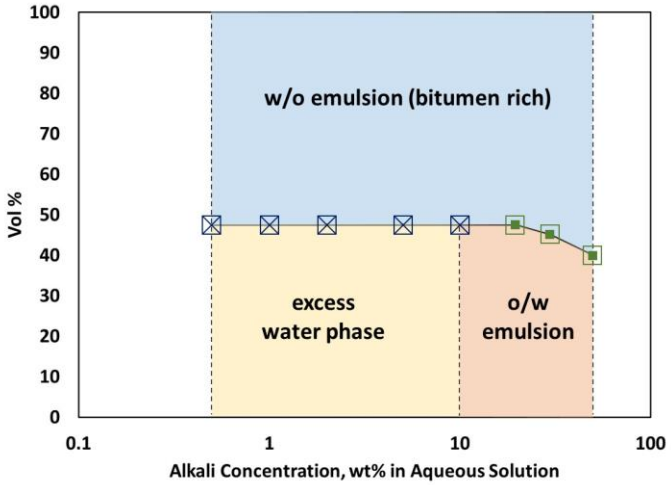

(d) Alkali: Pyrrolidine, WOR 5:5, Salinity: 100,000 ppm

Figure 4.12 Emulsion phase behavior of pyrrolidine samples at WOR 5:5 and 100°C

At higher salinities (30,000 and 100,000 ppm), bitumen-rich w/o emulsions were dominant over o/w emulsions.

▣ : water-in-oil emulsions (bitumen-rich) with oil-in-water emulsions (water-rich)

☒ : water-in-oil emulsions with excess water phase

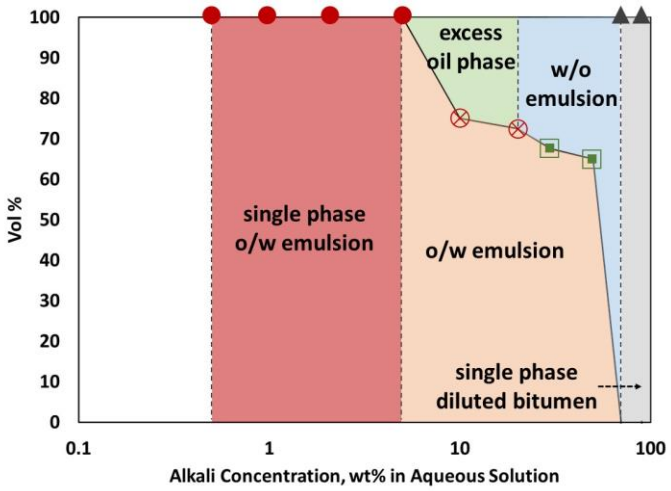

(a) Alkali: Pyrrolidine, WOR 7:3, Salinity: 0 ppm

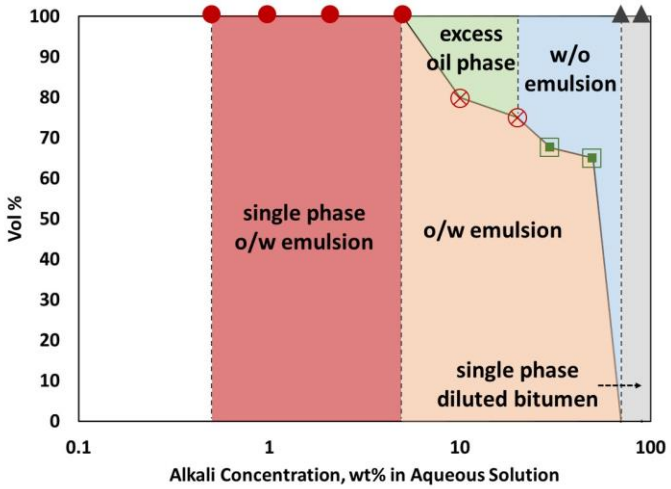

(b) Alkali: Pyrrolidine, WOR 7:3, Salinity: 1,000 ppm

Figure 4.13 Emulsion phase behavior of pyrrolidine samples at WOR 7:3 and 100°C

At low salinities (0 and 1,000 ppm), single-phase o/w emulsions were observed from 0.5 to 5 wt% pyrrolidine concentration. The o/w emulsion with the excess oil phase was dominant below 20 wt% pyrrolidine concentration.

● : single-phase oil-in-water emulsion
⊗ : oil-in-water emulsions with excess oil phase
▣ : water-in-oil emulsions (bitumen-rich) with oil-in-water emulsions (water-rich)
▲ : diluted bitumen

Figure continued

Figure continued

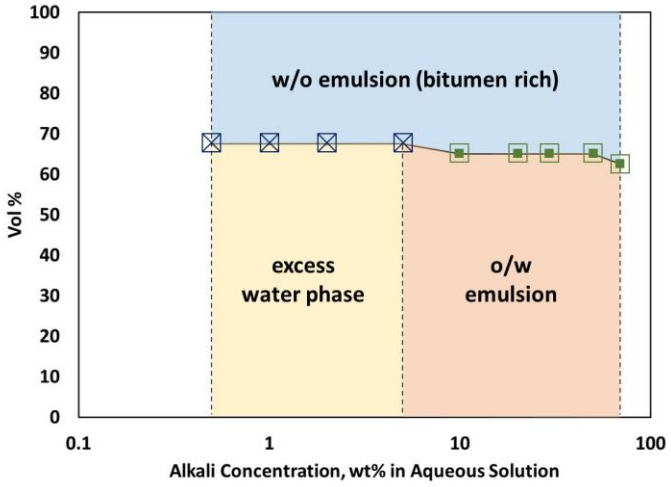

(c) Alkali: Pyrrolidine, WOR 7:3, Salinity: 30,000 ppm

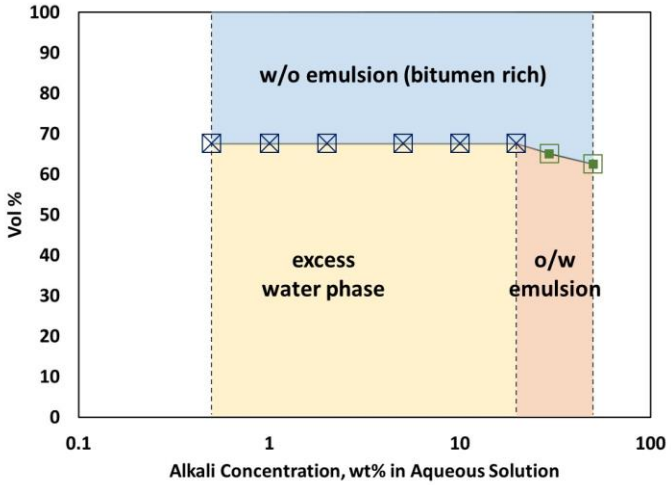

(d) Alkali: Pyrrolidine, WOR 7:3, Salinity: 100,000 ppm

Figure 4.13 Emulsion phase behavior of pyrrolidine samples at WOR 7:3 and 100°C

At higher salinities (30,000 and 100,000 ppm), bitumen-rich w/o emulsions were dominant over o/w emulsions.

▣ : water-in-oil emulsions (bitumen-rich) with oil-in-water emulsions (water-rich)

☒ : water-in-oil emulsions with excess water phase

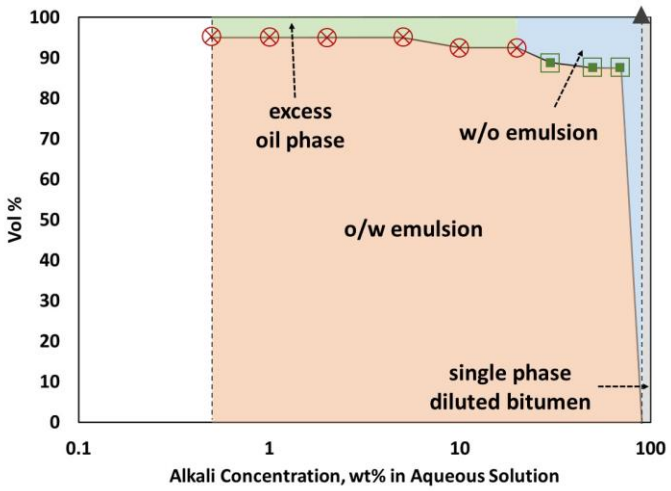

(a) Alkali: Pyrrolidine, WOR 9:1, Salinity: 0 ppm

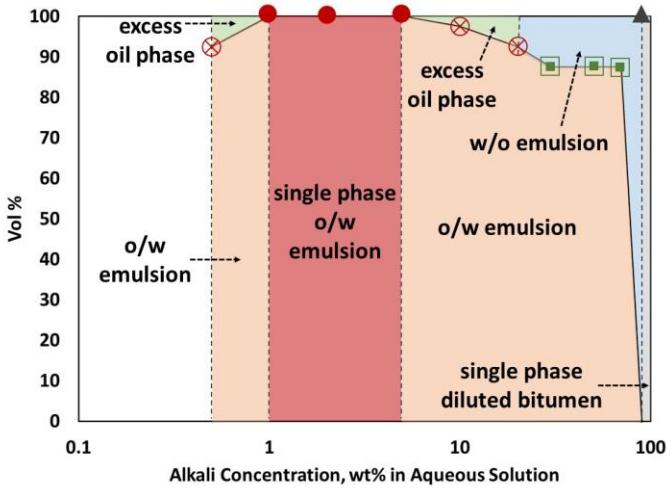

(b) Alkali: Pyrrolidine, WOR 9:1, Salinity: 1,000 ppm

Figure 4.14 Emulsion phase behavior of pyrrolidine samples at WOR 9:1 and 100°C

Single-phase o/w emulsions were observed at 1,000 ppm. At low salinities (0 and 1,000 ppm), the o/w emulsion with the excess oil phase was dominant below 20 wt% pyrrolidine concentration.

- ● : single-phase oil-in-water emulsion
- ⊗ : oil-in-water emulsions with excess oil phase
- ▣ : water-in-oil emulsions (bitumen-rich) with oil-in-water emulsions (water-rich)
- ▲ : diluted bitumen

Figure continued

Figure continued

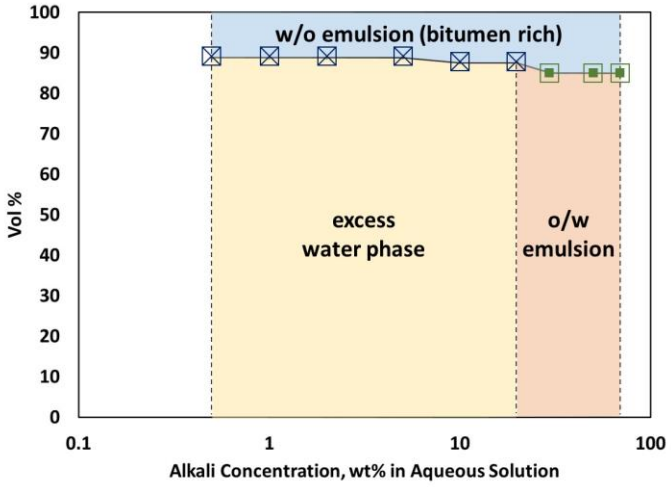

(c) Alkali: Pyrrolidine, WOR 9:1, Salinity: 30,000 ppm

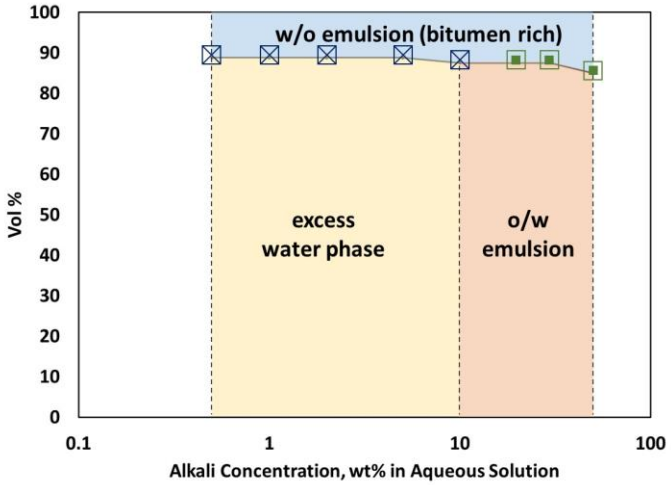

(d) Alkali: Pyrrolidine, WOR 9:1, Salinity: 100,000 ppm

Figure 4.14 Emulsion phase behavior of pyrrolidine samples at WOR 9:1 and 100°C

At higher salinities (30,000 and 100,000 ppm), bitumen-rich w/o emulsions were dominant over o/w emulsions.

▣ : water-in-oil emulsions (bitumen-rich) with oil-in-water emulsions (water-rich)

☒ : water-in-oil emulsions with excess water phase

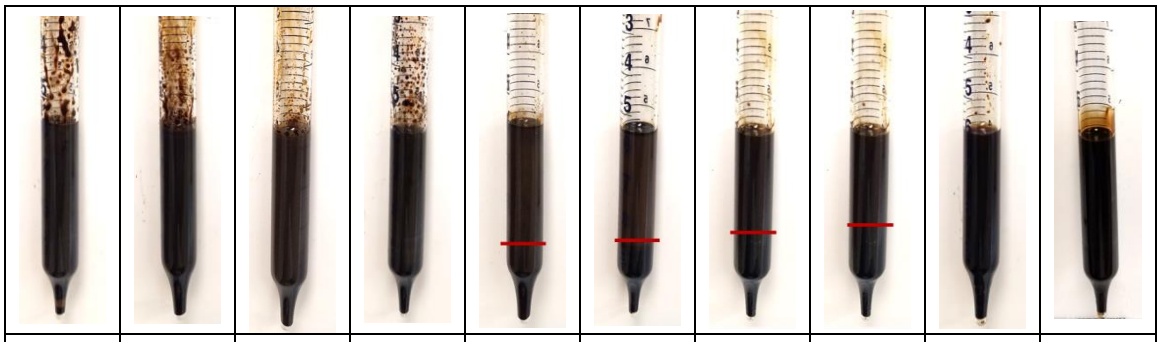

0.5 wt%	1 wt%	2 wt%	5 wt%	10 wt%	20 wt%	30 wt%	50 wt%	70 wt%	90 wt%

Figure 4.15 Emulsion phase behavior at different pyrrolidine concentrations: 0 ppm salinity, WOR 7:3, 100°C

From 0.5 to 5 wt% of pyrrolidine, a single-phase o/w emulsion was created. At 10 and 20 wt%, the o/w emulsion with the excess oil phase was observed. At 30 and 50 wt%, w/o emulsions (bitumen-rich) with o/w emulsion (water-rich) were observed. Note that even a small amount of bitumen in the aqueous phase can make o/w emulsions very dark. Above 70 wt%, bitumen was diluted by the pyrrolidine solution.

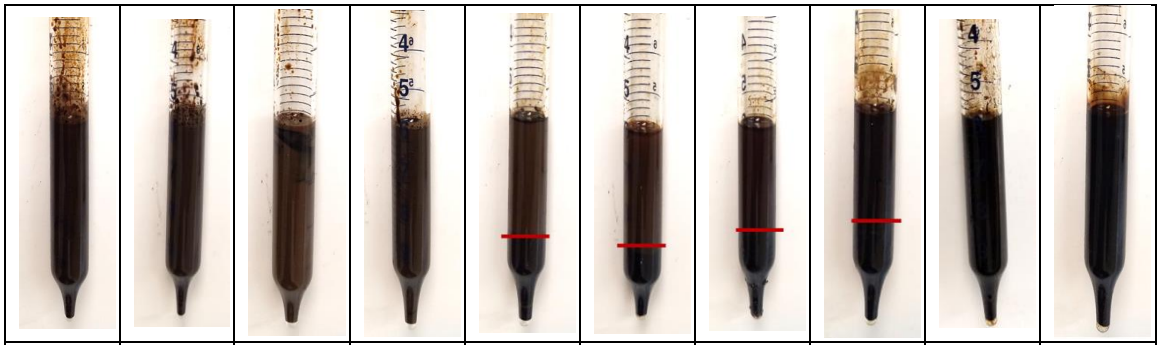

0.5 wt%	1 wt%	2 wt%	5 wt%	10 wt%	20 wt%	30 wt%	50 wt%	70 wt%	90 wt%

Figure 4.16 Emulsion phase behavior at different pyrrolidine concentrations: 1,000 ppm salinity, WOR 7:3, 100°C

From 0.5 to 5 wt% of pyrrolidine, a single-phase o/w emulsion was created. At 10 and 20 wt%, o/w emulsions with an excess oil phase were observed. At 30 and 50 wt%, w/o emulsions (bitumen-rich) with o/w emulsion (water-rich) were observed. Note that even a small amount of bitumen in the aqueous phase can make o/w emulsions very dark. Above 70 wt%, bitumen was diluted by the pyrrolidine solution.

4.3.2. The Amount of Bitumen in Emulsions

The phase behavior and the bitumen content of these samples are presented in **Figure 4.17** for DEA, **Figure 4.18** and **Table 4.3** for TETA, and **Figure 4.19** and **Table 4.4** for pyrrolidine. For DEA samples, there were two emulsions at these conditions: bitumen-rich and water-rich o/w emulsions. After demulsification, the measurement of oil content in each emulsion showed that the bitumen content in the water-rich emulsion was too small to be measured. Note that the color of bitumen in this research is complete black. Therefore, even a very small amount bitumen dissolve in water-rich emulsion could result in an opaque phase. Essentially, the entire volume of the bitumen (i.e. 2.4 ml) in the total 8-ml sample was measured in the bitumen-rich o/w emulsion, the volume of which was 3.3 - 3.4 ml at 0.5 - 5 wt% DEA at 25°C, and 3.6 - 4.2 ml at 0.5 - 5 wt% DEA at 50°C. That is, the oil contents in these water-external emulsions were more than 70 vol% at 25°C and 57 vol% at 50°C.

For TETA samples, the o/w emulsion at 2 wt% TETA showed the highest bitumen concentration among the three TETA concentrations. Also, the bitumen concentration in emulsion tends to increase with increasing temperature. As a result, the o/w emulsion at 2 wt% TETA at 80°C is a single phase containing all the bitumen.

For pyrrolidine samples, a single-phase o/w emulsion was created with 0.5 wt% pyrrolidine sample for all temperatures. These emulsion samples have the maximum bitumen content, 2.4 ml, which is 30% of the entire emulsion volume. At pyrrolidine concentration of 2 wt% and 5 wt%, the o/w emulsion with the excess oil phase was observed. The amount of the excess oil phase decreased with increasing temperature. At 100°C, the excess oil phase was not observed as the bitumen was completely emulsified in water.

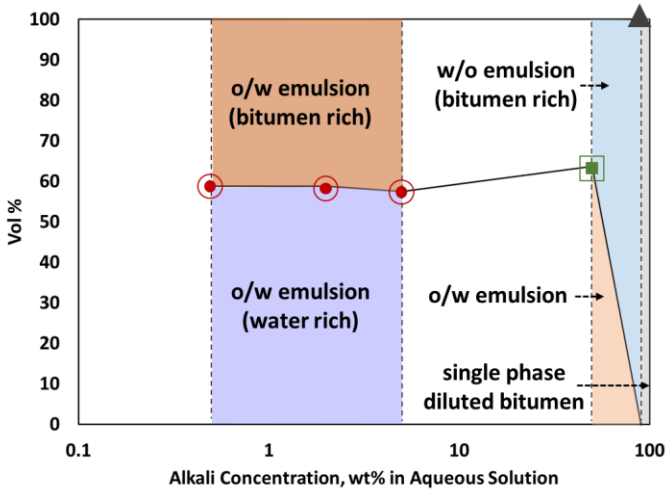

(a) Alkali: DEA, WOR 7:3, Salinity: 1,000 ppm, Temperature: 25°C

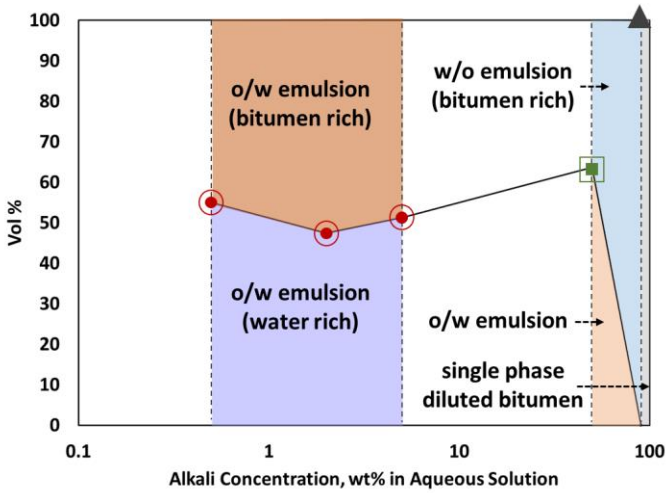

(b) Alkali: DEA, WOR 7:3, Salinity: 1,000 ppm, Temperature: 50°C

Figure 4.17 Phase Behavior of emulsions with DEA at 25°C and 50°C

A single-phase o/w emulsion was not observed. Two o/w (bitumen-rich and water-rich) emulsions were observed up to 5 wt% DEA concentration. Essentially, the entire volume of the bitumen (2.4 ml) in the total 8-ml sample was measured in the bitumen-rich o/w emulsion.

▲ : a single phase diluted bitumen

◉ : oil-in-water emulsions (bitumen rich) with oil-in-water emulsions (water rich)

▣ : water-in-oil emulsions (bitumen rich) with oil-in-water emulsions (water rich)

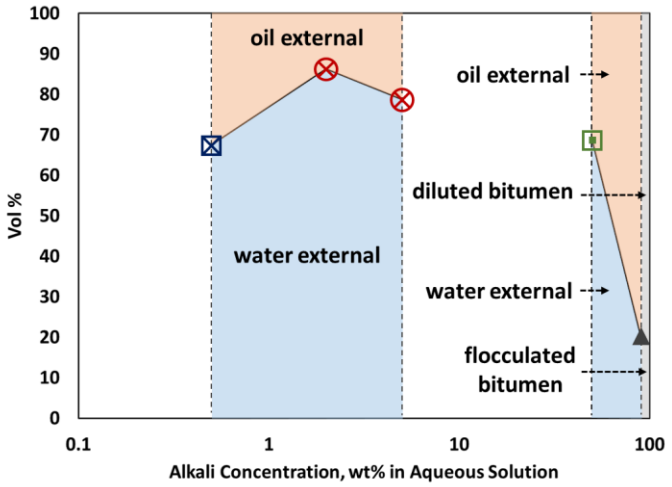

(a) Alkali: TETA, WOR 7:3, Salinity: 1,000 ppm, Temperature: 25°C

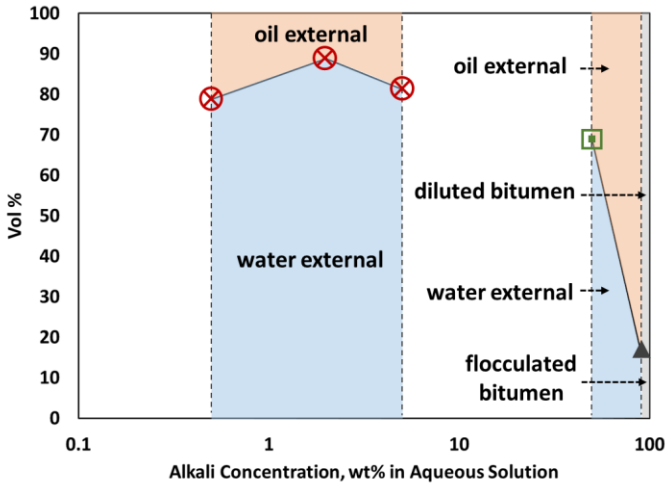

(b) Alkali: TETA, WOR 7:3, Salinity: 1,000 ppm, Temperature: 50°C

Figure 4.18 Phase Behavior of emulsions with TETA at 25°C, 50°C, and 80°C

● : a single phase oil-in-water emulsion
⊗ : oil-in-water emulsions with excess oil phase
▣ : water-in-oil emulsions (bitumen-rich) with oil-in-water emulsions (water-rich)
▲ : diluted bitumen

Figure continued

Figure continued

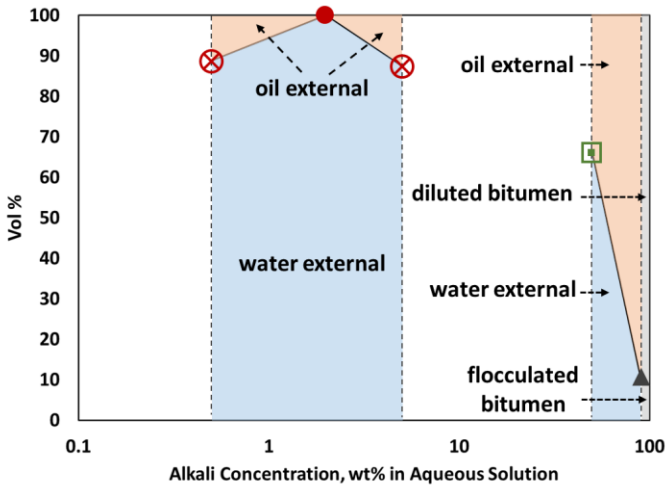

(c) Alkali: TETA, WOR 7:3, Salinity: 1,000 ppm, Temperature: 80°C

Figure 4.18 Phase Behavior of emulsions with TETA at 25°C, 50°C, and 80°C

At 25°C, the w/o emulsion with the excess water phase was observed at 0.5 wt%, and the o/w emulsion with the excess oil phase was observed at 2 wt% and 5 wt%. At 50°C, the o/w emulsion with the excess oil phase was observed at 0.5 wt%, 2 wt% and 5 wt%. At 80°C, the single phase o/w emulsion was observed only at 2 wt%, and the o/w emulsion with the excess oil phase was observed at 0.5 wt% and 5 wt%. For 90 wt% at all temperatures, inhomogenously diluted bitumen resulted in a small amount of flocculated bitumen at the bottom.

● : a single phase oil-in-water emulsion
⊗ : oil-in-water emulsions with excess oil phase
▣ : water-in-oil emulsions (bitumen-rich) with oil-in-water emulsions (water-rich)
▲ : diluted bitumen

Table 4.3 Bitumen amount in emulsions for TETA samples (Salinity 1,000 ppm, WOR 7:3)

The amount of bitumen is 2.4 ml in the total of 8 ml of each sample. Samples with 2 wt% TETA show the highest concentration of bitumen in o/w emulsions for all temperatures.

a. Temperature 25°C

TETA Concentration [wt%]	Emulsion Type	Emulsion Volume [ml]	Volumetric Composition of Emulsion			
			Bitumen		Brine	
			[ml]	[vol.%]	[ml]	[vol.%]
0.5	w/o	2.6	2.4	92.3	0.2	7.7
2	o/w	6.9	1.3	18.8	5.6	81.2
5	o/w	6.3	0.7	11.1	5.6	88.9

b. Temperature 50°C

TETA Concentration [wt%]	Emulsion Type	Emulsion Volume [ml]	Volumetric Composition of Emulsion			
			Bitumen		Brine	
			[ml]	[vol.%]	[ml]	[vol.%]
0.5	o/w	6.3	0.7	11.1	5.6	88.9
2	o/w	7.1	1.5	21.1	5.6	78.9
5	o/w	6.5	0.9	13.8	5.6	86.2

c. Temperature 80°C

TETA Concentration [wt%]	Emulsion Type	Emulsion Volume [ml]	Volumetric Composition of Emulsion			
			Bitumen		Brine	
			[ml]	[vol.%]	[ml]	[vol.%]
0.5	o/w	7.1	1.5	21.1	5.6	78.9
2.0	o/w	8.0	2.4	30.0	5.6	70.0
5.0	o/w	7.0	1.4	20.0	5.6	80.0

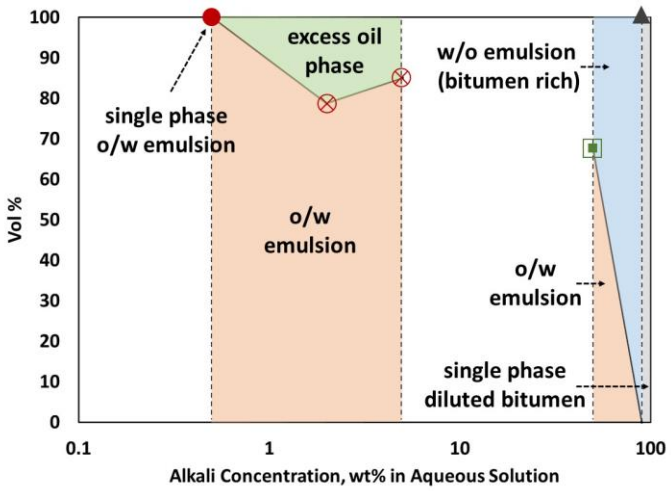

(a) Alkali: Pyrrolidine, WOR 7:3, Salinity: 1,000 ppm, Temperature: 25°C

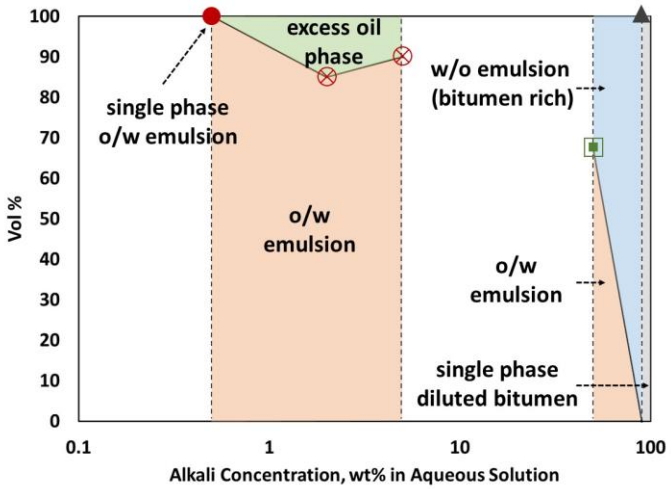

(b) Alkali: Pyrrolidine, WOR 7:3, Salinity: 1,000 ppm, Temperature: 50°C

Figure 4.19 Phase Behavior of emulsions with pyrrolidine at 25°C, 50°C, and 80°C

● : a single phase oil-in-water emulsion
⊗ : oil-in-water emulsions with excess oil phase
▣ : water-in-oil emulsions (bitumen-rich) with oil-in-water emulsions (water-rich)
▲ : diluted bitumen

Figure continued

Figure continued

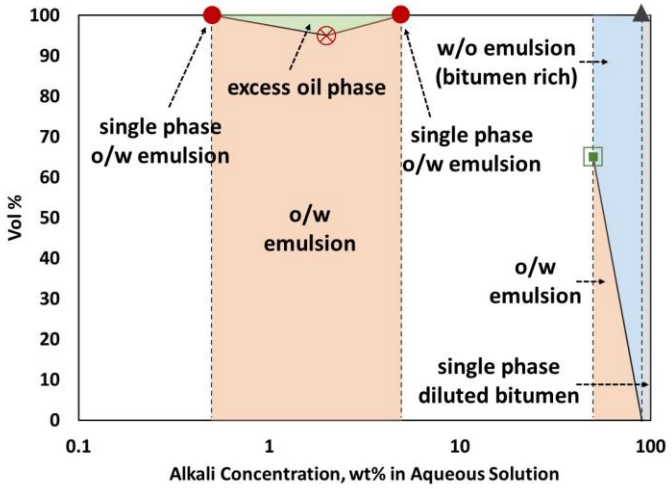

(c) Alkali: Pyrrolidine, WOR 7:3, Salinity: 1,000 ppm, Temperature: 80°C

Figure 4.19 Phase Behavior of emulsions with pyrrolidine at 25°C, 50°C, and 80°C

The 0.5 wt% pyrrolidine sample created the single-phase o/w emulsion at all temperatures. At pyrrolidine concentrations below 5 wt%, it clearly shows that the vol% of o/w emulsions became larger with increasing temperature, indicating o/w emulsions turned into a single-phase o/w emulsion. At 100°C, these o/w emulsions became a single-phase.

● : a single phase oil-in-water emulsion
⊗ : oil-in-water emulsions with excess oil phase
▣ : water-in-oil emulsions (bitumen-rich) with oil-in-water emulsions (water-rich)
▲ : diluted bitumen

Table 4.4 Bitumen amount in emulsions for pyrrolidine samples (Salinity 1,000 ppm, WOR 7:3)

Samples with 0.5 wt% pyrrolidine created a single-phase o/w emulsion at all temperatures. It is clear that, as temperature increases, the bitumen content in emulsions also increases for a given o/w emulsion.

a. Temperature 25°C

Pyrrolidine Concentration [wt%]	Emulsion Type	Emulsion Volume [ml]	Volumetric Composition of Emulsion			
			Bitumen		Brine	
			[ml]	[vol.%]	[ml]	[vol.%]
0.5	o/w	8.0	2.4	30	5.6	70
2	o/w	6.3	0.7	11	5.6	89
5	o/w	6.8	1.2	18	5.6	82

b. Temperature 50°C

Pyrrolidine Concentration [wt%]	Emulsion Type	Emulsion Volume [ml]	Volumetric Composition of Emulsion			
			Bitumen		Brine	
			[ml]	[vol.%]	[ml]	[vol.%]
0.5	o/w	8.0	2.4	30	5.6	70
2	o/w	6.8	1.2	18	5.6	82
5	o/w	7.2	1.6	22	5.6	78

c. Temperature 80°C

Pyrrolidine Concentration [wt%]	Emulsion Type	Emulsion Volume [ml]	Volumetric Composition of Emulsion			
			Bitumen		Brine	
			[ml]	[vol.%]	[ml]	[vol.%]
0.5	o/w	8.0	2.4	30	5.6	70
2	o/w	7.6	2.0	26	5.6	74
5	o/w	8.0	2.4	30	5.6	70

4.3.3. Viscosity of Emulsions

Results of the viscosity measurement are summarized in **Table 4.5** and **Figure 4.20** for DEA, **Table 4.6** and **Figure 4.21** for TETA, and **Table 4.7** and **Figure 4.22** for pyrrolidine. Shear-thinning behavior was observed for all fluids studied, except for the original bitumen. The shear-thinning behavior indicates hydrodynamic interaction and deformation of dispersed droplets (Nizamidin et al. 2015; Pal 1996). However, the w/o emulsion at 50 wt% alkali concentration was only weakly shear-thinning likely because there was only a small amount of dispersed water in this oil-external emulsion (Pal 2000).

The bitumen content and temperature affect the viscosity of o/w emulsions in a complex manner. With increasing temperature, the bitumen content tends to increase in the o/w emulsion, but the viscosity of bitumen itself decreases. The effect of temperature on the o/w emulsion viscosity can be observed for the case of 0.5 wt% pyrrolidine, i.e., the viscosities of the single-phase o/w emulsion with 0.5 wt% pyrrolidine at 25°C were similar to those at 50°C. At 80°C, however, the o/w emulsion became much less viscous especially at lower shear rates.

The effect of an increased oil content in o/w emulsion can be observed for the viscosity data obtained for 2 wt% pyrrolidine samples at 25°C and 50°C, where the o/w emulsion viscosity increases with increasing temperature. The data for 5 wt% pyrrolidine samples at the three temperatures in Table 4.7 show that the viscosity of o/w emulsion decreased with increasing temperature in spite of the increased oil content at 80°C.

For DEA samples, viscosities of o/w emulsions at different DEA concentrations show similar values at a given temperature. This trend could be due to the similar bitumen content and volumetric concentration for all o/w emulsions. The temperature effect on the viscosity of o/w emulsions are more evident at higher shear rate; e.g., o/w emulsions at 50°C were less viscous than those at 25°C.

As expected, w/o emulsions created with 50 wt% alkali were more viscous than o/w emulsions created with lower alkali concentrations. The effect of temperature on viscosity reduction is more prominent for w/o emulsions as the external phase is oil. For samples of 50 wt% DEA and 50 wt% pyrrolidine, w/o emulsions were substantially less viscous than the original bitumen at a given temperature, indicating the dilution of bitumen by an organic alkali.

The viscosity of the bitumen measured by the same rheometer (Model: ARES LS-1 from TA Instruments) was 9,040 cp at 50°C and 690 cp at 80°C. Newtonian behavior was confirmed for the bitumen sample. At 25°C, the bitumen viscosity was not measured by the rheometer because of the limitation in torque. However, Baek et al. (2019a) presented a viscosity correlation for this bitumen based on measurements using an in-line viscometer, which calculates 447,000 cp at 25°C.

In comparison with the original bitumen, it was possible to achieve the significant viscosity reduction by creating o/w emulsion. For samples with DEA, bitumen-rich o/w emulsions are 3 to 4 orders of magnitude less viscous at 25°C, and 2 orders of magnitude less viscous at 50°C. For samples with TETA, o/w emulsions are 4 to 5 orders of magnitude less viscous at 25°C, 2 to 3 orders of magnitude less viscous at 50°C, and 1 to 2 orders of magnitude less viscous at 80°C. For samples with pyrrolidine, o/w emulsions are 4 to 6 orders of magnitude less viscous at 25°C, 2 to 3 orders of magnitude less viscous at 50°C, and 1 to 2 orders of magnitude less viscous at 80°C.

In steam injection process like SAGD, in-situ shear rates are expected to be below 10.0 sec^{-1}. **Figure 4.23** plots viscosities measured at three shear rates, 1.0, 5.6, and 10.0 sec^{-1} at different temperatures. It shows that, in general, the viscosities of o/w emulsions are insensitive to temperature at a given low shear rate for all organic alkalis.

The insensitivity of o/w emulsion viscosity gives the validation of this experiment regarding temperature. The temperature range of this experiment was from 25 to 80°C, whereas steam injection temperature for SAGD is usually much higher. However, this research focuses on the reaction and emulsification of bitumen with an organic alkali at the steam chamber edge. While an organic alkali is injected with steam at high temperature (e.g. 200°C), bitumen emulsification and the emulsion drainage occur at lower temperatures near thermal front (i.e. the steam chamber edge). Therefore, the insensitivity of the emulsion mobility to temperature is going to help increase the "transition zone" in which a meaningful amount of bitumen transport occurs.

Table 4.5 Emulsion viscosity of DEA samples (Salinity 1,000 ppm, WOR 7:3)

a. Temperature 25°C

DEA Concentration	0.5 wt%	2 wt%	5 wt%	50 wt%	90 wt%
Emulsion Type	o/w	o/w	o/w	w/o	dilution
Shear Rate [1/sec]	Viscosity [cp]	Viscosity [cp]	Viscosity [cp]	Viscosity [cp]	Viscosity [cp]
0.1	76.4	- (*)	266.8	- (*)	86.0
0.2	134.6	- (*)	184.5	2001.8	79.2
0.3	144.8	- (*)	148.4	2088.2	49.7
0.6	105.9	447.7	130.7	2332.6	30.3
1.0	107.0	249.7	104.7	2217.7	21.6
1.8	82.6	163.8	82.1	1850.7	16.1
3.2	97.4	109.6	65.3	1610.2	13.0
5.6	84.4	97.9	58.2	1580.6	12.5
10.0	48.3	73.6	53.4	1531.6	14.3
17.8	37.2	59.9	50.7	1402.2	14.5
31.6	31.0	51.3	50.0	1355.7	14.1
56.2	31.1	43.7	48.5	1429.3	16.1
100.0	19.5	41.9	49.2	1375.6	21.3

b. Temperature 50°C

DEA Concentration	0.5 wt%	2 wt%	5 wt%	50 wt%	90 wt%
Emulsion Type	o/w	o/w	o/w	w/o	dilution
Shear Rate [1/sec]	Viscosity [cp]	Viscosity [cp]	Viscosity [cp]	Viscosity [cp]	Viscosity [cp]
0.1	255.5	215.0	320.0	262.6	92.1
0.2	215.1	174.9	237.5	249.7	84.1
0.3	179.0	133.5	161.8	237.0	67.0
0.6	144.2	108.5	121.0	217.2	47.6
1.0	114.5	85.3	96.4	199.1	37.5
1.8	89.9	65.0	76.4	180.1	31.6
3.2	63.1	49.9	59.9	163.6	26.5
5.6	44.7	41.2	47.6	148.5	24.7
10.0	33.2	31.2	34.4	135.3	24.7
17.8	27.4	20.6	21.6	120.8	26.1
31.6	26.0	14.9	15.0	107.1	27.0
56.2	22.2	13.7	12.7	97.4	30.1
100.0	22.3	12.7	12.6	91.8	33.4

(*) Measurement error due to the torque limit of the rheometer.

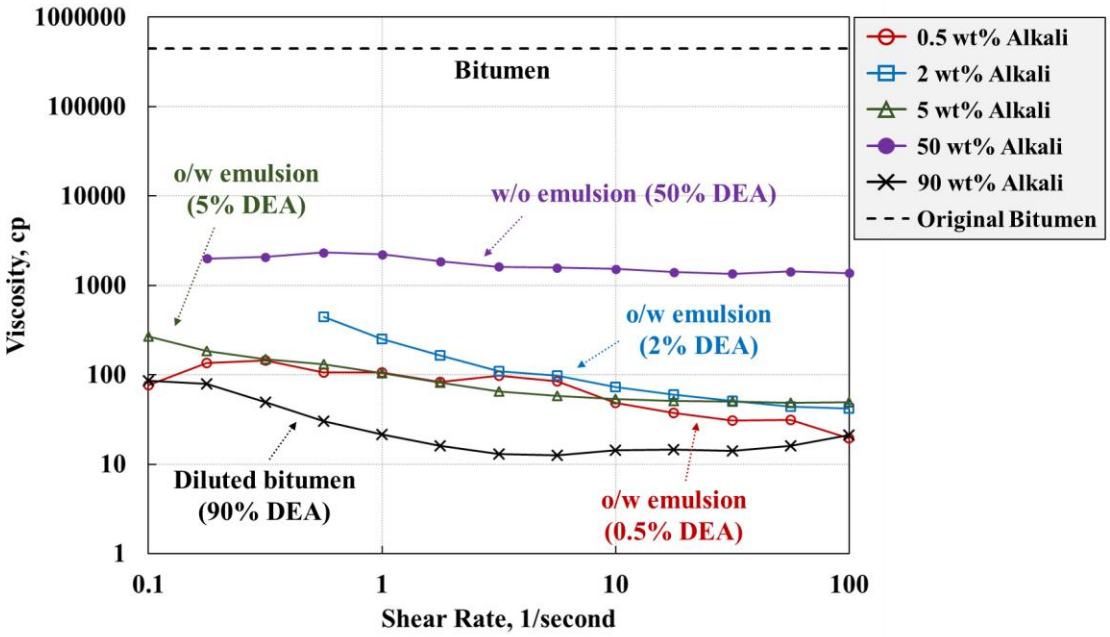

(a) Alkali: DEA, WOR 7:3, Salinity: 1,000 ppm, Temperature: 25°C

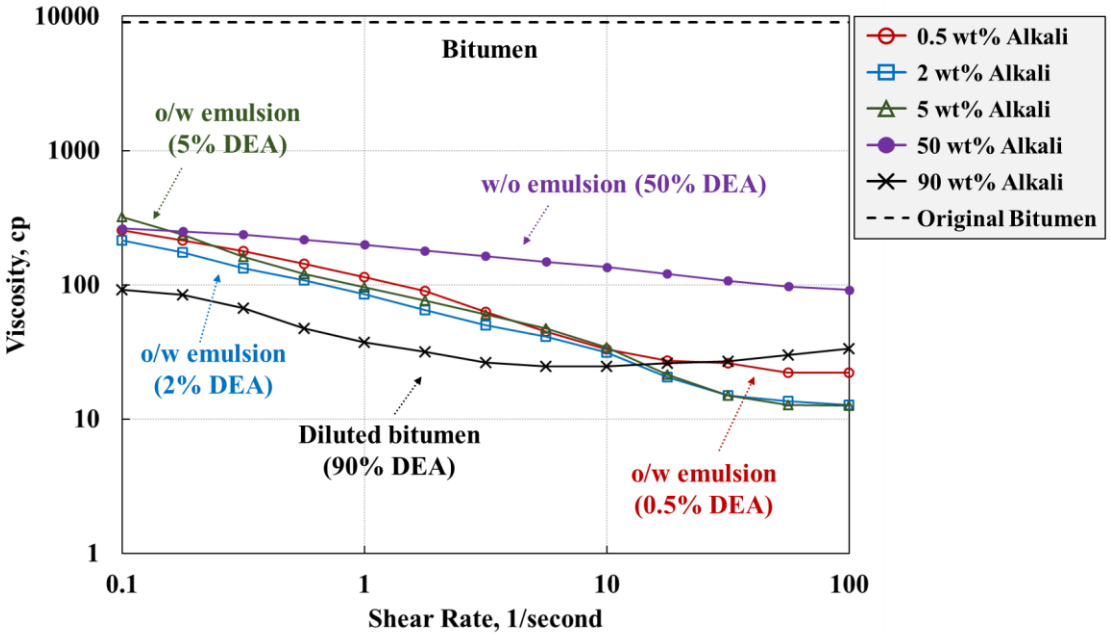

(b) Alkali: DEA, WOR 7:3, Salinity: 1,000 ppm, Temperature: 50°C

Figure 4.20 Emulsion viscosity of DEA samples

Table 4.6 Emulsion viscosity of TETA samples (Salinity 1,000 ppm, WOR 7:3)

a. Temperature 25°C

TETA Concentration	0.5 wt%	2 wt%	5 wt%	50 wt%	90 wt%
Emulsion Type	w/o	o/w	o/w	w/o	dilution
Shear Rate [1/sec]	Viscosity [cp]	Viscosity [cp]	Viscosity [cp]	Viscosity [cp]	Viscosity [cp]
0.1	155360.0	447.3	210.4	100360.0	1577.9
0.2	153030.0	302.3	115.4	102540.0	1482.7
0.3	146430.0	186.9	74.3	103500.0	1231.5
0.6	133340.0	87.2	57.7	104700.0	800.9
1.0	120010.0	59.8	39.6	105050.0	454.5
1.8	107110.0	37.1	26.1	100410.0	314.2
3.2	93112.3	19.9	12.5	91256.3	170.6
5.6	83634.3	12.4	6.4	82145.4	124.8
10.0	74869.9	9.6	4.4	78709.1	112.8
17.8	63073.3	6.1	3.8	69098.2	103.9
31.6	49191.5	4.1	2.7	58675.6	93.4
56.2	34652.3	3.3	2.5	45412.5	89.9
100.0	26195.7	4.7	2.4	- (*)	90.0

b. Temperature 50°C

TETA Concentration	0.5 wt%	2 wt%	5 wt%	50 wt%	90 wt%
Emulsion Type	o/w	o/w	o/w	w/o	dilution
Shear Rate [1/sec]	Viscosity [cp]	Viscosity [cp]	Viscosity [cp]	Viscosity [cp]	Viscosity [cp]
0.1	363.9	405.3	440.4	5741.9	629.1
0.2	287.5	240.6	379.6	5832.2	577.6
0.3	209.2	200.4	274.8	5891.7	519.9
0.6	136.1	164.4	192.4	5936.3	449.7
1.0	90.3	138.0	135.5	5867.7	381.8
1.8	55.6	110.0	98.6	5768.8	323.2
3.2	34.8	78.9	79.9	5578.6	255.4
5.6	17.6	40.9	41.5	5296.5	264.3
10.0	13.0	15.8	32.9	5166.0	184.0
17.8	9.0	7.4	18.2	4862.9	122.6
31.6	5.2	4.5	8.7	4779.5	109.6
56.2	4.2	2.8	6.2	4991.3	66.0
100.0	3.8	2.3	4.4	4943.8	49.1

(*) Measurement error due to the torque limit of the rheometer.

Table continued

Table continued

c. Temperature 80°C

TETA Concentration	0.5 wt%	2 wt%	5 wt%	50 wt%	90 wt%
Emulsion Type	o/w	o/w	o/w	w/o	dilution
Shear Rate [1/sec]	Viscosity [cp]	Viscosity [cp]	Viscosity [cp]	Viscosity [cp]	Viscosity [cp]
0.1	354.6	178.6	194.2	927.4	333.9
0.2	239.3	114.8	144.5	873.8	272.1
0.3	196.0	84.9	110.3	841.3	219.2
0.6	218.9	69.4	84.2	823.7	189.1
1.0	130.4	61.5	64.1	800.8	153.2
1.8	96.6	46.2	47.5	791.3	122.7
3.2	80.3	34.2	34.3	773.9	99.2
5.6	57.9	26.9	22.1	760.7	79.1
10.0	41.7	18.9	15.6	758.3	65.7
17.8	29.4	16.4	10.2	758.2	53.2
31.6	21.3	12.2	7.2	756.3	43.5
56.2	13.9	9.1	4.7	778.0	33.7
100.0	7.8	6.7	3.9	777.1	27.0

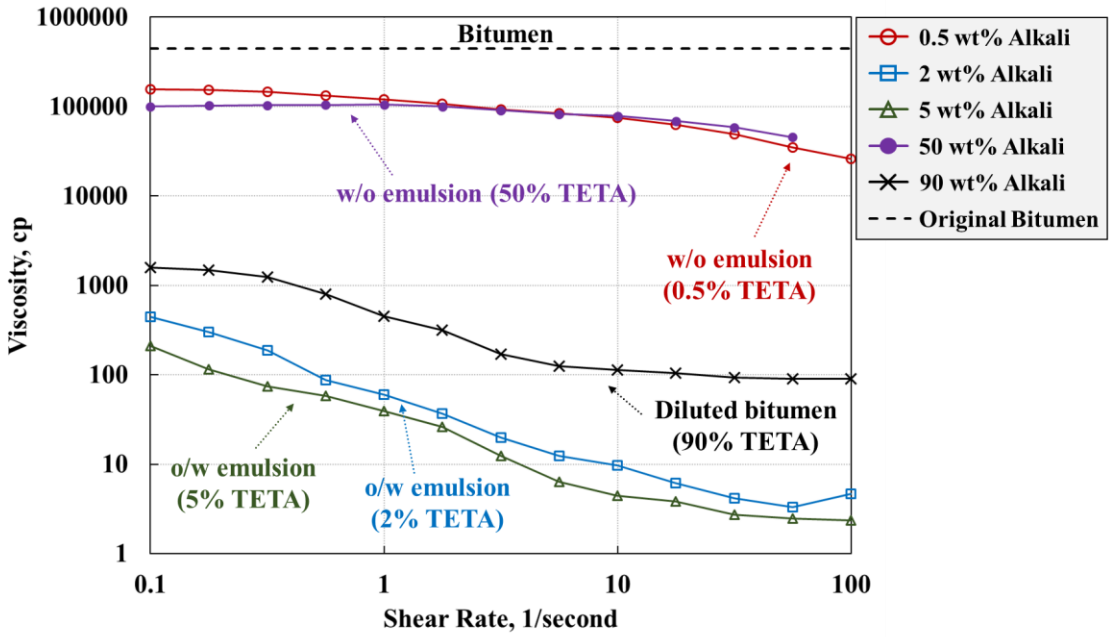

(a) Alkali: TETA, WOR 7:3, Salinity: 1,000 ppm, Temperature: 25°C

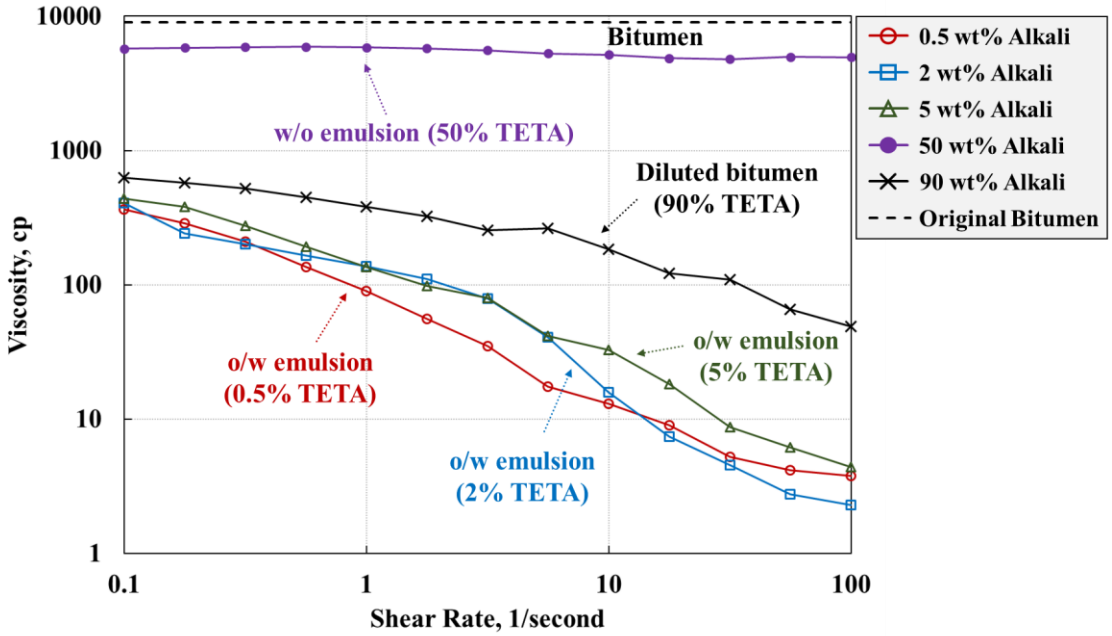

(b) Alkali: TETA, WOR 7:3, Salinity: 1,000 ppm, Temperature: 50°C

Figure 4.21 Emulsion viscosity of TETA samples

Figure continued

Figure continued

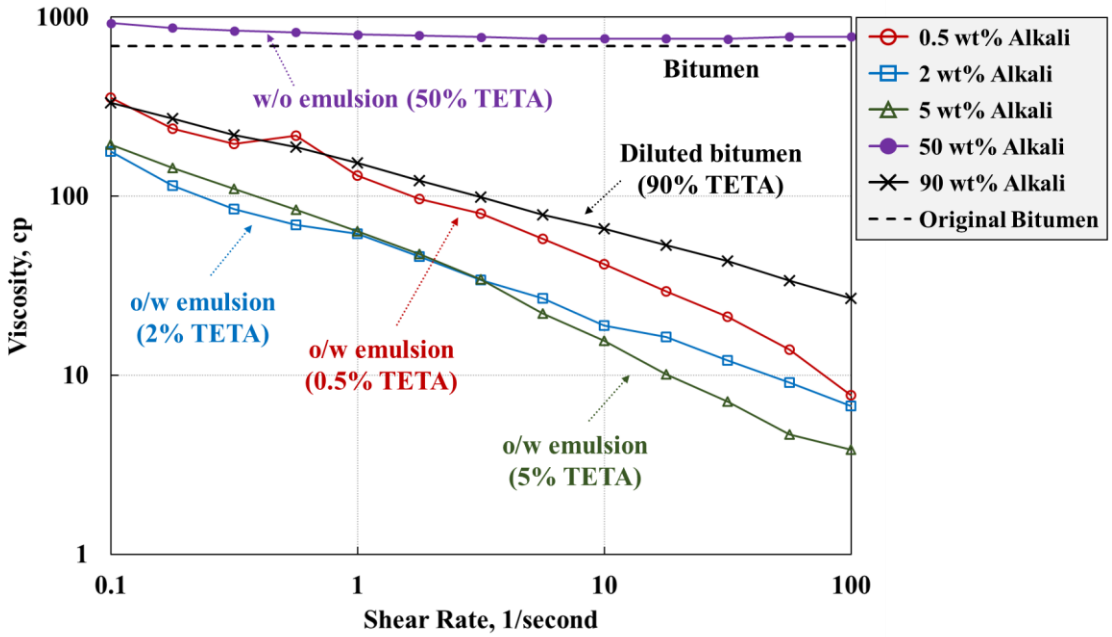

(c) Alkali: TETA, WOR 7:3, Salinity: 1,000 ppm, Temperature: 80°C

Figure 4.21 Emulsion viscosity of TETA samples

Table 4.7 Emulsion viscosity of pyrrolidine samples (Salinity 1,000 ppm, WOR 7:3)

a. Temperature 25°C

Pyrrolidine Concentration	0.5 wt%	2 wt%	5 wt%	50 wt%	90 wt%
Emulsion Type	o/w	o/w	o/w	w/o	dilution
Shear Rate [1/sec]	Viscosity [cp]	Viscosity [cp]	Viscosity [cp]	Viscosity [cp]	Viscosity [cp]
0.1	176.0	83.3	130.0	17801.3	102.2
0.2	168.0	65.5	103.5	17761.2	63.5
0.3	112.4	44.5	75.8	17535.3	42.7
0.6	69.9	30.0	55.6	16793.4	29.2
1.0	40.1	20.3	36.3	15750.8	22.2
1.8	25.7	13.0	22.7	14370.6	16.4
3.2	14.6	8.0	15.4	13659.8	13.4
5.6	11.1	4.9	10.2	13014.9	11.7
10.0	8.2	3.9	8.0	10400.0	11.2
17.8	6.7	2.8	6.4	8296.3	10.0
31.6	5.5	2.2	5.2	7167.6	9.4
56.2	4.9	1.8	4.6	5863.5	8.6
100.0	4.5	1.6	4.2	5115.7	9.2

b. Temperature 50°C

Pyrrolidine Concentration	0.5 wt%	2 wt%	5 wt%	50 wt%	90 wt%
Emulsion Type	o/w	o/w	o/w	w/o	dilution
Shear Rate [1/sec]	Viscosity [cp]	Viscosity [cp]	Viscosity [cp]	Viscosity [cp]	Viscosity [cp]
0.1	235.1	176.7	132.6	- (*)	54.5
0.2	177.2	167.3	105.8	2006.4	56.7
0.3	125.3	146.5	86.8	1993.8	61.1
0.6	81.9	134.3	72.4	1971.3	56.8
1.0	57.1	108.9	65.2	2022.9	50.5
1.8	43.9	80.4	54.0	1898.1	44.3
3.2	29.1	31.4	46.7	1896.1	39.8
5.6	17.5	19.0	39.5	1801.6	47.1
10.0	10.9	19.1	31.5	1737.1	45.0
17.8	7.9	7.7	21.9	1678.3	37.0
31.6	6.0	4.4	13.4	1557.0	34.5
56.2	4.7	2.8	3.6	1488.0	32.1
100.0	3.9	2.3	2.9	1438.6	29.6

(*) Measurement error due to the torque limit of the rheometer.

Table continued

Table continued

c. Temperature 80°C

Pyrrolidine Concentration	0.5 wt%	2 wt%	5 wt%	50 wt%	90 wt%
Emulsion Type	o/w	o/w	o/w	w/o	dilution
Shear Rate [1/sec]	Viscosity [cp]	Viscosity [cp]	Viscosity [cp]	Viscosity [cp]	Viscosity [cp]
0.1	53.5	74.5	25.7	540.0	46.6
0.2	37.1	62.3	22.0	518.6	43.8
0.3	30.4	50.0	19.3	513.2	33.7
0.6	25.8	38.4	17.3	478.5	29.2
1.0	22.2	29.2	14.1	418.0	30.2
1.8	18.7	23.0	12.5	365.8	29.1
3.2	15.6	16.5	9.3	309.1	27.0
5.6	12.3	13.3	8.4	264.6	24.8
10.0	8.3	10.0	6.0	225.6	23.7
17.8	6.3	5.7	4.9	193.0	22.9
31.6	5.3	4.4	4.4	164.3	22.5
56.2	4.8	2.8	4.0	136.4	22.4
100.0	4.0	2.6	3.8	132.5	22.0

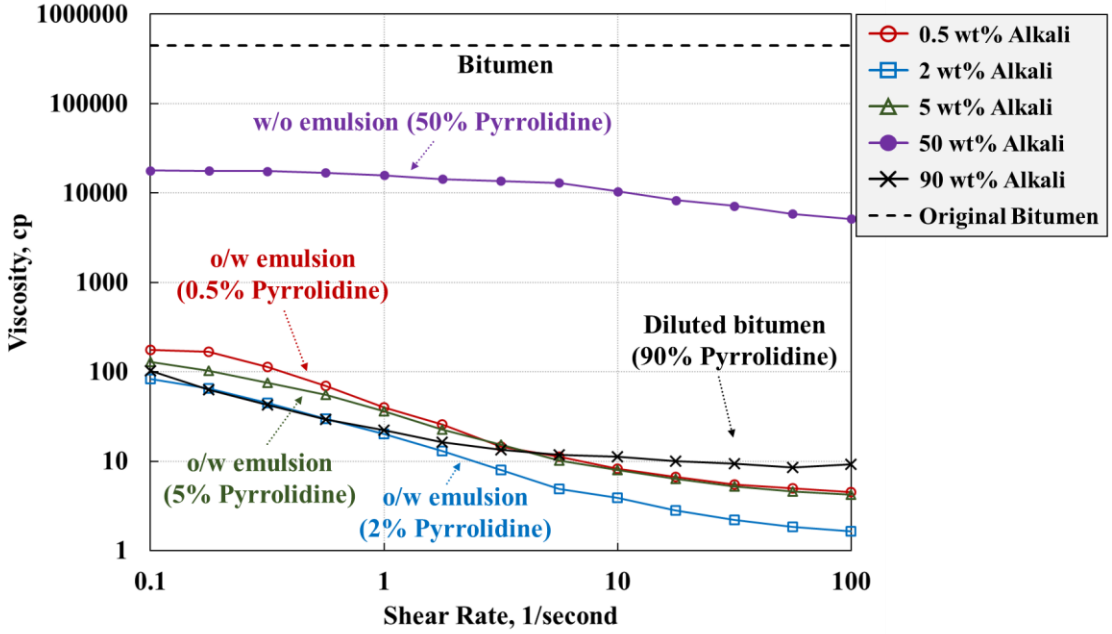

(a) Alkali: Pyrrolidine, WOR 7:3, Salinity: 1,000 ppm, Temperature: 25°C

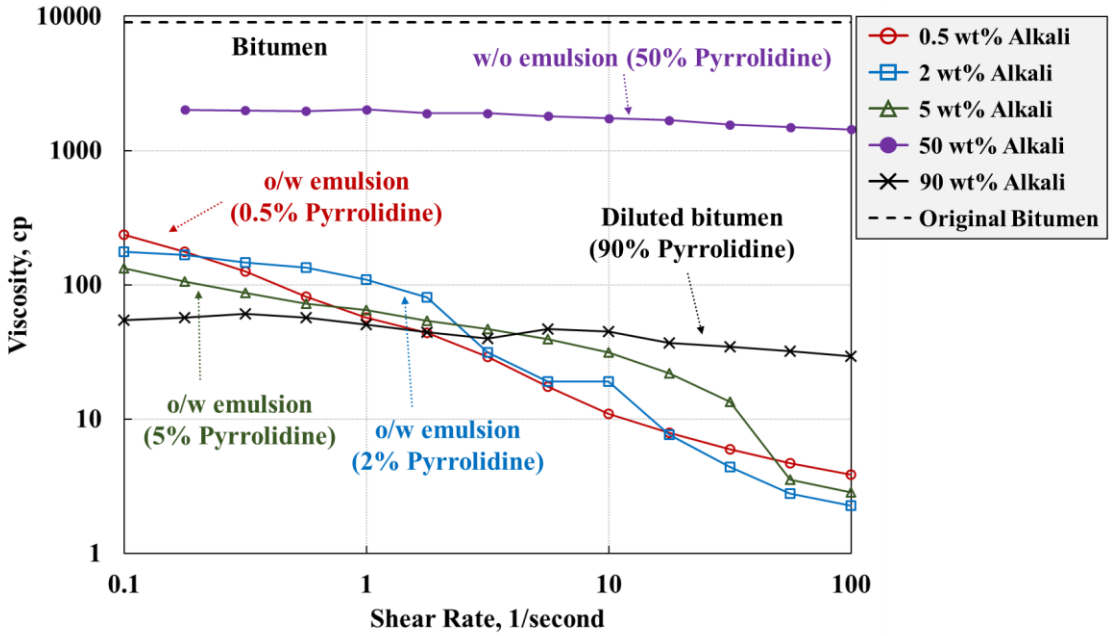

(b) Alkali: Pyrrolidine, WOR 7:3, Salinity: 1,000 ppm, Temperature: 50°C

Figure 4.22 Emulsion viscosity of pyrrolidine samples

Figure continued

Figure continued

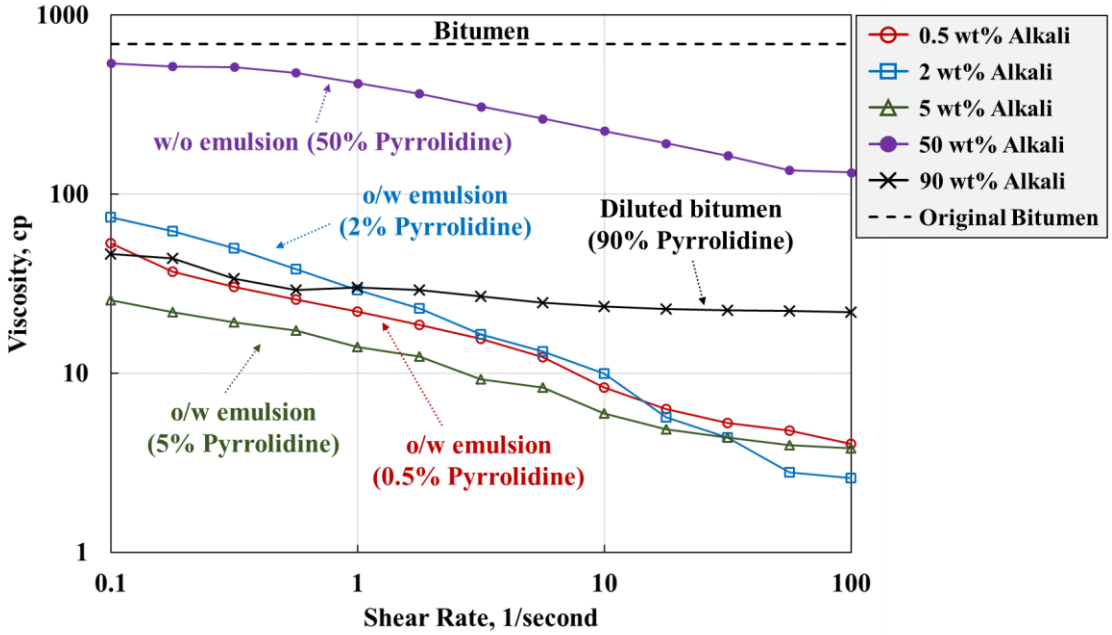

(c) Alkali: Pyrrolidine, WOR 7:3, Salinity: 1,000 ppm, Temperature: 80°C

Figure 4.22 Emulsion viscosity of pyrrolidine samples

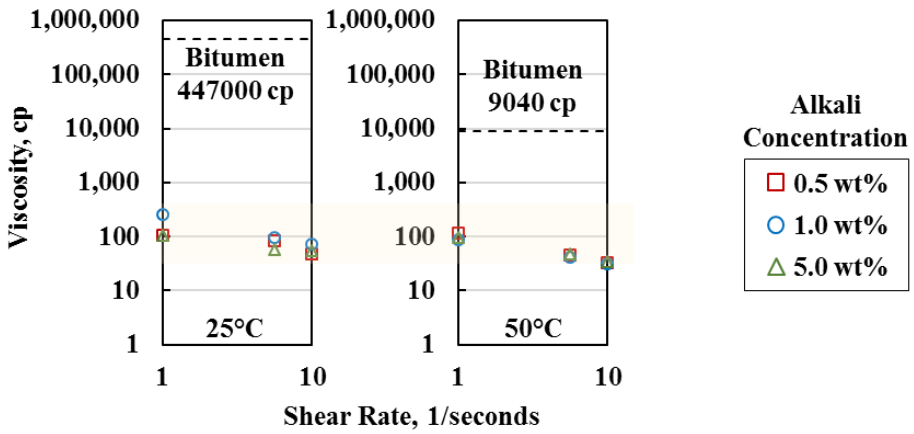

(a) o/w emulsion viscosity for DEA samples at 25°C and 50°C

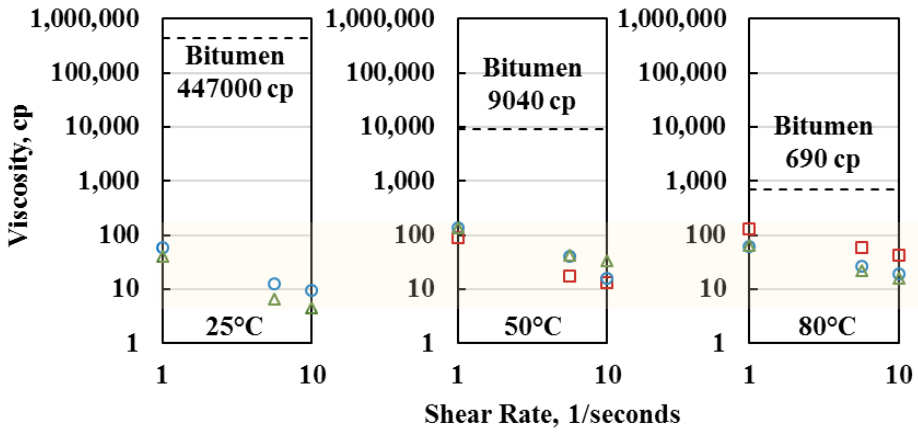

(b) o/w emulsion viscosity for TETA samples at 25°C, 50°C, and 80°C

Figure 4.23 Viscosity of o/w emulsions at different temperatures at low shear rates

Figure continued

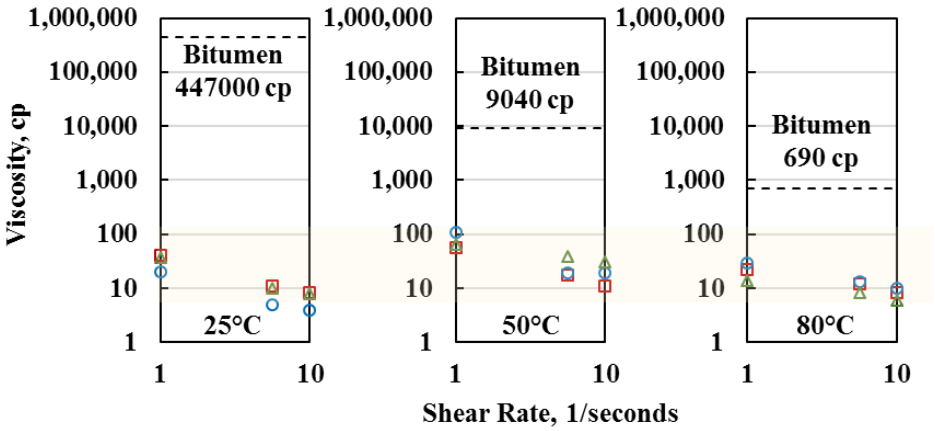

(c) o/w emulsion viscosity for pyrrolidine samples at 25°C, 50°C, and 80°C

Figure 4.23 Viscosity of o/w emulsions at different temperatures at low shear rates

4.4. Chemical Structure of Organic Alkalis on Bitumen Emulsification

Experimental results clearly show that different organic alkalis resulted in different emulsion phase behavior such as emulsion types, bitumen content in emulsions, and emulsion viscosity. In this research, bitumen was emulsified with natural surfactants that were activated by the reaction of an organic alkali with acidic components in bitumen (**Figure 4.24**). It is reasonable to assume that the natural surfactants (soaps) created from the same bitumen were similar. Then, the different phase behavior with different organic alkalis (DEA, TETA, and pyrrolidine) is largely attributed to differences of the organic alkali as a co-solvent in the bitumen/NaCl-brine/alkali mixture. That is, the chemical structure of an organic alkali can result in different emulsion phase behavior with bitumen.

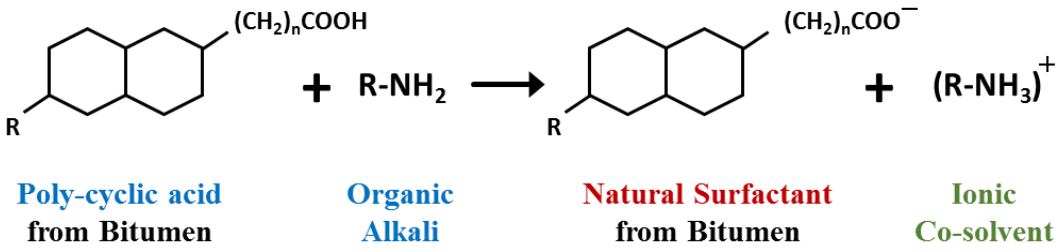

Figure 4.24 Example of the chemical reaction to activate natural surfactants in bitumen

Properties of DEA, pyrrolidine, and TETA are summarized in **Table 4.8**. DEA and pyrrolidine are secondary amines and similar to each other in terms of MW and chemical formula. However, the important difference is that DEA has an aliphatic hydrocarbon chain, whereas pyrrolidine has a cyclic structure. TETA contains three two-carbon aliphatic segments and 4 nitrogen atoms.

Table 4.8 Properties of organic alkalis

Organic Alkali	Chemical Formula	MW [g/mol]	Hansen Solubility Parameter (Hansen 2007)		
			Dispersion	Polarity	Hydrogen
Diethylamine (DEA)	$C_4H_{11}N$	73	14.9	2.3	6.1
Pyrrolidine	C_4H_9N	71	17.9	6.5	7.4
Triethylenetetramine (TETA)	$C_6H_{18}N_4$	146	Not available		

The emulsion phase behavior showed that TETA was effective in o/w emulsification of bitumen only at high temperatures. At WOR 7:3 and 1,000 ppm, for example, TETA gave a single-phase o/w emulsion at 100°C. At temperatures below 100°C, however, the o/w emulsion with a small amount of bitumen was created along with the excess bitumen phase. With 4 nitrogen atoms in the structure, TETA is the most polar compound among the three organic alkalis, resulting in a large solubility in water. The high polarity tends to make TETA sensitive to temperature in terms of affinity for the bitumen in the presence of water (Baek et al. 2019a). It is likely that TETA's polarity is too high for o/w emulsification of the bitumen for a wide range of temperatures.

In comparison to DEA and TETA, pyrrolidine created the single-phase o/w emulsion behavior at a wider range of temperatures. Also, the o/w emulsions created with pyrrolidine showed superior fluidity and rapid coalescence behavior after mixing when the o/w emulsion co-existed with the excess oil phase. This type of qualitative observations in addition to the emulsion color and texture is a widely used technique for the identification of low IFT emulsions (Chang et al. 2019).

Potential reasons for pyrrolidine to be superior to DEA and TETA as a co-solvent may include the higher level of affinity for bitumen, which is often highly asphaltic. The

steric effect of the organic alkali is an important factor that determines the shape of the co-solvent, which in turn affects the size of asphaltenes aggregation in the bitumen emulsification. Asphaltenes are a group of complex compounds with multi-benzene rings. According to Larichev et al. (2016), planar molecules (e.g., cyclic hydrocarbons due to the steric effect on their shapes) can fit into the asphaltene structure and replace asphaltene molecules with relatively small hydrocarbons. For example, Larichev et al. (2016) observed that cyclohexanol disaggregated asphaltenes whereas 1-hexanol aggregated asphaltenes, although they are similar in terms of MW and chemical formula. The steric effect likely makes pyrrolidine more compatible with the asphaltic bitumen than DEA or TETA. Although pyrrolidine has a greater polarity than DEA, our results showed that the steric effect on the molecular shape is more important than polarity as a co-solvent to create o/w emulsions with bitumen.

The Hansen solubility dispersion parameter can be a good indicator for the affinity for bitumen. Larichev et al. (2016) observed the disaggregation of asphaltenes when the Hansen solubility dispersion parameter of the chemical increases from 14.5 to 20. The Hansen solubility dispersion parameter is 14.9 for DEA and 17.9 for pyrrolidine (Hansen 2007). Larichev et al. (2016) studied the relationship between the dispersion parameter and asphaltene aggregation, based on which the size of asphaltene aggregation with pyrrolidine could be about 12% smaller than that with DEA.

4.5. Conclusions

The main idea of this research is to use an organic alkali as a steam additive to improve SAGD, and induce the o/w bitumen emulsification. The central question was whether an organic alkali can form o/w emulsions that contain a meaningful amount of bitumen, and that are much less viscous than the original bitumen. Therefore, this research investigated the fundamental data of phase behavior and viscosity for emulsions created by mixtures of Athabasca bitumen, organic alkalis, and NaCl brine. The emulsion phase behavior was summarized with more than 300 samples with different alkali concentrations, brine salinities, and WORs at 100°C. Viscosities and bitumen contents in emulsions were measured at 25°C, 50°C and 80°C for selected emulsion samples at 7:3 WOR and 1,000 ppm salinity.

- It was possible to create o/w emulsions by adding a small amount of an organic alkali to Athabasca bitumen and NaCl brine. Results showed that o/w emulsions appeared at low alkali concentrations (below 20 wt% and as low as 0.5 wt%) and low salinities (0 and 1,000 ppm). As an organic alkali concentration increased, w/o emulsions appeared. A diluted bitumen was observed at 90 wt% alkali in the aqueous solution.
- As a bitumen carrier, in general, o/w emulsions created by pyrrolidine contain higher bitumen amounts in comparison to DEA or TETA. For pyrrolidine samples, the single-phase o/w emulsion, which maximize the utilization of aqueous phase as a bitumen carrier, was observed at various conditions at 100°C: (1) for WOR 9:1, 1 to 5 wt% pyrrolidine at 1,000 ppm, (2) for WOR 7:3, 0.5 to 5 wt% pyrrolidine at 0 and 1,000 ppm, and (3) for WOR 5:5, 1 to 10 wt% pyrrolidine at 0 ppm. For samples of 0.5 wt% pyrrolidine with WOR 7:3 at 1,000 ppm, the single-phase o/w emulsion was observed for all temperatures from 25 to 100°C.

- The o/w emulsions created in this research were much less viscous than the original bitumen. They were 3 to 6 orders of magnitude less viscous at 25°C, 2 to 3 orders of magnitude less viscous at 50°C, and 1 to 2 orders of magnitude less viscous at 80°C. The insensitivity of the o/w emulsion mobility to temperature is going to help increase the "transition zone" in which a meaningful amount of bitumen transport occurs.
- Pyrrolidine was superior to DEA and TETA as a co-solvent for the o/w emulsification of bitumen. The results indicate that it is important to consider the affinity of the organic alkali to bitumen for o/w emulsification at a wide range of temperatures. Important factors for this purpose include the polarity, the steric effect that affects the molecular shape, and the Hansen solubility parameter of organic alkalis.

5. Preliminary Study on SAS for Heavy Oil Recovery [3]

This research investigates the use of SAS to improve the displacement efficiency of polymer flooding. Unlike the conventional SP or ASP flooding, this research focuses on the application of SAS as a sole chemical additive to polymer solution without any additional chemicals or salinity gradient. A single SAS is not expected to reduce IFT to ultra-low level of 10^{-3} dynes/cm. The key is the incremental oil recovery by IFT reduction using SAS without creating Winsor type III micro-emulsions. Therefore, the proposed method may be more properly denoted as "improved polymer flooding" or "low-tension polymer flooding" than surfactant-polymer (SP) flooding which achieves ultra-low IFT between the displacing and displaced phases.

5.1. Materials

Oil The same dehydrated Athabasca bitumen (in the previous two chapters) was used for experiments in this research. The experiments were conducted at 95°C, at which the oil viscosity was measured to be 276 cp.

Brine The reservoir brine and the injection brine were set to be 5 wt% NaCl and 0.1 wt% NaCl, respectively. The simple brine composition with no hardness allowed us to focus on evaluating the effect of a SAS on heavy oil recovery.

[3] This chapter was published in the following paper. Baek conducted all experiment and analyzed most of data as the first author of this paper.

- Baek, K., Argüelles-Vivas, F.J., Abeykoon, G.A., Okuno, R. and Weerasooriya, U.P. 2019. Application of Ultrashort Hydrophobe Surfactants with Cosolvent Characters for Heavy Oil Recovery. *Energy and Fuels* 33: 8241-8249. https://doi.org/10.1021/acs.energyfuels.9b01716

Surface Active Solvent (SAS)

A SAS consists of a short hydrophobe (e.g. carbon number lower than C_8) with a certain amount of propylene oxide (PO) units and the sufficient ethylene oxide (EO) units. It has characters of a solvent (i.e. a short hydrophobe head), hydrophobicity by PO units, and hydrophilicity by EO units. A larger number of PO results in a higher level of hydrophobicity and a lower IFT. Depending on brine salinity, brine hardness, and temperature, EO number should be adjusted for aqueous stability. Chang et al. (2019) discussed details of alkoxylated alcohols and other surfactants along with co-solvents.

In this research, a SAS was synthesized by alkoxylation of phenol; i.e. phenol-xPO-yEO. Phenol was selected as the basis for the affinity to heavy oil in this research. Its aromatic structure is known to be compatible with asphaltene-rich heavy oil because the steric effect of the benzene ring can reduce the size of asphaltic components' aggregation (Larichev et al. 2016). Larichev et al. (2016) presented that planar molecules (e.g., cyclic structures) could fit into the asphaltene structure and replace asphaltene molecules with relatively small hydrocarbons.

The number of PO units was limited to 7 (i.e. x = 7) to prevent a SAS having too long hydrocarbon chains which become similar to conventional surfactants such as Guerbet alcohol based surfactants. Also, it was found that four (x = 4) was the minimum PO number to create surface activity (i.e. IFT reduction) on solvents. Therefore, the PO numbers of 4 and 7 were investigated. The number of EO units ranged from 5 to 30 for phenol-4PO-yEO and from 5 to 40 for phenol-7PO-yEO. Phenol-4PO-yEOs and phenol-7PO-yEOs were provided from Harcros Chemicals.

Polymer

HPAM polymer, Flopaam 3630S (SNF), was used for a polymer flooding and an improved polymer flooding with a glass-bead pack. The polymer concentration was 0.22 wt%, which gave the viscosity of approximately 40 cp at injection conditions, corresponding to the field conditions of interest (7 times less viscous than the displaced oil). **Figure 5.1** gives the measured viscosities of the polymer solution at different shear rates at 95°C. The polymer-solution viscosity clearly decreased with increasing brine salinity. The effect of the SAS on the polymer-solution viscosity was not observed.

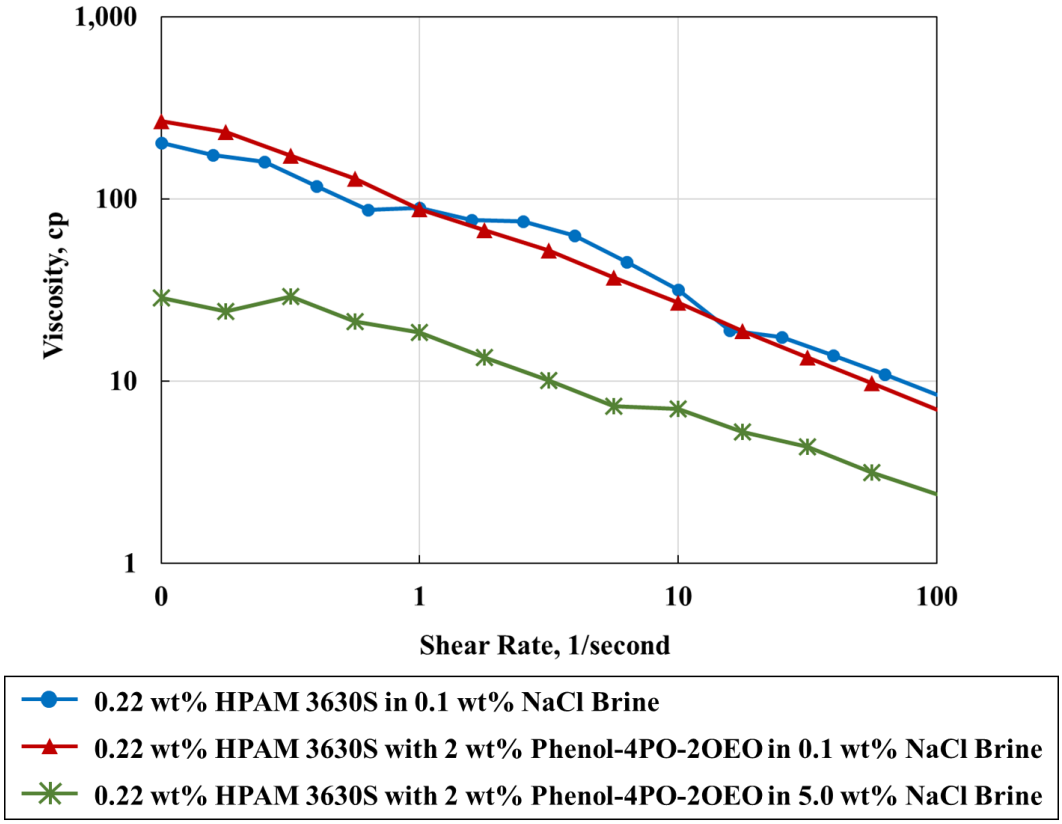

Figure 5.1 Polymer viscosity: 0.22 wt% HPAM 3630S at 95°C

Glass-bead pack

A cylinder was packed with glass beads as a porous medium. The cylinder is 50 cm long, and its internal volume is 8.2 ml. The porous medium contained particles with diameters ranging from 106 μm to 125 μm (the sieve number 120). The porosity and permeability of the porous media were measured to be 33% and 9.5 Darcy, representing the clean-sand facies of a heavy oil reservoir in Alberta, Canada.

5.2. Phase Behavior and IFT

Among 12 SASs (phenol-4PO-yEO: y = 5, 10, 15, 20, 25, and 30, and phenol-7PO-yEO: y = 5, 10, 15, 20, 30, and 40), phenol-4PO-20EO was eventually selected as the optimal SAS for heavy oil displacement. This section presents the screening procedure to select the optimal SAS through the aqueous stability test and the emulsion phase behavior test at 95°C.

SASs were subject to aqueous stability tests at 3 concentrations (0.5, 1, and 2 wt%) in the injection brine (0.1 wt% NaCl). Samples were aged at 4 different temperatures (25, 40, 80, and 95°C) for 2 days. Aqueous stability was confirmed by visual observation as to whether the solution was clear or cloudy (opaque), and whether it showed any phase separation. **Table 5.1** shows that 6 SASs passed the aqueous stability test at 95°C. They were phenol-4PO-yEO (y = 15, 20, 25, and 30) and phenol-7PO-yEO (y = 30 and 40).

These SASs were subject to the emulsion phase behavior test. The objective was to find a low IFT mixing behavior at 95°C. For each sample, 4 ml of the solution was prepared in an 8-ml borosilicate test tube. Samples were prepared at 3 different solvent concentrations (0.5, 1, and 2 wt% in aqueous phase) with 6 different salinities (0, 0.1, 0.5, 1, 2, and 3 wt% NaCl). Water-oil-ratio (WOR) was fixed at 7:3 (i.e., 70 vol% aqueous

phase and 30 vol% oil). Samples were aged at 95°C for 5 days before reporting the phase behavior.

Phase behavior test is summarized in **Table 5.2** and **Figure 5.2**. Total 13 samples with 4 SASs resulted in low IFT: phenol-4PO-20EO, phenol-4PO-25O, phenol-7PO-30EO, and phenol-7PO-40EO. Emulsion phases illustrated in Figure 5.2 were unstable macro-emulsions. They were separated into the oil phase and the aqueous phase by the 7th-day after mixing. Samples were evaluated by visual observation in terms of fluidity, color, and droplet size in the aqueous phase. Phenol-4PO-20EO and phenol-7PO-30EO resulted in the best phase behavior. Considering the injection brine salinity (0.1 wt% NaCl), 2 wt% phenol-4PO-20EO was selected as the optimum SAS and its concentration.

The critical micelle concentration (CMC) of phenol-4PO-20EO was 0.008 wt% (by the pendant drop method), as shown in **Figure 5.3**. The IFT between the heavy oil and the 2 wt% phenol-4PO-20EO solution was 0.39 dynes/cm at 95°C (by the spinning drop method). In comparison, the IFT between the heavy oil and the 0.1 wt% NaCl brine at 95°C is approximately 11 dynes/cm (Isaacs and Smolek 1983).

The IFT reduction from 11 to 0.39 dynes/cm resulted in a good mixing behavior. It created a single-phase mixture immediately after mixing, and slowly separated into the oil phase and the aqueous phase (Figure 5.2). Based on the method introduced in Kumar et al. (2012), the excess oil phase in the sample was confirmed to be oil-external, because it was dissolved in toluene, but not in water. The oil concentration in the aqueous phase with 2 wt% phenol-4PO-20EO was measured to be less than 1 vol%. The aqueous phase was actually transparent, light brown liquid. It is likely that the viscosity of this aqueous phase is similar to the viscosity of the external phase (brine or polymer).

The IFT between the heavy oil and the 2 wt% phenol-4PO-20EO solution with 0.05 wt% HPAM 3630s polymer resulted in 0.41 dynes/cm, which is close to the IFT without

polymer. It was not possible to measure IFT at higher polymer concentrations because an oil droplet did not elongate properly in a viscous surrounding phase. Previous studies indicated that the effect of polymer on the IFT between the aqueous and oleic phases depends on oil composition, surfactant(s), and polymer among many other factors. Khan et al. (2008) found that the surface tension of an anionic surfactant (sodium dodecyl sulfate or sodium dodecylbenzene sulfonate) solution increased with increasing polymer concentration (polyacrylamide, partially hydrolyzed polyacrylamide, or xanthan gum). However, the range of CMC did not change significantly in their research.

SiTu et al. (2017) reported that the IFT between n-decane and the mixture of benzyl substituted alkyl sulfobetaine and polyether nonionic surfactant solution increased with increasing polymer concentration. They used partly hydrolyzed polyacrylamide (HPAM), hydrophobically modified polyacrylamide (HMPAM), and co-polymer. However, Situ et al. (2017) also found that HPAM polymer did not change the IFT between Daqing crude oil and the surfactant solution likely because of acidic components in the crude oil.

In this research, with the high acid number (3.56 mg-KOH-g-oil), the IFT values measured with/without 0.05 wt% HPAM polymer indicate that the IFT is approximately 0.4 dynes/cm the between heavy oil and the 2 wt% phenol-4PO-20EO solution with/without HPAM polymer. i.e. polymer does not affect the IFT value of a non-ionic SAS with an acidic heavy oil.

Table 5.1 Aqueous stability test in brine salinity 0.1 wt% NaCl.

SAS	Concentration	Stability: S (stable), C (cloudy), PS (phase separation)			
		Temperature			
		25°C	40°C	80°C	90°C
Phenol-4PO-5EO	0.5 wt%	S	S	C	C
	1 wt%	S	C	C	C
	2 wt%	S	C	C	PS
Phenol-4PO-10EO	0.5 wt%	S	S	S	C
	1 wt%	S	S	C	C
	2 wt%	S	S	C	C
Phenol-4PO-15EO	0.5 wt%	S	S	S	S
	1 wt%	S	S	S	C
	2 wt%	S	S	S	C
Phenol-4PO-20EO	0.5 wt%	S	S	S	S
	1 wt%	S	S	S	S
	2 wt%	S	S	S	S
Phenol-4PO-25EO	0.5 wt%	S	S	S	S
	1 wt%	S	S	S	S
	2 wt%	S	S	S	S
Phenol-4PO-30EO	0.5 wt%	S	S	S	S
	1 wt%	S	S	S	S
	2 wt%	S	S	S	S
Phenol-7PO-5EO	0.5 wt%	S	C	PS	PS
	1 wt%	C	C	PS	PS
	2 wt%	C	C	PS	PS
Phenol-7PO-10EO	0.5 wt%	S	S	PS	PS
	1 wt%	S	C	PS	PS
	2 wt%	S	S	PS	PS
Phenol-7PO-15EO	0.5 wt%	S	S	C	PS
	1 wt%	S	S	S	PS
	2 wt%	S	S	S	PS
Phenol-7PO-20EO	0.5 wt%	S	S	S	PS
	1 wt%	S	S	S	PS
	2 wt%	S	S	S	PS
Phenol-7PO-30EO	0.5 wt%	S	S	S	S
	1 wt%	S	S	S	S
	2 wt%	S	S	S	S
Phenol-7PO-40EO	0.5 wt%	S	S	S	S
	1 wt%	S	S	S	S
	2 wt%	S	S	S	S

Table 5.2 Phase behavior test result at 95°C

Phenol-4PO-20EO, phenol-4PO-25EO, phenol-7PO-30EO and phenol-7PO-40EO resulted in low IFT emulsion.
(E = oil-in-water macro-emulsion / N = no emulsion / Blank = not tested)

Phenol-4PO-xEO					Phenol-7PO-xEO				
EO #	Salinity [wt%]	Concentration [wt%]			EO #	Salinity [wt%]	Concentration [wt%]		
		0.5	1	2			0.5	1	2
15	0	N			30	0	N	E	E
	0.1	N				0.1	N	E	E
	0.5	N				0.5	N	N	N
	1	N				1	N	N	N
	2	N				2	N	N	N
	3	N				3	N	N	N
20	0	N	E	E	40	0	N	E	E
	0.1	N	E	E		0.1	N	N	N
	0.5	N	N	N		0.5	N	N	N
	1	N	N	N		1	N	N	N
	2	N	N	N		2	N	N	N
	3	N	N	N		3	N	N	N
25	0	N	E	E					
	0.1	N	N	E					
	0.5	N	N	N					
	1	N	N	N					
	2	N	N	N					
	3	N	N	N					
30	0	N	N	N					
	0.1	N	N	N					
	0.5	N	N	N					
	1	N	N	N					
	2	N	N	N					
	3	N	N	N					

Brine Salinity [wt%]	SAS				
	Concentration [wt%]	Phenol-4PO-20EO	Phenol-4PO-25EO	Phenol-7PO-30EO	Phenol-7PO-40EO
0	1				
	2				-
0.1	1		-		
	2				-

Figure 5.2 Phase behavior test result at 95°C

Phenol-4PO-20EO and phenol-7PO-30EO resulted in low IFT mixing behavior

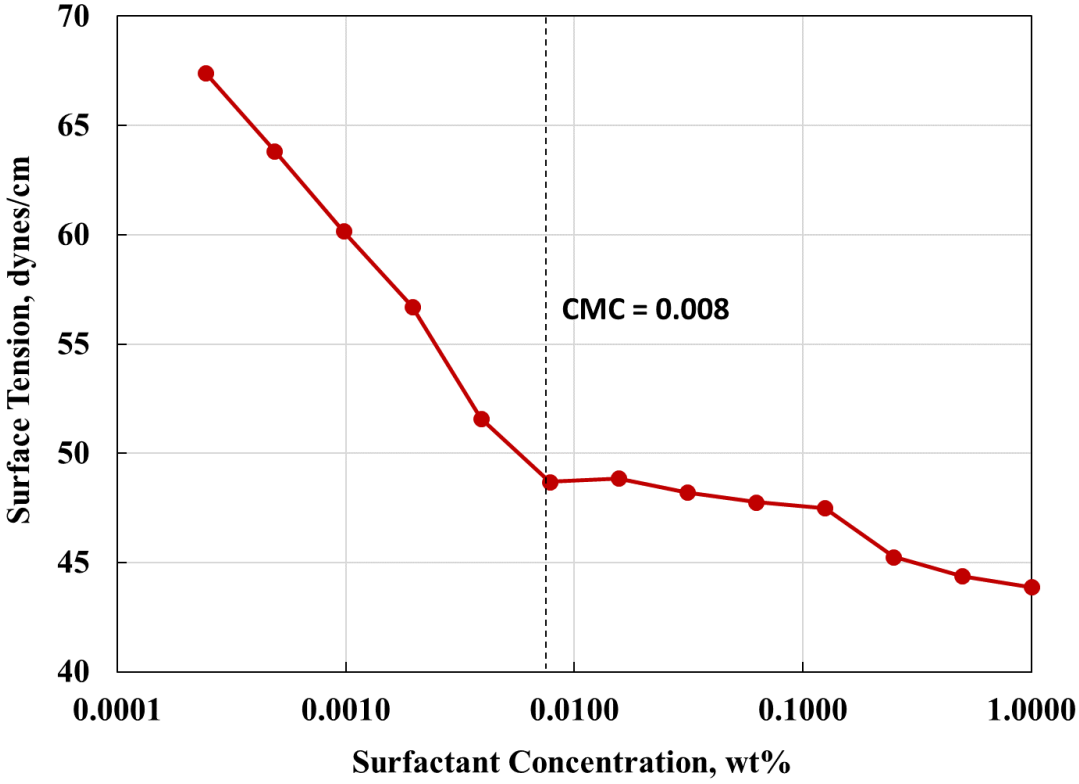

Figure 5.3 CMC (critical micelle concentration) of phenol-4PO-20EO

The IFT was measured by the pendant drop method at the room temperature.

5.3. Oil Displacement and Fractional Flow Calculation

5.3.1. Oil Displacement Results

Water flooding, polymer flooding, and improved polymer flooding by adding phenol-4PO-20EO were conducted. With the objective of quantifying the incremental recoveries by the polymer flooding and the improved polymer flooding, all displacements were conducted in the secondary-recovery mode.

Three flooding experiment results are summarized in **Table 5.3**. The phenol-4PO-20EO was injected as part of two pore volumes (PV) of polymer solution for the improved polymer flooding in this experiment, but it would be a slug for oil-displacement fronts in field applications.

Figure 5.4 shows a schematic of the experimental setup. There were three accumulators for the heavy oil, the initial reservoir brine (5 wt% NaCl), and the injection fluids. The injection fluids were 0.1 wt% NaCl brine for the water flooding, 0.22 wt% polymer in 0.1 wt% NaCl brine for the polymer flooding, and 2 wt% phenol-4PO-20EO with 0.22 wt% polymer in 0.1 wt% NaCl brine for the improved polymer flooding. The system pressure and the injection flow rate were controlled by ISCO pumps. The system temperature was kept at 95°C in a Blue-M oven. System pressure and temperature were monitored and recorded by a data-acquisition system.

The general experimental procedure is described here. First, the porous medium and all flow-lines were cleaned with toluene and dried at 95°C for 1 day. After that, the system was evacuated for at least 2 hours. Then, the glass-bead pack was saturated with the reservoir brine (5 wt% NaCl). Based on the volume injected, the pore volume of the glass-bead pack was measured. The reservoir brine was injected for several pore volumes to calculate the permeability of the glass-bead pack with Darcy's equation. Thereafter, the

oil was injected. The reservoir brine was collected from the outlet during the oil injection. Oil breakthrough and water recovery were measured to determine the initial oil and water saturations for the subsequent oil displacement experiment. Several pore volumes of oil were injected to estimate the end-point relative permeability to oil.

Total 2 PV of the injection fluid was injected at the injection rate of 0.2 ml/hr, which corresponds to 1 ft/day in the porous medium. The corresponding shear rate in the porous medium was approximately 8 sec^{-1} based on the correlation of Cannella et al. (1988). The oil recovery was measured by a graduated cylinder at the effluent. After 2 pore volume injection (PVI), more than 200 ml of injection fluid was additionally injected to estimate the end-point relative permeability to the injection fluid.

The capillary number of the water flooding was 3.4×10^{-8}, which is in the normal range of water flooding (Lake et al. 2014). The capillary number of the polymer flooding was 4.4×10^{-6} because of the increased viscosity of the displacing fluid. The capillary number of the improved polymer flooding was 1.2×10^{-4} because of the IFT reduction by the SAS (2 wt% phenol-4PO-20EO).

Figure 5.5 presents the cumulative oil recovery for each flooding experiment. The water flooding case defines the basis for evaluating the polymer flooding, which in turn gives the basis for evaluating the improved polymer flooding. The oil recovery at 1 PVI was 27% for the water flooding case, 50% for the polymer flooding case, and 79% for the improved polymer flooding. The oil recovery at 2 PVI was 30% for the water flooding case, 62% for the polymer flooding case, and 84% for the improved polymer flooding. That is, the SAS (2 wt% phenol-4PO-10EO in this research) added to the polymer solution yielded an incremental recovery of 29% in comparison to the polymer flooding case at 1 PVI.

The water flooding showed the water breakthrough at 0.2 PVI, which resulted from the adverse effect of low-viscosity water on the efficiency of oil displacement by water. The polymer flooding case showed a delayed breakthrough around 0.5 PVI, which resulted in a twofold increase in oil recovery at 2 PVI in comparison to the water flooding case. The improved polymer flooding showed the breakthrough around 0.7 PVI resulting in the aforementioned increase in oil recovery in comparison to the polymer flooding. This improvement by the addition of the SAS to polymer was attributed to the lowered IFT (from 11 to 0.39 dynes/cm) because that is the main difference from the polymer-alone injection. The effect of lowered IFT on polymer flooding was confirmed by matching experimental results with fractional flow theory in the following section.

5.3.2. Fractional Flow Calculation

Results from the oil displacement experiments were matched by fractional flow theory (Pope 1980). The main purpose was to evaluate the effect of the reduced IFT on the improved polymer flood in comparison to the water and polymer floods.

It was assumed that there was no oil in the aqueous phase during the improved polymer flooding. This assumption was validated by the phase behavior test that resulted in less than 1 vol% of oil in the aqueous phase. Therefore, the viscosity of the displacing fluid for the improved polymer flooding was assumed to be same as the polymer solution viscosity.

Figure 5.6 presents the relative permeability curves required to match the data for the water flooding, the polymer flooding, and the improved polymer flooding. The end-point relative permeabilities for heavy oil and brine (dots) were measured during the experiment. The end-point relative permeability for the SAS-polymer solution and the exponent of each curve were calibrated to match the breakthrough times and oil recoveries.

The capillary end effect for each oil displacement was estimated by Rapoport and Leas number (Rapoport and Leas 1953). The scaling coefficient for the polymer flooding and the improved polymer flooding was 42.3 cp·cm^2/min, indicating no capillary end effect. The scaling coefficient of the water flooding was 0.33 cp·cm^2/min that might indicate the possibility of capillary end effect. Therefore, the fractional flow was matched with the polymer flooding first. The water flooding was matched with the same relative permeability curves that were used for the polymer flooding.

After that, a new set of relative permeability curves was constructed with the lowered residual oil saturation for the improved polymer flooding from 0.3 to 0.05. This residual oil saturation reduction was attributed to the reduced IFT by the addition of the SAS, which is the main difference between the polymer flood and the improved polymer flood. Figure 5.5 shows that the fractional flow curves are in good agreement with the cumulative oil recovery data. In particular, the agreement in terms of water and polymer breakthrough times can be confirmed by the changes in oil production rate. Figure 5.5 also shows the agreement in terms of the ultimate oil recovery factors.

Table 5.3 Summary of oil displacement experiments

Experiment		Water Flooding	Polymer Flooding	Improved Polymer Flooding
Glass-bead pack	Porosity	33%	33%	33%
	Permeability	9.65 Darcy	9.49 Darcy	9.45 Darcy
	Oil Viscosity at 95°C	276 cp	276 cp	276 cp
	Reservoir Brine	5 wt% NaCl	5 wt% NaCl	5 wt% NaCl
Injection Fluids (Secondary Flooding)	Brine	0.1 wt% NaCl	0.1 wt% NaCl	0.1 wt% NaCl
	Polymer	N/A	0.22 wt% HPAM 3630S	0.22 wt% HPAM 3630S
	SAS	N/A	N/A	2 wt% Phenol-4PO-20EO
	Viscosity at 8 sec^{-1}	N/A	40 cp	40 cp
Injection Rate		0.2 ml/hr	0.2 ml/hr	0.2 ml/hr
Capillary Number (N_C)		3.4×10^{-8}	4.4×10^{-6}	1.2×10^{-4}
Pore Volume Injection (PVI)		2 PVI	2 PVI	2 PVI
Water Breakthrough		0.2 PVI	0.5 PVI	0.7 PVI
Oil Recovery at 1 PVI		27%	50%	79%
Oil Recovery at 2 PVI		30%	62%	84%

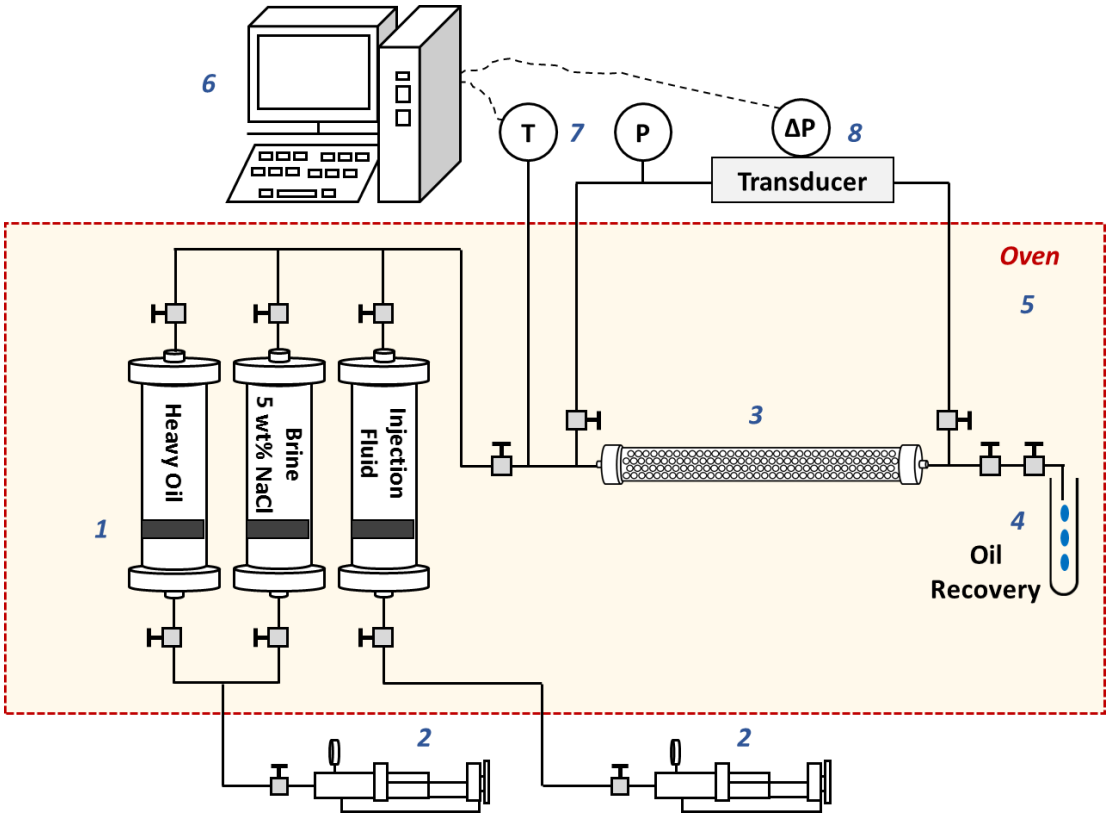

1. Accumulators
2. ISCO Pump
3. Glass-bead pack
4. Graduated Cylinder
5. Blue M Oven
6. Data-acquisition system
7. Temperature Gauge
8. Pressure Transducer

Figure 5.4 Schematic of the experimental set-up for oil displacement

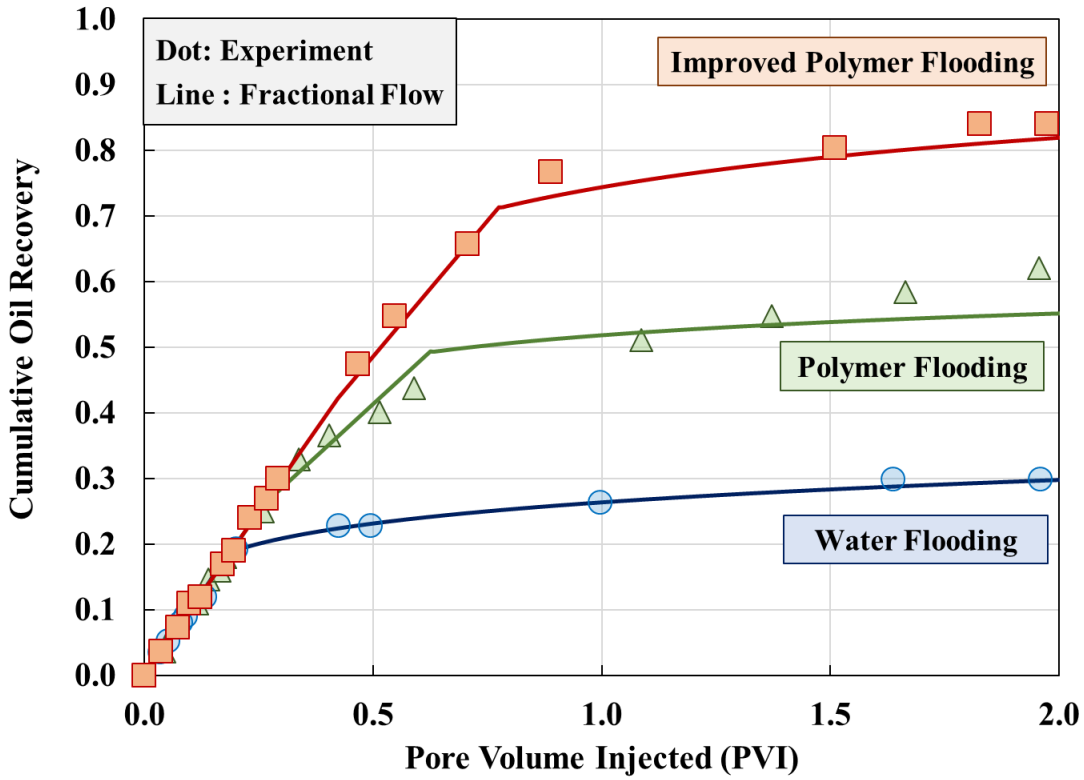

Figure 5.5 Oil displacement results

The cumulative oil recovery factors at 2 PVI was 30% for water flooding, 62% for polymer flooding, and 84% for the improved polymer flooding. The oil recovery data were matched by fractional flow calculation by using the parameters given in Figure 5.6.

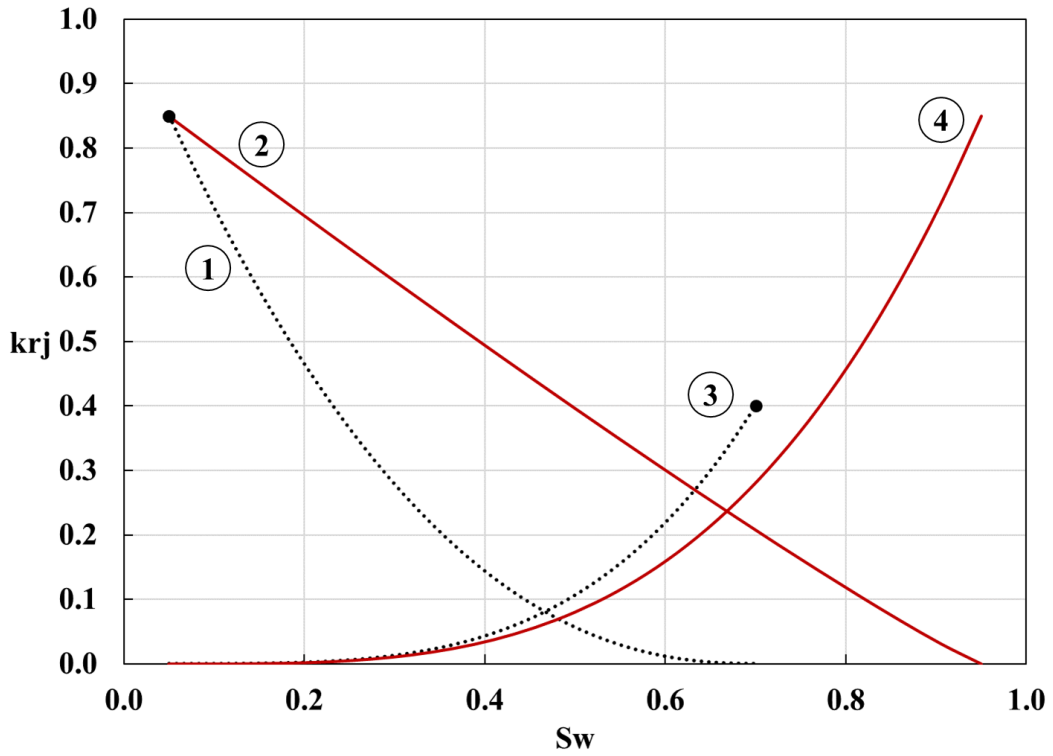

1	kro (Water flooding, Polymer flooding)	3	krw (Water flooding, Polymer flooding)
2	kro (Improved polymer flooding)	4	krw (Improved polymer flooding)

	Water Flooding Polymer Flooding	Improved Polymer Flooding
S_{wr}	0.05	0.05
S_{or}	0.3	0.05
k^o_{rw}	0.4	0.85
k^o_{ro}	0.85	0.85
n_w	3.6	3.4
n_o	2.3	1.1

Figure 5.6 Relative permeability for the fractional flow calculation

The same relative permeability curve was used for water flooding and polymer flooding. A relative permeability curve was constructed for improved polymer flooding. The shaded parameters (green) in the table were measured and shown as dots in the figure. The other parameters were determined by matching the oil displacement results.

5.4. Potential Advantage of SAS

The SAS is designed to have multiple functions in one compound. That is, it has characters of solvent (i.e., phenol in this experiment), and its PO and EO units respectively give the hydrophobicity and hydrophilicity. The aqueous stability of the SAS at the desired temperature and the brine composition can be found by changing the EO number. As shown with phenol-xPO-yEO in this experiment, the optimal selection of the SAS for a given oil displacement can be done in a systematic manner.

The result of the improved polymer flooding suggests a potential opportunity of enhanced heavy oil recovery by using a simple non-ionic SAS as a sole additive to widely-used polymer flooding. Results so far indicate that the improved polymer flooding relies on the effect of a SAS on oil displacement efficiency.

Unlike the conventional SP and ASP flooding, the ultra-low IFT (e.g., 10^{-3} dynes/cm) was not achieved during the improved polymer flooding; however, using only one additive to the traditional polymer flooding yields the simplicity of the method implementation. In general, ASP flooding requires various types of chemicals: an alkali, a polymer, surfactants, co-surfactants, and co-solvents. The design and implementation become inevitably more complicated as the number of additives increases.

Also, the SAS is relatively less expensive than conventional surfactants; for example, the cost is expected to be about 1.25 USD/lb (100% active basis) because the base solvent (e.g., phenol) is not expensive. Furthermore, the non-ionic SAS is expected to have little adsorption on rock surfaces (Fortenberry et al. 2015; Upamali et al. 2018). This would also contribute to simpler and less expensive implementation.

5.5. Conclusions

This was a preliminary study of SAS to improve the displacement efficiency of polymer flooding. Phenol-4PO-20EO was used as a sole additive to the conventional polymer flooding for heavy oil recovery.

The optimal EO and PO numbers were found in terms of phase behavior and IFT at 95°C. Heavy oil displacements (276 cp at 95°C) through the glass-bead pack were conducted by the water flooding, the polymer flooding, and the improved polymer flooding. Each flooding result was compared to quantify the effect of the simple non-ionic SAS on heavy oil displacement. Key conclusions are as follows:

- The selection of the optimal SAS can be done in a systematic manner as demonstrated with phenol-xPO-yEO in this research. This non-ionic SAS was made by the alkoxylation of phenol that shows a high level of affinity for the heavy oil studied in this research. Then, the optimal ranges of EO and PO numbers were found at reservoir conditions in terms of temperature and brine salinity.
- Phenol-4PO-20EO was selected as the optimal SAS for the improved-polymer flooding at 95°C. The IFT between the heavy oil and the 2 wt% phenol-4PO-20EO solution was measured to be 0.39 dynes/cm at 95°C. This is a substantially lower IFT compared to the IFT between the heavy oil and the brine without phenol-4PO-20EO, 11 dynes/cm at 95°C.
- The improved polymer flooding resulted in 79% oil recovery after 1 PVI. It was 52% more recovery than the water flooding, and 29% more recovery than the polymer flooding. The polymer flooding improved the oil recovery efficiency by increasing the water viscosity. The polymer flooding was improved by the addition of 2 wt% phenol-4PO-20EO, which reduced the IFT between the displacing and the displaced phases. The fractional flow theory along with the experimental results indicated that the

lowered IFT resulted in the significant reduction of residual oil saturation during the improved polymer flooding.

- The experimental results suggest a new opportunity of enhanced heavy oil recovery by adding a slug of the SAS to the conventional polymer flooding. The injection solution was composed of one non-ionic SAS and one polymer without any alkali, co-surfactants, and co-solvents. Depending on the cost of the base solvent (e.g. phenol in this research), the cost of SAS can be lower than conventionally used surfactants for ASP and SP.
- As a preliminary study, the experimental conditions in this research were simplified. The reservoir brine and the injection brine were composed of NaCl only. There was no slug control during the improved polymer flooding such as a certain pore volume of SAS-polymer solution slug followed by polymer drive. Therefore, the further research on the improved polymer should be subject to reservoir conditions and injection strategies that are more relevant to an oil field. For example:
  - Reservoir oil
  - Reservoir conditions: pore size distribution, permeability, porosity, temperature
  - Brine salinity and composition
  - Optimum slug size of SAS-polymer solution

6. Improved Polymer Flooding using SAS for North-Sea Heavy Oil Reservoir

The preliminary study on the improved polymer flooding (Chapter 5) shows the potential advantage of using a SAS as a single additive to polymer for the incremental heavy oil recovery. In this chapter, the improved polymer flooding is studied for a heavy oil reservoir in North Sea, where the original operation plan is straight polymer flooding. The main difference between the improved polymer flooding in this research and the conventional SP flooding is that there is no micro-emulsion in the improved polymer flooding. The expected mechanism of SAS is IFT reduction by a few orders of magnitude. It will cause capillary desaturation by increasing capillary number, leading to less snap-off (or trapping-off) of oil.

It is well known that we can reduce the residual oil saturation (or remaining oil saturation) by increasing capillary number (Figure 2.3). Capillary number is defined as follows:

$$\text{Capillary number, Nc} = \frac{k\Delta P}{\sigma L}$$

where k is permeability, ΔP is pressure drop, σ is interfacial tension (IFT), and L is the length of core. At a given system, permeability (k) and length (L) are fixed. Therefore, capillary number can be increased by increasing pressure drop (ΔP) or reducing IFT.

The typical IFT values between oil and brine range between 15 - 20 dynes/cm. If a SAS could reduce IFT to 0.01 - 0.1 dynes/cm, the capillary number can be increased by 2 - 3 orders of magnitude. When this increased capillary number lies above its critical capillary number, we can reduce the residual oil saturation and increase oil recovery.

Recently, there are several studies focusing on the interfacial elasticity to achieve the incremental oil recovery (Bidhendi et al. 2018; Chávez-Miyauchi et al. 2016 and 2020). These studies attempted to explain the mechanism of the low salinity water injection by increasing the interfacial elasticity between the oil phase and the brine phase. The higher interfacial elasticity reduced the snap-off of oil in porous media and resulted in more continuous oil flow, and finally, more oil recovery. It was found that a non-ionic surfactant improved the interfacial elasticity between the oil phase and the aqueous phase (Chávez-Miyauchi et al. 2016). In addition, acidic components (or asphaltenes) are known to increase the interfacial elasticity (Reilly et al. 2018). Therefore, it is expected that the interfacial elasticity between the heavy oil and the aqueous phase would be high with a non-ionic SAS.

The goal of this research is to find the mechanism of the incremental oil recovery using the SAS. The question is: **under what condition, does the improved polymer flooding increase the oil recovery in comparison to straight polymer flooding?** To answer this question, an optimum SAS and its slug size were found for a substantial increase in oil recovery. Phase behavior (mixing and separation behavior), IFT measurement, viscosity measurement, and sandpack flooding were conducted under the actual reservoir conditions.

Section 6.1 summarized materials for this experiment. Then, phase behavior study including IFT measurement is described in Sections 6.2 and 6.3. Tracer test and in-situ polymer viscosity measurement are explained in Sections 6.4 and 6.5.

Sandpack flooding results with different injection schemes are summarized in Section 6.6. Section 6.7 presents the case that the improved polymer flooding did not work. In Section 6.8, I discuss the conditions required for the successful improve polymer flooding with experimental data. Section 6.9 draws conclusions of this chapter.

6.1. Materials

Oil Field

The reservoir is located in North Sea. This is an unconsolidated sand reservoir containing heavy oil (about 500 cp) at the reservoir temperature of 38°C. The reservoir brine salinity is 56,456 ppm. At the current stage, the operation plan is straight polymer flooding.

Table 6.1 Heavy oil properties

Property		Value	Method
Molecular Weight		428 g/mol	Freezing Point Depression
Acid Number		8.08 mg-KOH/g-oil	ASTM D 664
SARA	Saturates	53.5 wt%	Liquid-Solid Chromatography
	Aromatics	22.8 wt%	
	Resins	20.8 wt%	
	Asphaltenes	2.9 wt% (Pentane insoluble)	
Viscosity (dead oil)		3,160 cp (at 38°C) 500 cp (at 61°C)	In-house rheometer

Heavy Oil

An analogous heavy oil (dead oil) was tested in this research. The properties of analogous heavy oil are closed to those of heavy oil from the actual reservoir. Basic properties of the heavy oil were measured by Exova laboratory (Edmonton, Alberta, Canada). The molecular weight (MW) of the heavy oil was measured to be 428 g/mol by freezing point depression. Simulated distillation analysis was performed up to 720°C. SARA analysis gave the following composition: 53.5 wt% saturates, 22.8 wt% aromatics,

20.8 wt% resins and 2.9 wt% asphaltenes. This is a very acidic oil with the total acid number of 8.08 mg-KOH/g-oil. The properties of heavy oil are summarized in **Table 6.1**. To match the oil viscosity of 500 cp, the experimental temperature was set to be 61°C.

Sandpack

The dimension of a sandpack is 30.48 cm (= 1 foot) length and 2.54 cm (= 1 inch) diameter. The grain size distribution of the reservoir is illustrated in **Figure 6.1**. A sandpack was prepared to match the cumulative grain size distribution. Ottawa sand was filtered with five different grain sizes. Before packing sand, the filtered sand was acidized by 10 wt% HCl solution (2.7 Molarity of HCl, pH = -0.44). After acidizing, each filtered sand was re-filtered by the same sieve number. The grain size distribution of the sandpack is summarized in **Figure 6.2** and **Table 6.2**.

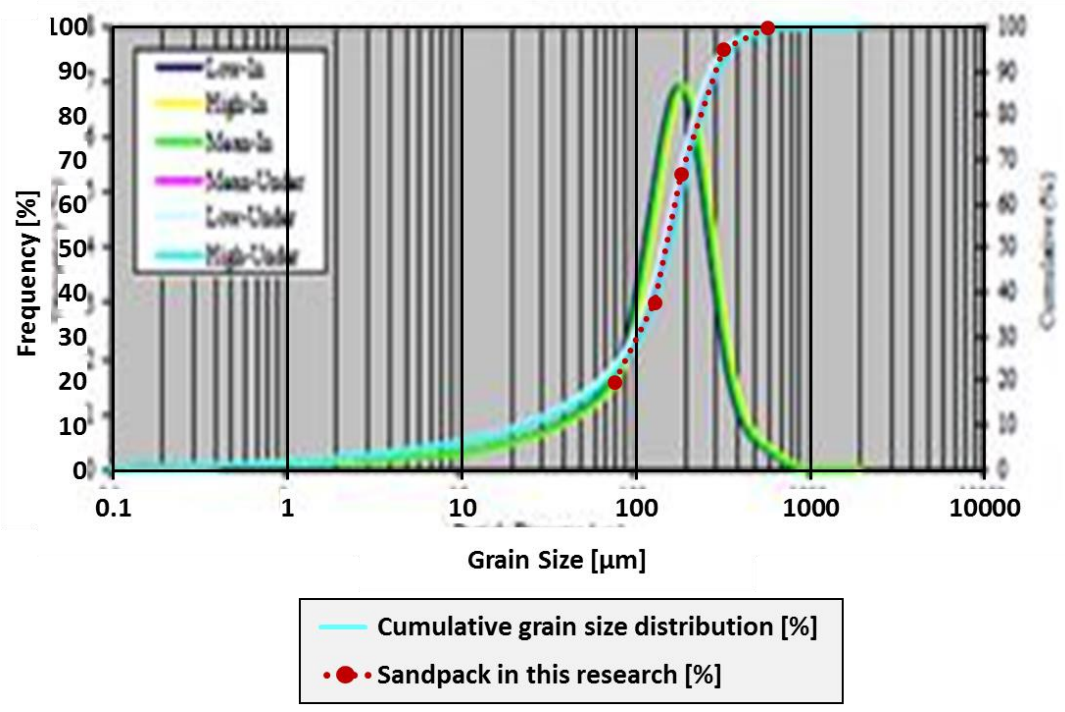

Figure 6.1 Reservoir grain size distribution

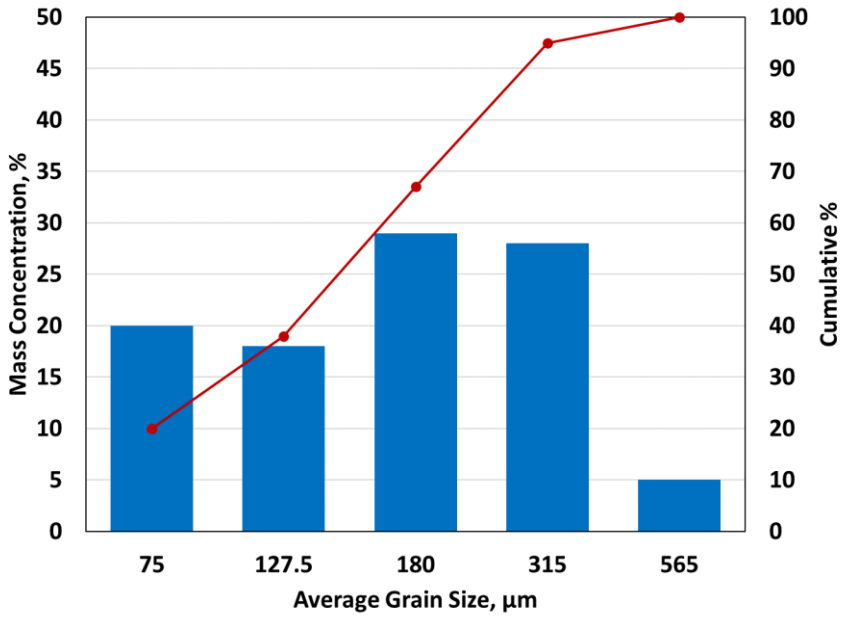

Figure 6.2 Sandpack grain size distribution

Table 6.2 Sand filtering to match the grain size distribution

Sieve #	Lower Limit [µm]	Upper Limit [µm]	Average Size [µm]	Frequency [%]	Cumulative [%]
325	45	105	75	20	20
140	105	150	127.5	18	38
100	150	210	180	29	67
70	210	420	315	28	95
40	420	710	565	5	100

To improve the visual observation during sandpack flooding, a sandpack accumulator was made of a transparent polycarbonate. A block of polycarbonate was purchased from Boedeker Plastics (product name: TECANAT ® PC Unfilled

Polycarbonate) and a sandpack accumulator was manufactured by the machine-shop in this department. The detailed design and photos of the accumulator is shown in **Figure 6.3**.

The operation temperature of polycarbonate ranges from -30 to 121°C. The maximum pressure depends on the thickness of an accumulator. With 1.9-cm thickness, it can handle up to 27.6 bars (= 400 psi) (confirmed by the machine-shop in this department). Polycarbonate is not compatible with a strong acid, a strong base, acetone, and toluene, none of which was used in this experiment. The fluids injected in the accumulator were reservoir brine, polymer solution, DI water (for cleaning), IPA (for cleaning), and hexane (for cleaning).

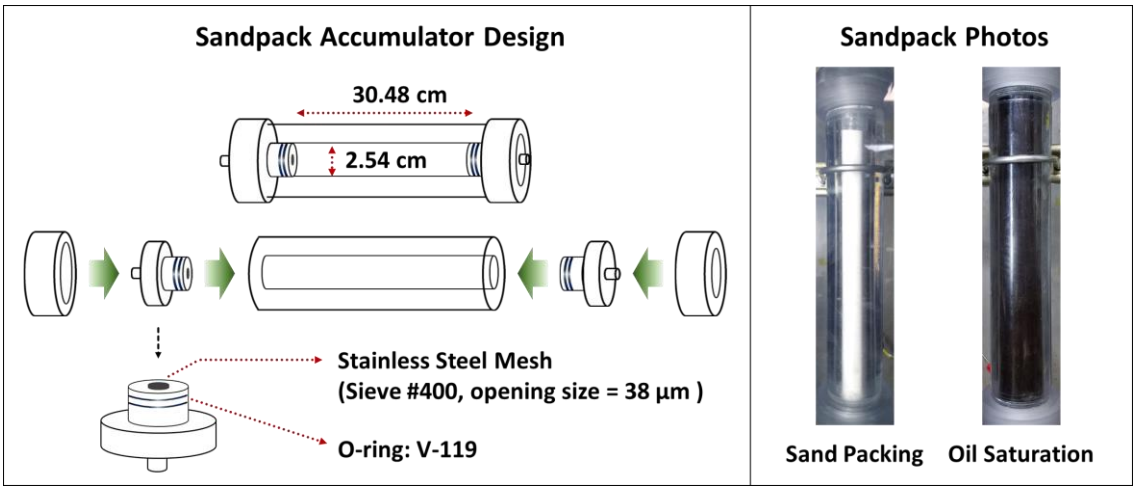

Figure 6.3 Transparent sandpack accumulator (polycarbonate)

Brine

The salinity of the reservoir brine is 56,456 ppm. According to the operation plan, the produced reservoir brine is going to be used for polymer flooding. Therefore, the

salinity of the injection brine and the reservoir brine is set to be same. The composition of brine is summarized in **Table 6.3**.

Table 6.3 Brine composition

Ions	Concentration [mg/L]
Na^+	18,387
K^+	200
Ca^{2+}	2,015
Mg^{2+}	958
Cl^-	34,883
SO_4^{2-}	13
Total Dissolved Solid (TDS)	56,456

Polymer

In this research, partially hydrolyzed polyacrylamide (HPAM) polymer, Flopaam 3630S (SNF), was used for a polymer flooding and an improved polymer flooding. This is a powder type polymer with an approximate molecular weight of 20 million Dalton.

The polymer concentration was 0.54 wt% in the reservoir brine, which gave the viscosity of approximately 60 cp at the shear rate of 7 sec^{-1}. For the improved polymer flooding, a target concentration of a SAS was directly added in the polymer solution.

Special cares are required during polymer solution preparation and experiment. Polymer solutions can be easily degraded chemically or mechanically. Sorbie classified three different mechanisms of polymer degradation as follows (Sorbie 1991):

First, the chemical degradation is the breakdown of polymer molecules by contaminants like oxygen. Oxygen attacks the molecular structure of hydrolyzed polymer. The chemical degradation occurs not only in a reservoir but also in the process of polymer

solution preparation. Second, the mechanical degradation occurs due to high shear rate where the mechanical stress breaks the polymer structure. This occurs when a polymer solution passes through porous media at high rates. But also, the mechanical degradation could occur during polymer solution preparation when polymer is mixed at too high speed (rpm) and too long time. Third, the biological degradation refers microbial breakdown of polymer by bacteria. This can be prevented by the effective biocides.

In this research, a polymer solution and SAS-polymer solution were prepared in a way to avoid any degradations. The polymer solution and the SAS-polymer solution were prepared as follows. One batch of polymer solution was no more than 400 ml. The polymer was added after the brine (or brine + SAS) solution was prepared. While adding polymer powders in the brine (or brine + SAS) solutions, the extra caution is required. Polymer was added while the solution is under mixing at 500 rpm. Polymer powders should be sprinkled into the solution at the consistent rate (manually), so that no polymer aggregation occurred.

The mixing rate and time of the polymer (or SAS-polymer) solution was fixed at 500 rpm for 3 - 4 hours. After mixing, the solution was filtered through 1.2 μm filter. Filtration ratio (FR) was measured to confirm the quality (homogeneity) of the polymer solution. Filtration ratio (FR) was defined as the time (Δt_2) to collect 20 ml from 180 ml to 200 ml divided by the time (Δt_1) to collect 20 ml from 60 ml to 80 ml. The polymer solution is acceptable when FR is smaller than 1.2.

$$\text{Filtration Ratio, FR} = \frac{\Delta t_2}{\Delta t_1} = \frac{t_{200\text{ml}} - t_{180\text{ml}}}{t_{80\text{ml}} - t_{60\text{ml}}}$$

After filtration, the polymer solution was degassed by argon gas for more than 1 hour. This is the step to remove any oxygen in the solution. It is ideal to use the prepared

polymer solution right after degassing. Otherwise, the polymer solution should be kept in a refrigerator until its usage.

Figure 6.4 gives the measured viscosities of the polymer solution and or the SAS-polymer solution at different shear rates at 61°C. The effect of the SAS on the polymer-solution viscosity was not observed.

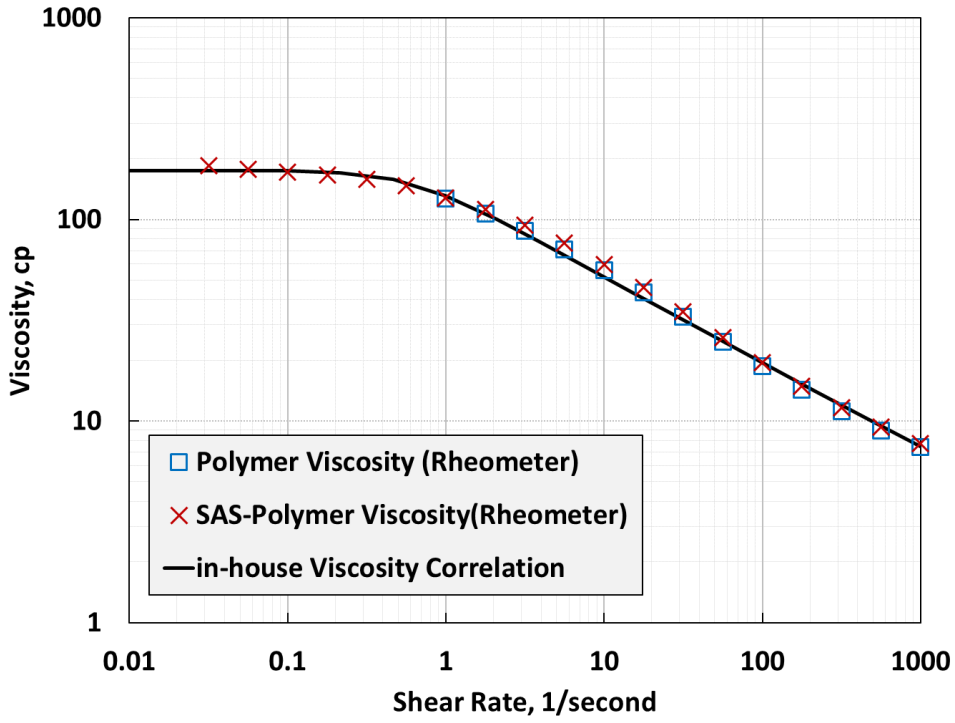

- **Polymer Solution**

Polymer	**0.54 wt% HPAM 3630S (Flopaam, SNF)**
Brine	**56,456 ppm TDS**

- **SAS-Polymer Solution**

Surface Active Solvent	**0.5 wt% 2-EH-7PO-15EO**
Polymer	**0.54 wt% HPAM 3630S (Flopaam, SNF)**
Brine	**56,456 ppm TDS**

Figure 6.4 Polymer viscosity at 61°C (bulk phase viscosity measured by rheometer)

Surface Active Solvent (SAS)

A total of 12 SASs of 2-etheylhexanol(2-EH)-xPO-yEO and phenol-xPO-yEO with different numbers of x and y were tested. The list of SAS is **Table 6.4.** All SASs were provided from Harcros chemicals.

Table 6.4 SAS list

2-EH (2-ethylhexanol)		Phenol	
-xPO	-yEO	-xPO	-yEO
4PO	15	4PO	15
4PO	20	4PO	20
4PO	25	4PO	30
7PO	8	7PO	15
7PO	15	7PO	20
7PO	20	7PO	30

6.2. IFT and CMC Measurement

IFT was measured by a spinning drop tensiometer at 61°C. The concentration of the SAS was 1 wt% in the aqueous solution. The brine salinity was matched to the reservoir brine at 56,456 ppm. IFT was also measured at different salinities from zero ppm (DI water) to 107,266 ppm, proportionally changing with the reservoir brine composition. Results of the IFT measurement are summarized in **Table 6.5** (for 2-EH-xPO-yEO) and in **Table 6.6** (for phenol-xPO-yEO).

Table 6.5 IFT measurement of 2-EH-xPO-yEO solution with heavy oil

Salinity [ppm]	IFT [dynes/cm] (Concentration = 1 wt% / Temperature = 61°C)					
	2-EH-4PO			2-EH-7PO		
	15EO	20EO	25EO	8EO	15EO	20EO
0	1.05	4.02	7.40	(-)	0.27	0.44
5,646	0.77	2.45	4.82	(-)	0.26	0.43
28,228	0.43	0.73	2.32	(-)	0.094	0.19
56,456 (*)	0.20	0.37	0.87	(-)	0.025	0.10
84,684	0.088	0.220	0.290	(-)	(-)	0.045
107,266	0.040	0.134	0.193	(-)	(-)	0.017

Note (*) reservoir brine
(-) it does not pass the aqueous stability

Table 6.6 IFT measurement of phenol-xPO-yEO solution with heavy oil

Salinity [ppm]	IFT [dynes/cm] (Concentration = 1 wt% / Temperature = 61°C)					
	Phenol-4PO			Phenol-7PO		
	15EO	20EO	30EO	15EO	20EO	30EO
0	11.28	14.89	14.63	1.22	2.77	6.77
5,646	6.95	11.25	13.01	1.10	1.71	4.63
28,228	1.81	4.26	8.46	0.68	0.86	2.90
56,456 (*)	1.26	1.80	2.68	0.35	0.49	1.13
84,684	0.91	1.25	1.92	(-)	0.31	0.65
107,266	(-)	0.96	1.47	(-)	0.24	0.49

Note (*) reservoir brine
(-) it does not pass the aqueous stability

Results of the IFT measurement show two important trends as shown in **Figure 6.5** and **Figure 6.6**. First, at a given PO number, lower EO number results in lower IFT. This confirms the surface activity of the SAS: propylene oxide (PO) increases affinity for oil and decrease IFT; and ethylene oxide (EO) increases aqueous stability, but increases IFT.

Second, at a given SAS, IFT becomes lower with increasing salinity. As a result, IFT shows the lowest value near its aqueous stability limit, e.g. 2-EH-7PO-15EO or phenol-7PO-15EO. Therefore, the optimum SAS can be found with the combination of PO and EO numbers that is near the aqueous stability limit and results in the lowest IFT, as shown in **Figure 6.7**.

With IFT results, 2-EH-7PO-15EO was selected as the optimum SAS. Then, the critical micelle concentration (CMC) was measured to decide the optimal concentration of 2-EH-7PO-15EO. IFT was measured with the different concentrations of 2-EH-7PO-15EO in the reservoir brine. The same spinning drop tensiometer was used for IFT measurement at 61°C. The result is summarized in **Figure 6.8** and **Table 6.7**. It was found that the CMC of 2-EH-7PO-15EO was 0.025 wt% in the reservoir brine and the IFT was stable at 0.025 dynes/cm above CMC.

Based on the CMC measurement, the concentration of 2-EH-7PO-15EO was set as 0.5 wt% in polymer solution to keep the concentration above CMC during sandpack floods considering possible lost (i.e. adsorption) in a sandpack. Note that the total concentration of surfactants in SP or ASP flooding is usually 1 wt% (Fortenberry et al. 2015; Sharma et al. 2015; Sharma et al. 2018; Tagavifar et al. 2018; Upamali et al. 2018).

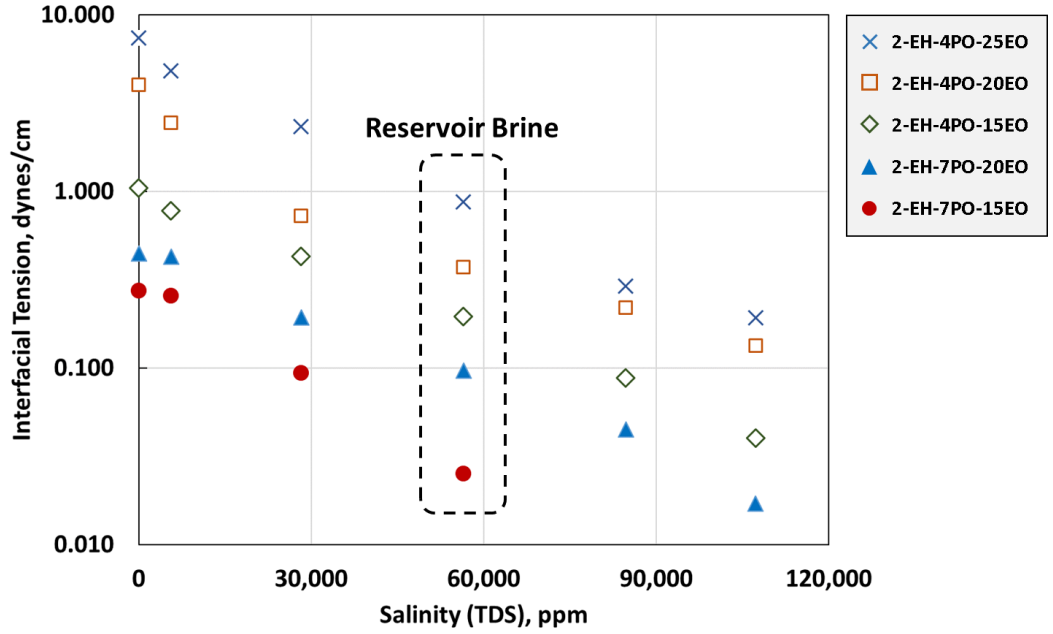

Figure 6.5 IFT of 1 wt% 2-EH-xPO-yEO with heavy oil at 61°C

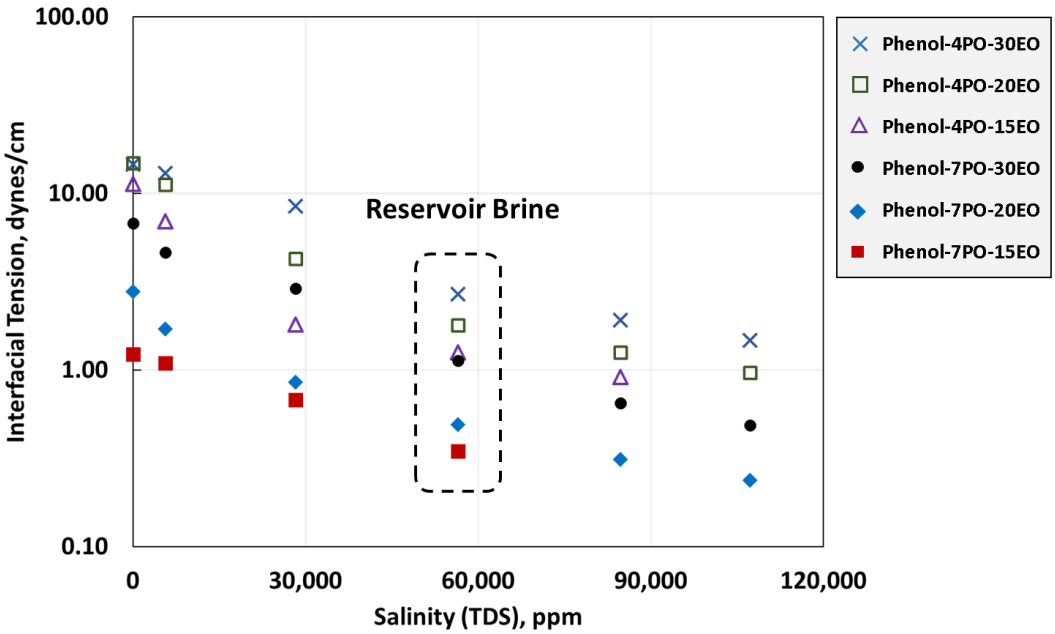

Figure 6.6 IFT of 1 wt% Phenol-xPO-yEO with heavy oil at 61°C

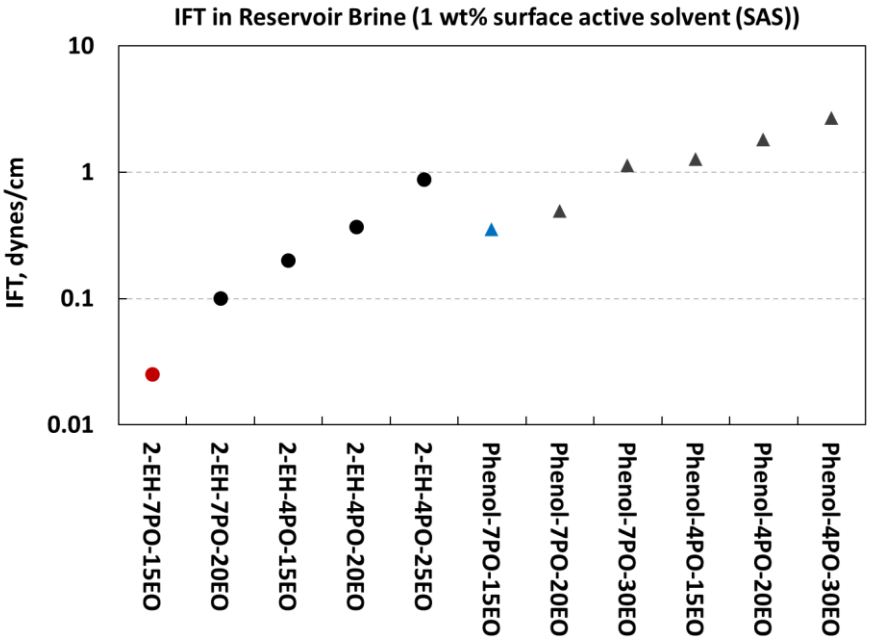

Figure 6.7 IFT of 1 wt% SAS with heavy oil at 61°C in the reservoir brine

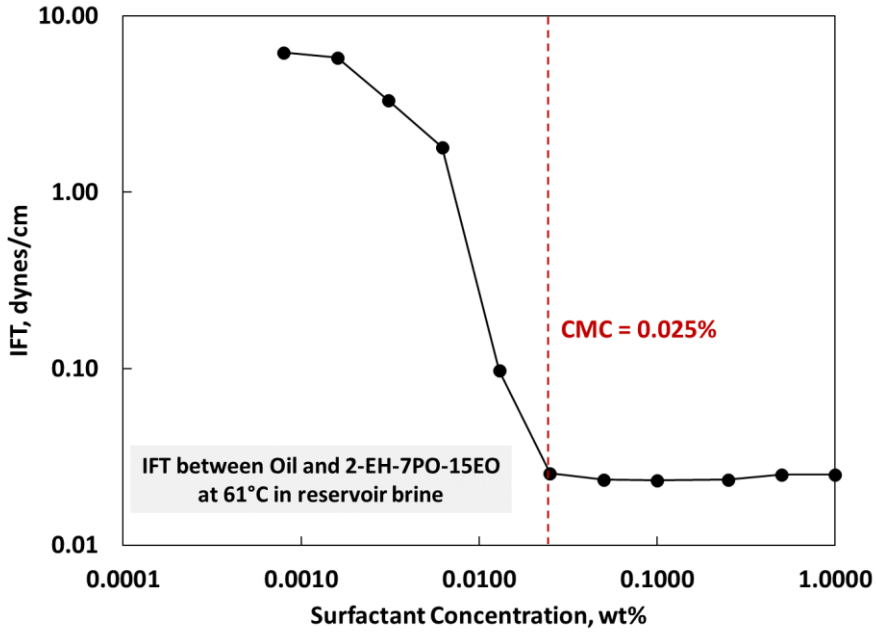

Figure 6.8 CMC of 2-EH-7PO-15EO in the reservoir brine at 61°C

Table 6.7 CMC of 2-EH-7PO-15EO in the reservoir brine at 61°C

2-EH-7PO-15EO Concentration in Reservoir Brine [wt%]	IFT [dynes/cm]
0	15.8
0.0008	6.19
0.0016	5.79
0.0031	3.30
0.0062	1.80
0.013	0.098
0.025	0.025
0.05	0.023
0.1	0.023
0.25	0.023
0.5	0.025
1	0.025

6.3. Phase Behavior in Pipette

From IFT measurement results, 4 SASs were selected for the further analysis on phase behavior in a pipette: 2-EH-7PO-15EO (0.025 dynes/cm), 2-EH-7PO-20EO (0.096 dynes/cm), 2-EH-4PO-15EO (0.20 dynes/cm), and phenol-7PO-15EO (0.36 dynes/cm), which were the order of the low IFT among 12 SASs. Samples were prepared in 10-ml Pyrex pipettes. The concentration of SASs was 1 wt%. Water-oil-ratio (WOR) was 7:3 (i.e. 70 vol.% aqueous phase and 30 vol.% oil phase). The brine salinity was 56,456 ppm (at reservoir condition). The temperature was 61°C.

For all samples, macro-emulsions were observed. There was no micro-emulsion. After mixing, a single-phase macro-emulsion was created. Then, these macro-emulsions broke into the oil phase and the aqueous phase as the aqueous phase separated out from the oil phase. After long time, there were two phases as follows: oil phase with a very small amount of water and aqueous phase with a negligible amount of oil.

The separation test is summarized in **Figure 6.9**, **Figure 6.10**, and **Table 6.8**. From the left, the composition of the aqueous phase is (1) only reservoir brine, (2) 1 wt% 2-EH-7PO-15EO, (3) 1 wt% 2-EH-7PO-20EO, (4) 2-EH-4PO-15EO, and (5) 1 wt% phenol-7PO-15EO in the reservoir brine. The result of 1 wt% 2-EH-7PO-15EO is the average of 5 samples as shown in **Figure 6.11**.

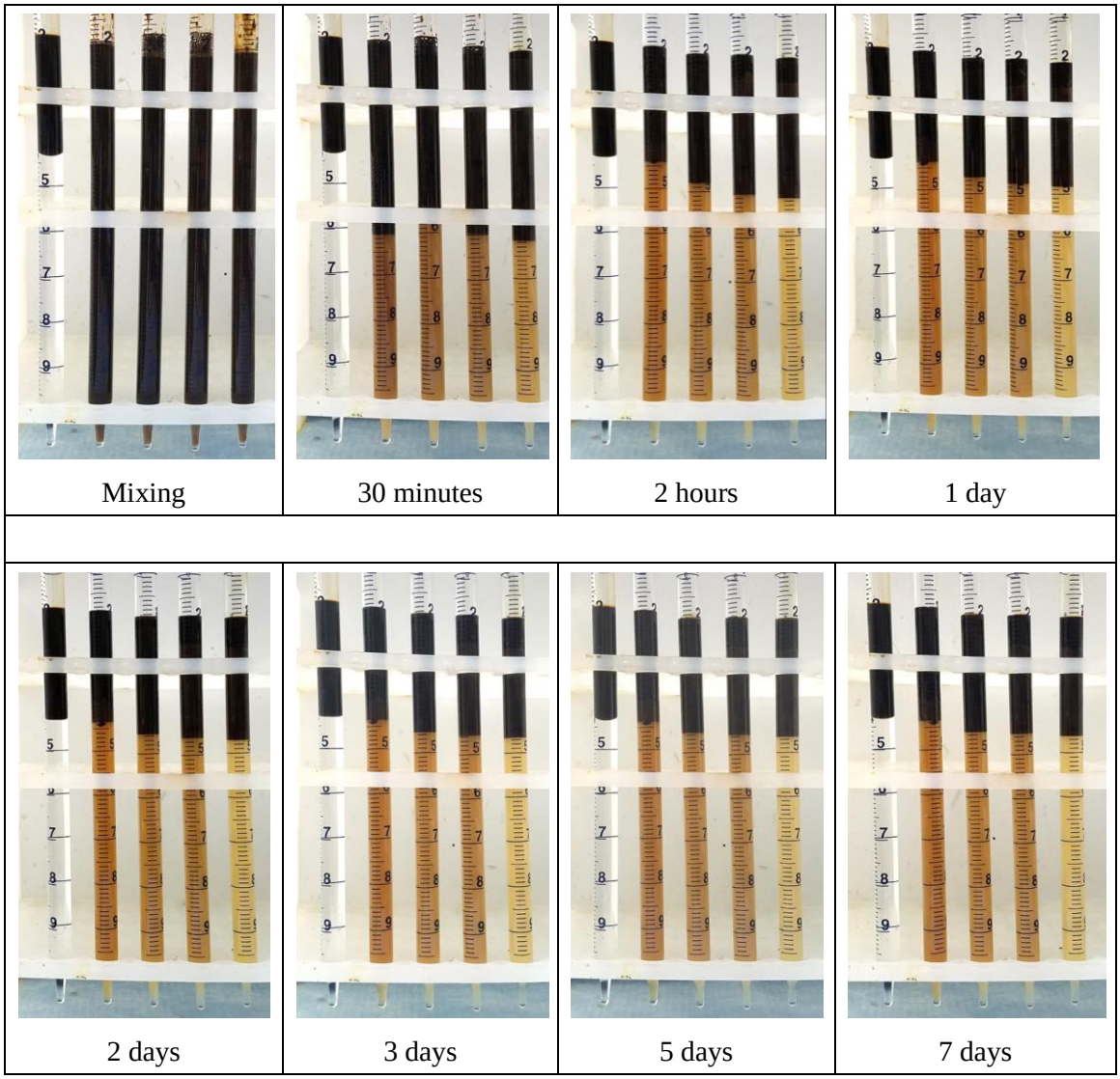

Figure 6.9 Phase separation after mixing

From the left, the composition of the aqueous phase is (1) only reservoir brine, (2) 1 wt% 2-EH-7PO-15EO, (3) 1 wt% 2-EH-7PO-20EO, (4) 1 wt% 2-EH-4PO-15EO, and (5) 1 wt% phenol-7PO-15EO in the reservoir brine. The separation was measured for 11 days. Water content (vol.%) in the oil phase did not change a lot after 7days. Note that the oil amount in the aqueous phase is negligible. Since the heavy oil is very dark black, only a tiny amount of heavy oil can make aqueous phase brown.

Table 6.8 Phase separation after mixing: water content [vol.%] in the oil phase

Aqueous Phase	IFT [dynes/cm]	Water Content in Oil Phase [vol.%]	
		After 1 day	After 11 days
1 wt% 2-EH-7PO-15EO	0.025	7.6	2.0
1 wt% 2-EH-7PO-20EO	0.096	8.4	4.4
1 wt% 2-EH-4PO-15EO	0.20	11.1	4.4
1 wt% Phenol-7PO-15EO	0.36	14.3	8.0

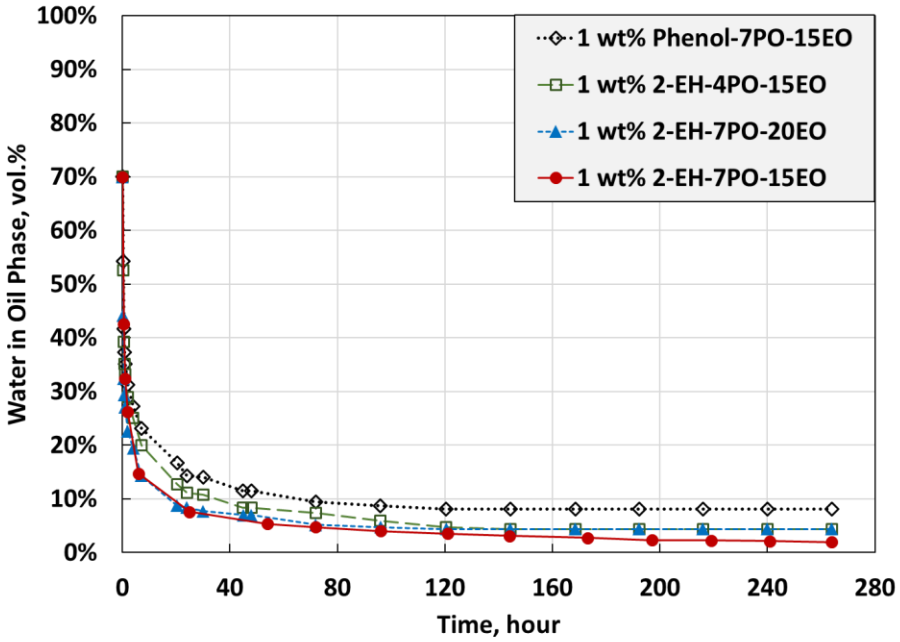

Figure 6.10 Phase separation trend for different SASs

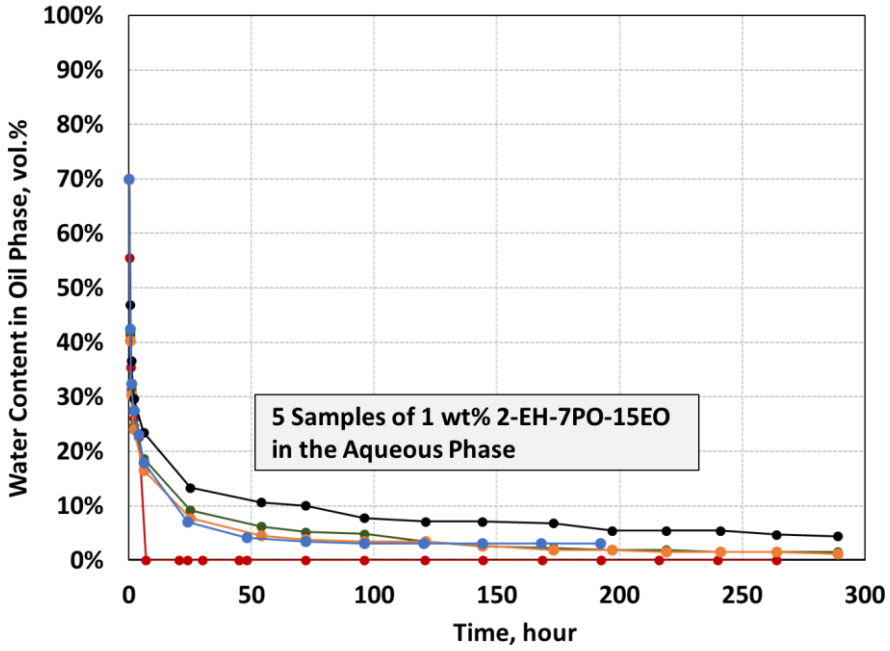

Figure 6.11 Phase separation: 5 samples of 1 wt% 2-EH-7PO-15EO

The separation trend clearly shows that lower IFT samples resulted in the faster emulsion separation and the lower amount of water (vol.%) in the oil phase. This means we can expect better mixing with lowered IFT and the faster separation of emulsion. This is a qualitative confirmation of separation behavior because the mixing procedure and separation time scale are not relevant to actual field operations.

2-EH-7PO-15EO results in not only the lowest IFT, but also faster emulsion separation. To check the effect of concentration, the separation test for 0.5 wt% and 0.7 wt% of samples were compared with 1.0 wt% 2-EH-7PO-15EO sample. Because the CMC of 2-EH-7PO-15EO is 0.025 wt%, they have the same IFT (0.025 dynes/cm). The results are shown in **Figure 6.12** and **Table 6.9**. It shows that the lower concentrations resulted in the faster phase separation. This confirms that 0.5 wt% could be the optimal concentration rather than 1 wt% 2-EH-PO-15EO for sandpack flooding experiment.

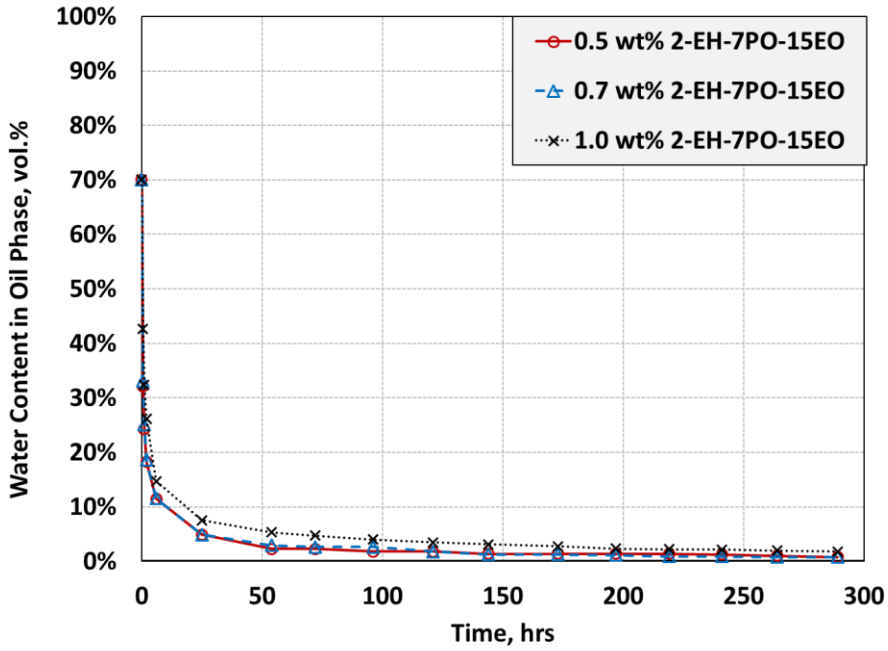

Figure 6.12 Phase separation test for different concentration of 2-EH-7PO-15EO: 0.5, 0.7, and 1.0 wt% in the aqueous phase

Table 6.9 Phase separation test for different concentration of 2-EH-7PO-15EO

Time	2-EH-7PO-15EO Concentration in Aqueous Phase		
	0.5 wt%	0.7 wt%	1.0 wt%
	Water Content in Oil Phase [vol.%]		
0	70.0	70.0	70.0
1 hour	24.3	33.1	42.6
6 hours	11.5	11.5	14.7
1 day	4.9	4.9	7.6
3 days	2.3	2.7	4.8
5 days	1.8	1.8	3.5
7 days	1.4	1.3	2.8
11 days	1.0	0.8	2.0

6.4. Sandpack Tracer Test

A tracer test was conducted to check the homogeneity of the sandpack. Two different salinity of brines were injected. First, the low salinity brine (14,114 ppm, 4 times lower salinity than the original salinity) was injected for 1 pore volume. Then, the high salinity brine (56,456 ppm, the original reservoir brine) was injected for 2 pore volumes. The pump injection rate was kept at 3 ml/hr, which corresponds to 1 ft/day. The normalized salinities of effluent samples were measured. The result is shown in **Figure 6.13**.

When there is no dispersion, the normalized salinity from zero (for 14,114 ppm) to one (for 56.456 ppm) would be plotted as a piston-like displacement. Dispersion makes the effluent concentration change smeared. The experimental data were matched with 1-D convection-dispersion (CD) equation. The analytical solution of CD equation is as follows (Lake et al. 2014, Chapter 5):

$$C_D = \frac{1}{2}\operatorname{erfc}\left(\frac{x_D - t_D}{2\sqrt{\frac{t_D}{N_{Pe}}}}\right) + \frac{e^{x_D N_{Pe}}}{2}\operatorname{erfc}\left(\frac{x_D + t_D}{2\sqrt{\frac{t_D}{N_{Pe}}}}\right)$$

Peclet number (N_{Pe}) is defined as follows:

$$N_{Pe} = \frac{uL}{\phi K_L}$$

where u is Darcy velocity (cm/s), L is distance (cm), ϕ is porosity, and K_L is a longitudinal dispersion coefficient (cm^2/s). In this tracer test, sandpack porosity (ϕ) was 0.32, length (L) was 31.7 cm, and Darcy velocity (u) = 1.3×10^{-4} cm/s. Therefore, experimental data can be matched by adjusting a longitudinal dispersion coefficient (K_L).

With $K_L = 5 \times 10^{-5}$ cm^2/s, experimental data was successfully matched with CD equation. The calculated Peclet Number (N_{Pe}) was 261. The parameters for CD equation are summarized in **Table 6.10**.

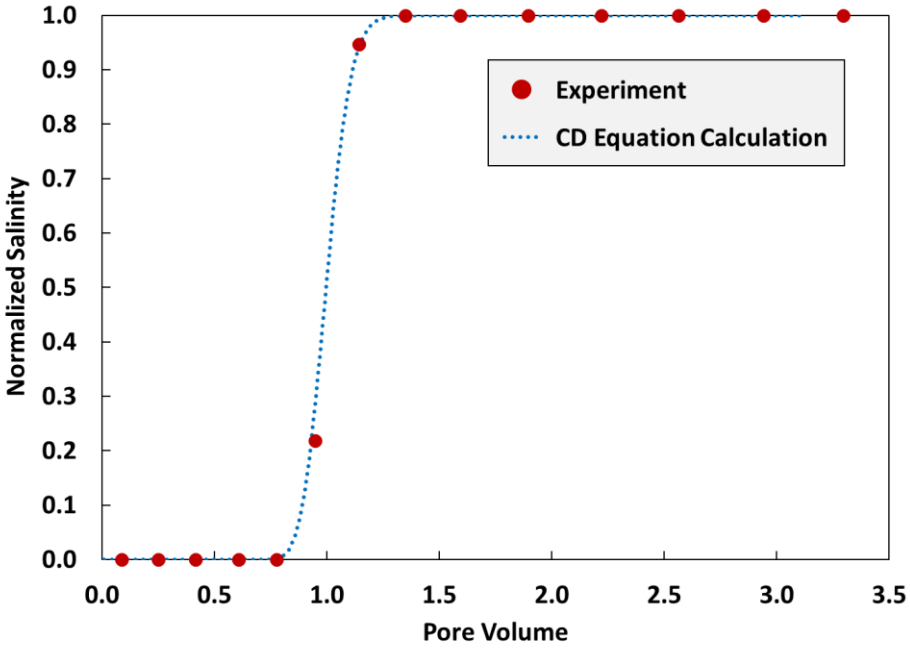

Figure 6.13 Sandpack tracer test

Table 6.10 Sandpack Tracer Calculation

Porosity	0.32
Distance (Sandpack Length)	31.7 cm
Darcy Velocity	1.3×10^{-4} cm/s
Longitudinal dispersion coefficient, K_L	5×10^{-5} cm^2/s
Longitudinal Dispersivity (α_L)	0.384615 cm
Peclet Number (N_{Pe})	261

Peclet number (N_{Pe}) can be expressed as a function of Dispersivity (α_L, cm). In this form, Peclet number (N_{Pe}) is independent of velocity (Lake et al. 2014, Chapter 5).

$$N_{Pe} = \frac{L}{\alpha_L}$$

and

$$\text{Longitudinal dispersion coefficient, } K_L = \alpha_L \times u$$

Dispersion coefficient (K_L) is a function of velocity for a given core (or a sandpack) (Ujfaludi 1986). Dispersivity (α_L) is a constant at a given core (or a sandpack). Therefore, at a given core dimension, Peclet number (N_{Pe}) is constant. This means, at a given core (or sandpack), one cannot change Peclet number (N_{Pe}) by increasing the flowrate.

6.5. In-Situ Polymer Viscosity: Viscoelastic Behavior

The bulk phase polymer viscosity measured by a rheometer shows shear-thinning behavior (Figure 6.4). However, in-situ HPAM polymer viscosity shows a viscoelastic behavior in porous media: polymer viscosity decreases as shear rates increase up to a certain point, and then the in-situ viscosity increases as shear rate increases above that point.

In-situ viscoelastic behavior of HAPM polymer can be found in many studies (Han et al. 1995; Hincapie 2016; Rock et al. 2017; Skauge et al. 2018; Sorbie 1991). Different studies resulted in different viscoelastic behaviors at different shear rates. The viscoelastic behavior is a complex mechanism related to the type of porous media, polymer types and concentrations, and brine compositions and concentrations. Therefore, it is important to measure in-situ polymer viscosity before sandpack flooding experiment.

The compositions of brine, polymer solution and SAS-polymer solution were described in Figure 6.4. The experimental set-up for in-situ viscosity measurement was illustrated in **Figure 6.14**. The system pressure was controlled by ISCO pumps and the temperature was kept in a Blue M oven at 61°C. After 3 hours of evacuation, the sandpack was filled with brine to measure a porosity. Then, the pressure drops at different brine injection rates were measured to determine a permeability. After determining the porosity and permeability, the polymer solution was injected for more than one pore volume to displace the brine completely. Because this is a miscible displacement (brine displaced by water-soluble polymer solution) with no salinity difference, the single-phase Darcy equation is used to calculate the viscosity of polymer.

After displacing brine, the pressure drops at different polymer injection rates were measured to determine the viscosities of the polymer solution at different shear rates. Then, polymer in the sandpack was displaced by the SAS-polymer solution. The SAS-polymer

solution was injected for more than one pore volume to displace the polymer solution completely. After displacing the polymer solution, the pressure drops at different SAS-polymer injection rates were measured to determine the viscosities of the SAS-polymer solution at different shear rates.

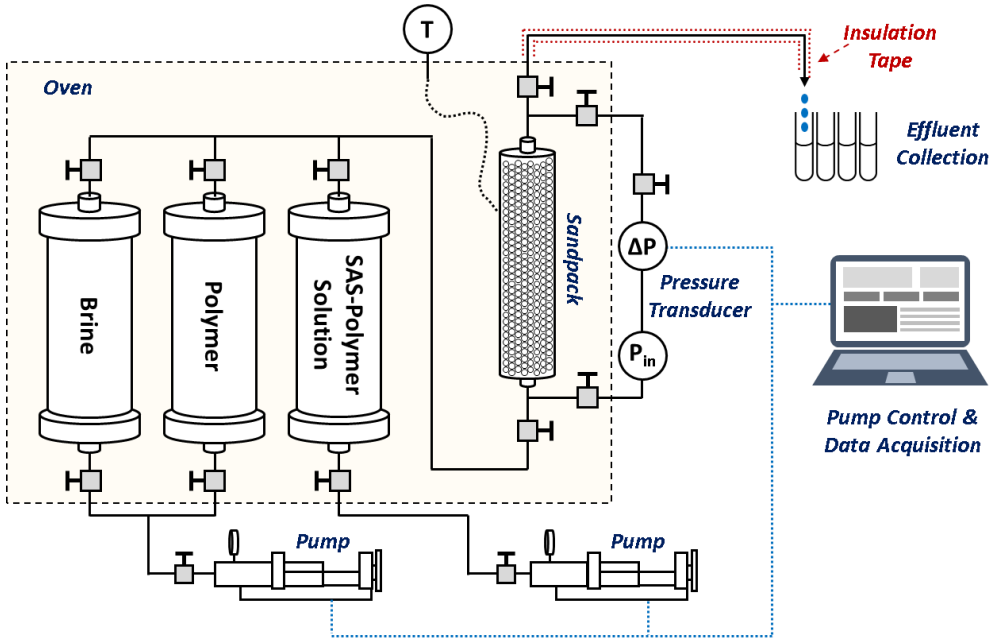

Figure 6.14 Experimental set-up for in-situ viscosity measurement

Polymer (or SAS-polymer) viscosity can be calculated by Darcy's equation with a measured permeability (k), the dimension of a porous media (Length and Area), and measured pressure drops (ΔP) at different injection rates (q):

$$\mu = \frac{k}{q} A \frac{\Delta P}{L}$$

Shear rate calculation is based on the bundle of tubes model. Hirasaki and Pope (1974) provided in-situ shear rate equation derived from modified Blake-Kozeny model as follows:

$$\dot{\gamma} = \left(\frac{3n+1}{4n}\right)^{\frac{n}{n-1}} \frac{12u}{\sqrt{150k\phi}}$$

where u is Darcy velocity (superficial velocity). k is permeability and ϕ is porosity. n is power index from the power law model of bulk viscosity.

Cannella et al. (1988) introduced the correction factor C on the in-situ shear rate equation as follows:

$$\dot{\gamma} = C\left(\frac{3n+1}{4n}\right)^{\frac{n}{n-1}} \frac{u}{\sqrt{k\phi}}$$

where u is Darcy velocity (superficial velocity). k is permeability and ϕ is porosity. n is power index from the power law model of bulk viscosity. They tested this model to Berea sandstone and suggested C = 6. For a sandpack, C = 4 was matched with experimental data in other literature (Koh et al. 2018). In this research, in-situ shear rate equation by Cannella et al. (1988) was applied with C = 4.

It was found that HPAM polymer reduced the permeability of porous media mainly because of polymer adsorption (Gogarty 1967; Hirasaki and Pope 1974; Mishra et al. 2014; Smith 1970; Sorbie 1991; White et al. 1973; Zaitoun and Chauveteau 1998). For in-situ viscosity calculation, the permeability reduction should be considered because 1) the original brine permeability will result in higher viscosity than the actual in-situ viscosity, 2) permeability will change the in-situ shear-rate calculation result.

The porosity and brine permeability of sandpack were 0.32 and 9.5 Darcy, respectively. The effective permeability of polymer and SAS-polymer solutions were determined to be 2.9 Darcy instead of the original permeability.

Figure 6.15 shows in-situ viscosity of polymer and SAS-polymer solution with and without permeability reduction. It clearly shows that the effective permeability for polymer should be adjusted to 2.9 Darcy to get the correct in-situ viscosity. The in-situ viscosity calculation results are summarized in **Table 6.11** for polymer, and **Table 6.12** for SAS-polymer.

The viscoelastic behavior was observed at the shear rates greater than 10 sec^{-1}. This viscoelastic behavior is in line with Rock et al. (2017), who measured in-situ HPAM polymer viscosity in a sandpack. Like bulk viscosity measurement (Figure 6.4), there was no effect of the SAS on in-situ polymer viscosity.

In this research, the maximum injection rate of the polymer solution and the SAS-polymer solution was 3 ml/hr that corresponded to an in-situ shear rate of 4.4 sec^{-1}. Therefore, no in-situ viscoelastic behavior was expected for the polymer solution or the SAS-polymer solution during the flooding.

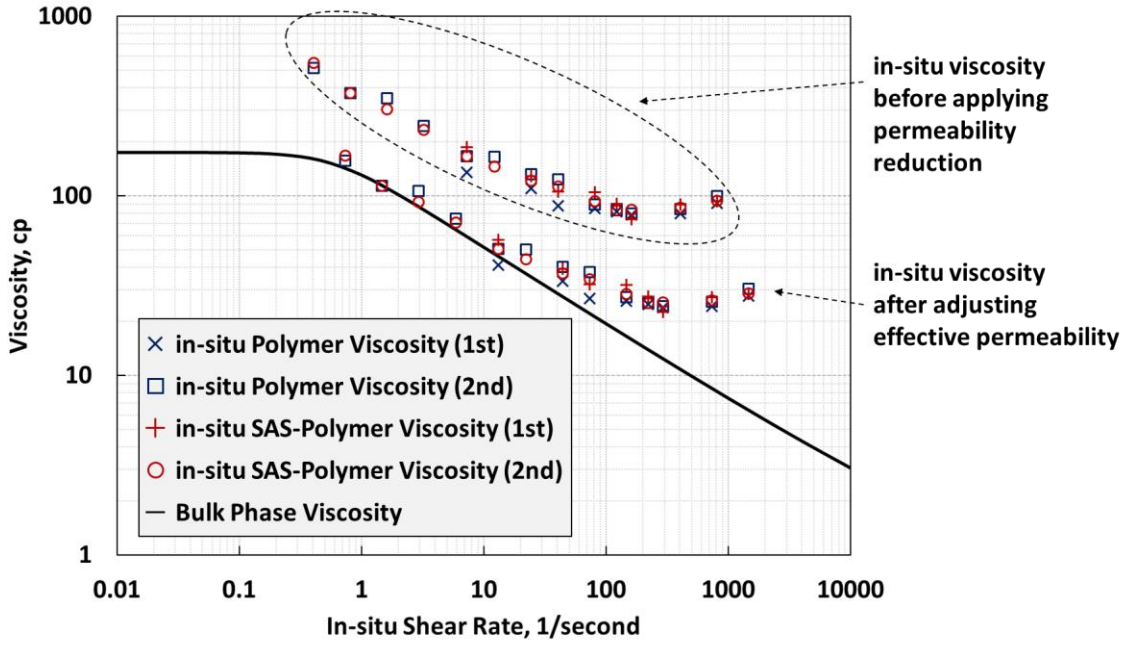

Figure 6.15 In-situ polymer and SAS-polymer viscosity measurement: viscoelastic behavior

Table 6.11 In-situ polymer viscosity calculation

- Sandpack porosity = 0.32
- Sandpack permeability = 9.5 Darcy (Brine permeability)
- Effective permeability = 2.9 Darcy (Adjusted for polymer and SAS-polymer solutions)

Pump Injection Rate	Velocity		In-situ Shear Rate	Polymer Solution in-situ Viscosity			
	Superficial ($u = q/A$)	Interstitial ($v = u/\phi$)		1st Measurement		2nd Measurement	
				ΔP	μ	ΔP	μ
[ml/hr]	[cm/hr]	[cm/hr]	[1/sec]	[bar]	[cp]	[bar]	[cp]
0.5	0.1	0.2	0.7			0.038	156.0
1	0.2	0.5	1.5			0.055	113.5
2	0.3	1.0	2.9			0.103	106.4
4	0.6	2.0	5.9			0.145	74.5
9	1.4	4.5	13.2	0.179	41.0	0.221	50.4
15	2.4	7.5	22.1			0.365	50.1
30	4.8	15.0	44.1	0.490	33.6	0.586	40.2
50	7.9	24.9	73.6	0.648	26.7	0.910	37.5
100	15.9	49.9	147.1	1.262	26.0	1.324	27.2
150	23.8	74.8	220.7	1.806	24.8	1.848	25.3
200	31.8	99.8	294.3	2.310	23.8	2.358	24.3
500	79.5	249.5	735.7	5.881	24.2	6.226	25.6
1000	159.0	499.0	1471.4	13.445	27.7	14.700	30.2

(Blank) No measurement

Table 6.12 In-situ SAS-polymer solution viscosity calculation

- Sandpack porosity = 0.32
- Sandpack permeability = 9.5 Darcy (Brine permeability)
- Effective permeability = 2.9 Darcy (Adjusted for polymer and SAS-polymer solutions)

Pump Injection Rate	Velocity		In-situ Shear Rate	SAS-Polymer Solution in-situ Viscosity			
				1st Measurement		2nd Measurement	
	Superficial ($u = q/A$)	Interstitial ($v = u/\phi$)		ΔP	μ	ΔP	μ
[ml/hr]	[cm/hr]	[cm/hr]	[1/sec]	[bar]	[cp]	[bar]	[cp]
0.5	0.1	0.2	0.7			0.041	167.4
1	0.2	0.5	1.5			0.055	113.5
2	0.3	1.0	2.9			0.090	92.2
4	0.6	2.0	5.9			0.138	70.9
9	1.4	4.5	13.2	0.248	56.7	0.221	50.4
15	2.4	7.5	22.1			0.324	44.4
30	4.8	15.0	44.1	0.572	39.2	0.538	36.9
50	7.9	24.9	73.6	0.779	32.1	0.834	34.3
100	15.9	49.9	147.1	1.551	31.9	1.379	28.4
150	23.8	74.8	220.7	2.006	27.5	1.848	25.3
200	31.8	99.8	294.3	2.193	22.6	2.468	25.4
500	79.5	249.5	735.7	6.633	27.3	6.357	26.2
1000	159.0	499.0	1471.4	13.734	28.3	13.852	28.5

(Blank) No measurement

6.6. Sandpack Flooding Experiment

The application of SAS to the secondary flooding is expected to be more promising than to the tertiary flooding because it does not aim to achieve ultra-low IFT. Therefore, all sandpack flooding experiments were conducted as the secondary mode: direct polymer injection without water injection (i.e., the initial water saturation is the residual water saturation.).

The experimental conditions are summarized in **Table 6.13**. Polymer flooding was conducted as the base line of comparison with the improved polymer flooding. Three improved polymer floods were conducted with three different slug sizes. For all experiments, HPAM 3630S polymer concentration was 0.54 wt%. The brine salinity was 56,456 ppm for both initial brine and injection solutions (Table 6.3). No salinity gradient was applied during oil recovery. The total pore volume injection (PVI) was 5 PVI for all experiment. The three different slug sizes of SAS-polymer solution were 1) 0.5 PVI of 0.1 wt% 2-EH-7PO-15EO in 0.54 wt% polymer, 2) 0.1 PVI of 0.5 wt% 2-EH-7PO-15EO in 0.54 wt% polymer, and 3) 0.5 PVI of 0.5 wt% 2-EH-7PO-15EO in 0.54 wt% polymer. The different slug sizes were tested to evaluate the effect of 2-EH-7PO-15EO concentration and retention on the final oil recovery.

The experimental set-up for sandpack flooding is illustrated in **Figure 6.16**. Here is the general procedure of sandpack flooding. The sandpack and all flow-lines were cleaned and dried at 61°C for 1 day. After that, the system was evacuated for at least 3 hours. Then, the sandpack was saturated with the brine (56,456 ppm). Based on the volume injected, the pore volume of the sandpack was measured. The brine was injected for several pore volumes to calculate the permeability of the sandpack with Darcy's equation.

Table 6.13 Secondary sandpack flooding scheme

	Polymer Flooding	Improved Polymer Flooding	Improved Polymer Flooding	Improved Polymer Flooding
Experiment	Flood #1	Flood #2	Flood #3	Flood #4
Temperature	61°C	61°C	61°C	61°C
Porous Medium	Ottawa Sand	Ottawa Sand	Ottawa Sand	Ottawa Sand
Porosity	32%	35%	34%	33%
Permeability	9.0 Darcy	9.6 Darcy	9.4 Darcy	9.3 Darcy
Pore Volume	64.7 ml	66.5 ml	66.7 ml	64.4 ml
Initial Oil Saturation	56.5 ml (87%)	56.4 ml (85%)	58 ml (87%)	54.3 ml (84%)
Initial Water Saturation	8.2 ml (13%)	10.1 ml (15%)	8.7 ml (13%)	10.1 ml (16%)
Brine Salinity	56,456 ppm	56,456 ppm	56,456 ppm	56,456 ppm
Oil Viscosity	500 cp	500 cp	500 cp	500 cp
Polymer Viscosity	60 cp (at 7 sec^{-1})	60 cp (at 7 sec^{-1})	60 cp (at 7 sec^{-1})	60 cp (at 7 sec^{-1})
SAS-Polymer Slug	-	0.5 PVI 0.1 wt% 2-EH-7PO-15EO 0.54 wt% HAPM 3630S 56,456 ppm Brine	0.1 PVI 0.5 wt% 2-EH-7PO-15EO 0.54 wt% HAPM 3630S 56,456 ppm Brine	0.5 PVI 0.5 wt% 2-EH-7PO-15EO 0.54 wt% HAPM 3630S 56,456 ppm Brine
Polymer Injection	5 PVI 0.54 wt% HAPM 3630S 56,456 ppm Brine	4.5 PVI 0.54 wt% HAPM 3630S 56,456 ppm Brine	4.9 PVI 0.54 wt% HAPM 3630S 56,456 ppm Brine	4.5 PVI 0.54 wt% HAPM 3630S 56,456 ppm Brine

After measuring the porosity and permeability, the sandpack was saturated with the heavy oil by displacing brine with oil. The oil was injected under the reasonable pressure drop (about 1 bar, or 15 psi) to avoid the over-saturation of oil that resulted in the initial water saturation of the sandpack below its S_{wr}. Total 200 ml of heavy oil was injected at 10 ml/hr for 20 hours. Oil saturation in the sandpack is shown in **Figure 6.17**. A very stable brine displacement was observed during oil saturation.

Brine was collected from the outlet during the oil injection. Oil breakthrough and water recovery were measured to determine the initial oil and water saturations for the subsequent oil displacement experiment. Several pore volumes of heavy oil were injected to estimate the end-point relative permeability to oil.

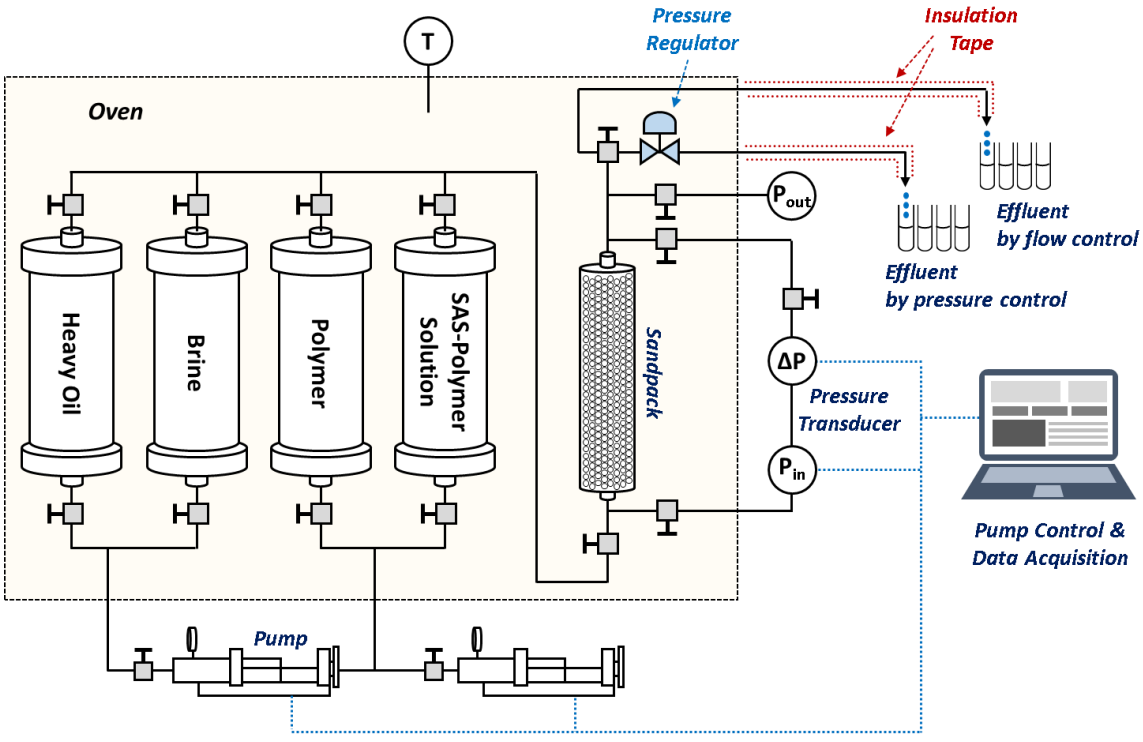

Figure 6.16 Experimental set-up for sandpack flooding

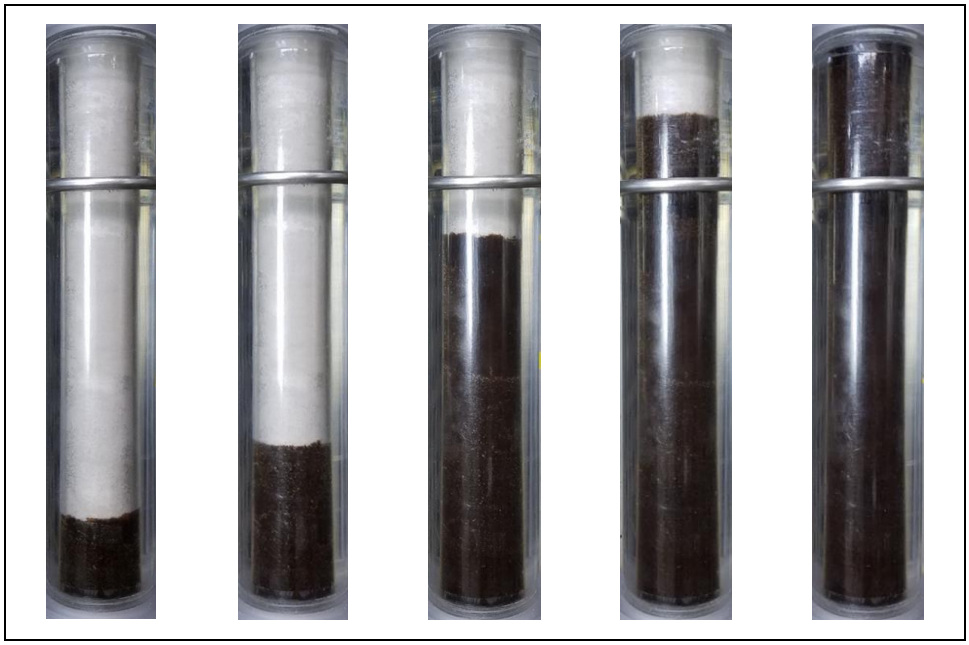

Figure 6.17 Sandpack oil saturation (photos)

For the secondary polymer flooding, a total of 5 PVs of polymer solution was injected. Polymer injection rate was controlled by the constant pressure drop of 0.44 bar/meter (= 2 psi/ft), which is the operation scheme planned by the oil company in the target reservoir. The outlet pressure was set-up at 3.45 bars (50 psi) by back pressure regulator (BPR). The injection pump was under constant pressure control to keep the pressure drop at 0.44 bar/meter (= 2 psi/ft). After water breakthrough, however, the pump flow rate was fluctuating to keep the constant pump pressure, resulting in a lot of noise in pressure drop measurement as shown in **Figure 6.20**.

On average, the injection rate was 1 ml/hr until water breakthrough and 3 ml/hr after polymer breakthrough to keep the pressure drop of 0.22 - 0.44 bar/meter (1 - 2 psi/ft). Therefore, for improved polymer flooding, the injection rate was controlled by the constant flow rate of the pump. For the secondary improved polymer flooding, the SAS-polymer

slug was injected at 1 ml/hr followed by straight polymer flooding at 1 ml/hr. Then, the polymer injection rate was increased to 3 ml/hr after polymer breakthrough. The polymer injection was continued until the total PVI reached 5 pore volume including the SAS-polymer slug.

The result of the secondary polymer flooding (Flood #1) is summarized in **Table 6.14**, **Figure 6.18**, **Figure 6.19**, and **Figure 6.20**. Water breakthrough occurred before 0.28 PVI. Based on oil cut, polymer breakthrough was confirmed at 0.6 PVI. Oil recovery (%OOIP) increased to 47% at 1 PVI, 60% at 2 PVI, 64% at 3 PVI. The final oil recovery at 5 PVI was 66%.

The result of the improved polymer flooding (Flood #2) with 0.5 PVI of 0.1 wt% 2-EH-7PO-15EO is summarized in **Table 6.15**, **Figure 6.21**, **Figure 6.22**, and **Figure 6.23**. Water breakthrough occurred before 0.31 PVI. Based on oil cut, polymer breakthrough was confirmed at 0.73 PVI. Oil recovery (%OOIP) increased to 63% at 1 PVI, 72% at 2 PVI, 78% at 3 PVI. The final oil recovery at 5 PVI was 82%.

The result of the improved polymer flooding (Flood #3) with 0.1 PVI of 0.5 wt% 2-EH-7PO-15EO is summarized in **Table 6.16**, **Figure 6.24**, **Figure 6.25**, and **Figure 6.26**. Water breakthrough occurred before 0.31 PVI. Based on oil cut, polymer breakthrough was confirmed at 0.72 PVI. Oil recovery (%OOIP) increased to 63% at 1 PVI, 74% at 2 PVI, 78% at 3 PVI. The final oil recovery at 5 PVI was 82%.

The result of the improved polymer flooding (Flood #4) with 0.5 PVI of 0.5 wt% 2-EH-7PO-15EO is summarized in **Table 6.17, Figure 6.27**, **Figure 6.28**, and **Figure 6.29**. Water breakthrough occurred before 0.3 PVI. Based on oil cut, polymer breakthrough was confirmed at 0.75 PVI. Oil recovery (%OOIP) increased to 70% at 1 PVI, 82% at 2 PVI, 89% at 3 PVI. The final oil recovery at 5 PVI was 93%.

Table 6.14 The secondary polymer flooding result (Flood #1)

PVI	Oil Recovery [%OOIP]	Oil Cut [%]	Oil Saturation in Sandpack [%]
0.28	28	69	63
0.37	32	48	59
0.6	40	20	53
1.0	47	16	46
1.4	53	13	41
2.0	60	9	35
2.5	63	7	32
3.0	64	3	31
5.0	66	1	30

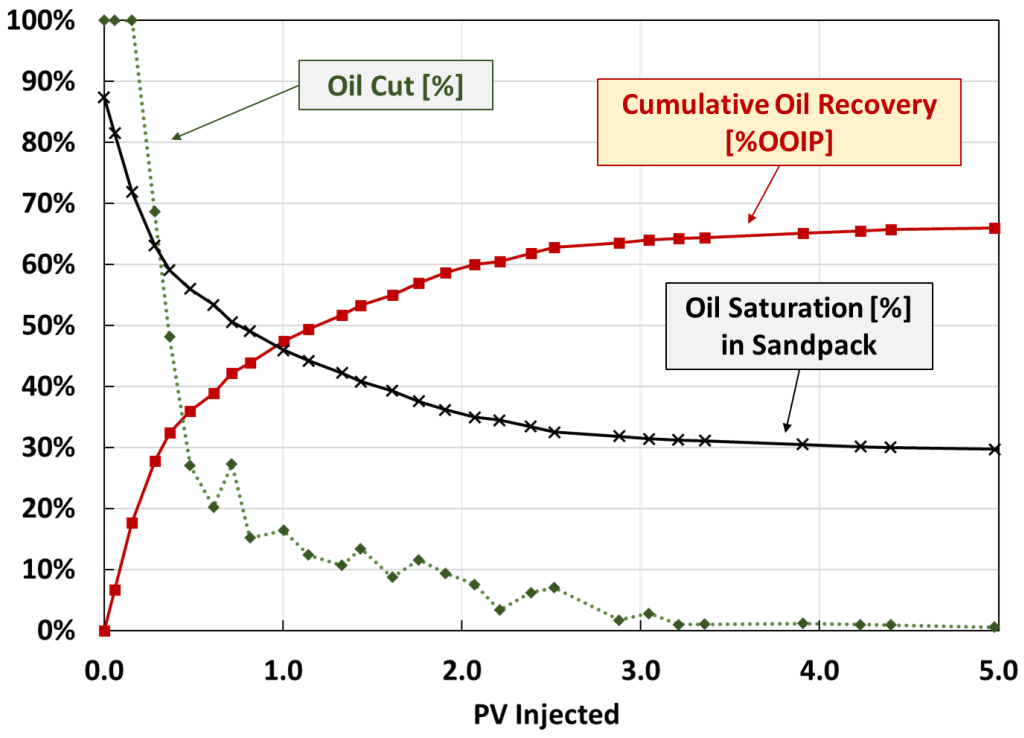

Figure 6.18 The secondary polymer flooding result (Flood #1)

							
PVI	Start	0.7	1.0	2.0	3.0	4.0	5.0
Oil Recovery [%OOIP]	-	40	47	60	64	65	66

Figure 6.19 The secondary polymer flooding (Flood #1): sandpack photos

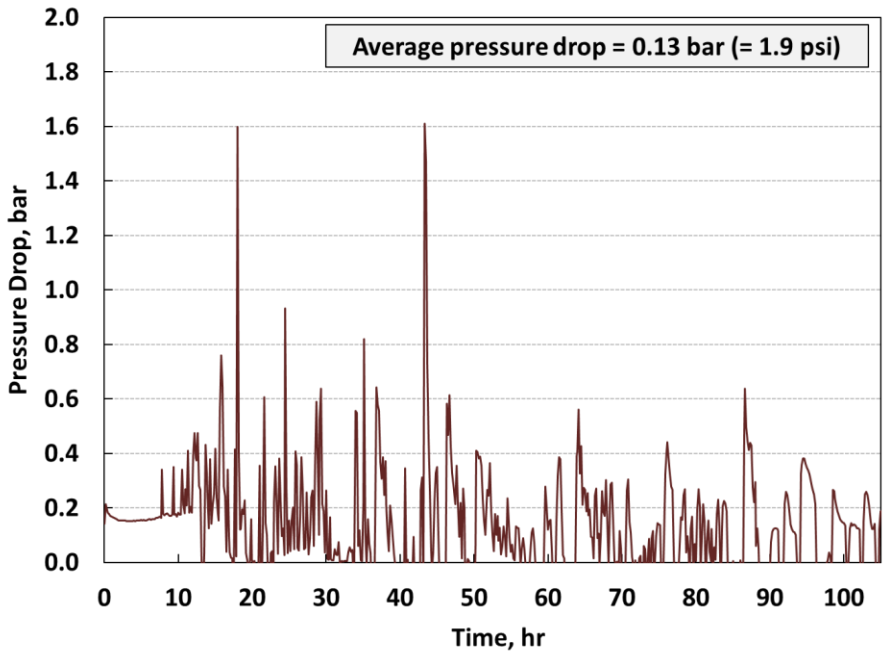

Figure 6.20 The secondary polymer flooding (Flood #1): pressure drop

Table 6.15 The secondary improved polymer flooding result (Flood #2)

PVI	Oil Recovery [%OOIP]	Oil Cut [%]	Oil Saturation in Sandpack [%]
0.31	37	99	54
0.49	51	54	42
1.05	63	13	31
1.45	68	8	28
2.2	74	6	22
2.8	77	3	19
3.5	80	3	17
4.5	82	1.4	15
5.0	82	0.8	15

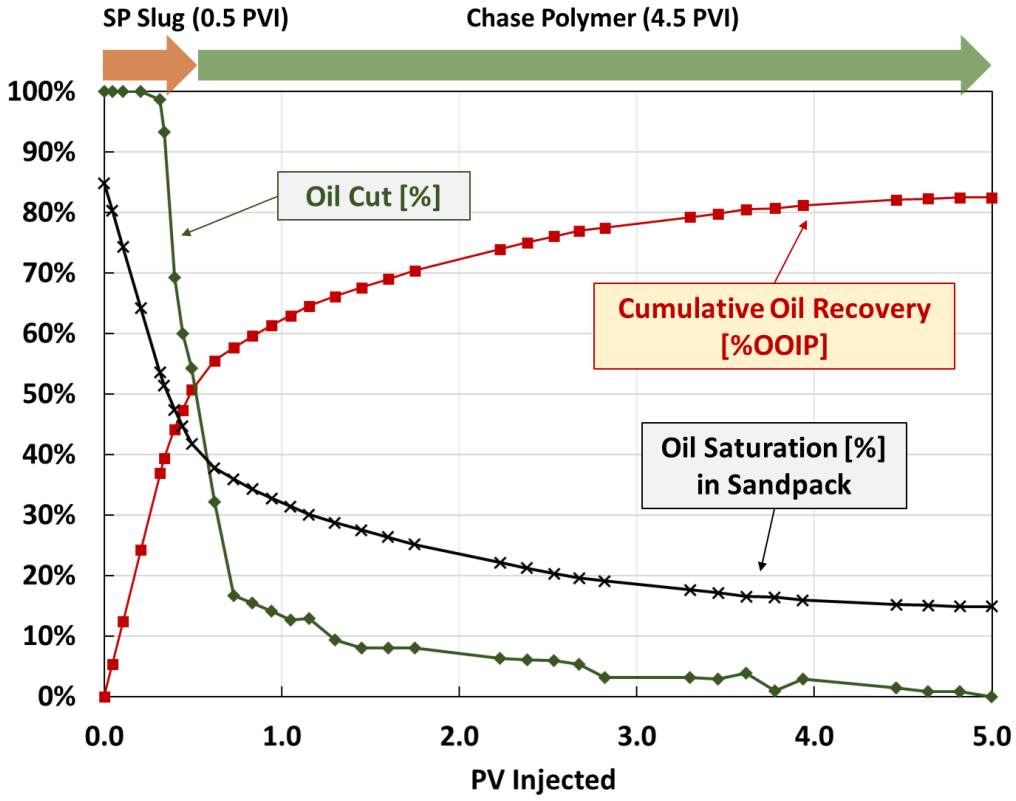

Figure 6.21 The secondary improved polymer flooding result (Flood #2)

Total PVI	Start	0.3	0.5	1.0	1.5	2.0	3.0	4.0	4.5	5.0
Slug PVI	-	SAS 0.3	SAS 0.5	Poly. 0.5	Poly. 1.0	Poly. 1.5	Poly. 2.5	Poly. 3.5	Poly. 4.0	Poly. 4.5
Oil Rec. [%OOIP]	0	37	51	63	68	72	78	81	82	82

Figure 6.22 The secondary improved polymer flooding (Flood #2): sandpack photos

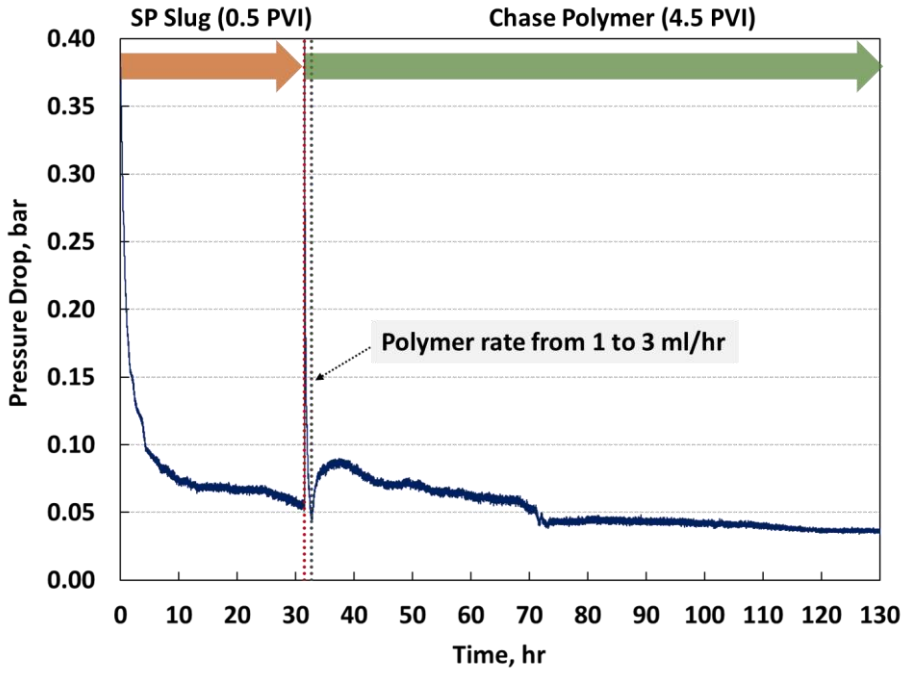

Figure 6.23 The secondary improved polymer flooding (Flood #2): pressure drop

Table 6.16 The secondary improved polymer flooding result (Flood #3)

PVI	Oil Recovery [%OOIP]	Oil Cut [%]	Oil Saturation in Sandpack [%]
0.31	35	90	57
0.47	44	42	49
1.05	63	21	32
1.5	70	10	26
2.4	76	5	21
2.9	78	3	19
3.5	80	3	17
4.0	81	0.8	17
5.0	82	0.3	16

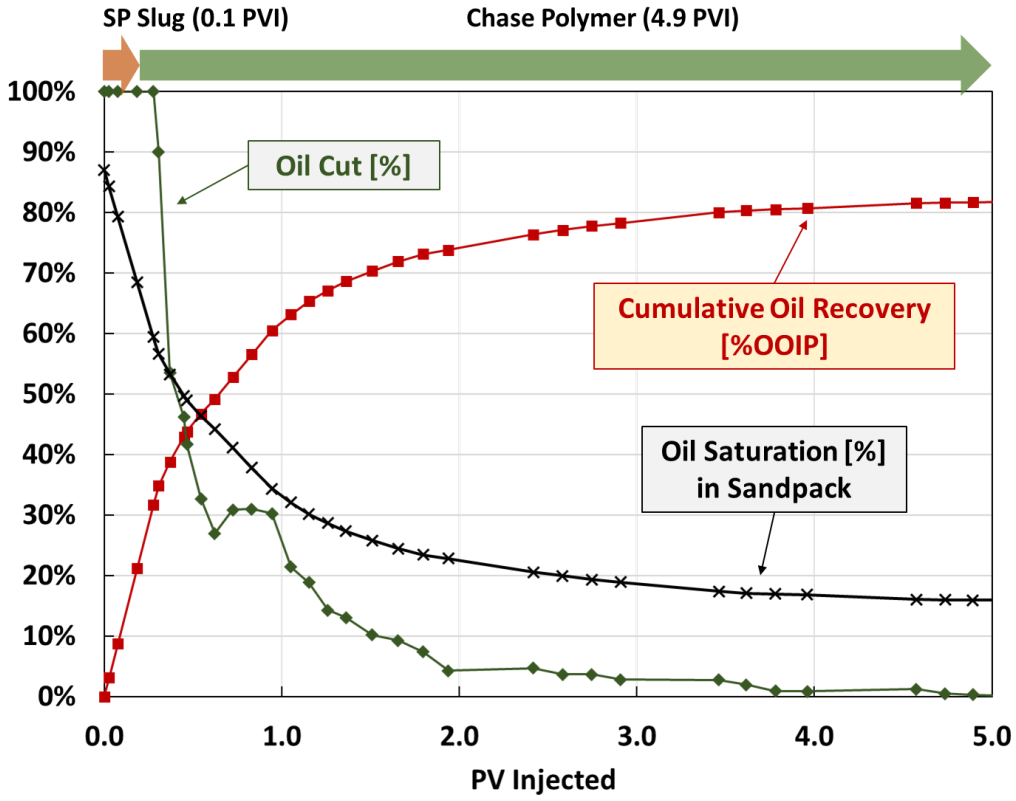

Figure 6.24 The secondary improved polymer flooding result (Flood #3)

Total PVI	Start	0.1	0.5	1.1	2.1	2.5	3.1	3.5	4.1	5.0
Slug PVI	-	SAS 0.1	Poly. 0.4	Poly. 1.0	Poly. 2.0	Poly. 2.4	Poly. 3.0	Poly. 3.4	Poly. 4.0	Poly. 4.9
Oil Rec. [%OOIP]	0	35	45	63	74	76	78	80	81	82

Figure 6.25 The secondary improved polymer flooding (Flood #3): sandpack photos

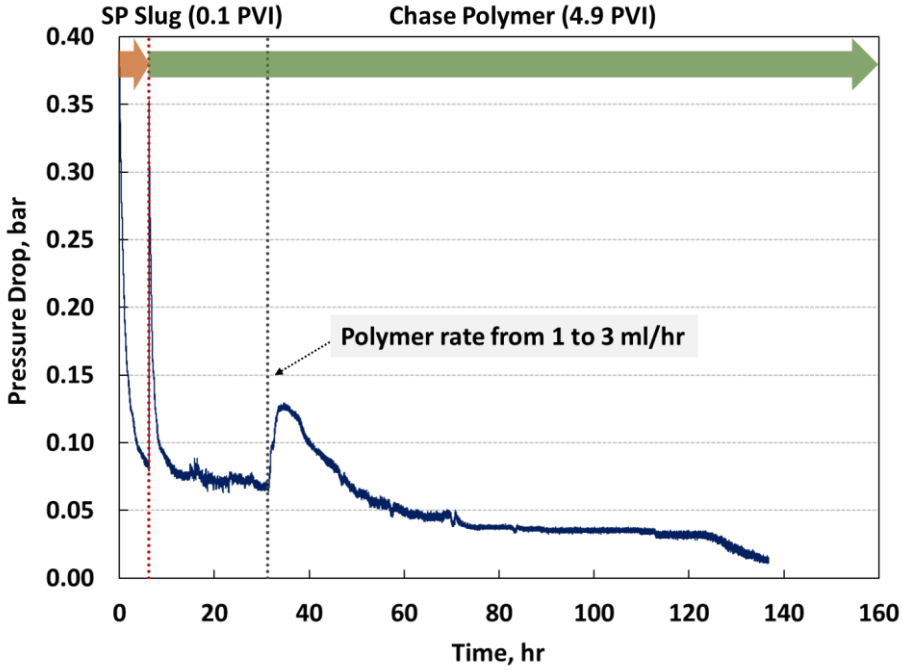

Figure 6.26 The secondary improved polymer flooding (Flood #3): pressure drop

Table 6.17 The secondary improved polymer flooding result (Flood #4)

PVI	Oil Recovery [%OOIP]	Oil Cut [%]	Oil Saturation in Sandpack [%]
0.3	35	94	54
0.54	55	50	38
1.1	71	17	25
1.5	78	13	19
2.0	82	8	15
2.4	87	7	11
3.0	89	3	9
4.1	92	2	7
5.0	93	0.4	6

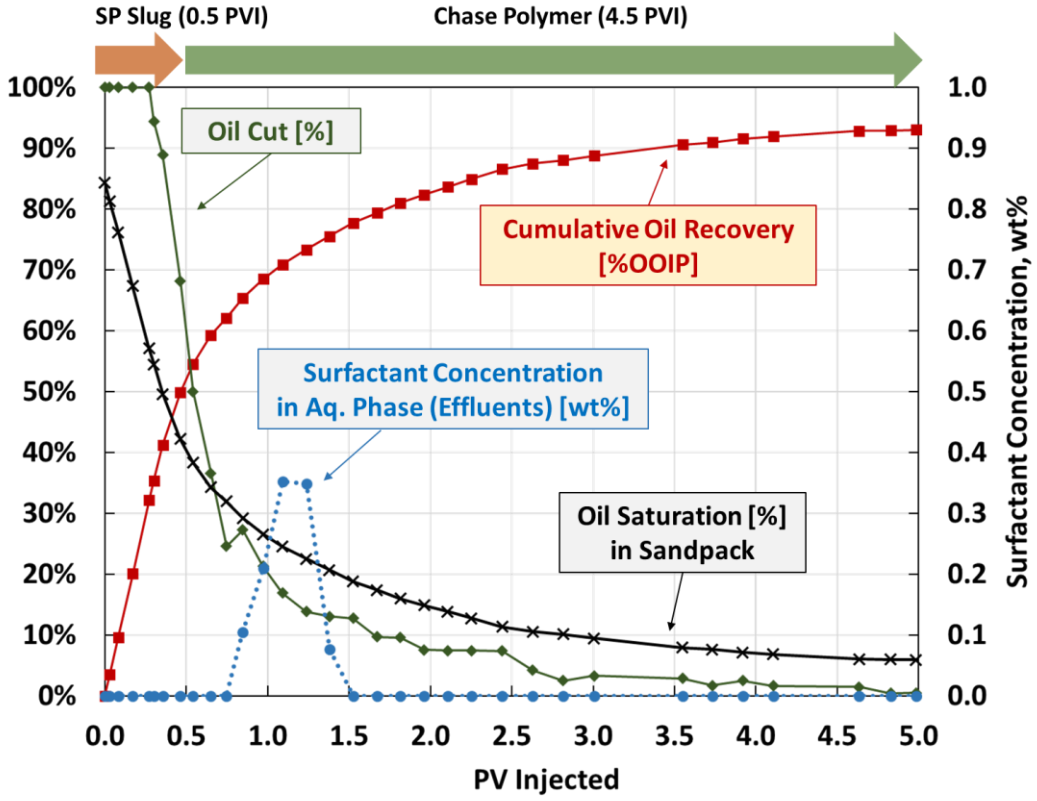

Figure 6.27 The secondary improved polymer flooding result (Flood #4)

Total PVI	Start	0.3	0.5	0.7	1.2	2.0	2.8	3.7	4.5	5.0
Slug PVI	-	SAS 0.3	SAS 0.5	Poly. 0.2	Poly. 0.7	Poly. 1.5	Poly. 2.3	Poly. 3.2	Poly. 4.0	Poly. 4.5
Oil Rec. [%OOIP]	0	35	51	60	73	82	88	91	92	93

Figure 6.28 The secondary improved polymer flooding (Flood #4): sandpack photos

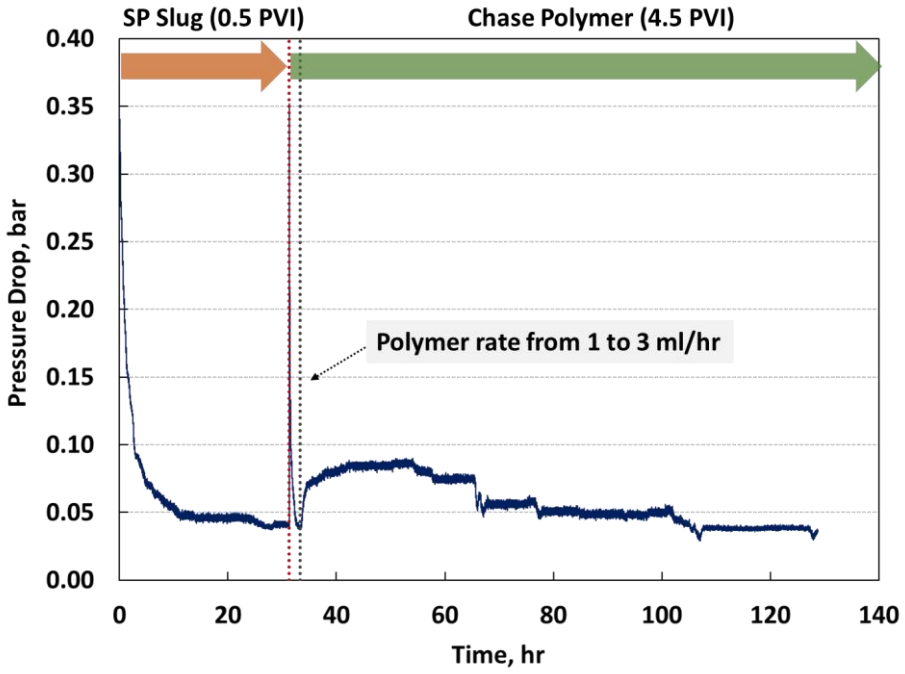

Figure 6.29 The secondary improved polymer flooding (Flood #4): pressure drop

The comparison among 4 sandpack floods is summarized in **Figure 6.30**. It clearly shows that the improved polymer flooding can achieve an incremental oil recovery compared to the polymer flooding. At 1 PVI, the incremental oil recovery of the improved polymer was 16% for Flood #2 and #3, and 23% for Flood #4. At 2 PVI, the incremental oil recovery became 12%, 14%, and 22% for Flood #1, #2, and #3. At 5 PVI, the final incremental oil recovery was 16% for Flood #2 and #3, and 27% for Flood #4. After 1 PVI until 5 PVI, the improved polymer flooding consistently achieved the incremental oil recovery about 12 - 16 % for Flood #2 and #3, and 22 - 27 % for Flood #4.

The result is promising because the only difference between the polymer flooding and the improved polymer flooding was a small amount of SAS-polymer slug (2-EH-7PO-15EO in polymer solution). For Flood #2 and #3, the same amount of SAS-polymer slug was injected with either 0.5 PVI of 0.1 wt% 2-EH-7PO-15EO or 0.1 PVI of 0.5 wt% 2-EH-7PO-15EO. For Flood #4, 5 times larger quantity of SAS-polymer slug was injected with 0.5 PVI of 0.5 wt% 2-EH-7PO-15EO. Compared to the conventional ASP flooding that used about 1 wt% of surfactant combination with additional co-solvents, a smaller amount of a SAS was used for the improved polymer flooding, but it achieved a significant incremental oil recovery.

The main reason for the incremental oil recovery was the delayed polymer breakthrough time. For all experiment, water breakthrough time was similar to each other (around 0.3 PVI). However, after water breakthrough, the oil cut until polymer breakthrough was higher for the improved polymer flooding cases. Flood #4 shows the most delayed polymer breakthrough, and the oil cut after polymer breakthrough was higher compared to Flood #2 or #3.

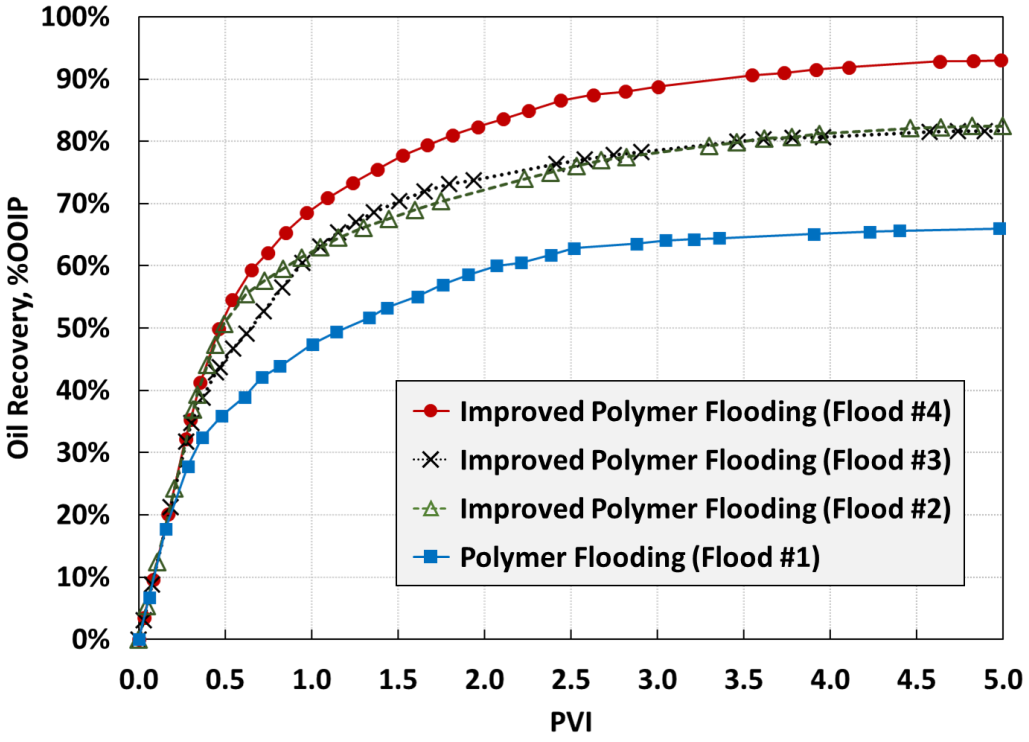

	SAS-Polymer Slug	Polymer Drive
Flood #1	-	5.0 PVI
Flood #2	0.1 wt% 2-EH-7PO-15EO, 0.5 PVI	4.5 PVI
Flood #3	0.5 wt% 2-EH-7PO-15EO, 0.1 PVI	4.9 PVI
Flood #4	0.5 wt% 2-EH-7PO-15EO, 0.5 PVI	4.5 PVI

PVI	Oil Recovery [%OOIP]			
	Flood #1	Flood #2	Flood #3	Flood #4
0.5	36	51	45	51
1.0	47	63	63	70
1.5	54	68	70	78
2.0	60	72	74	82
2.5	63	76	76	87
3.0	64	78	78	89
3.5	64	80	80	91
4.0	65	81	81	92
4.5	66	82	82	93
5.0	66	82	82	93

Figure 6.30 Oil recovery comparison among 4 sandpack flooding experiment

The delayed polymer breakthrough and higher oil cuts indicate the SAS (2-EH-7PO-15EO) improved the relative permeability of oil. It successfully reduced IFT between the displaced fluid (heavy oil) and the displacing fluid (polymer solution) and reduced the residual oil saturation. Note that the IFT between the heavy oil and the reservoir brine is 15.8 dynes/cm and it can be reduced to 0.025 dynes/cm with 2-EH-7PO-15EO (Table 6.7). With 9.5-Darcy permeability, 30.48-cm length, and 0.44-bar/meter pressure drop, the capillary numbers (Nc) are 2.7×10^{-5} for the polymer flooding and 1.7×10^{-2} for the improved polymer flooding. Lowered residual oil (or remaining oil) saturation could be achieved by capillary desaturation at this high capillary number.

The same amount of 2-EH-7PO-15EO was injected for Flood #2 and #3. They were designed to compare different slug injection schemes between the lower concentration with the lager PVI (Flood #2) and the higher concentration with lower PVI (Flood #3). A meaningful difference between Floods #2 and #3 was not observed but they show slightly different oil recoveries from the water breakthrough through 2.5 PVI. Whereas Flood #2 showed a larger oil bank right after the water breakthrough with a smaller oil cut later, Flood #3 showed a smaller oil bank right after the water breakthrough with a larger oil cut until 2.5 PVI. After 2.5 PVI, the oil recovery becomes nearly the same for both cases.

The surfactant retention was measured carefully in a separate flooding experiment. A total of 0.5 PV of 0.5 wt% SAS-polymer solution was injected in the brine-saturated sandpack with no oil. The concentrations of 2-EH-7PO-15EO in effluent samples were measured in high performance liquid chromatography (HPLC). The retention was measured to be 0.055 mg/g-rock as shown in **Table 6.18**.

Only 47% of the total injected 2-EH-7PO-15EO was measured in the aqueous phase of effluent samples for Flood #4 (Figure 6.27). For Floods #2 and #3, there was no 2-EH-

7PO-15EO measured in effluent samples. This indicated that a large amount of 2-EH-7PO-15EO was partitioning into the oil phase. According to the overall material balance, excepted retention (0.055 mg/g) in the sandpack, 2-EH-7PO-15EO was distributed about 53% in the aqueous phase and 47% in the oil phase for Flood #4.

When the surfactant retention was calculated only with the SAS recovered in the aqueous phase (i.e. 53% of 2-EH-7PO-15EO), the surfactant retention becomes 0.24 mg/g. This can be viewed as the maximum surfactant loss during sandpack flooding, considering any possible additional surfactant loss in the oil phase. Therefore, it is realistic to conclude that the surfactant retention was higher than 0.055 mg/g (lower limit), but lower than 0.24 mg/g (upper limit).

Table 6.18 2-EH-7PO-15EO retention in the sandpack

Total Injection	0.178 g
Recovered Mass	0.158 g
Loss	0.020 g
Sand Mass	360.5 g
Retention	0.055 mg/g

The result of 2-EH-7PO-15EO retention in the sandpack indicates that the partitioning coefficient is an important factor to determine the distribution of 2-EH-7PO-15EO in the oil phase and the aqueous phase. According to the overall material balance of 2-EH-7PO-15EO in Flood #4, an "apparent" partitioning coefficient of 2-EH-7PO-15EO was approximately 0.9 (i.e. 53% in the aqueous phase and 47% in the oil phase). A separate experiment was conducted for the equilibrium partitioning coefficient of 2-EH-7PO-15EO to supplement the overall material balance analysis.

Samples were prepared with 5 different 2-EH-7PO-15EO concentrations (0.1, 0.2, 0.3, 0.4, and 0.5 wt%) in the aqueous phase. For each sample, salinity was fixed at the reservoir brine (56,456 ppm) and the equal volume between the aqueous and oil phases. Also, samples were prepared with and without polymer to confirm the effect of polymer on the surfactant partitioning behavior. While samples were aged at 61°C for 5 days, they were mixed by a vortex mixer 8 times for the first 2 days. Then, samples were taken out to the room temperature and aged for additional 5 days for equilibration. Note that effluent samples from the sandpack flooding was also rested in the room temperature. The concentration of 2-EH-7PO-15EO in the aqueous phase was measured by HPLC. The concentration of 2-EH-7PO-15EO in the oil phase was calculated based on the material balance. The results are summarized in **Table 6.19**.

The results show that the overall concentration of 2-EH-7PO-15EO affects the partitioning coefficient. The partitioning coefficient became larger as the total concentration decreased. The possible explanation is based on the interaction between salt ions (in the aqueous phase) and EO groups in the SAS. When the SAS concentration is low, there are not enough EO groups against salt ions pushing the SAS into the oil phase. As the EO concentration increases, the larger amount of SAS can stay in the aqueous phase, resulting in the reduction of partitioning coefficient. More data of the partitioning coefficient is required to confirm this explanation.

Table 6.19 2-EH-7PO-15EO partitioning coefficient

(a) Samples without polymer

Total 2-EH-7PO-15EO Concentration in Samples [wt%]	Concentration in Each Phase (average of 3 measurement)		Partitioning Coefficient $K = C_{oil}/C_{aq.}$
	$C_{aq.}$ [wt%] (in aqueous phase)	$C_{oil.}$ [wt%] (in oil phase)	
0.1	0.0201	0.0799	3.98
0.2	0.0577	0.1423	2.47
0.3	0.0982	0.2018	2.05
0.4	0.1570	0.2430	1.55
0.5	0.1808	0.3192	1.76

(b) Samples with polymer (0.54 wt% HPAM 3630s)

Total 2-EH-7PO-15EO Concentration in Samples [wt%]	Concentration in Each Phase (average of 3 measurement)		Partitioning Coefficient $K = C_{oil}/C_{aq.}$
	$C_{aq.}$ [wt%] (in aqueous phase)	$C_{oil.}$ [wt%] (in oil phase)	
0.1	0.0168	0.0832	4.97
0.2	0.0548	0.1452	2.65
0.3	0.0921	0.2079	2.26
0.4	0.1293	0.2707	2.09
0.5	0.1920	0.3080	1.60

From 0.1 wt% to 0.5 wt% 2-EH-7PO-15EO, the partitioning coefficient ranged from 1.55 to 3.98. These values are greater than the apparent partitioning coefficient from the overall material balance of Flood #4. The discrepancy likely came from the equilibrium status after the proper vortex mixing of samples, which did not happen inside porous media during sandpack flooding. Effluent samples after the insufficient mixing during sandpack flooding may have resulted in more 2-EH-7PO-15EO partitioning in the aqueous phase.

Sandpack flooding results showed that the improved polymer flooding with a SAS can increase oil recovery compared to the straight polymer flooding. Does this method work for other cases? For example, does it work in a sandstone? Does it work for light oil recovery? Although it is not possible to test all different cases, I am going to present one case that the improved polymer flooding did not work well in the next section.

6.7. Improved Polymer Flooding for Light Oil Recovery in Sandstones

This is a counter example for light oil recovery in a sandstone core. The oil properties are summarized in **Table 6.20**. Dead oil viscosity at the reservoir temperature 77°C is 2.2 cp. Total acid number is 0.17 mg-KOH/g. SARA analysis shows that there are almost no resins and asphaltenes in this light oil. The reservoir brine salinity is 68,413 ppm as shown in **Table 6.21**.

Based on phase behavior and IFT measurement, 1 wt% 2-EH-4PO-15EO was selected as an optimal SAS. The original IFT between light oil and brine is 14.7 dynes/cm. IFT can be reduced to 0.28 dynes/cm by 1 wt% 2-EH-4PO-15EO (**Table 6.22**), although this IFT is one order magnitude greater than the case presented in the previous section.

The secondary and tertiary core floods were designed to evaluate the improved polymer flooding for light oil recovery. The core flooding design is summarized in **Table 6.23**. A Boise sandstone core was prepared with 1.5-inch diameter and 1-foot length. Instead of a sandpack accumulator, a core holder was used. Other than that, the experimental set-up was similar to the one for sandpack flooding (Figure 6.16).

For water flooding, 0.1 wt% NaCl was prepared. A total of 2 PV of brine was injected at 5 ft/day. The injection rate was set to avoid the capillary end effect by getting Rapoport-Leas number above 1 $cp \cdot cm^2/min$. At the end of water flooding, the injection rate was increased to 50 ft/day for a while to confirm no additional oil recovery.

For SAS-polymer injection, 0.08 wt% HAPM 3630s (Flopaam, SNF) polymer and 1 wt% 2-EH-4PO-15EO were mixed in 0.1 wt% NaCl brine. The target viscosity of the SAS-polymer soliton was 10 cp at the injection rate. For the tertiary flooding, a total of 3 PV was injected after water flooding. For the secondary flooding, a total of 4 PV of the SAS-polymer solution was injected. There was no polymer drive after SAS-polymer injection.

Table 6.20 Light oil properties

Average Molecular Weight		210 g/mol
Acid Number		0.17 mg-KOH/g
Dead Oil Viscosity at 77°C		2.2 cp
SARA	Saturates	71.6 wt%
	Aromatics	24.8 wt%
	Resins	3.4 wt%
	Asphaltenes (Pentane insoluble)	0.1 wt%

Table 6.21 Reservoir brine composition

Ions	Concentration [mg/L]
Na^{+}	25,423
Ca^{2+}	1,110
Mg^{2+}	181
Cl^{-}	41,683
SO_4^{2-}	16
Total Dissolved Solid (TDS)	68,413

Table 6.22 IFT between light oil and brine

	IFT [dynes/cm]
Light Oil and 0.1 wt% NaCl Brine	14.7
Light Oil and 0.1 wt% NaCl Brine with 1 wt% 2-EH-4PO-15EO	0.28

Table 6.23 Core flooding scheme for light oil recovery

		Tertiary Flooding	Secondary Flooding
Temperature		77°C	77°C
Porous Medium		Boise Sandstone (1.5-inch dia. / 1-foot long)	Boise Sandstone (1.5-inch dia. / 1-foot long)
Porosity		35%	33%
Permeability		2,019 mD	2,341 mD
Initial Oil Saturation		61%	63%
Reservoir Brine		68,413 ppm	68,413 ppm
Oil Viscosity		2.2 cp	2.2 cp
Brine Viscosity		0.37 cp	0.37 cp
Polymer Viscosity		10 cp (at the injection rate)	10 cp (at the injection rate)
Water Injection	PVI	2 PVI	
	Salinity	0.1 wt% NaCl	-
	Injection Rate	6.35 cm/hr (5 ft/day)	
SAS-Polymer Injection	PVI	3 PVI	4 PVI
	Salinity	0.1 wt% NaCl	0.1 wt% NaCl
	Composition	0.08 wt% HPAM 3630S 1 wt% 2EH-4PO-15EO	0.08 wt% HPAM 3630S 1 wt% 2EH-4PO-15EO
	Injection Rate	1.27 cm/hr (1 ft/day)	1.27 cm/hr (1 ft/day)

The oil recovery results are illustrated in **Figure 6.31** and **Figure 6.32**. For the tertiary flooding, oil recovery was 49% (OOIP) after 2 PVI of water injection. However, SAS-polymer injection achieved only 6% additional oil recovery. The final oil recovery after 5 PVI was 55% (OOIP). The secondary improved polymer flooding shows similar result. The final oil recovery after 4 PVI was 54% (OOIP). The tertiary flooding and the secondary flooding show no difference in term of the final oil recovery. However, the secondary flooding could be beneficial for the faster oil recovery at the earlier PVI.

Overall, the improved polymer flooding of light oil in a sandstone did not achieve a substantial increase in oil recovery. The experimental conditions were quite different from the previous heavy oil case (Section 6.6). The oil has a low acid number with a small amount of resins and a negligible amount of asphaltenes. The permeability of the sandstone core was not as high as the permeability of a sandpack. Although it achieved an IFT reduction from 14.7 to 0.28 dynes/cm, it was not as low as the heavy oil case of 0.025 dynes/cm in the previous section. The capillary number with the reduced IFT (0.28 dynes/cm) was 2×10^{-4}. The water saturation in a sandstone core was higher than the water saturation in the sandpack. These differences man result in low oil recovery. The next section will provide a discussion of the conditions conducive to a successful improved polymer flooding.

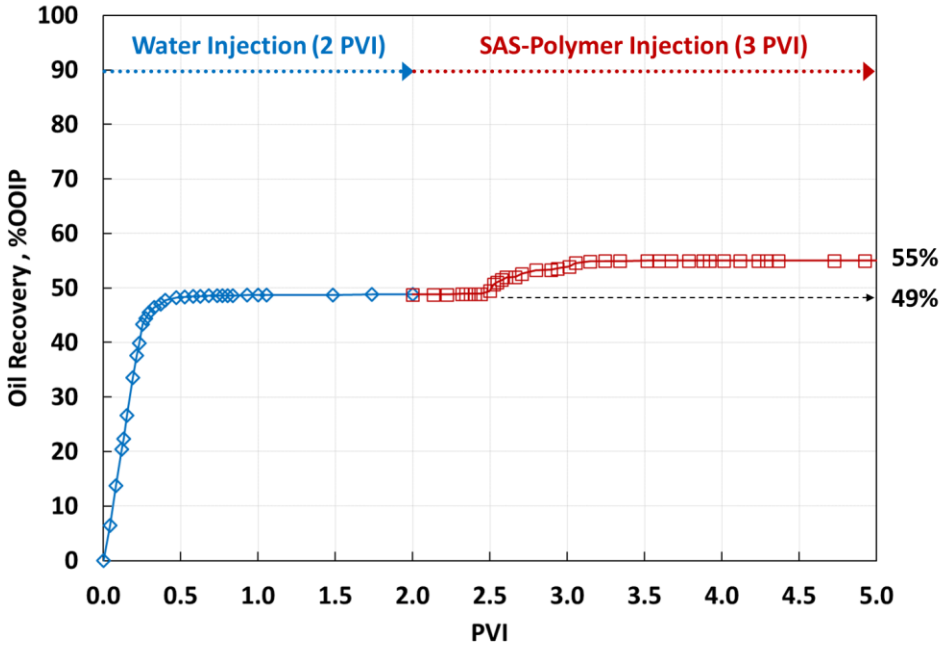

Figure 6.31 The tertiary improved polymer flooding for light oil recovery

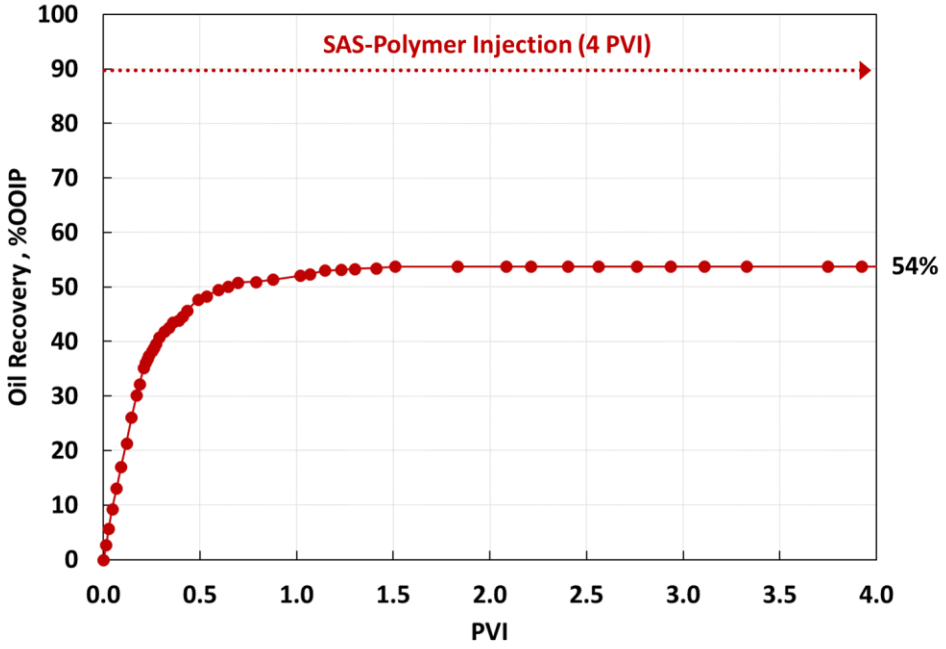

Figure 6.32 The secondary improved polymer flooding for light oil recovery

6.8. Discussion about Conditions for SAS-Improved Polymer Flooding

Water flooding is not an efficient oil recovery method for heavy oil production due to an adverse mobility ratio. It will result in an inefficient volumetric sweep with channeling of the injected water under reservoir heterogeneities. For more efficient heavy oil displacement, the injected water needs to be viscosified by polymer. With a fixed oil viscosity, the mobility ratio can be reduced by increasing the water viscosity. Theoretically, water viscosity can be easily increased to several-hundred centipoise as long as the polymer is stable at the injection solution. In actual oil fields, however, the viscosity of the injection fluid is limited by operating conditions, such as project cash flow, injection rate, injectivity, and chemical cost. More constraints are expected for off-shore reservoirs because of the limited space for surface facilities.

The target heavy oil reservoir in this research is in the North Sea. The viscosity of the heavy oil is 500 cp at the reservoir conditions (125 bars and 38°C). The unconsolidated sand reservoir gives a porosity of 35% porosity and a permeability of 10 Darcy. The distance between the injector well and the producer well is 250 m. According to the original operation scheme, polymer flooding is planned with pressure drop control at 0.44 bar/meter (= 2 psi/ft) (a total pressure drop of 110 bars from the injector to the producer). Considering the oil viscosity (500 cp), it seems to be reasonable to have polymer viscosity around few-hundred centipoise. However, the planned polymer viscosity is only 20 cp.

One aspect of the limited polymer viscosity is its injection rate. For example, if we apply a simple Darcy equation to estimate the polymer injection rate in the reservoir, the rate of 20 cp polymer solution is about 1.27 cm/hr (= 1 ft/day) when the relative permeability of water is 0.1. The actual rate will be much slower in a three-dimensional heterogeneous reservoir. If the polymer viscosity is increased to 500 cp, which is equal to the oil viscosity, the flow rate becomes 25 times smaller. It will take decades to inject one

pore volume of polymer solution into the reservoir; it is economically infeasible to have the viscosity ratio of unity.

A similar case is the previous pilot test by Chevron in Captain Field in the North Sea (Poulsen et al. 2018). It is a sand reservoir of heavy oil with 31% porosity and 5 Darcy permeability. Chevron produced heavy oil (up to 150 cp) by injecting 20 cp polymer solution. They selected the polymer viscosity of 20 cp based on the economic point of view, although the polymer injectivity was not an issue up to 200 cp.

It is often inevitable to have an unfavorable mobility ratio during polymer flooding for heavy oil recovery, especially in off-shore reservoirs. Surfactant-polymer (SP) flooding could be an alternative solution to enhance the recovery of heavy oil. While keeping polymer viscosity, surfactant(s) could give a potential incremental oil recovery with IFT reduction. This potential could be greater for heavy oil displacement compared to light oil displacement as discussed later in this section.

SP flooding has been studied for a long time in the literature. A field test for SP flooding can be found in early 1960s, known as "micellar-polymer flooding" (Gogarty 1978; Ondrusek 1988; Thomas and Farouq Ali 1992). Theories on SP flooding were established through many studies (Austad et al. 1994; Hirasaki 1981; Hirasaki et al. 2011; Pope et al. 1979; Thomas and Farouq Ali 1992). SP flooding is usually considered as a tertiary flooding after water flooding. It is important to create an oil bank by coalescence of dispersed oil droplets that have been made by the preceding water flood. Usually, more than two surfactants are used to create type-III micro-emulsion phase behavior with ultra-low IFT (10^{-3} dynes/cm) with salinity gradient. The low-tension polymer flooding by BP (Kalpakci et al. 1990) and Equinor (Maldal et al. 1998) were the traditional SP flooding in terms of IFT and the number of surfactants.

The improved polymer flooding is designed to improve the oil recovery efficiency of polymer flooding with an adverse mobility ratio by reducing the IFT between the oleic and aqueous phases. This is a simplified version of the conventional SP flooding; i.e., it does not consider a complex micro-emulsion phase behavior, but aim only at reducing the IFT between the oleic and aqueous phases so that it yields a reduced residual oil saturation and a delayed breakthrough of polymer. Unlike the conventional SP flooding, the improved polymer flooding uses single SAS (as a surfactant) with no other chemicals or salinity gradient. When applied to an undeveloped reservoir with a high oil saturation (e.g., the reservoir in the North Sea), the improved polymer flooding with a moderate reduction in IFT may yield an enhanced displacement efficiency of heavy oil without having to form an oil bank from oil droplets dispersed in the high-saturation water phase.

From the operational point of view, the improved polymer flooding can have several advantages in off-shore reservoirs. The off-shore platform has limited space for facilities to handle the large quantity of chemicals. That is, it is more advantageous to use fewer chemicals. Salinity gradient is also more difficult for off-shore reservoirs because either the sea water or the produced water (i.e. reservoir brine) is often the water source for injection. Salinity gradient could be possible when there is salinity difference between the sea water and the reservoir brine. However, the injection of sea water may cause scale precipitation when it is mixed with the reservoir brine.

The mechanism of the improved polymer flooding can be explained with two fundamentals: capillary desaturation and fractional flow theory. Capillary number increases with higher permeability, higher pressure drop, lower IFT, and shorter length.

$$\text{Capillary number, Nc} = \frac{k\Delta P}{\sigma L}$$

where k is permeability, ΔP is pressure drop, σ is interfacial tension (IFT), and L is length.

The length is often uncontrollable for an actual oil displacement. Increasing the pressure drop to increase the capillary number is also limited. A large pressure drop means a large injection rate. For polymer injection, however, a large flow rate may cause the mechanical degradation of polymer near the injector. Also, the injection pressure cannot exceed the fracture pressure. The operator for the North Sea heavy oil reservoir has planned the operating pressure drop at 0.44 bar/meter (= 2 psi/ft). Therefore, IFT reduction is essentially the only way to increase the capillary number.

Then, how much should the capillary number be increased for reducing the residual oil saturation? There are several experimental data for the capillary desaturation of sandstones. For Berea sandstone, the critical capillary number was found in the range of 10^{-5} to 10^{-6}. The residual oil saturation reduced to smaller than 10% when the capillary number was in the range of 10^{-2} to 10^{-3} (Chatzis and Morrow 1984; Garnes et al. 1990; Fulcher et al. 1985). A similar trend was found with reservoir sandstones (Tarbert and ORE sandstones) from the Oseberg Field in the North Sea (Garnes et al. 1990). For Bentheimer sandstone, the critical capillary number was found in the range of 1×10^{-4} and the residual oil saturation became smaller than 5% in the range of 3×10^{-4} (Qi et al. 2017).

A similar capillary desaturation curve is expected for an unconsolidated sand reservoir, although high permeability may result in more rapid decline of oil saturation beyond the critical capillary number (Lake et al. 2014). We can expect that, for a high-permeability sandpack (e.g. 10 Darcy), the critical capillary number would be about 10^{-4} and the residual oil saturation would become less than 10% at the capillary number of 10^{-2}. This trend is schematically shown in Figure 2.3.

In this research, the improved polymer flooding with 2-EH-7PO-15EO reduced IFT from 15.8 to 0.025 dynes/cm (i.e., a reduction by 3 orders of magnitude). This IFT

reduction could increase the capillary number from 2.7×10^{-5} to 1.7×10^{-2}. The critical capillary number and a rapid capillary desaturation of the sandpack are expected to be within this range. As a result, the residual oil saturation can be significantly reduced for the improved polymer flooding in comparison to straight polymer flooding. The experimental data show that the improved polymer flooding resulted in 6% of remaining oil saturation in the sandpack, whereas the remaining oil saturation after 5 PVI polymer flooding was still 30%. Note again that the IFT of 0.025 dynes/cm is not an ultra-low value (i.e. range of 10^{-3} dynes/cm) that is usually required for an efficient tertiary recovery.

Another mechanism to explain the improved polymer flooding is the fractional flow theory. Let's assume two example cases of light oil (1 cp) and heavy oil (500 cp) with similar relative permeability curves as shown in **Figure 6.33**. Two sets of curves represent the relative permeability of water (and polymer) flooding and SP flooding. For SP flooding, the residual oil saturation decreases from 24% to 5%, representing a possible capillary desaturation of the residual oil saturation from 24% (for water flooding and polymer flooding) to 5% (for SP flooding).

The fractional flow of water, polymer and SP solution based on the relative permeability (Figure 6.33) is shown in **Figure 6.34**. The tangent line on each fractional flow represents breakthrough of the secondary mode water flooding, polymer flooding, and SP flooding. According to this example case, water flooding was enough for light oil (1 cp) recovery, and polymer (5 cp) flooding for light oil displacement does not result in a meaningful incremental oil recovery. Water flooding recovers 61% (OOIP) oil recovery at breakthrough of 0.52 PVI. Polymer flooding achieves only 8% more oil recovery at breakthrough of 0.73 PVI.

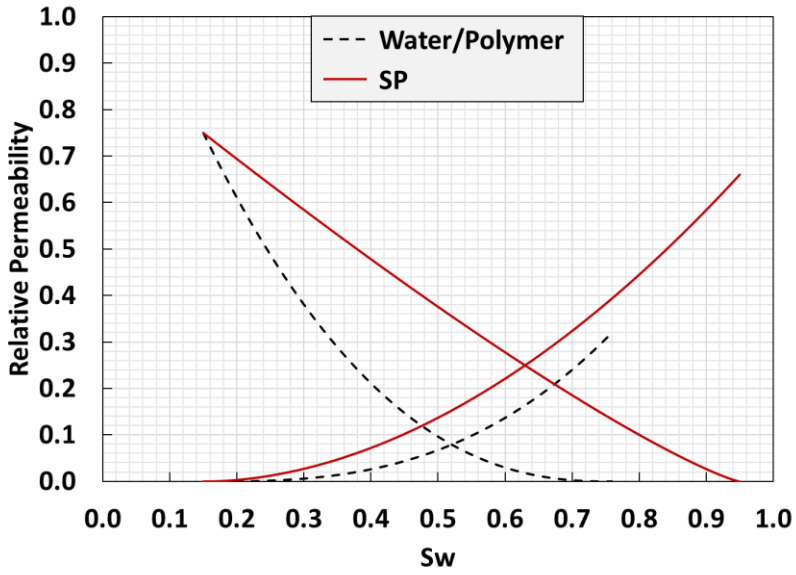

	Water / Polymer	SP
S_{wr}	0.15	0.15
S_{or}	0.24	0.05
k^0_{rw}	0.32	0.66
k^0_{ro}	0.75	0.75
n_w	2.8	1.9
n_o	2.4	1.2

Figure 6.33 Example cases: relative permeability of light oil and heavy oil

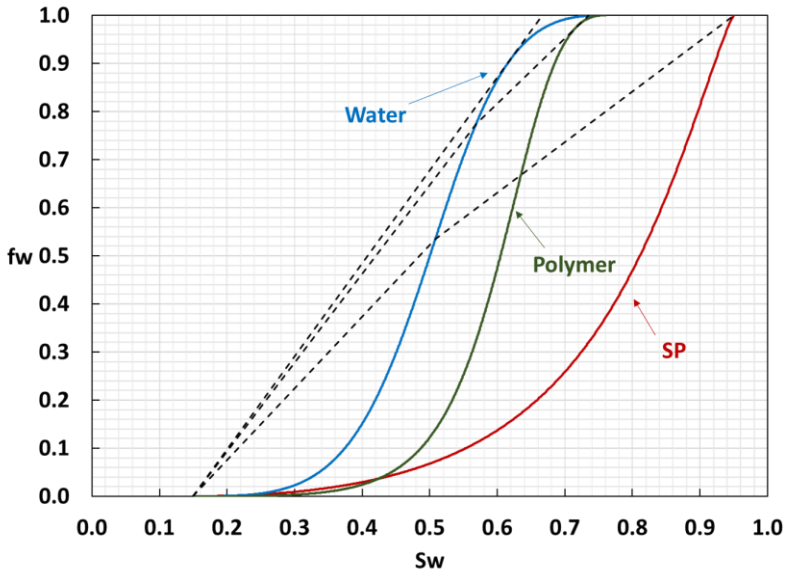

(a) Fractional flow of light oil displacement: Oil 1 cp / Polymer 5 cp

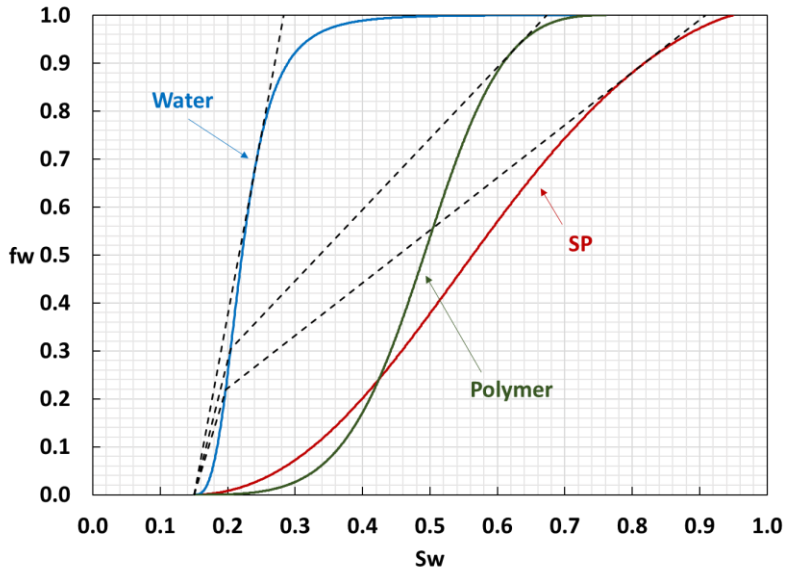

(b) Fractional flow of heavy oil displacement: Oil 500 cp / Polymer 300 cp

Figure 6.34 Example cases: fractional flow of light oil and heavy oil

Figure continued

Figure continued

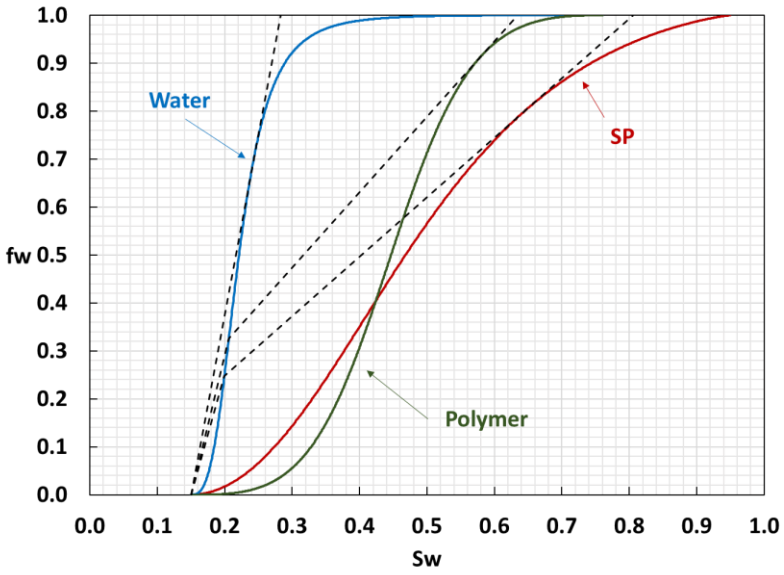

(c) Fractional flow of light oil displacement: Oil 500 cp / Polymer 140 cp

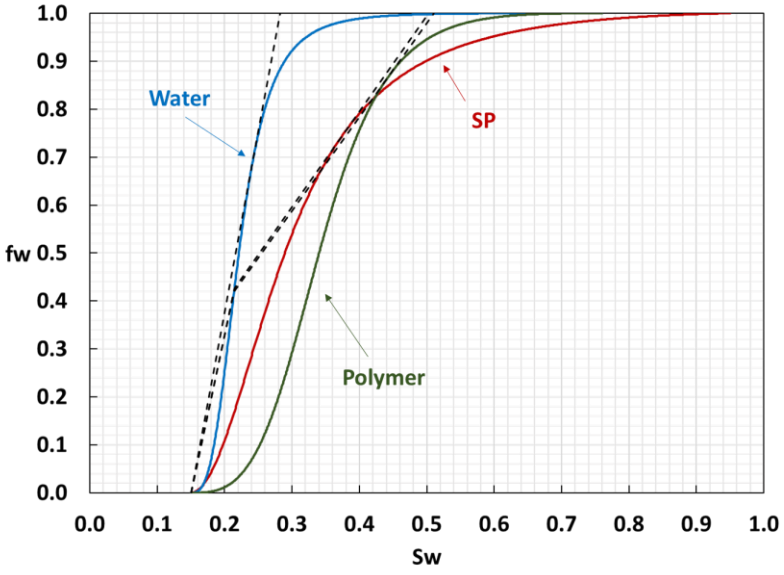

(d) Fractional flow of heavy oil displacement: Oil 500 cp / Polymer 20 cp

Figure 6.34 Example cases: fractional flow of light oil and heavy oil

For the example of the heavy oil case, water flooding is very inefficient with early breakthrough. In this example case, water flooding for 500 cp heavy oil displacement recovers 16% (OOIP) oil recovery at breakthrough of 0.13 PVI. The effect of polymer (300 cp) is prominent for heavy oil recovery (Figure 6.34(b)). It delays breakthrough time and achieves a lot more incremental oil recovery compared to water flooding. However, as polymer viscosity decreases to 140 cp (Figure 6.34(c)) and to 20 cp (Figure 6.34(d)), the polymer breakthrough time gets faster with a less amount of oil recovery at breakthrough.

When the performance of polymer flooding becomes less effective under the adverse mobility ratio, the improved polymer flooding can give potential to achieve more oil recovery. According to the fractional flow of polymer and SP solution, the improved polymer flooding can increase oil recovery with delayed breakthrough time and higher oil cut after breakthrough. This interpretation corresponds to experimental data of the improved polymer flooding in the previous section (Section 6.6).

Fractional flow calculation was applied to match two sandpack flooding results, Flood #1 (Polymer flooding) and Flood #4 (0.5 PVI of 0.5 wt% SAS slug) (Section 6.6). **Figure 6.35** shows the relative permeability curve to match experimental data. In addition to basic assumptions of fractional flow, it was assumed that the initial water saturation is equal to the residual water saturation. End-point relative permeabilities of water and oil were matched with measured data. Other parameters of relative permeability curves were adjusted.

For fluid properties, measured viscosities of brine (0.7 cp) and oil (500cp) were applied. Polymer viscosity was assumed to be 100 cp, which corresponds to the in-situ polymer viscosity at the shear rate of 2 sec^{-1}. Since polymer viscosity was not constant during sandpack flooding, this assumption will give the largest error in matching fractional

flow calculation with the experimental result. Polymer retentions were set as 250 mg/g for polymer flooding and 50 mg/g for the improved polymer flooding.

Figure 6.36 shows the fractional flow and the oil recovery result. Fractional flow calculation matched the improved flooding better than polymer flooding. A possible reason is the fluctuation of polymer viscosity during polymer flooding because of the unstable pressure drop control. Except the oil recovery around polymer breakthrough, however, the calculation result gives a good agreement with sandpack flooding result. According to the calculation, the residual oil saturation was reduced from 24.5% to 5%. This indicates that the capillary number during the improved polymer flooding reached beyond its critical capillary number and achieved the significant reduction of the residual oil saturation.

Under the adverse mobility ratio (or unfavorable viscosity ratio), there was not meaningful difference on oil recovery at the breakthrough time between the polymer flooding and the improved polymer flooding in these simplified fractional-flow calculations. The incremental oil recovery (27%) of the improved polymer flooding was mainly from the higher oil cut after breakthrough. This observation was confirmed by fractional flow calculation.

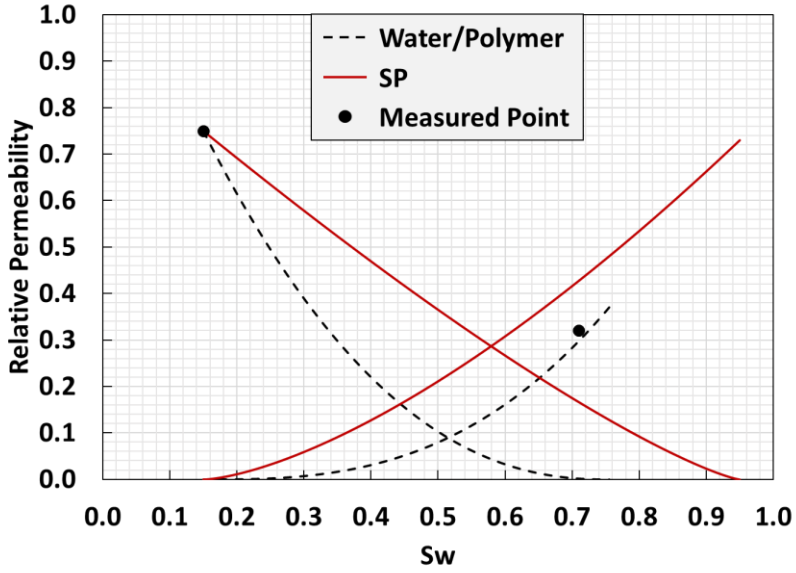

	Water / Polymer	SP
S_{wr}	0.15	0.15
S_{or}	0.245	0.05
k^0_{rw}	0.37	0.73
k^0_{ro}	0.75	0.75
n_w	2.8	1.5
n_o	2.3	1.25

- Viscosity: Oil 500 cp / Brine 0.7 cp / Polymer (& SP) solution 100 cp
- Adjusted polymer retention: 250 mg/g (for polymer flooding) and 50 mg/g (for SP flooding)

Figure 6.35 Relative permeability curve to match sandpack flooding data

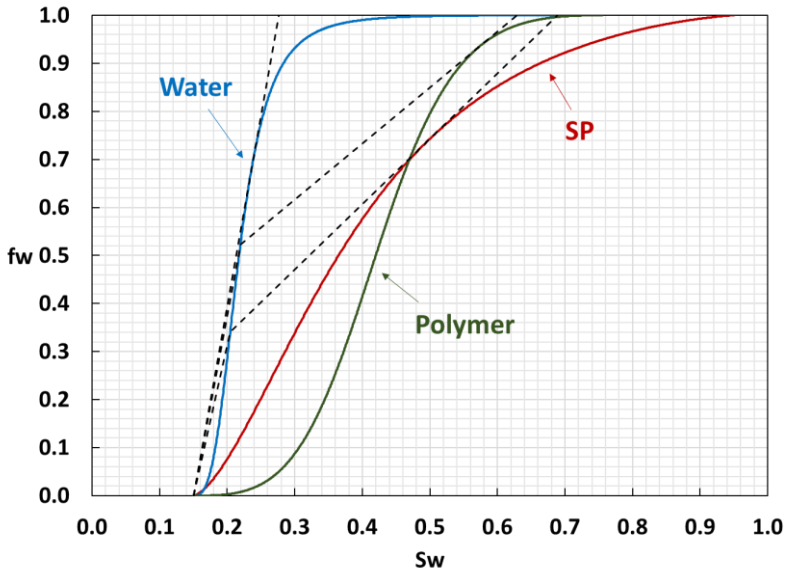

(a) Fractional Flow

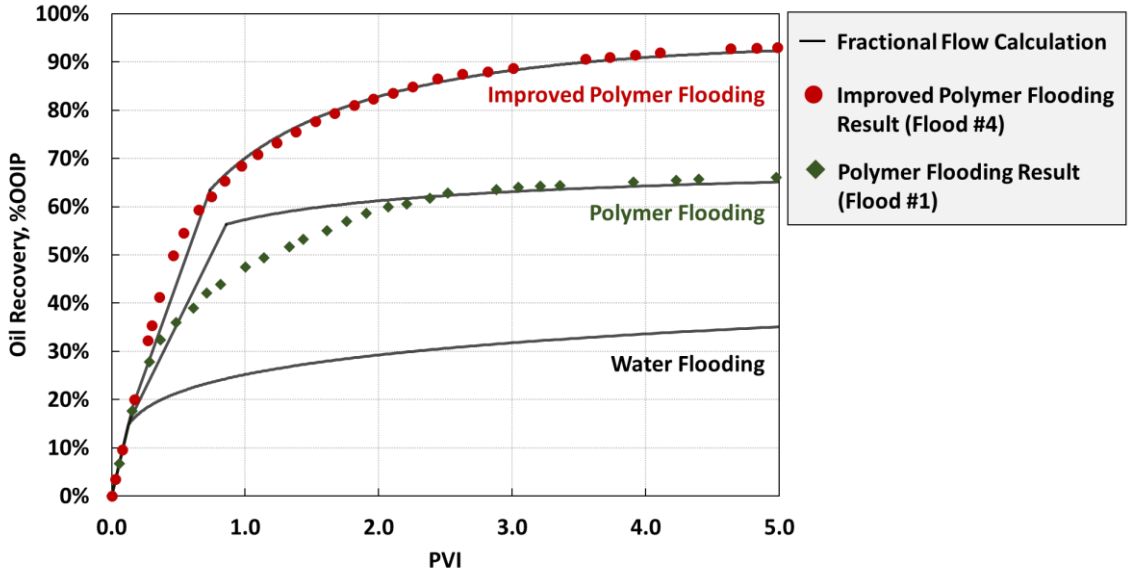

(b) Oil Recovery (%OOIP)

Figure 6.36 Fractional flow calculation to match sandpack flooding data

Another possible mechanism of the improved polymer flooding is the reduction of snap-off (or trapping off) of oil with high elasticity which has been studied for the low salinity water flooding (Bidhendi et al. 2018; Chávez-Miyauchi et al. 2016 and 2020). The less snap-off resulted in a continuous oil flow and lower residual oil saturation by a less amount of oil left behind oil flow. The interfacial viscoelasticity consists of the interfacial elasticity and the interfacial viscosity. According to Chávez-Miyauchi et al. (2016), the interfacial elasticity decreased as the brine salinity increased while the interfacial viscosity remained almost constant. Therefore, the low salinity brine keeps the higher interfacial elasticity.

The interfacial viscosity between the oil and aqueous phases decreases with a surfactant (or a co-solvent) (Fortenberry et al. 2015; Wasan et al. 1979). According to Chávez-Miyauchi et al. (2016), both the interfacial viscosity and the interfacial elasticity decreased with a non-ionic surfactant. However, the interfacial elasticity was consistently larger than the interfacial viscosity over the entire salinity range tested in the research. Therefore, it was possible to keep the interfacial viscoelasticity between the oil phase and the aqueous phase with a non-ionic surfactant. Also, it was found that a non-ionic surfactant resulted in significantly higher interfacial elasticity compared to cationic surfactants (Georgieva et al. 2009). In addition, acidic components (or asphaltenes) are known to increase the interfacial elasticity (Reilly et al. 2018).

Heavy oil in this research shows a high acid number: 8.08 mg-KOH/g-oil. With high interfacial elasticity between heavy oil and aqueous phases, highly acidic heavy oil could flow as a continuous oil phase with less snap-off of oil droplets. This can reduce the residual oil saturation during the improved polymer flooding.

Based on the discussion of capillary desaturation and fractional flow, the most important factor for the improved polymer flooding is the IFT reduction that is low enough

to reach a capillary number of 10^{-2}. In this research, IFT was reduced by 2-EH-7PO-15EO from 15.8 to 0.025 dynes/cm and the corresponding capillary number increased from 2.7×10^{-5} to 1.7×10^{-2}. In the study of Panthi et al. (2019), they used phenol-7PO-15EO to reduce IFT to 0.035 dynes/cm. Their improved polymer flooding achieved a meaningful incremental oil recovery with capillary numbers ranged from 0.99×10^{-2} to 3.99×10^{-2}.

At the current research status, the improved polymer flooding is suggested for heavy oil recovery when the oil exists as a continuous phase in the reservoir (i.e., the secondary flooding rather than the tertiary). As shown in the previous section (Section 6.7), this simplified SP flooding may not be effective for the tertiary flooding of light oil displacement, in which the water flooding likely yields a high displacement efficiency. A similar case can be found in Bataweel et al. (2012), which was a tertiary SP flooding for light oil displacement in sandstone. No salinity gradient was applied. They used either single amphoteric (not specified) or single anionic surfactant (not specified) to reduce the IFT to 0.022 - 0.072 dynes/cm. The polymer viscosity was high enough to achieve a mobility ratio smaller than one. However, they achieved only about 14 - 17% incremental oil recovery after the water flooding.

The effect of oil and porous medium properties on the performance of the improved polymer flooding should be investigated in the future. Figure 6.33 showed that the improved polymer flooding with the preceding water flooding unlikely achieved capillary desaturation in the Boise Sandstone core with the IFT of 0.28 dyne/cm for the light oil used. It is fundamentally important for a successful application of SAS to exhibit capillary desaturation for a given oil and porous medium in the secondary-mode flooding. Such an improved polymer flood is expected to yield a delayed polymer breakthrough as shown in Section 6.6.

As for any enhanced oil recovery methods, the oil saturation is an important factor for a successful application of improved polymer flooding. The improved polymer flooding was tested at very low oil saturation by injecting the SAS-polymer solution after Flood #1 (polymer flooding, Section 6.6). The oil saturation in the sandpack was 30% after polymer flooding (Flood #1). After 3 PVI of the additional SAS-polymer solution into this sandpack, only 6% more oil was recovered. This result indicates that, at very low oil saturation, the improved polymer flooding without ultra-low IFT micro-emulsions could not form an oil bank by the coalescence of oil droplets in the sand pack.

6.9. Conclusions

Improved polymer flooding was tested for heavy oil recovery in a sandpack. Experimental conditions were matched to the heavy oil reservoir in the North Sea. Given the limited sources for injection water and space on the off-shore platform, the improved polymer flooding was designed with no alkali injection and no salinity gradient. A SAS, 2-EH-7PO-15EO, was tested as a sole additive to the polymer solution. Four different sandpack floods for heavy oil recovery were conducted with different slug sizes and concentrations. The key conclusions are as follows:

- The optimal SAS was selected through IFT measurements in this research. Each SAS gave the lowest IFT near its solubility limit. After mixing, the lower IFT resulted in the faster phase separation into the oil and aqueous phases.
- 2-EH-7PO-15EO was selected as the optimum SAS in this research. The IFT between the heavy oil and the aqueous solution was 0.025 dynes/cm at 61°C. The CMC of 2-EH-7PO-15EO was 0.025 wt% in the reservoir brine at 61°C. 2-EH-7PO-15EO gave the lowest IFT, the fastest phase separation, and the lowest water content (vol.%) in the oil phase among the 12 SASs tested.
- The surface retention of 2-EH-7PO-15EO was 0.055 mg-SAS/g-rock, which is substantially smaller than typical values reported for ionic surfactants in the conventional SP. The small retention of SAS in the reservoir means an effective use of the injected SAS for sweeping/displacing heavy oil.
- The improved polymer flooding (Flood #2, #3, and #4) achieved a meaningful incremental oil recovery compared to the polymer flooding (Flood #1). The oil recovery (%OOIP) at 1 PVI was 47% for Flood #1, 63% for Flood #2 and #3, and 70% for Flood #4. After 1 PVI until 5 PVI, the improved polymer flooding consistently

achieved the incremental oil recovery about 12 - 16 % for Flood #2 and #3, and 22 - 27 % for Flood #4.

- The expected mechanism of the improved polymer flooding is the capillary desaturation by increasing capillary number through the IFT reduction by SAS. Another possible mechanism is higher interfacial elasticity of highly acidic heavy oil with a non-ionic SAS. Both mechanisms are expected to reduce the oil snap-off in heavy oil displacement by polymer solution. The conditions conducive to a successful application of the improved polymer flooding include a heavy oil reservoir of well-sorted porous media at high oil saturation with no preceding water flood.
- At the current research stage, the improved polymer flooding with SAS unlikely make an oil bank from dispersed oil droplets in the continuous water phase in the porous medium. Therefore, a continuous oil phase in the reservoir is an important factor for the successful improved polymer flooding by SAS. The improved polymer flooding can be more effective under the adverse mobility ratio when the performance of straight polymer flooding is not effective. With IFT reduction, the improved polymer flooding can increase oil recovery with the reduced oil saturation, the delayed polymer breakthrough, and the higher oil cut after breakthrough.
- The experimental results suggest a potential advantage of the improved polymer flooding. A SAS-polymer slug was composed of one non-ionic SAS and one polymer without any alkali, co-surfactants, and co-solvents. The conventional ASP flooding that typically uses about 1 wt% of surfactant in combination with additional co-solvents. A smaller amount of a SAS was used for the improved polymer flooding and achieved the significant incremental oil recovery.

7. Summary, Conclusions, and Recommendations for Future Research

7.1. Summary and Conclusions

This dissertation focused on the experimental study of dimethyl ether (DME), organic alkalis (diethylamine (DEA), triethylenetetramine (TETA), and pyrrolidine), and a surface active solvent (SAS) as a potential additive to the conventional heavy oil method such as steam injection and polymer flooding.

For bitumen recovery in SAGD, a water-soluble solvent, DME, is expected to reduce the bitumen viscosity by dilution and reduce the cumulative steam-oil ratio (CSOR) with a lowered steam chamber edge temperature. Prior to designing steam injection experiments or simulation studies, the phase behavior data are required to understand the property of DME - bitumen mixtures. The major contribution of this research is the fundamental phase behavior data such as bubble point, viscosity, density, and the viscosity model of DME - bitumen mixture.

Organic alkalis were investigated to utilize the condensed water that is the most abundant component in SAGD. The main idea was to induce bitumen-in-water emulsions, so that emulsified bitumen can also flow in the aqueous phase as well as the separate bitumen flow. This research provided phase behavior data including bitumen emulsification, bitumen content (vol.%) in oil-in-water emulsions, and emulsion viscosity. It was found that induced bitumen-in-water emulsions can be an effective bitumen carrier containing a meaningful amount of bitumen with viscosity a lot lower than the original bitumen viscosity.

For heavy oil recovery, the SAS-improved polymer flooding was studied for the incremental oil recovery compared to the straight polymer flooding. A SAS was the only additive to polymer with no additional chemicals such as co-surfactant, co-solvents, or

alkalis. Also, there was no salinity gradient necessary in the SAS-improved polymer flooding. This research provided the procedure to select an optimum SAS and the results of the lab-scale improved polymer floods based on the field operation plan for North Sea heavy oil reservoir. The sandpack flooding results showed the significant incremental oil recovery with a small amount of a SAS. The experimental data suggested that a successful application of the improved polymer flooding would be in a heavy oil reservoir of high-permeability unconsolidated sand with no preceding water flood.

7.2. Recommendations for Future Research

For the use of DME and organic alkalis for bitumen recovery in steam injection, this research provided the fundamental phase behavior data and viscosity data for DME - bitumen mixtures and bitumen emulsification with organic alkalis. The future research includes steam injection experiments and simulation studies. The steam injection experiment can be divided into two steps. The simulation study will be the last step to match experimental data and predict a field scale production.

The first step can be a steam injection for heavy oil recovery in a small-scale sandpack (or sandstone). This experiment is a simple and fast way to compare oil recovery between the only steam injection process and the co-injection process of steam and solvent. Oil recovery, pressure drop, effluent emulsification, and solvent recovery can be measured by this experiment.

A small-scale sandpack experiment is essential to measure in-situ emulsion properties. For example, it will confirm the oil-in-water emulsification of bitumen under a low shear rate by gravity drainage in porous media. In-situ emulsion viscosity can be measured as a function of different shear rates and pore sizes. The organic alkali retention in a sandpack is important parameter to design a steam injection experiment. The relative

permeability of oil-in-water emulsions should be measured to calculate the in-situ flow of bitumen-containing phases.

The next experiment will be a steam experiment with a large size sandpack, for which a high capacity steam generator is required to mimic SAGD operation. In addition to experimental data from small-scale sandpack experiments, this experiment can provide steam chamber characteristics, such as chamber growth, chamber edge temperature, and heat loss. Steam-oil-ratio, which is the most critical factor to determine the economic feasibility of SAGD, can be compared between steam-only injection and the co-injection of steam and solvent.

For the improved polymer flooding, this research shows the significant incremental oil recovery using a SAS for heavy oil recovery in a sandpack. It seems that the type of oil (heavy or light) is an important factor to determine the performance of the improved polymer flooding. It is recommended to compare the results of the improved polymer flooding with different oil properties such as heavy oil, light oil, acidic oil, and non-acidic oil.

More details of improved polymer flooding can be explained with the IFT measurement between the oil phase and the aqueous phase from effluents of sandpack flooding. Especially, the IFT of effluent samples after breakthrough will be important to explain the higher oil cut after breakthrough, where the SAS concentration in the aqueous phase seems negligible.

The improved polymer flooding was studied for the actual reservoir in the North Sea. A simulation study is required to predict oil production for the pilot test. First, simulation study should match the lab-scale experiment. Then, the simulation model can be developed for the field scale. The IFT reduction by SAS may affect the sweep efficiency

with the altered relative permeability of oil and water. The simulation study would help find an optimal injection scheme for SAS-polymer slug and polymer chase in the reservoir.

Since SAS is a new type of a surfactant, it is recommended to study the interaction between SAS and oil in addition to IFT. This will be studies on chemical properties such as interfacial viscoelasticity, wettability alteration, surfactant retention, and partitioning coefficient. With the systematic change of PO and EO units, this study will help to design the optimum SAS for the improved polymer flooding.

The effect of the base solvent that makes the hydrophobe of SAS can be an interesting topic. In this research, only two types of solvent were tested (e.g. 2-ethylhexanol or phenol). However, any kinds of secondary or tertiary alcohols with a short carbon chain could be a good candidate to make SAS. In addition, SAS as a short hydrophobe surfactant may result in better tolerance at higher temperature and hardness of brine in comparison to the conventional surfactants. This study will expand the opportunity of using of SAS in various chemical EOR processes.

Glossary

Roman Symbols

cp	centipoise (= mPa·s)
K	Kelvin (temperature)
mD	millidarcy (=10^{-3} Darcy)
N_C	capillary number
o/w	oil-in-water emulsions
P	pressure
ppm	parts per million
sec	second
T	temperature
V	volume
v	volume fraction
vol%	volume percent
W	aqueous phase
w/o	water-in-oil emulsions
wt%	weight percent
x	mole fraction
μ	viscosity
ρ	density

Abbreviations

AAD	average absolute deviation
AARD	average absolute relative deviation
ASP	alkali - surfactant - polymer
API	American petroleum institute
CMC	critical micelle concentration
CSOR	cumulative steam-to-oil ratio
EO	ethylene oxide
EOR	enhanced oil recovery
ES-SAGD	expanding-solvent-SAGD
HPAM	partially hydrolyzed polyacrylamide
HMPAM	hydrophobically modified polyacrylamide
IFT	interfacial tension
MW	molecular weight, g/mol

OOIP	original oil in place
SAGD	steam-assisted gravity drainage
SAP	solvent-aided-process
SARA	saturates, asphaltenes, resins and aromatics
SOR	steam-oil ratio
SAS	surface active solvent
SP	surfactant - polymer
PO	propylene oxide
PV	pore volume
PVI	pore volume injection, or pore volume injected
WOR	water oil ratio

Chemicals

2-EH	2-ethylhexanol
DME	dimethyl ether
DEA	diethyl amine
KOH	potassium hydroxide
HCl	hydrochloric acid
TETA	triethylenetetramine
NaCl	sodium chloride

References

Abdurahman, N.H., Rosli, Y.M., Azhari, N.H. and Hayder, B. A. 2012. Pipeline Transportation of Viscous Crudes as Concentrated Oil-in-Water Emulsions. *Journal of Petroleum Science and Engineering* 90-91: 139-144. https://doi.org/10.1016/j.petrol.2012.04.025

Acevedo, S., Gutierrez, X. and Rivas, H. 2001. Bitumen-in-Water Emulsions Stabilized With Natural Surfactants. *Journal of Colloid and Interface Science* 242: 230-238. https://doi.org/10.1006/jcis.2001.7728

Aitkulov, A., Luo, H., Lu, J. and Mohanty, K.K. 2017. Alkali-Cosolvent-Polymer Flooding for Viscous Oil Recovery: 2D Evaluation. *Energy and Fuels* 31:7015-7025. https://doi.org/10.1021/acs.energyfuels.7b00790

Alberta Energy Regulator (AER). 2012. *Identification of Enhanced Oil Recovery Potential in Alberta*. Phase 2 Final Report for Energy Resource Conservation Board.

Alkindi, A., Al-Azri, N., Said, D., AlShuaili, K. and te Riele, P. 2016. Persistence in EOR-Design of a Field Trial in a Carbonate Reservoir Using Solvent-based Water-Flood Process. Presented at the SPE EOR Conference at Oil and Gas West Asia, Muscat, Oman, 21-23 March. SPE-179838-MS. https://doi.org/10.2118/179838-MS

Al-Yaari, M., Hussein, I., Al-Sarkhi, A., Abbad, M. and Change, F. 2015. Effect of Water Salinity on Surfactant-Stabilized Water–Oil Emulsions Flow Characteristics. *Experimental Thermal and Fluid Science* 64: 54-61. https://doi.org/10.1016/j.expthermflusci.2015.02.001

Al-Sahhaf, T., Elsharkawy, A. and Fahim, M. 2008. Stability of Water-in-Crude Oil Emulsions: Effect of Oil Aromaticity, Resins to Asphaltene Ratio, and pH of Water. *Petroleum Science and Technology* 26: 2009-2022. https://doi.org/10.1080/10916460701428904

Argillier, J., Henaut, I., Gateau, P., Heraud, J.P. and Glenat, P., 2005. Heavy Oil Dilution. SPE paper presented at the 2005 SPE International Thermal Operations and Heavy Oil Symposium, Calgary, Alberta, Canada, 1-3 November. SPE-97763-MS. https://doi.org/10.2118/97763-MS

Arrhenius, S. 1887. Uber die Dissociation der in Wasser Gelosten Stoffe (On the Dissociation of Substances Dissolved in Water). *Z. Phys. Chem*. 1: 631-648.

Ashrafizadeh, S.N. and Kamran, M. 2010. Emulsification of Heavy Crude Oil in Water for Pipeline Transportation. *Journal of Petroleum Science and Engineering* 71: 205-211. https://doi.org/10.1016/j.petrol.2010.02.005

Ashrafizadeh, S.N., Motaee, E. and Hoshyargar, V. 2012. Emulsification of Heavy Crude Oil in Water by Natural Surfactants. *Journal of Petroleum Science and Engineering* 86-87: 137-143. https://doi.org/10.1016/j.petrol.2012.03.026

Austad, T., Fjelde, I., Veggeland, K. and Taugbøl, K. 1994. Physicochemical principles of low tension polymer flood. *Journal of Petroleum Science and Engineering* 10(03): 255-269. https://doi.org/10.1016/0920-4105(94)90085-X

Azom, P.N. and Srinivasan, S. 2009. Mechanistic Modeling of Emulsion Formation and Heat Transfer During the Steam-Assisted Gravity Drainage (SAGD) Process. SPE Annual Technical Conference and Exhibition, 4-7 October, New Orleans, Louisiana. SPE-124930-MS. https://doi.org/10.2118/124930-MS

Baek, K., Argüelles-Vivas, F.J., Okuno, R., Sheng, K., Sharma, H. and Weerasooriya, U.P. 2018. Emulsification of Athabasca Bitumen by Organic Alkali: Emulsion Phase Behavior and Viscosity for Bitumen/Brine/Triethylenetetramine. *Journal of Petroleum Science and Engineering* 168: 359-369. https://doi.org/10.1016/j.petrol.2018.04.063

Baek, K., Sheng, K., Argüelles-Vivas, F.J. and Okuno, R. 2019a. Comparative Study of Oil-Dilution Capability of Dimethyl Ether and Hexane as Steam Additives for Steam-Assisted Gravity Drainage. *SPE Reservoir Evaluation & Engineering* 22(03): 1030-1048. SPE-187182-PA. https://doi.org/10.2118/187182-PA

Baek, K., Argüelles-Vivas, F.J., Okuno, R., Sheng, K., Sharma, H. and Weerasooriya, U.P. 2019b. An Experimental Study of Emulsion Phase Behavior and Viscosity for Athabasca Bitumen/Diethylamine/Brine Mixtures. *SPE Reservoir Evaluation & Engineering* 22(2): 628-641. SPE-189768-PA. https://doi.org/10.2118/189768-PA

Baek, K., Okuno, R., Sharma, H. and Weerasooriya, U.P. 2019c. Oil-in-Water Emulsification of Athabasca Bitumen with Pyrrolidine Solution, *Fuel* 246: 425-442. https://doi.org/10.1016/j.fuel.2019.02.123

Baek, K., Argüelles-Vivas, F.J., Abeykoon, G.A., Okuno, R. and Weerasooriya, U.P. 2019d. Application of Ultrashort Hydrophobe Surfactants with Cosolvent Characters for Heavy Oil Recovery. *Energy and Fuels* 33: 8241-8249. https://doi.org/10.1021/acs.energyfuels.9b01716

Bahmanabadi, H., Hemmati, M., Shariatpanahi, H. Masihi, M. and Karambeigi, M.S. 2016. Phase Behavior and Rheology of Emulsions in an Alkaline/Cosolvent/Crude Oil/Brine System. *Petroleum Science and Technology* 34 (3): 207-215. https://doi.org/10.1080/10916466.2015.1017648

Ballard, N., Salsamendi, M., Carretero, P., and Asua, J.M. 2015. An Investigation Into the Nature and Potential of In-Situ Surfactants for Low Energy Miniemulsification. *Journal of Colloid and Interface Science* 458: 69-78. http://dx.doi.org/10.1016/j.jcis.2015.07.041

Barton, A.F., 1991. *CRC Handbook of Solubility Parameters and Other Cohesion Parameters*. CRC press.

Bataweel, M.A., Shivaprasad, A.Y. and Nasr-El-Din, H.A. 2012. Low-Tension Polymer Flooding Using Amphoteric surfactant in High Salinity/High Hardness and High Temperature Conditions in Sandstone Cores. SPE EOR Conference at Oil and Gas West Asia, 16-18 April, Muscat, Oman. SPE-155676-MS. https://doi.org/10.2118/155676-MS

Bera, A., Ojha, K., Kumar, T. and Mandal, A. 2012. Phase Behavior and Physicochemical Properties of (Sodium Dodecyl Sulfate + Brine + Propan-1-ol + Heptane) Microemulsions. *J. Chem. Eng. Data* 57 (3): 1000-1006. https://doi.org/10.1021/je2013796

Bibette, J., Roux, D., and Pouligny, B. 1992. Creaming of Emulsions: the Role of Depletion Forces Induced by Surfactant. *Journal de Physique II*, 2(3): 401-424. https://doi.org/10.1051/jp2:1992141

Bidhendi, M.M., Garcia-Olvera, G., Morin, B., Oakey, J.S. and Alvarado, V. 2018. Interfacial Viscoelasticity of Crude Oil/Brine: An Alternative Enhanced-Oil-Recovery Mechanism in Smart Waterflooding. *SPE Journal* 23(03): 803-818. https://doi.org/10.2118/169127-PA

Bryan, J. and Kantzas, A. 2007a. Enhanced Heavy-Oil Recovery by Alkali-Surfactant Flooding. SPE Annual Technical Conference and Exhibition, 11-14 November, Anaheim, California, U.S.A. SPE-110738-MS. https://doi.org/10.2118/110738-MS

Bryan, J. and Kantzas, A. 2007b. Potential for Alkali-Surfactant Flooding in Heavy Oil Reservoirs Through Oil-in-Water Emulsification. Canadian International Petroleum Conference, 12-14 June, Calgary, Alberta. PETSOC-2007-134. https://doi.org/10.2118/09-02-37

Bryan, J., Mai, A. and Kantzas, A. 2008. Investigation Into the Processes Responsible for Heavy Oil Recovery by Alkali-Surfactant Flooding. SPE Symposium on Improved Oil Recovery, 20-23 April, Tulsa, Oklahoma, USA. SPE-113993-MS. https://doi.org/10.2118/113993-MS

Butler, R. M. 2001. Some Recent Developments in SAGD. *Journal of Canadian Petroleum Technology* 40(1). PETSOC-01-01-DAS. https://doi.org/10.2118/01-01-DAS

Cannella, W.J., Huh, C. and Seright, R.S. 1988. Prediction of Xanthan Rheology in Porous Media. SPE Annual Technical Conference and Exhibition, 2-5 October, Houston, Texas. SPE-18089-MS. https://doi.org/10.2118/18089-MS

Cenovus Energy. 2012. *Suffield Conventional Heavy Oil Chemical Flood 2011 Annual Report*. IETP Project 03-053

Chang, H.L. 2013. Chapter 10. ASP Process and Field Results. *in Enhanced Oil Recovery - Field Case Studies*. 1st Edition. Elsevier. ISBN: 978-0-12-386545-8

Chang, L., Pope, G.A., Jang, S.H. and Tagavifar. 2019. Prediction of microemulsion phase behavior from surfactant and co-solvent structures. *Fuel* 237: 494-514. https://doi.org/10.1016/j.fuel.2018.09.151

Chávez-Miyauchi, T.E., Firoozabadi, A. and Fuller, G.G. 2016. Nonmonotonic Elasticity of the Crude Oil–Brine Interface in Relation to Improved Oil Recovery. *Langmuir* 32(9): 2192-2198. https://doi.org/10.1021/acs.langmuir.5b04354

Chávez-Miyauchi, T.E., Lu, Y. and Firoozabadi, A. 2020. Low salinity water injection in Berea sandstone: Effect of wettability, interface elasticity, and acid and base functionalities. *Fuel* 263. https://doi.org/10.1016/j.fuel.2019.116572

Chatzis, I. and Morrow, N.R. 1984. Correlation of Capillary Number Relationships for Sandstone. *Society of Petroleum Engineers* 24(05): 555-562. SPE-10114-PA. https://doi.org/10.2118/10114-PA

Computer Modelling Group. 2014. STARS Version 2014 User Guide. Calgary, Alberta, Canada: CMG

Cooke Jr, C. E., Williams, R. E. and Kolodzie P. A. 1974. Oil Recovery by Alkaline Waterflooding. *Journal of Petroleum Technology* 26(12): 1365-1374. SPE-4739-PA. https://doi.org/10.2118/4739-PA

Dehaghani, A.H.S. and Badizad, M.H., 2016. Experimental Study of Iranian Heavy Crude Oil Viscosity Reduction by Diluting with Heptane, Methanol, Toluene, *Gas Condensate and Naphtha. Petroleum* 2(4), pp.415-424. https://doi.org/10.1016/j.petlm.2016.08.012

Delamaide, E. 2014. Polymer Flooding of Heavy Oil - From Screening to Full-Field Extension. SPE Heavy and Extra Heavy Oil Conference: Latin America, 24-26 September, Medellín, Colombia. SPE-171105-MS. https://doi.org/10.2118/171105-MS

Delamaide, E., Zaitoun, A., Renard, G. and Tabary, R. 2014a. Pelican Lake Field: First Successful Application of Polymer Flooding In a Heavy-Oil Reservoir. *SPE Reservoir Evaluation & Engineering* 17(03): 340-354. SPE-165234-PA. https://doi.org/10.2118/165234-PA

Delamaide, E., Bazin, B., Rousseau, D. and Degre, G. 2014b. Chemical EOR for Heavy Oil: The Canadian Experience. SPE EOR Conference at Oil and Gas West Asia, 31 March-2 April, Muscat, Oman. SPE-169715-MS. https://doi.org/10.2118/169715-MS

Delamaide, E. 2017. Using Horizontal Wells for Chemical EOR: Field Cases. *Georesursy* 19(3): 166-175. https://doi.org/10.18599/grs.19.3.3

Dong, M., Ma, S. and Liu, Q. 2009. Enhanced Heavy Oil Recovery Through Interfacial Instability: A Study of Chemical Flooding for Brintnell Heavy Oil. *Fuel* 88: 1049–1056. https://doi.org/10.1016/j.fuel.2008.11.014

Ezeuko, C.C., Wang, J. and Gates, I.D. 2013. Investigation of Emulsion Flow in Steam-Assisted Gravity Drainage. *SPE Journal* 18(03): 440-447. SPE-157830-PA. https://doi.org/10.2118/157830-PA

Fan, T. and Buckley, J. 2007. Acid Number Measurements Revisited. *SPE Journal* 12(4): 496-500. SPE-99884-PA. https://doi.org/10.2118/99884-PA

Feng, A., Zhang, G., Ge, J., Jiang, P., Pei, H., Zhang, J. and Li, R. 2012. Study of Surfactant-Polymer Flooding in Heavy Oil Reservoirs. SPE Heavy Oil Conference Canada, 12-14 June, Calgary, Alberta, Canada. SPE-157621-MS. https://doi.org/10.2118/157621-MS

Fortenberry, R., Kim, D., Nizamidin, N., Adkins, S., Arachchilage, G., Koh, H.S., Weerasooriya, U.P. and Pope, G.A. 2015. Use of Cosolvents to Improve Alkaline/Polymer Flooding. *SPE Journal* 20(2). SPE-166478-PA. https://doi.org/10.2118/166478-PA

Fu, L., Zhang, G., Ge, J., Liao, K., Pei, H., Jiang, P. and Li, X. 2016. Study on Organic Alkali-Surfactant-Polymer Flooding for Enhanced Ordinary Heavy Oil Recovery. *Colloids and Surfaces A: Physicochemical and Engineering Aspects* 508: 230-239. https://doi.org/10.1016/j.colsurfa.2016.08.042

Fulcher, R.A. Jr., Ertekin, T. and Stahl, C.D. 1985. Effect of Capillary Number and Its Constituents on Two-Phase Relative Permeability Curves. *Journal of Petroleum Technology* 37(02). SPE-12170-PA. https://doi.org/10.2118/12170-PA

Gao, J., Okuno, R. and Li, H.A. 2017. An Experimental Study of Multiphase Behavior for n-Butane/Bitumen/Water Mixtures. *SPE Journal* 22 (3): 783-798. SPE-180736-PA. https://doi.org/10.2118/180736-PA

Gao, J., Okuno, R. and Li, H.A. 2018. A Phase-Behavior Study for n-Hexane/Bitumen and n-Octane/Bitumen Mixtures. *SPE Journal* 23 (1): 128-144. SPE-186097-PA. https://doi.org/10.2118/186097-PA

Garnes, J.M., Mathisen, A.M., Scheie, A. and Skauge, A. 1990. Capillary Number Relations for Some North, Sea Reservoir Sandstones. SPE/DOE Enhanced Oil Recovery Symposium, 22-25 April, Tulsa, Oklahoma. SPE-20264-MS. https://doi.org/10.2118/20264-MS

Gates, I.D., 2007. Oil Phase Viscosity Behavior in Expanding-Solvent Steam-Assisted Gravity Drainage. *Journal of Petroleum Science and Engineering* 59 (1-2): 123-134. https://doi.org/10.1016/j.petrol.2007.03.006

Ge, J., Feng, A., Zhang, G., Jiang, Ping., Pei, H., Li, R. and Fu, X. 2012. Study of the Factors Influencing Alkaline Flooding in Heavy-Oil Reservoirs. *Energy and Fuels* 26 (5): 2875–2882. https://doi.org/10.1021/ef3000906

Georgieva, D., Schmitt, V., Leal-Calderon, F. and Langevin, D. 2009. On the Possible Role of Surface Elasticity in Emulsion Stability. *Langmuir* 25(10): 5565-5573. https://doi.org/10.1021/la804240e

Ghannam, M.T. and Esmail. N. 2007. Flow Enhancement of Medium-Viscosity Crude Oil. *Petroleum Science and Technology* 24(8): 985-999. https://doi.org/10.1081/LFT-200048166

Ghannam, M.T., Hasan, S.W., Abu-Jdayil, B. and Esmail, N. 2012. Rheological Properties of Heavy & Light Crude Oil Mixtures for Improving Flowability. Journal of *Petroleum Science and Engineering* 81: 122-128. https://doi.org/10.1016/j.petrol.2011.12.024

Glandt, C.A. and Chapman, W.G. 1995. The Effect of Water Dissolution on Oil Viscosity. *SPE Reservoir Engineering* 10 (1): 59-64, SPE-24631-PA. https://doi.org/10.2118/24631-PA

Gogarty, W.B. 1967. Mobility Control With Polymer Solutions. *Society of Petroleum Engineers Journal* 7(2): 161-173. SPE-1566-B. https://doi.org/10.2118/1566-B

Gogarty, W.B. 1978. Micellar/Polymer Flooding An Overview. *Society of Petroleum Engineers* 30(08). SPE-7041-PA. https://doi.org/10.2118/7041-PA

Groot, J.A.W.M., Eikmans, D., Fadili, A. and Romate, J.E. 2016a. Field-Scale Modeling and Sensitivity Analysis of DME Enhanced Waterflooding. Presented at the SPE EOR Conference at Oil and Gas West Asia, Muscat, Oman, 21-23, March. SPE-179798-MS. https://doi.org/10.2118/179798-MS

Groot, J.A.W.M., Chernetsky, A., te Riele, P.M., Dindoruk, B., Cui, J., Wilson, L.C. and Ratnakar, R. 2016b. Representation of Phase Behavior and PVT Workflow for DME Enhanced Water-Flooding. Presented at the SPE EOR Conference at Oil and

Gas West Asia, Muscat, Oman, 21-23, March. SPE-179771-MS. https://doi.org/10.2118/179771-MS

Gupta, S., Gittins, S. and Picherack, P. 2005. Field Implementation of Solvent Aided Process. *Journal of Canadian Petroleum Technology* 44 (11): 8-13. PETSOC-05-11-TN1. https://doi.org/10.2118/05-11-TN1

Gupta, S.C. and Gittins, S.D. 2006. Christina Lake Solvent Aided Process Pilot. *Journal of Canadian Petroleum Technology* 45 (9): 15-18. PETSOC-06-09-TN. https://doi.org/10.2118/06-09-TN

Haddadnia, A., Azinfar, B., Zirrahi, M. and Hassanzadeh, H. 2018. Thermophysical Properties of Dimethyl Ether/Athabasca Bitumen System. *The Canadian Journal of Chemical Engineering* 96 (2): 597-604. https://doi.org/10.1002/cjce.23009

Han, X., Wang, W. and Xu, Y. 1995. The Viscoelastic Behavior of HPAM Solutions in Porous Media and It's Effects on Displacement Efficiency. International Meeting on Petroleum Engineering, 14-17 November, Beijing, China. SPE-30013-MS. https://doi.org/10.2118/30013-MS

Hansen, C.M. 1967. *The Three Dimensional Solubility Parameter and Solvent Diffusion Coefficient: Their Importance in Surface Coating Formulation*. Danish Technical Press.

Hansen, C.M. 2007. *Hansen Solubility Parameters: A User's Handbook*, Second Edition, CRC Press. ISBN 9780849372483

Hasan, S.W., Ghannam, M.T. and Esmail, N. 2010. Heavy Crude Oil Viscosity Reduction and Rheology for Pipeline Transportation. *Fuel* 89(5): 1095-1100. https://doi.org/10.1016/j.fuel.2009.12.021

Healy, R.N., Reed, R.L. and Stenmark, D.G. 1976. Multiphase Microemulsion Systems. *Society of Petroleum Engineers* 16(03). SPE-5565-PA. https://doi.org/10.2118/5565-PA

Hincapie, R.E. 2016. *Pore-Scale Investigation of the Viscoelastic Phenomenon during Enhanced Oil Recovery (EOR) Polymer Flooding through Porous Media*. PhD Dissertation. The Clausthal University of Technology. ISBN: 978-3-86948-531-7

Hirasaki, G.J. and Pope, G.A. 1974. Analysis of Factors Influencing Mobility and Adsorption in the Flow of Polymer Solution Through Porous Media. *Society of Petroleum Engineers Journal* 14(04): 337-346. SPE-4026-PA. https://doi.org/10.2118/4026-PA

Hirasaki, G.J. 1981. Application of the Theory of Multicomponent, Multiphase Displacement to Three-Component, Two-Phase Surfactant Flooding 21(02). *Society of Petroleum Engineers Journal* 21(02). SPE-8373-PA. https://doi.org/10.2118/8373-PA

Hirasaki, G.J., Miller, C.A. and Puerto, M. 2011. Recent Advances in Surfactant EOR. *SPE Journal* 16(04). SPE-115386-PA. https://doi.org/10.2118/115386-PA

Hocine, S., Magnan, A., Degre, G., Rousseau, N. and Rousseau, D. 2014. Alkaline-Free Surfactant Polymer Process for Heavy Oil. SPE EOR Conference at Oil and Gas West Asia, 31 March-2 April, Muscat, Oman. SPE-169697-MS. https://doi.org/10.2118/169697-MS

Ihmels, E.C. and Lemmon, E.W. 2007. Experimental Densities, Vapor Pressures, and Critical Point, and a Fundamental Equation of State for Dimethyl Ether. *Fluid Phase Equilibria* 260: 36-48. https://doi.org/10.1016/j.fluid.2006.09.016

Isaacs, E.E. and Smolek, K.F. 1983. Interfacial tension behavior of athabasca bitumen/aqueous surfactant systems. *The Canadian Journal of Chemical Engineering* 61(2): 233-240. https://doi.org/10.1002/cjce.5450610215

Ivory. J.J., Zheng, R., Nasr, T.N., Deng, X., Beaulieu, G. and Heck, G. 2008. Investigation of Low Pressure ES-SAGD. Presented at 2008 SPE International Thermal Operations and Heavy Oil Symposium, Calgary, Alberta, Canada, October 20-23. SPE-117759-MS. https://doi.org/10.2118/117759-MS

Jia, W. and Okuno, R. 2018. Modeling of Asphaltene and Water Associations in Petroleum Reservoir Fluids Using Cubic-Plus-Association EOS. *AIChE Journal* 64(9): 3429-3442. https://doi.org/10.1002/aic.16191

Kalpakci, B., Arf, T.G., Barker, J.W., Krupa, A.S., Morgan, J.C. and Neira, R.D. 1990. The Low-Tension Polymer Flood Approach to Cost-Effective Chemical EOR. SPE/DOE Enhanced Oil Recovery Symposium, 22-25 April, Tulsa, Oklahoma. SPE-20220-MS. https://doi.org/10.2118/20220-MS

Kang, X., Zhang, J., Sun, F., Zhang, F., Feng, G., Yang, J., Zhang, X. and Xiang, W. 2011. A Review of Polymer EOR on Offshore Heavy Oil Field in Bohai Bay, China. SPE Enhanced Oil Recovery Conference, 19-21 July, Kuala Lumpur, Malaysia. SPE-144932-MS. https://doi.org/10.2118/144932-MS

Kar, T., Williamson, M. and Hascakir, B. 2014. The Role of Asphaltenes in Emulsion Formation for Steam Assisted Gravity Drainage (SAGD) and Expanding Solvent - SAGD (ES-SAGD). SPE Heavy and Extra Heavy Oil Conference: Latin America, 24-26 September, Medellín, Colombia. SPE-171076-MS. https://doi.org/10.2118/171076-MS

Kariznovi, M., Nourozieh. H., Guan. J. and Abedi J. 2013. Measurement and Modeling of Density and Viscosity for Mixtures of Athabasca Bitumen and Heavy n-Alkane. *Fuel* 112: 83-95. https://doi.org/10.1016/j.fuel.2013.04.071

Keshavarz, M., Okuno, R. and Babadagli, T. 2014. Efficient Oil Displacement Near the Chamber Edge in ES-SAGD. *Journal of Petroleum Science and Engineering* 118: 99-113. https://doi.org/10.1016/j.petrol.2014.04.007

Keshavarz, M., Okuno, R. and Babadagli, T. 2015. Optimal Application Conditions for Steam/Solvent Coinjection. *SPE Reservoir Evaluation & Engineering* 18 (1): 20-38. SPE-165471-PA. https://doi.org/10.2118/165471-PA

Khan, Y.K., Samanta, A., Ojha, K. and Mandal, A. 2008. Interaction between aqueous solutions of polymer and surfactant and its effect on physicochemical properties. *Asia-Pacific Journal of Chemical Engineering* 3: 579-585. https://doi.org/10.1002/apj.212

Kim, M., Abedin, A., Lele, P., Guerrero, A. and Sinton, D. 2017. Microfluidic Pore-Scale Comparison of Alcohol- and Alkaline-Based SAGD Processes. *Journal of Petroleum Science and Engineering* 154: 139-149. https://doi.org/10.1016/j.petrol.2017.04.025

Kokal, S. 2005. Crude-Oil Emulsions: A State-of-the-Art Review. *SPE Production & Facilities* 20(1). SPE-77497-PA. https://doi.org/10.2118/77497-PA

Koh, H., Lee, V.B. and Pope, G.A. 2018. Experimental Investigation of the Effect of Polymers on Residual Oil Saturation. *SPE Journal* 23(01): 1-17. SPE-179683-PA. https://doi.org/10.2118/179683-PA

Kumar, R. and Mohanty, K.K. 2010. ASP Flooding of Viscous Oils. SPE Annual Technical Conference and Exhibition, 19-22 September, Florence, Italy. SPE-135265-MS. https://doi.org/10.2118/135265-MS

Kumar, R., Dao, E. and Mohanty, K.K. 2012. Heavy-Oil Recovery by In-Situ Emulsion Formation. *SPE Journal* 17(2). SPE-129914-PA. https://doi.org/10.2118/129914-PA

Lake, L.W., Johns, R., Rossen, B. and Pope, G.A. 2014. *Fundamentals of Enhanced Oil Recovery*. Society of Petroleum Engineers. ISBN: 978-1-61399-328-6

Larichev, Y.V., Nartova, A.V. and Martyanov, O.N. 2016. The Influence of Different Organic Solvents on the Size and Shape of Asphaltene Aggregates Studied via Small-Angle X-Ray Scattering and Scanning Tunneling Microscopy. *Adsorption Science and Technology* 34(2-3): 244-257. https://doi.org/10.1177/0263617415623440

Leaute, R.P. and Carey B.S. 2002. Liquid Addition to Steam for Enhancing Recovery of Bitumen With CSS: Evolution of Technology from Research Concept to a Field Pilot at Cold Lake. Presented at the SPE/Petroleum Society of CIM/CHOA Paper Number 79011, Calgary, Alberta, Canada, November 4-7. PETSOC-2005-161. https://doi.org/10.2118/2005-161

Li. W., Mamora, D.D. and Li, Y., 2011a. Light- and Heavy-Solvent Impacts on Solvent-Aided-SAGD Process: A Low-Pressure Experimental Study. *Journal of Canadian Petroleum Technology* 50 (4): 19-30. SPE-133277-PA. https://doi.org/10.2118/133277-PA

Li. W., Mamora, D.D. and Li, Y., 2011b. Solvent-Type and -Ratio Impacts on Solvent-Aided SAGD Process. *SPE Reservoir Evaluation & Engineering* 14 (3): 320-331. SPE-130802-PA. https://doi.org/10.2118/130802-PA

Liu, J., Adegbesan, K.O. and Bai, J. 2012. Suffield Area, Alberta, Canada - Caen Polymer Flood Pilot Project. SPE Heavy Oil Conference Canada. 12-14 June, Calgary, Alberta, Canada. SPE-157796-MS. https://doi.org/10.2118/157796-MS

Liu, Q., Dong, M., Yue, X. and Hou, J. 2006. Synergy of Alkali and Surfactant in Emulsification of Heavy Oil in Brine. Colloids and Surfaces *A: Physicochemical*

and Engineering Aspects 273: 219-228. https://doi.org/10.1016/j.colsurfa.2005.10.016

Liu, Q., Dong, M., Ma, S. and Tu, Y. 2007. Surfactant Enhanced Alkaline Flooding for Western Canadian Heavy Oil Recovery, *Colloids and Surfaces A: Physicochem. Eng. Aspects* 293: 63-71. https://doi.org/10.1016/j.colsurfa.2006.07.013

Lu, C., Liu, H., Zhao, W., Lu, K., Liu, Y., Tian, J. and Tan, X. 2017. Experimental Investigation of In-Situ Emulsion Formation to Improve Viscous-Oil Recovery in Steam-Injection Process Assisted by Viscosity Reducer. *SPE Journal* 22(1): 130-137. SPE-181759-PA. https://doi.org/10.2118/181759-PA

Lu, Q., Ning, Y., Wang, J. and Yang, X. 2015. Full Field Offshore Surfactant-Polymer Flooding in Bohai Bay China. SPE Asia Pacific Enhanced Oil Recovery Conference, 11-13 August, Kuala Lumpur, Malaysia. SPE-174591-MS. https://doi.org/10.2118/174591-MS

Maldal, T., Gilje, E., Kristensen, R., Karstad, T., Nordbotten, A., Schilling, B.E.R. and Vikane, O. 1998. Evaluation and Economical Feasibility of Polymer-Assisted Surfactant Flooding for the Gullfaks Field, Norway. *SPE Reservoir Evaluation & Engineering* 1(02): 161-168. SPE-35378-PA. https://doi.org/10.2118/35378-PA

Malkin, A.Y., Rodionova, G., Simon, S., Ilyin, S.O., Arinina, M.P., Kulichikhin, V.G. and Sjöblom, J. 2016. Some Compositional Viscosity Correlations for Crude Oils from Russia and Norway. *Energy and Fuels* 30: 9322-9328. https://doi.org/10.1021/acs.energyfuels.6b02084

McInnis, L.E., Hunter, K.D., Ellis-Toddington, T.T. and Grawbarger, D.J. 2013. Case Study of the Taber Mannville B ASP Flood. SPE Enhanced Oil Recovery Conference, 2-4 July, Kuala Lumpur, Malaysia. SPE-165264-MS. https://doi.org/10.2118/165264-MS

Mehrotra, A.K. and Svrcek. W.Y. 1986. Viscosity of Compressed Athabasca Bitumen. *The Canadian Journal of Chemical Engineering* 64 (5): 844-847. https://doi.org/10.1002/cjce.5450640520

Michailidou, E.K., Assael, M.J., Huber. M.L. and Perkins. R.A. 2013. Reference Correlation of the Viscosity of n-Hexane From the Triple Point to 600 K and up to

100 MPa, *Journal of Physical and Chemical Reference Data* 42 (3): 1-12. https://doi.org/10.1063/1.4818980

Mishra, S., Bera, A. and Mandal, A. 2014. Effect of Polymer Adsorption on Permeability Reduction in Enhanced Oil Recovery. *Journal of Petroleum Engineering*. http://dx.doi.org/10.1155/2014/395857

Mohebati, M.H., Maini, B.B., and Harding, T.G. 2012. Numerical-Simulation Investigation of the Effect of Heavy-oil Viscosity on the Performance of Hydrocarbon Additives in SAGD. *SPE Reservoir Evaluation & Engineering* 15 (02): 165-181. SPE-138151-PA. https://doi.org/10.2118/138151-PA

Murphy Oil Corporation. 2016. *SEAL Polymer Project Scheme Approval No. 11320C*. Annual Performance Presentation.

Nasr, T.N., Beaulieu, G., Golbeck, H. and Heck, G. 2003. Novel Expanding Solvent-SAGD Process "ES-SAGD". *Journal of Canadian Petroleum Technology* 42 (1): 13-16. https://doi.org/10.2118/03-01-TN

Nizamidin, N., Weerasooriya, U.P. and Pope, G.A. 2015. Systematic Study of Heavy Oil Emulsion Properties Optimized With a New Chemical Formulation Approach: Particle Size Distribution. *Energy and Fuel* 29: 7065-7079. https://doi.org/10.1021/acs.energyfuels.5b01818

Nourozieh, H., Kariznovi, M., Guan, J. and Abedi, J. 2013. Measurement of Thermophysical Properties and Modeling for Pseudo-Binary Mixtures of n-Decane and Athabasca Bitumen. *Fluid Phase Equilibria* 347: 62-75. https://doi.org/10.1016/j.fluid.2013.03.010

Nourozieh, H., Kariznovi, M. and Abedi, J. 2015a. Density and Viscosity of Athabasca Bitumen Samples at Temperatures Up to 200C and Pressures Up to 10 MPa. *SPE Journal*, 18 (03): 375-386. SPE-176026-PA. https://doi.org/10.2118/176026-PA

Nourozieh, H., Kariznovi, M. and Abedi, J. 2015b. Viscosity Measurement and Modeling for Mixtures of Athabasca Bitumen/Hexane. *Journal of Petroleum Science and Engineering* 129: 159-167. https://doi.org/10.1016/j.petrol.2015.03.002

Nourozieh, H., Kariznovi, M. and Abedi, J. 2015c. Viscosity Measurement and Modeling for Mixtures of Athabasca Bitumen/n-Pentane at Temperatures Up to 200°C. *SPE Journal*, 20 (02): 226-238. SPE-170252-PA. https://doi.org/10.2118/170252-PA

Nourozieh, H., Kariznovi, M. and Abedi, J. 2015d. Experimental and Modeling Studies of Phase Behavior for Propane/Athabasca Bitumen Mixtures. *Fluid Phase Equilibria* 397: 37-43. https://doi.org/10.1016/j.fluid.2015.03.047

Nourozieh, H., Kariznovi, M. and Abedi, J. 2017. Solubility of n-Butane in Athabasca Bitumen and Saturated Densities and Viscosities at Temperatures Up to 200°C. *SPE Journal* 22 (01): 94-102. SPE-180927-PA. https://doi.org/10.2118/180927-PA

Okuno, R. 2018. "Coinjection of Dimethyl Ether and Steam for Bitumen and Heavy Oil Recovery," PCT Application Serial Number: PCT/US17/45724, U.S. Patent Application Serial Number: 15/670973, August 7, 2017. https://worldwide.espacenet.com/publicationDetails/originalDocument?FT=D&date=20180215&DB=&locale=en_EP&CC=WO&NR=2018031463A1&KC=A1&ND=4, notice of allowance on August 27, 2018. Issued on November 13, 2018 as U.S. Patent No. 10,125,591. Canada Application Serial No. 3,033,003.

Okuno, R., Weerasooriya, U., and Baek, K.H. 2019. "Methods for the Recovery of Heavy Hydrocarbons," A provisional application was submitted on April 16, 2019. US Patent Office Serial Number: 62/834,573.

Ondrusek, P.S. 1988. Micellar/Polymer Flooding in the Bradford Field. *Society of Petroleum Engineers* 40(08). SPE-15550-PA. https://doi.org/10.2118/15550-PA

Pal, R. 1996. Effect of Droplet Size on the Rheology of Emulsions. *AIChE Journal* 42(11): 3181-3190. https://doi.org/10.1002/aic.690421119

Pal, R. 2000. Shear Viscosity Behavior of Emulsions of Two Immiscible Liquids. *Journal of Colloid and Interface Science* 225: 359-366. https://doi.org/10.1006/jcis.2000.6776

Panthi, K., Weerasooriya U.P. and Mohanty, K.K. 2019. Chemical Flood of a Viscous Oil with Novel Surfactants. SPE Annual Technical Conference and Exhibition, 30 September - 2 October, Calgary, Alberta, Canada. SPE-196198-MS. https://doi.org/10.2118/196198-MS

Pei, H., Zhang, G., Ge, J., Jin, L. and Ma, C. 2013. Potential of Alkaline Flooding to Enhance Heavy Oil Recovery Through Water-in-Oil Emulsification. *Fuel* 104: 284-293. https://doi.org/10.1016/j.fuel.2012.08.024

Petersen, M.A. and Grade, H. 2011. Analysis of Steam Assisted Gravity Drainage Produced Water using Two-Dimensional Gas Chromatography with Time-of-Flight Mass Spectrometry. *Ind. Eng. Chem. Res*. 50(21): 12217-12224. https://doi.org/10.1021/ie200531h

Pope, G.A., Wang, B. and Tsaur, K. 1979. A Sensitivity Study of Micellar/Polymer Flooding. *Society of Petroleum Engineers* 19(06). SPE-7079-PA. https://doi.org/10.2118/7079-PA

Pope, G.A. 1980. The Application of Fractional Flow Theory to Enhanced Oil Recovery. *SPE Journal* 20(03): 191-205. SPE-7660-PA. https://doi.org/10.2118/7660-PA

Poulsen, A., Shook, G.M., Jackson, A., Ruby, N., Charvin, K., Dwarakanath, V., Thach, S. and Ellis, M. 2018. Results of the UK Captain Field Interwell EOR Pilot. SPE Improved Oil Recovery Conference, 14-18 April, Tulsa, Oklahoma, USA. SPE-190175-MS. https://doi.org/10.2118/190175-MS

Qi, P., Ehrenfried, D.H., Koh, H. and Balhoff, M.T. 2017. Reduction of Residual Oil Saturation in Sandstone Cores by Use of Viscoelastic Polymers. *SPE Journal*. SPE-179689-PA. https://doi.org/10.2118/179689-PA

Ramos-Pallares, F., Schoeggl, F.F., Taylor, S.D., Satyro, M.A. and Yarranton, H.W. 2015. Predicting the Viscosity of Hydrocarbon Mixtures and Diluted Heavy Oils Using the Expanded Fluid Model. *Energy and Fuels* 30 (5): 3575-3595. https://doi.org/10.1021/acs.energyfuels.5b01951

Rapoport, L.A. and Leas, W.J. 1953. Properties of Linear Waterfloods. *Journal of Petroleum Technology* 5(05): 140-148. SPE-213-G. https://doi.org/10.2118/213-G

Razi, M., Sinha, S., Waghmare, P.R., Das, S. and Thundat. T. 2016. Effect of Steam-Assisted Gravity Drainage Produced Water Properties on Oil/Water Transient Interfacial Tension. *Energy and Fuels* 30(12): 10714-10720. https://doi.org/10.1021/acs.energyfuels.6b01686

Reilly, T., Medina, B., Lehmann, T. and Alvarad, V. 2018. Select Naphthenic Acids Beneficially Impact Oil-Water Dynamics During Smart Waterflooding. SPE Annual Technical Conference and Exhibition, 24-26 September, Dallas, Texas, USA. SPE-191455-MS. https://doi.org/10.2118/191455-MS

Robins, M.M. and Hibberd, D.J. 1998. Emulsion Flocculation and Creaming. *In Modern Aspects of Emulsion Science, Royal Society of Chemistry*, Chapter 4. pp. 115-144.

Rock, A., Hincapie R.E., Wegner, J. and Ganzer, L. 2017. Advanced Flow Behavior Characterization of Enhanced Oil Recovery Polymers using Glass-Silicon-Glass Micromodels that Resemble Porous Media. SPE Europec featured at 79th EAGE Conference and Exhibition, 12-15 June, Paris, France. SPE-185814-MS. https://doi.org/10.2118/185814-MS

Saki, M. and Khaz'ali, A.R. 2017. Influence of Surfactant Type, Surfactant Concentration, and Salinity on Interfacial Tension of a Brine/Live Oil/Surfactant Fluid System: A Case Study of Iranian Asmari Oil Reservoir. *Iranian Journal of Oil & Gas Science and Technology* 6(1): 01-12. https://doi.org/10.22050/ijogst.2017.44341

Salager, J. L., Loaiza-Maldonado, I., Minana-Perez, M. and Silva, F. 1982. Surfactant-Oil-Water Systems Near the Affinity Inversion Part I: Relationship Between Equilibrium Phase Behavior and Emulsion Type and Stability. *Journal of Dispersion Science and Technology* 3: 279-292. https://doi.org/10.1080/01932698208943642

Schorling, P., Kessel, D. and Rahimian, I. 1999. Influence of the Crude Oil Resin/Asphaltene Ratio on the Stability of Oil/Water Emulsions. *Colloids and Surfaces A: Physicochemical and Engineering Aspects* 152: 95-102. https://doi.org/10.1016/S0927-7757(98)00686-4

Sharma, H., Dufour, S., Arachchilage, G.W.P.P., Weerasooriya, U.P., Pope, G.A. and Mohanty, K.K. 2015. Alternative alkalis for ASP flooding in anhydrite containing oil reservoirs. *Fuel* 140: 407-420. https://doi.org/10.1016/j.fuel.2014.09.082

Sharma, H., Panthi, K. and Mohanty, K.K. 2018. Surfactant-Less Alkali-Cosolvent-Polymer Floods for an Acidic Crude Oil. *Fuel* 215: 484-491. https://doi.org/10.1016/j.fuel.2017.11.079

Sharma, J. and Gates, I.D. 2010. Multiphase Flow at the Edge of a Steam Chamber. *Canadian Journal of Chemical Engineering* 88(3): 312-321. https://doi.org/10.1002/cjce.20280

Shamekhi, H., Kantzas, A., Bryan, J.L. and Su, S. 2013. Insights into Heavy Oil Recovery by Surfactant, Polymer and ASP Flooding. SPE Heavy Oil Conference-Canada, 11-13 June, Calgary, Alberta, Canada. SPE-165440-MS. https://doi.org/10.2118/165440-MS

Shen, C. 2013. Chapter 17. SAGD for Heavy Oil Recovery. *in Enhanced Oil Recovery - Field Case Studies*. 1st Edition. Elsevier. ISBN: 978-0-12-386545-8

Sheng, J.J. 2014. A Comprehensive Review of Alkaline-Surfactant-Polymer (ASP) Flooding. *Asia-Pacific Journal of Chemical Engineering* 9: 471-489. https://doi.org/10.1002/apj.1824

Sheng, J.J. 2015. Investigation of Alkaline–Crude Oil Reaction. *Petroleum* 1(1): 31-39. https://doi.org/10.1016/j.petlm.2015.04.004

Sheng, K., Okuno, R. and Wang, M. 2018. Dimethyl Ether as an Additive to Steam for Improved Steam-Assisted Gravity Drainage. *SPE Journal*. SPE-184983-PA. https://doi.org/10.2118/184983-PA

Sheng, K., Argüelles-Vivas, F.J., Baek, K.H. and Okuno, R. 2019. An Experimental Study of Emulsion Flow in Alkaline/Solvent Coinjection with Steam for Heavy-Oil/Bitumen Recovery. *SPE Reservoir Evaluation & Engineering*. SPE-190224-PA. https://doi.org/10.2118/190224-PA

Shi, X. and Okuno, R. 2018. Analytical Solution for Steam-Assisted Gravity Drainage With Consideration of Temperature Variation Along the Edge of a Steam Chamber. *Fuel* 217: 262-274. https://doi.org/10.1016/j.fuel.2017.12.110

SiTu, W., Lu, H., Ruan, C., Zhang, L., Zhu, Y. and Zhang, L. 2017. Effect of polymer on dynamic interfacial tensions of sulfobetaine solutions. *Colloids and Surfaces A: Physicochemical and Engineering Aspects* 533: 231-240. https://doi.org/10.1016/j.colsurfa.2017.09.006

Skauge, A., Zamani, N., Jacobsen, J.G., Shiran, B.S., Al-Shakry, B. and Skauge, T. 2018. Polymer Flow in Porous Media: Relevance to Enhanced Oil Recovery. *Colloids Interfaces* 2(3). https://doi.org/10.3390/colloids2030027

Smith, F.W. 1970. The Behavior of Partially Hydrolyzed Polyacrylamide Solutions in Porous Media. *Journal of Petroleum Technology* 22(02): 148-156. SPE-2422-PA. https://doi.org/10.2118/2422-PA

Sorbie, K.S. 1991. *Polymer-Improved Oil Recovery*. Springer Netherlands. ISBN 978-0-216-92693-6

Srivastava, P. and Castro, L. 2011. Successful Field Application of Surfactant Additives to Enhance Thermal Recovery of Heavy Oil. SPE Middle East Oil and Gas Show and Conference, 25-28 September, Manama, Bahrain. SPE-140180-MS. https://doi.org/10.2118/140180-MS

Tagavifar, M., Herath, S., Weerasooriya, U.P., Sepehrnoori, K. and Pope, G.A. 2018. Measurement of Microemulsion Viscosity and Its Implications for Chemical Enhanced Oil Recovery. *SPE Journal* 23(01): 66-83. SPE-179672-PA. https://doi.org/10.2118/179672-PA

Thomas, S. and Farouq Ali, S.M. 1992. Micellar-Polymer Flooding: Status And Recent Advances. *Petroleum Society of Canada* 31(08). https://doi.org/10.2118/92-08-05

Ujfaludi, L. 1986. Longitudinal dispersion tests in non-uniform porous media. *Hydrological Sciences Journal* 31(4): 467-474. https://doi.org/10.1080/02626668609491067

Upamali, K.A.N., Liyanage, P.J., Jang, S.H., Shook, E., Weerasooriya, U.P. and Pope, G.A. 2018. New Surfactants and Cosolvents Increase Oil Recovery and Reduce Cost. *SPE Journal* 23(06): 2202-2217. SPE-179702-PA. https://doi.org/10.2118/179702-PA

USGS (U.S. Geological Survey). 2007. *Heavy Oil and Natural Bitumen Resources in Geological Basins of the World*. Report 2007-1084. https://pubs.usgs.gov/of/2007/1084

Venkatramani, A. and Okuno, R. 2017. Compositional Mechanisms in SAGD and ES-SAGD With Consideration of Water Solubility in Oil. *SPE Reservoir Evaluation*

& Engineering 20 (03): 681-697. SPE-180737-PA. https://doi.org/10.2118/180737-PA

Venkatramani, A. and Okuno, R. 2018. Mechanistic Simulation Study of Expanding-Solvent Steam-Assisted Gravity Drainage Under Reservoir Heterogeneity. *Journal of Petroleum Science & Engineering* 169: 146-156. https://doi.org/10.1016/j.petrol.2018.04.074

Vittoratos, E. and Kovscek, A. 2017. Doctrines and Realities in Reservoir Engineering. SPE Western Regional Meeting, 23-27 April, Bakersfield, California. SPE-185633-MS. https://doi.org/10.2118/185633-MS

Walther, C. 1931. The Evaluation of Viscosity Data. *Erdol Teer* 7: 382–384.

Wang, M., Baek, K., Abeykoon, G.A., Argüelles-Vivas, F.J. and Okuno, R. 2019. A Comparative Study of Ketone and Surfactant for Enhancement of Water Imbibition in Fractured Porous Media. *Energy and Fuels* 34(5): 5159-5167. https://doi.org/10.1021/acs.energyfuels.9b03571

Wasan, D.T., McNamara, J.J., Shah, S.M., Sampath, K. and Aderangi, N. 1979. The Role of Coalescence Phenomena and Interfacial Rheological Properties in Enhanced Oil Recovery: An Overview. *Journal of Rheology* 23(2): 181-207. https://doi.org/10.1122/1.549524

Wassmuth, F.R., Green, K., Arnold, W. and Cameron, N. 2009. Polymer Flood Application to Improve Heavy Oil Recovery at East Bodo. *Journal of Canadian Petroleum Technology* 48(02): 55-61. https://doi.org/10.2118/09-02-55

Watson, A., Trahan, G.A. and Sorensen, W. 2014. An Interim Case Study of an Alkaline-Surfactant-Polymer Flood in the Mooney Field, Alberta, Canada. SPE Improved Oil Recovery Symposium, 12-16 April, Tulsa, Oklahoma, USA. SPE-169154-MS. https://doi.org/10.2118/169154-MS

Weerasooriya, U., Mohanty, K.K., Okuno, R., Baek, K.H., Panthi, K., Sharma, H., Ghosh, P., and Abeykoon, G.A. 2019a. "Alkoxylate Emulsions," WIPO Application No.: PCT/US2019/25873, April 4, 2019. US Patent Office Serial Number: 62/732,234.

Weerasooriya, U., Mohanty, K.K., Okuno, R., Baek, K.H., Panthi, K., Sharma, H., Ghosh, P., and Abeykoon, G.A. 2019b "Methods for Hydrocarbon Recovery Using

Alkoxylate Emulsions," WIPO Application No.: PCT/US2019/25871, April 4, 2019. US Patent Office Serial Number: 62/732,234.

White, J.L., Goddard, J.E. and Phillips, H.M. 1973. Use of Polymers To Control Water Production in Oil Wells. *Journal of Petroleum Technology* 25(02): 143-150. SPE-3672-PA. https://doi.org/10.2118/3672-PA

Winsor, P.A. 1948. Hydrotropy, Solubilisation and Related Emulsification Processes. *Transactions of the Faraday Society* 44: 376-398. https://doi.org/10.1039/TF9484400376

Wu, J., Liu, Z., Bi, S. and Meng, X. 2003. Viscosity of Saturated Liquid Dimethyl Ether From (227 to 343) K. *Journal of Chemical & Engineering Data* 48: 426-429. https://doi.org/10.1021/je0256232

Wu. J., Liu, Z., Wang, B. and Pan, J. 2004. Measurement of the Critical Parameters and the Saturation Densities of Dimethyl Ether. *Journal of Chemical & Engineering Data* 49: 704-708. https://doi.org/10.1021/je034251+

Wu, J. and Yin, J. 2008. Vapor Pressure Measurements of Dimethyl Ether From (213 to 393) K. *Journal of Chemical & Engineering Data* 53: 2247-2249. https://doi.org/10.1021/je800375t

Xia, L., Lu, S. and Cao, G. 2004. Stability and Demulsification of Emulsions Stabilized by Asphaltenes or Resins. *Journal of Colloid and Interface Science* 271: 504-506. https://doi.org/10.1016/j.jcis.2003.11.027

Xiao, R., Teletzke, G., Lin, M., Glotzbach, R., Aitkulov, A., Yeganeh, M., Jaishankar, A. and Hegner, J. 2017. A Novel Mechanism of Alkaline Flooding to Improve Sweep Efficiency for Viscous Oils. SPE Annual Technical Conference and Exhibition, 9-11 October, San Antonio, Texas, USA. SPE-187366-MS. https://doi.org/10.2118/187366-MS

Yan, Z., Elliott, J. and Masliyah, J. 1999. Roles of Various Bitumen Components in the Stability of Water-in-Diluted-Bitumen Emulsions. *Journal of Colloid and Interface Science* 220: 329-337. https://doi.org/10.1006/jcis.1999.6533

Yang, X., Verruto, V. and Kilpatrick, P. 2007. Dynamic Asphaltene−Resin Exchange at the Oil/Water Interface: Time-Dependent W/O Emulsion Stability for

Asphaltene/Resin Model Oils. *Energy and Fuels* 21 (3): 1343-1349. https://doi.org/10.1021/ef060465w

Yarranton, H., Hussein, H. and Masliyah, J. 2000. Water-in-Hydrocarbon Emulsions Stabilized by Asphaltenes at Low Concentrations. *Journal of Colloid and Interface Science* 228: 52-63. https://doi.org/10.1006/jcis.2000.6938

Ye, Z., Zhang, F., Han, L., Luo, P., Yang, J. and Chen, H. 2008. The effect of temperature on the interfacial tension between crude oil and gemini surfactant solution. *Colloids and Surfaces A: Physicochemical and Engineering Aspects* 322(1–3): 138-141. https://doi.org/10.1016/j.colsurfa.2008.02.043

Zaitoun, A. and Chauveteau, G. 1998. Effect of Pore Structure and Residual Oil on Polymer Bridging Adsorption. SPE/DOE Improved Oil Recovery Symposium, 19-22 April, Tulsa, Oklahoma. SPE-39674-MS. https://doi.org/10.2118/39674-MS

Zeidani, K. and Gupta, S. 2013. Surfactant-Steam Process: An Innovative Enhanced Heavy Oil Recovery Method for Thermal Applications. SPE Heavy Oil Conference-Canada, 11-13 June, Calgary, Alberta, Canada. SPE-165545-MS. https://doi.org/10.2118/165545-MS

Zhang, J., Ravikiran, R., Freiberg, D. and Thomas, C.P. 2012. ASP Formulation Design for Heavy Oil. SPE Improved Oil Recovery Symposium, 14-18 April, Tulsa, Oklahoma, USA. SPE-153570-MS. https://doi.org/10.2118/153570-MS

Zhang, J., Tian, D., Lin, M., Yang, Z. and Dong, Z. 2016. Effect of Resins, Waxes and Asphaltenes on Water-Oil Interfacial Properties and Emulsion Stability. *Colloids and Surfaces A: Physicochemical and Engineering Aspects* 507: 1-6. https://doi.org/10.1016/j.colsurfa.2016.07.081

Zhu, D. and Okuno, R. 2016. Multiphase Isenthalpic Flash Integrated With Stability Analysis. *Fluid Phase Equilibria* 423: 203-219. https://doi.org/10.1016/j.fluid.2016.04.005

Zou, X., Zhang, X. and Shaw, J. M. 2007. Phase Behavior of Athabasca Vacuum Bottoms + n-Alkane Mixtures. *SPE Production & Operations* 22 (02): 265-272. SPE-97661-PA. https://doi.org/10.2118/97661-PA